DISS. ETH NO. 25080

ASTRAL MICROTUBULE DYNAMICS IN *SACCHAROMYCES CEREVISIAE*

A thesis submitted to attain the degree of

DOCTOR OF SCIENCES of ETH Zürich
DR. SC. ETH ZÜRICH

presented by

XIUZHEN CHEN
MSC., NIBS, BEIJING
BORN 26 NOVEMBER 1985
CITIZEN OF CHINA

accepted on the recommendation of
Prof. Dr. Yves Barral
Prof. Dr. Michel Steinmetz
Prof. Dr. Benoît Kornmann
Prof. Dr. Iva Tolić
Prof. Dr. Gábor Székely

2018

ACKNOWLEDGMENTS

I thank my supervisor Yves Barral for giving me the opportunity to conduct my thesis research in his lab. It has been a time filled with sweat and tears but also rewarding moments. Yves has been a great scientific mentor throughout these years, I truly enjoyed and appreciate those meetings where Yves let me have a peek of how the thinking was done. Those moments are absolutely among my favourites of the lab life and have a large impact on me as a scientist. I thank Yves for his trust, a challenging project, and a network of amazing collaborators. Yves made it possible for me to work with fellows expertise in structural biology and mathematical modelling. I thank Prof. Michel Steinmetz from the Paul Scherer Institute and his lab (in particular Marcel Stangier) for working alongside with me and for stimulating discussions. I thank Lukas Widmer and his supervisor Prof. Jörg Stelling from BSSE for seeing more in my data than I did and a great time working together. I am grateful that Marcel and Lukas always traveled to Zurich for our meetings, it has been a wonderful experience working with both of them.

I wholeheartedly thank Prof. Iva Tolić and her team for developing the Low light tracking tool and for making it available to the community. None of the work presented here would be possible if not for the tracking tool, which helped me reshape my project and encouraged me to continue this work in moments of weakness.

I would also like to thank the members of my thesis committee: Prof. Michel Steinmetz, Prof. Benoît Kornmann, Prof. Iva Tolić, and Prof. Gábor Székely, who have supported me greatly with advice throughout my entire PhD.

I thank the entire Barral lab for discussions and suggestions. I am grateful to my subgroup colleagues Nana, Matze, and Jette for helping me getting started in the lab and for our subgroup meetings where everything could be discussed. I thank Mattia for translating my abstract into Italian. I would like to thank Rupali for being the best desk mate and for valuable scientific discussions.

Finally, I want to thank my best friend and life partner Daniele for encouraging me to embark on this adventure, helping me to automatize the image analysis pipeline, teaching me to code in MATLAB, and to write in LaTeX. I would also like to thank him for his contagious passion for science, unconditional support, boundless patience, and his amazing ability to encouraging me in whatever I choose to do!

ABSTRACT

Microtubules are dynamic cytoskeletal filaments that undergo alternate growth and shrinkage phases by incorporating or disassembling their building blocks, the $\alpha\beta$-tubulin dimers. This 'dynamic instability' hallmark of microtubules allows the microtubule cytoskeleton to be remodelled rapidly over the course of the cell cycle or upon external stimuli, supporting a broad range of critical cellular functions. Many microtubule-associated proteins (MAPs) contribute to this remodelling process by promoting microtubule assembly (named polymerase) or disassembly (named depolymerase). However, how these MAPs coordinate with each other and with cellular signals is poorly understood, partly due to the difficulty of qualitatively assessing microtubule dynamics in living cells at high spatio-temporal resolution. An example is the kinesin Kip2, which has been shown to be a microtubule polymerase in vitro. Yet it is unclear why and how Kip2 requires its cargo Bik1 (homolog of CLIP170) to polymerize microtubules in vivo. Here we use *S.cerevisiae* as a model system to investigate how the kinesin Kip2 concerts its motor and polymerase activities through phosphoregulation to maintain the length and organization of astral microtubules (aMTs).

First, we developed a novel computer-assisted framework to quantify aMT dynamics in vivo with high precision. Using this framework, we found that Kip2 uses its motor domain to translocate along the microtubule lattice and to polymerize microtubule at plus-ends. Strikingly, its cargo protein Bik1 (CLIP-170 homolog) is indispensable for Kip2 motor domain to make the transition into polymerase upon arrival at the plus-end. Indeed, failure of interacting with Bik1 renders the abundant Kip2 at plus-end inactive in polymerizing microtubules. The successful transition is achieved by retaining Kip2 on plus-ends by Bik1. Once its low-complexity N-terminus is phosphorylated, it triggers its interaction with the coiled-coil domain of Kip2, dissociates itself from Bik1, and hence from the plus-end. Furthermore, using homology-based structural modelling and experimental validation both in vivo and in vitro, we identified distinct tubulin interfaces within Kip2 motor domain that are involved in binding microtubule lattice to translocate and in binding free tubulin dimers to polymerize, respectively. Collectively, we demonstrate a novel mechanism with which MAPs cooperatively polymerize microtubules. We report the first 'motor domain' with dual function of motility and microtubule polymerization.

Interestingly, we also revealed an unexpected role of yeast microtubule-organizing center (MTOC), the spindle pole body (SPB) in controlling the dynamics of microtubule plus-ends. Kip2 recruitment and loading along microtubule lattice is prohibited in a Bik1 dependent manner, except near the minus-end or at SPB, which is strongly promoted by polo-like kinase Cdc5 mediated phosphorylation of a SPB component Spc72. Due to the high processivity of Kip2 translocation, the activity of a SPB recruiting Kip2 is transmitted to the amount of Kip2 on the plus-end, which in turn affects the dynamics of plus-end. Preliminary results indicate that hypo-phosphorylated Kip2 is no longer recruited to SPB as efficiently. We propose that Bik1 inhibits the random loading of Kip2 along the microtubule lattice by preventing the dissociation of hypo-phosphorylated Kip2 at plus-ends. Therefore, only phosphorylated Kip2 freely diffuses in cytoplasm, which has low affinity to microtubules. Release of hypo-phosphorylated Kip2 from plus-end allows the random loading of Kip2 along the microtubule lattice, which is likely the case in the absence of Bik1.

Finally, we investigated the factors contributing to the establishment and maintenance of the asymmetric organization of aMTs on the two sides of the mitotic spindles. We show that spatial signals, and not SPB history, determines the asymmetry. Furthermore, imbalanced kinase activities between the bud and mom compartments contribute to the aMT asymmetry. Most importantly, the biased activity of mitotic SPBs recruiting Kip2 regulates aMT asymmetry.

SOMMARIO

I microtubuli sono filamenti dinamici del citoscheletro che subiscono fasi alterne di crescita e decrescita incorporando o smontando i loro elementi costitutivi, i dimeri di α-tubulina e β-tubulina. Questa caratteristica, chiamata ïnstabilità dinamica"dei microtubuli, consente di rimodellare rapidamente il citoscheletro dei microtubuli nel corso del ciclo cellulare o su stimoli esterni, supportando un'ampia gamma di funzioni cellulari critiche. Molte proteine associate ai microtubuli (MAP) contribuiscono a questo processo di rimodellamento promuovendo l'assemblaggio dei microtubuli (denominato polimerizzazione) o la loro scomposizione (denominata depolimerizzazione). Tuttavia, il modo in cui queste MAP si coordinano tra loro e con i segnali cellulari risulta ancora poco chiaro. Tutto ciò è dovuto, in parte, alla difficoltà di valutare in modo qualitativo la dinamica dei microtubuli in vivo con un'alta risoluzione spaziale e temporale. Qui utilizziamo *S.cerevisiae* come sistema modello per studiare il modo in cui la chinesina Kip2 organizza le sue attività motorie e di polimerizzazione attraverso la fosforegolazione, al fine di preservare la lunghezza dei microtubuli astrali (aMTs).

Innanzitutto, abbiamo sviluppato un nuovo framework computerizzato per quantificare la dinamica dei aMT in vivo con alta precisione. Usando questo framework, abbiamo scoperto che la chinesina Kip2 utilizza il suo dominio motorio per traslocarsi lungo il reticolo di microtubuli e per polimerizzarli al terminale positivo. Sorprendentemente, una volta raggiunto il terminale positivo, la proteina di carico Bik1 (omologo di CLIP-170) è indispensabile per poter tramutare la funzione della chinesina Kip2 da proteina motore a polimerasi. In effetti, il fallimento dell'interazione con Bik1 rende inattiva Kip2 al terminale del microtubulo polimerizzante, anche se presente in abbondanza. Il successo di questa transizione si ottiene mantenendo Kip2 al terminale positivo. Una volta che il dominio N-terminale di bassa complessità di Kip2 accumula fosforilazione, si innesca la interazione con il suo stesso dominio 'coiled-coil', permettendo la dissociazione da Bik1, e quindi dal terminale positivo. Inoltre, utilizzando la modellazione strutturale basata sull'omologia unita alla convalidazione sperimentale sia in vivo che in vitro, abbiamo identificato delle interfacce di tubulina distinte all'interno del dominio motore di Kip2. Queste interfacce si legano al reticolo dei microtubuli per permettere la traslocazione di Kip2 e sono anche in grado di legarsi, rispettivamente, anche ai dimeri liberi di tubulina per permettere la loro polimerizzazione. Quindi, dimostriamo un nuovo meccanismo con cui le MAP polimerizzano in

modo cooperativo i microtubuli. Segnaliamo il primo "dominio motore"con doppia funzione di motilità e polimerizzazione dei microtubuli.

Abbiamo rivelato un ruolo inaspettato del "microtubule-organizing center"(MTOC) degli lieviti, chiamato 'spindle pole body' (SPB, equivalente del centrosoma) nel controllo della dinamica ai terminali dei microtubuli. Il reclutamento ed il caricamento di Kip2 lungo il reticolo dei microtubuli è proibito in un modo dipendente da Bik1, eccetto al terminale negativo o allo SPB. In questi due casi specifici il reclutamento è fortemente promosso dalla fosforilazione della proteina Spc72, componente dello SPB, mediata dalla polo-like chinasi Cdc5. A causa dell'elevata processività della traslocazione di Kip2, l'attività di uno SPB che recluta Kip2 si riflette nella quantità della stessa Kip2 al terminale positivo, che a sua volta influisce sulla sua dinamica. I risultati preliminari indicano che solo Kip2 in forma fosforilata può essere reclutata dallo SPB. Noi proponiamo che Bik1 inibisca il caricamento casuale di Kip2 lungo il reticolo di microtubuli impedendo la dissociazione di Kip2 non fosforilata ai terminali positivi. Pertanto, solo Kip2 fosforilata si diffonde liberamente nel citoplasma con scarsa affinità ai microtubuli. Il rilascio di Kip2 non fosforilata dal terminale positivo consente il caricamento casuale di Kip2 lungo il reticolo dei microtubuli, come probabilmente avviene in mancanza di Bik1. Infine, abbiamo studiato i fattori che contribuiscono alla creazione e al mantenimento dell'organizzazione asimmetrica dei microtubuli astrali ai due lati dei fusi mitotici. Dimostriamo che i segnali spaziali e non la storia dei SPB determinano l'asimmetria. Inoltre, le attività di chinasi sbilanciate tra i compartimenti del germoglio e della cellula madre contribuiscono all'asimmetria dei microtubuli astrali.

PUBLICATIONS

Parts of this thesis have been published in:
Lengefeld J., Yen E., Chen XZ., Leary A., Vogel J., Barral Y. Spatial cues and not spindle pole maturation drive the asymmetry of astral microtubules between new and pre-existing spindle poles. *Mol Biol Cell.,* 2017

Stangier M. M., Kumar A., Chen XZ., Farcas A., Barral Y., Steinmetz M. O. Structure-function relationship of the Bik1-Bim1 complex. *Structure* 2018

Parts of this thesis are manuscripts in preparation:
Chen XZ., Widmer L., Stangier M. M., Steinmetz M. O., Stelling J., Barral Y. A mechanism for the control of microtubule plus-end dynamics from the minus-end. *Manuscript in preparation.*

Chen XZ., Stangier M. M., Steinmetz M. O., Barral Y. Yeast CLIP170 turns kinesin Kip2 motor domain into microtubule polymerase at plus-end. *Manuscript in preparation.*

Contributions:
All experiments in this thesis were performed and analyzed by Xiuzhen Chen, with the exception of the data shown in Figure4.2B, Figure4.3AB, Figure4.4, and supplement Figure3, which were produced and analyzed by Mr. Marcel Stangier (Prof. Michel Steinmetz Laboratory, PSI), in Figure3.1 and Figure3.3ABC were produced by Xiuzhen Chen and analyzed by Mr. Lukas Widmer (Prof. Jörg Stelling Laboratory, BSSE), in Figure6.2, the last three Kip3 mutants (Kip3-pp1, Kip3-3A, and Kip3-pp1-3A) were produced and analyzed by Ms. Désirée Marchand, in Figure 5.5, which were produced by Xiuzhen Chen and analyzed by Mr. Jannik Hugener and Mr. Christian Doerig.

CONTENTS

1

INTRODUCTION

1.1 THE MICROTUBULE CYTOSKELETON

Cells are tasked with enormous amount of challenges. To function properly, they must be properly shaped, physically robust, and properly structured internally. They have to be able to rearrange their internal components as they grow, divide, respond to environmental stimuli, and fuse with neighbouring cells. Eukaryotic cells developed a system of filaments called cytoskeleton to cope with all these needs. The cytoskeleton's diverse functions originate from three families of filaments: microtubules, intermediate filaments, and actins, which are assembled from different protein molecules. Actin filaments accumulate at the cell periphery underlying the plasma membrane, are prompted to react quickly upon extracellular stimuli, and are most well know to drive cell motility (reviewed in [Suarez and Kovar, 2016, Davidson and Wood, 2016]). Intermediate filaments emanate from the nucleus and concentrate in the perinuclear region, extend throughout the cytoplasm to make contact with plasma membrane. Intermediate filaments are both highly rigid and highly dynamic, enabling them to be the main cytoskeleton to bear tension and absorb mechanical stress (reviewed in [Herrmann et al., 2007, Godsel et al., 2008]). Microtubules are essential for cell division and partitioning of genetic materials, they are also key factors in organizing organelle distribution, cargo transportation. Microtubules are also stable scaffold components of cilia, flagella, and the centriole [Desai and Mitchison, 1997], one of the most ancient features of eukaryotes.

Microtubule filaments are hollow cylinder structures composed by α/β-tubulin heterodimers in a head to tail manner, thus they are intrinsically polarized and their minus-ends (where α-tubulin is exposed) are anchored to microtubule-organizing centers (MTOCs), such that their plus-ends (where β-tubulin is exposed) radiate toward the edge of the cell (Figure 1.1). In majority of eukaryotes, except plants and early mammalian embryos, centrosomes function as MTOCs. Thus, the number and the distribution of MTOCs in each cell determines the overall pattern of microtubule cytoskeleton organization. As shown in Figure 1.1, microtubule cytoskeleton can appear differently between organisms. Mammalian cells assemble extremely abundant microtubules, in contrast budding yeast cells usually assemble limited numbers of microtubules, especially astral microtubules (aMT). Despite these differ-

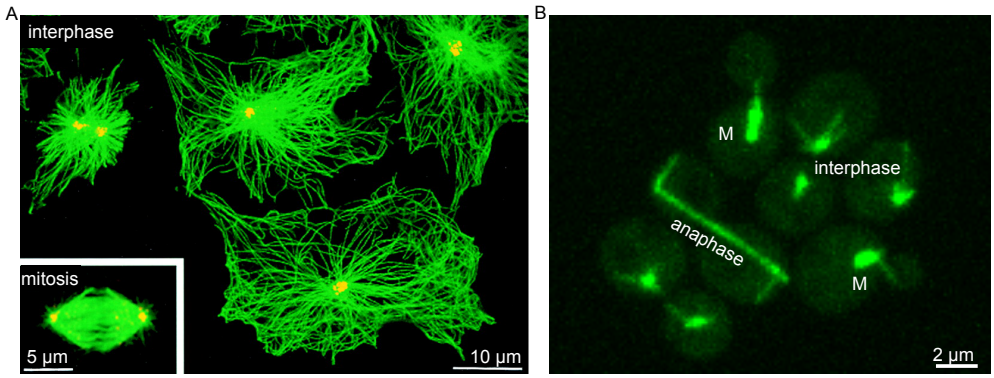

Figure 1.1 – Reorganization of microtubule cytoskeleton during the cell cycle. (A) Adapted from [Ohta et al., 2002]: Mammalian cells (CHO) demonstrate microtubules (green) and centrosome (yellow). (B) Microtubule cytoskeleton (green) during budding yeast mitosis. M: metaphase.

ences, the common theme is microtubules must be able to reorganize spatially and temporally rapidly, for instance, over the cell cycle progression. This is achieved by the dynamic instability of microtubules, with which microtubules alternate between growth and shrinkage phases continuously, any factors regulating the growth and shrinkage speeds, or the frequencies of catastrophe and rescue can contribute to the final organization of microtubules. Faithful execution of microtubule functions relies on its dynamic instability and the precise tuning of its dynamic instability by various microtubule associated proteins (MAPs) [Mitchison et al., 1984, Desai and Mitchison, 1997, Wade, 2009]. The importance of microtubule dynamic instability is most notable during mitosis, as highlighted by the fact that anticancer agents like Taxol inhibit cell division by stabilizing microtubules and suppressing their dynamics [Dumontet and Jordan, 2010].

1.1.1 *Microtubule Dynamic Instability*

Since the purification of α/β-tubulin heterodimers using their affinity for a mitosis drug colchicine [Shelanski and Taylor, 1968, Weisenberg et al., 1968], extensive biochemical and structural work has been done to understand how the dimers assemble into microtubules. In vitro, microtubules assembled from brain tubulins consist 10 to 15 protofilaments, with the vast majority having 14 protofilaments. Microtubules anchored to centrosomes and axonemes in vivo are dominantly consisting of 13 protofilaments [Evans et al., 1985]. GTP was copurified with tubulins in the original experiment and essential for microtubule assembling, now it is clear that each α/β-tubulin heterodimer

contains two GTP-binding sites (Figure 1.2A). The N-site (non-exchangeable) in the α-tubulin is buried in the intradimer interface [Nogales et al., 1998], and is constitutively occupied by GTP, which has been implied to promote the tubulin dimer stability. The nucleotide bound at the E-site (exchangeable) is exposed on the surface of an unbound dimer and the terminal dimer of a microtubule plus-end [Mitchison, 1993, Nogales, 2000]. Free α/β-tubulin dimers are not efficient at hydrolyzing GTP, but they can exchange bound GDP for GTP at the E-site, allowing them to be incorporated during polymerization (Figure 1.2B). Upon the incorporation of tubulin dimers onto the plus-ends of growing microtubules, their activities to hydrolyze GTP can be increased up to 50 fold [Vandecandelaere et al., 1999].

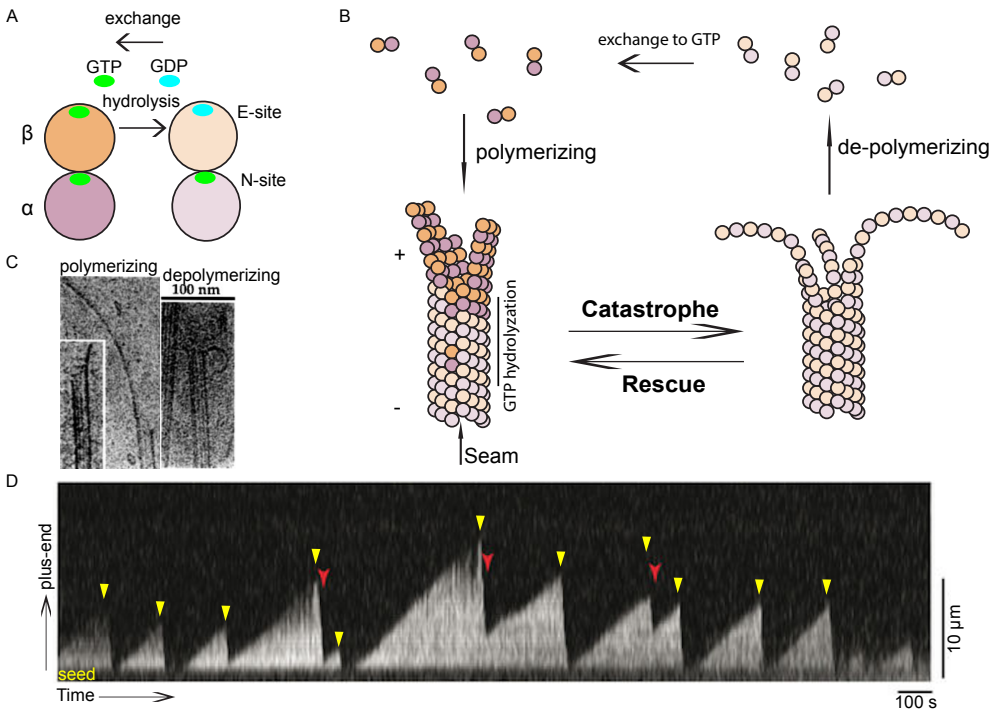

Figure 1.2 – Microtubule Dynamic Instability. (A) Cartoon of the α/β-tubulin heterodimer in which the β-tubulin bound GTP (on E-site) can be hydrolyzed, the α-tubulin bound GTP (on N-site) can not be exchanged or hydrolyzed. (B) Cartoon illustrating the protofilaments organization of microtubules and microtubule polymerization and depolymerization. Lateral interactions between protofilaments are α to α and β to β except at the seam. (C) Cryoelectron microscopy of polymerizing and depolymerizing microtubule plus-ends. (reprinted from [Chrétien et al., 1995]) (D) A typical kymograph of microtubule dynamic instability behaviour in vitro. The microtubule was nucleated from a GMPCPP seed in the presence of 12 μM tubulins and recorded with a TIRF microscope. The transitions from slow growth to fast shrinkage (catastrophe) are marked with yellow arrows. The opposite transitions (rescue) are less frequent and marked with red arrows. Adapted from [Aumeier et al., 2016].

The cartoon illustration of the microtubule dynamic instability in Figure 1.2B recapitulates our understanding so far. Microtubule polymerization occurs through the addition of GTP bound α/β-tubulin dimers onto microtubule ends. The addition of a GTP bound α/β-tubulin dimer activates GTP hydrolysis of the pre-assembled dimer, consequently most of the body of the microtubule contains GDP-bound tubulin. Morphology of growing microtubule ends show outwardly curved structures, presumably reflecting the conformation changes of tubulin dimers during polymerization. The GDP lattice is unstable but protected from depolymerizing by a stabilizing 'GTP' cap, which is a region of newly added GTP or GDP-Pi bound α/β-tubulin dimers. Loss of the cap leads to rapid depolymerization. The transition from polymerization to depolymerization is called catastrophe and the opposite switch is called rescue. We are having a pretty good understanding about catastrophe, but not so much for rescue, mainly due to the rareness of rescue events in reconstituted systems. In the following sections, I will summarize the evidences from biochemical and structural studies leading to this understanding or hypothesis on microtubule dynamics.

1.1.2 *GTP hydrolysis: the stabilizing cap model*

The GTP-tubulin cap model was proposed by [Mitchison et al., 1984] in light of the rapid depolymerization of sheared microtubules. Subsequent microtubule cutting experiments to remove the presumed 'cap' further suggested a stabilizing structure at or very near the plus-end of microtubules. Since microtubule growth involves the addition of GTP-bound tubulins, slowly hydrolyzable GTP analog GMPCPP was incorporated into microtubule plus-ends to test whether this analog can stabilize microtubles [Hyman et al., 1992]. GMPCPP strongly stabilize microtubules and dissociate slowly from plus-ends, When added to GDP-microtubules, GMPCPP also prevented depolymerization [Mickey and Howard, 1995]. Thus it is widely accepted that a region on microtubule plus-end with GTP not hydrolyzed yet or the hydrolysis intermediate Pi has not been released yet suppresses catastrophe.

Despite the compelling evidence of the existence of such a stablizing cap and the enormous efforts to visualize and measure the size of GTP-tubulin cap, the cap itself has never been directly observed (reviewed in [Erickson and O'Brien, 1992, Desai and Mitchison, 1997]). It was demonstrated by [Maurer et al., 2011] that EBs (end binding proteins) target themselves to growing plus-ends by recognizing a transient nucleotide-dependent state, mimicked by GTPγS (slowly hydrolyzable GTP analog)-bound microtubule lattice in vitro. And the idea of using EBs as a read out to estimate the size of the GTP-tubulin cap did provide valuable insights [Seetapun et al., 2012]. The authors

of [Seetapun et al., 2012] measured the brightness of EB1-GFP comets and calibrated with the number of EB1-GFP molecules present in the comets, they found that in vivo, the EB1 occupied region (presumably GTP-tubulin cap) can be as wide as 60 rows of tubulin dimers, dismissing the illusion of single layer of GTP-tubulin was sufficient to stabilize depolymerizing microtubules. A later study demonstrated that EB1-GFP proteins does not accumulate at the very tip of microtubule plus-end where fresh GTP-bound tubulins are just incorporated, instead they concentrate at about 100 nm (about 12.5 tubulin dimers) away from the very tip. And that the high affinity binding site for EB1 in growing microtubule plus-end could correspond to either GTP and/or GDP+Pi state [Maurer et al., 2014]. These studies suggests it is more precise to call the cap as 'nucleotide-dependent stabilizing cap', and that the cap is rather large. Further studies demonstrated that the size of this cap fluctuates depending on the growth speed of microtubules, and the longer the cap is, the stronger its activity is to protect the plus-end [Duellberg et al., 2016].

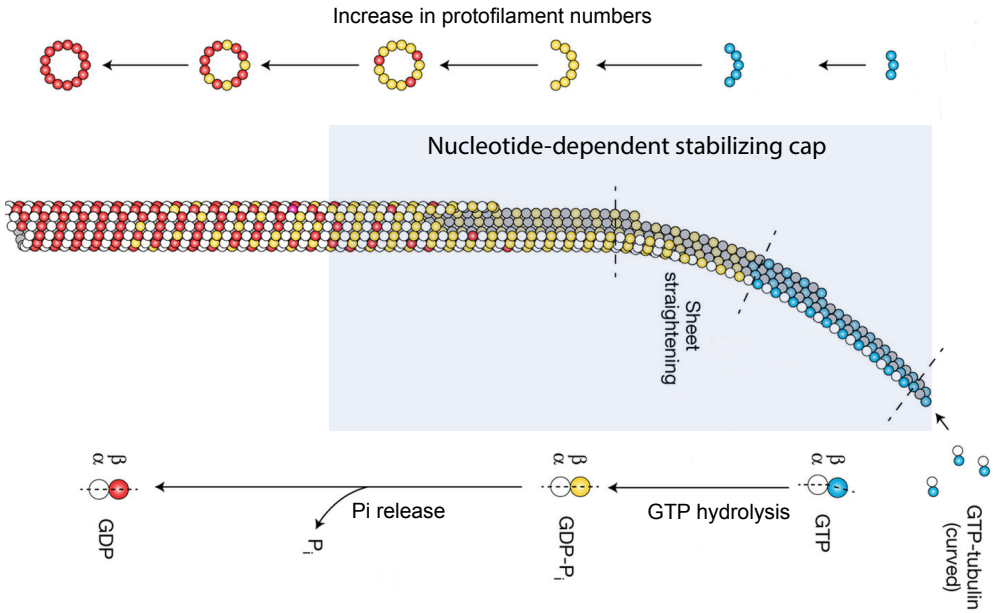

Figure 1.3 – Morphology and hypothesised nucleotide state of a growing microtubule plus-end basing on EBs binding sites and the chemical principle of GTP hydrolysis. Adapted from [Guesdon et al., 2016].

Another group of studies aim to gain insights into the structure of the stabilizing cap. [Chrétien et al., 1995] analyzed the plus-ends of microtubules nucleated by centrosomes by cryo-eletron microscopy (cryo-EM) (Figure 1.2C). The striking long protofilament sheets at polymerizing plus-ends were the first evidence that polymerization occurs through the extension of protofilaments

or dimers but not by addition of helical subunit. The straight and curved tubulin sheets have been observed repeatedly over the years. A recent cryo-EM tomography study again demonstrated the consistent morphology of polymerizing plus-ends [Guesdon et al., 2016]. The outward curved regions on the tip of plus-ends can now be explained by the curved conformation of freshly added GTP-bound tubulins [Buey et al., 2006, Rice et al., 2008, Nawrotek et al., 2011], which will be discussed in the next section.

To summarize, although we still can not directly visualize the stabilizing cap, with the accumulated biochemical and structural knowledge, we can depict the following model (shown in Figure 1.3). GTP-bound tubulins are intrinsically curved in solution and assemble into outwardly curved sheets that gradually straighten partially due to the increasing lateral forces. The transient state before the completion of GTP hydrolysis and the release of the γ-phosphate comprises the stabilizing cap. Slowly hydrolyzable analogs of GTP inhibits microtubule depolymerization but not polymerization, suggesting that GTP hydrolysis is not required for polymerization but rather for depolymerization. It is clear that any factors modulating GTP hydrolysis on growing microtubule plus-ends can regulate dynamic instability. And that accelerating GTP hydrolysis would weaken the stabilizing cap, one of such factors is EBs [Maurer et al., 2014, Zhang et al., 2015]. They recognize and promote an intermediate state generated during GTP hydrolysis. At the moment, whether GTP hydrolysis is initiated instantly upon tubulin dimer addition, whether the rather large EBs-binding region (GTP or GDP-Pi state) on growing plus-ends is a result of delayed GTP hydrolysis or delayed release of Pi, and whether or how the GTP hydrolysis or Pi release is directly coupled with the straightening of protofilament sheets is largely unknown and to be studied.

1.1.3 *Curvature of unpolymerized and polymerized tubulins*

Crystal structure of tubulin dimers alone is still missing due to their strong tendency to polymerize. But co-crystals of tubulin dimer in complex with a stathmin-like domain of the neural protein RB3 (called T2R structure [Gigant et al., 2000, Ravelli et al., 2004]) have been reported. In these structures, α/β-tubulin dimers adopt a curved conformation distinct from the their straight one when integrated in microtubule lattice, resembling the peeling protofilaments at shrinking microtubule plus-ends (Figure 1.2C). More recent co-crystals of tubulins in GTP bound form surprisingly demonstrated curved conformation as well [Nawrotek et al., 2011, Ayaz et al., 2012, Pecqueur et al., 2012], which revolutionized the model that GTP-bound tubulins adopt a straight conformation in order to be added to growing plus-ends. Moreover,

compelling biochemical and structural data support a model in which unpolymerized α/β-tubulin dimers is curved whether they are bound to GTP or GDP (reviewed in [Brouhard and Rice, 2014]).

At the centre of the current debate is how tubulin dimers get straightened after polymerization into microtubules. The first idea tested was whether GTP hydrolysis induces straightening. Comparison of cryo-EM reconstructions of GMPCPP-microtubles and GDP-microtubules revealed that GTP hydrolysis and λ-phosphate release left a hole in the E-site, loops from both tubulins but mostly α-tubulin move in to induce a longitudinal compaction between dimers [Alushin et al., 2014, Zhang et al., 2015]. In contrast, lateral contacts between tubulins were unchanged in different nucleotide states. This longitudinal compaction converts some of the energy from GTP hydrolysis into a mechanical form and stores it in the lattice as a strain. These advances prove that GTP hydrolysis induce conformational changes in microtubule plus-ends and thus induces depolymerization, but do not explain how or whether GTP hydrolysis is correlated with tubulin straightening. An alternative view basing on mathematical modelling suggests that the straightening process highly depends on the number of protofilaments and their lateral interactions [Jánosi et al., 1998]. Detailed structural studies of EB protein together with microtbules suggests that EB proteins not only accelerates GTP hydrolysis but also promotes seam closure [Zhang et al., 2015]. So it is possible that EB proteins facilitate tubulin straightening on polymerising plus-ends.

The unique curved conformation of unpolymerized and freshly polymerized tubulin dimers provides a simple mechanism for MAPs to discriminate tubulins in different states. Similar with EBs being able to recognize and bind to a transient, nucleotide-dependent state on polymerizing ends, MAPs can recognize growing or shrinking microtubule plus-ends by sensing and binding to curved tubulins. Plenty of work has been done to identify MAPs using this structural mechanism to selectively interact with distinct conformations of tubulins to control microtubule dynamics. I will introduce these examples in more detail in a later section.

1.1.4 *Kinetics of catastrophe*

The pioneering work to understand the kinetics of catastrophe and rescue was done to study the frequencies of catastrophe and rescue, together with the speeds of growth and shrinkage as a function of tubulin concentrations in vitro by [Walker et al., 1988]. Their early in vitro work suggested that catastrophe occurred with similar probability on newly formed and old microtubules, indicating that catastrophe was a single step process. Rescue events are rarely observed in vitro and are not well characterized. Experiments

conducted with modern technology thus higher spatiotemporal resolution baring similar ideas revealed that an increase in tubulin concentration indeed increased growth speed, but has moderate effect on catastrophe frequency. So the frequency of catastrophe is not highly dependent on growth speed [Gardner et al., 2011a], and that catastrophe occurred more frequently on older microtubules. This behaviour can be understood by considering microtubule catastrophe as a multistep process. Or that catastrophe requires the stabilizing cap on plus-end to evolve to become less effective. Thus, the ageing dependent catastrophe might reflect on the process of GTP hydrolysis and the structural change described in the last two sections or possibly the increased tapering of microtubule ends [Coombes et al., 2013].

In the original work [Gardner et al., 2011a] where the authors convincingly demonstrated the 'age' dependency of catastrophe, the effect of budding yeast Kinesin-8 Kip3 on catastrophe was studied by reconstituting Kip3 with tubulins. The authors found that Kip3 promotes catastrophe by accelerating the 'ageing' process. Recently, the curved tubulin specific affinity originated from the motor domain of Kip3 was identified [Arellano-Santoyo et al., 2017], and the stabilization of curved tubulin or the prevention of the tubulin straightening on plus-ends by Kip3 accelerates catastrophe. These results starts to explain how the 'ageing' process could be modulated by structural mechanisms.

It is clear that catastrophe is driven by GTP hydrolysis and plus-end structural changes, but the mechanisms and how the two aspects affect each other is still to be explored. To this day, no mathematical or computational model has integrated the biochemical, biophysical, and structural results. Such models will certainly provide valuable insights into the ageing process of microtubules.

Mathematical models integrate the biochemical, biophysical, and structural results could help the field to gain more insights into the multistep processes. Up to date, a multiple-protofilaments model proposed by [Bowne-Anderson et al., 2013] best explains the experimental data on GTP hydrolysis. This model predicts that GTP hydrolysis on growing plus-end undergoes a random-coupled mode, meaning that any GTP within the lattice has the same probability to be hydrolyzed except the one on the top of protofilaments, of which the hydrolysis must be activated upon the addition of a new tubulin dimer. This random-coupled GTP hydrolysis model explains the catastrophe as a multistep process. With the accumulating data on the structural change on plus-ends, a new model that integrates this aspect must be generated. Basing on the nature of GTP hydrolysis, it could well be that the addition of a new dimer initiates hydrolysis of the previous GTP, but the release of Pi

is a random process. The next major question is how GTP hydrolysis and tubulin structural change are unified on a growing plus-end.

1.1.5 *Mechanisms of rescue*

GTP hydrolysis determines the unstable nature of microtubules, and we have learned a great deal about catastrophe by studying pure tubulins in vitro. But the mechanisms of how microtubules stop depolymerizing and resume polymerizing again (rescue) is understudied mainly due to its low frequency in vitro. Although microtubules experience much higher frequency of rescue in living cells, it is essential to understand the basics of rescue by working with pure tubulins without MAPs.

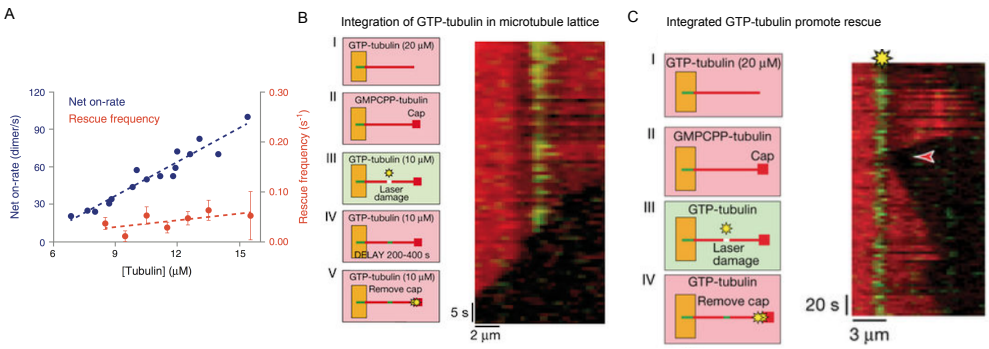

Figure 1.4 – Mechanisms of rescue. (A) Rescue events are not strongly correlated to tubulin concentration (7 to 14 μM). An increase of tubulin concentration siginificantly increase the tubulin on-rate but not rescue frequency. (reconstructed from [Walker et al., 1988]) (B) Photo-damage induce the integration of GTP-bound tubulin (green) into microtubule lattice (red). (C) Integrated GTP-bound tubulins promote rescue (red arrow). Yellow star represents the site of photo-damage. B and C reprinted from [Aumeier et al., 2016].

Despite difficulties, early in vitro studies have attempted to understand rescue and have left us with a great knowledge. [Walker et al., 1988] asked whether high concentrations of available free tubulins was enough to promote rescue. They found that although the on-rate of tubulins increased for about 5 fold by increasing tubulin concentrations from 7 to 14 μM, the frequency of rescue did not increase (Figure 1.4A). This suggests that rescue is unlikely to happen due to addition of tubulin dimers on depolymerizing plus-ends at the range of tubulin concentration below 14 μM.

Later a GTP-tubulin island model was proposed basing on a recombinant antibody that may specifically recognize GTP-tubulin in microtubules [Dimitrov et al., 2008]. This model does not involve the addition of tubulin dimers on depolymerizing plus-ends. This antibody not only recognizes the growing plus-end of microtubule but also dots along already polymerized

microtubules. This model was supported by several other works [Thoma et al., 2010, Bhattacharya et al., 2011, Nakata et al., 2011] but eventually it was always only a correlation. It was elusive whether the presence of a GTP-tubulin island in the lattice could promote rescue directly. The first step taken in this direction was introducing GMPCPP 'islands' into microtubules during growth [Tropini et al., 2012], the authors found that indeed these GMPCPP 'islands' can promote rescue directly, their rescue promoting activity rely on their size and composition. These work convincingly demonstrated that a GTP-like island within microtubule lattice could promote rescue. Recently, using micro-fluidic device and laser beam induced damage in microtubule lattice, [Aumeier et al., 2016] was able to demonstrate the integration of GTP-tubulins into the damaged site (Figure 1.4B), and that these GTP-tubulin islands were strongly correlated with rescue events. Moreover, not only photo-damage, but also mechanical damage like microtubule bending can induce the integration of GTP-bound tubulins. In summary, there is a wide range of evidence both in vitro and in vivo supporting the GTP-tubulin island model.

The GTP-tubulin island model explains microtubule rescue very well in situations where abundant microtubules are assembled and crowding microtubules start to bend and overlap with each other, where mechanical damages occur. It can not explain situations where no microtubule crowding and overlapping can be observed, like in budding yeast cytoplasm. Although it could be that other organelles like endoplasmic reticulum (ER) induce microtubule lattice damage and subsequent GTP-bound tubulin integration. An alternative model is emerging in light of a recent work demonstrated that liquid-like droplets can concentrate tubulins to about 4 fold of the background concentration [Woodruff et al., 2017]. Another study demonstrated that microtubule binding protein Tau is also able to form liquid-like droplet and concentrate tubulins for up to 20 fold [Hernández-Vega et al., 2017]. The highly concentrated tubulins in these droplets self-assemble into microtubules. The local high concentration of tubulin was obviously above the critical concentration of microtubule nucleation without seeds, so it is still possible that cells induce rescues by concentrating tubulins.

1.1.6 *Yeast tubulins*

Unlike the large number of genes coding for tubulins in mammalian cells [Ludueña, 1997], budding yeast has only two genes encoding for α-tubulin (TUB1 and TUB3) [Schatz et al., 1986] and one gene for β-tubulin (TUB2) [Neff et al., 1983], and no post translational modification has been identified on yeast tubulins. Almost all of the in vitro work with tubulins were done

with animal (Porcine or Bovine) brain tubulins due to their rich source and the technical difficulties in purifying yeast tubulins. But the biochemical differences between yeast and mammalian tubulins became important when some yeast +TIPs were shown to responded to yeast tubulins better. For instance, yeast XMAP215 homolog Stu2 accelerated polymerization of yeast tubulins to a much greater extent than of porcine brain tubulin, the concentration of Stu2 required to reach the same level of activity for yeast tubulin was two orders of magnitude lower than that for porcine brain tubulin [Podolski et al., 2014].

One of the parameters describing tubulin is the critical concentration for self assembly in vitro, this parameter varies upon temperature, concentration of magnesium and glycerol. For animal tubulins, the critical concentration under standard experimental conditions are between 15 to 25 μM leaning toward 15 μM. Under identical conditions, the critical concentration of budding yeast tubulins are only around 20% of that for animal tubulins [Davis et al., 1993]. A more recent measurement done by a different group obtained similar critical concentration of yeast tubulins at 0.18 mg/ml (which is around 1.788 μM) [Bode et al., 2003]. Consistently, critical cencentration of fission yeast tubulins is also in the range of 1.2 to 2 μM [Hussmann et al., 2016]. Comparison between budding yeast and mammalian microtubule cryo-EM structure in different nucleotide states suggests that GTP hydrolysis does not cause the interdimer interface compaction as observed with mammalian microtubule. Further more, Bim1 (budding yeast EB) binds not only between tubulin dimers but also within dimers [Howes et al., 2017].

These structural and biochemical differences may be important for certain yeast +TIPs to be at the highest activity, like Stu2, or the adaptation to the small size of yeast cells. On a side note, the two yeast α-tubulin variants have been shown to have distinct properties in vitro, tubulins containing Tub3 are less dynamic [Bode et al., 2003].

How abundant are tubulin dimers in the cytoplasm? Using cell volume and average protein copy number (average protein copy number between 12100 to 41000, cell volumn around 50 cubic μm) [Ghaemmaghami et al., 2003, Lu et al., 2007], the concentration is estimated between 0.4 to 1.4 μM without considering the fact that during metaphase the majority of tubulin is in the nucleus, this is much lower comparing to estimated concentrations in mammalian cells (between 7 to 14 μM). Thus the tubulin concentration in the cytoplasm during metaphase should be well below the critical concentration and various MAPs must be required to allow aMT growth and prevent their rapid growth.

For the microtubule cytoskeleton to execute its biological functions, various microtubule-associated proteins (MAPs) and molecular motors come into play, especially a special group of MAPs called plus-end tracking proteins (+TIPs). +TIPs are able to concentrate on growing or/and shrinking microtubule plus-ends, attaching the dynamic ends to cellular organelles, meanwhile allowing the dynamic polymerization and depolymerization of microtubules. These proteins are remarkable in several ways: firstly they are able to differentiate microtubule plus-ends from lattices, secondly they concentrate at and follow growing or shrinking plus-ends while tubulin dimers are being added or removed, thirdly they regulate the dynamic behaviour of microtubules.

The studies of +TIPs bloomed during the last decades thanks to the development of green fluorescent protein (GFP), which enabled identification of +TIPs with microscope based assays. The characterization of +TIPs mainly involved in vitro reconstitution with tubulin, biophysical, and structural studies, which generated a vast body of knowledge and revealed various mechanisms of +TIP targeting plus-ends and means of which +TIPs regulate catastrophe and rescue. In the following subsections I will introduce the classical +TIPs basing on the mechanisms through which they accumulate at plus-ends, integrated with a limited discussion on how they regulate microtubule dynamics with the focus of budding yeast +TIPs.

1.2.1 *EB proteins and their hitchhikers*

The most well studied group of autonomous plus-end tracking proteins are end-binding proteins (EBs). They are extremely conserved and present in all eukaryotic organisms [Lansbergen and Akhmanova, 2006]. Budding yeast and fission yeast express one protein from this family, Bim1 and Mal3, respectively, while nematodes have two. Fruit flies and mammalian cells express three EBs: EB1, EB2, and EB3 [Su and Qi, 2001]. EBs consist of three structural domains: the N-terminal calponin homology domain (CH domain), a linker followed by a coiled-coil domain (enables hybridization into homodimers), and the C-terminal EB homology domain (EBH domain) terminated by a EEY/F motif [Honnappa et al., 2005, Slep et al., 2005].

The extensive studies of EBs focused on their two structural features. The first is the CH domain and the linker region which specifically recognizes and tracks growing microtubule plus-ends [Slep and Vale, 2007, Xia et al., 2014]. High resolution cryo-EM based structure of microtubule with EB3 demonstrates that its CH domain binds to the microtubule lattice between two protofilaments with the preference for GTP-bound β-tubulin at plus-ends

[Zhang et al., 2015], allowing EBs to 'sense' the structural changes and the mechanic strain caused by GTP-hydrolysis. Moreover, EBs accelerate GTP hydrolysis to promote catastrophe. The second feature is their C-terminal domains (EBH domain and the EEY/F motif), which are docking sites of numerous +TIP called 'hitchhikers' [Honnappa et al., 2006, Weisbrich et al., 2007, Honnappa et al., 2009, Kumar et al., 2017]. The lab of Prof. Michel Steinmetz identified two short linear motifs that mediate the docking of their containing proteins on to the EBH domain of EBs: SxIP motif and LxxPTPh motif (where x can be any amino acid and h is a hydrophobic amino acid). The third large group of proteins hitchhike on EBs are 'cytoskeleton-associated protein and glycine-rich domain' (CAP-Gly domain) containing proteins, which specifically binds to the EEY/F motifs.

The structural details of EBH:SxIP [Honnappa et al., 2009], EBH:LxxPTPh [Kumar et al., 2017], and EEY/F:CAP-Gly [Honnappa et al., 2006, Weisbrich et al., 2007] interactions are now well characterized, the common theme is all these interactions are mediated by extremely conserved domains and rely on very small linear motifs. Usually, disrupting the small linear motifs (SxIP, LxxPTPh, and EEY/F) is enough to abolish these interactions. A large number of microtubule binding proteins containing these linear motifs have been identified and for many of these motifs, their ability to dock onto EBs have been experimentally validated. This make EBs a hub surrounded by many 'hitchhikers' that exert their own regulating effects on microtubule dynamics. Since +TIPs are usually multi-domain proteins, it is imaginable that these +TIPs compete, orderly bind one after another, or collaboratively enhance interaction between them. Here I will introduce several important examples of 'hitchhikers' containing different EB binding motifs.

1.2.1.1 *SxIP motif*

Since the first description of the 'SxIP' motif [Honnappa et al., 2009], there has been a large expansion of +TIPs, based on the presence of such an 'SxIP' motif. Representatives of this group of 'hitchhikers' are APC, CLASP1, CLASP2, MCAK, budding yeast Kar9, Kip2, and Ipl1 (reviewed in [Kumar and Wittmann, 2012]). Studies regarding these proteins revealed that the 'SxIP' mediated interactions require the 'SxIP' motif to be surrounded by unstructured and positively charged residues, such that strong electrostatic interactions with the negatively charged EBH domains can contribute to the originally weak encounter. Consequently, phosphorylation groups around the 'SxIP' motifs often tamper its interaction with EBs. For instance, multiple phosphorylation introduced by CDKs and GSK3 can abolish interaction between CLASP2 and EB1 [Watanabe et al., 2009, Kumar et al., 2009, Kumar

et al., 2012]. For budding yeast kineisn Kip2, phosphorylations introduced by kinases Dbf2 and Mck1 surrounding its 'SNIP' domain weaken its interaction with Bim1 [Drechsler et al., 2015]. The cell cycle-dependent phosphorylation provides an extra layer of regulation on 'SxIP' mediated interactions. Budding yeast Cdk1 directly phosphorylate the Aurora kinase Ipl1 to prevent Ipl1-Bim1 interaction until anaphase onset [Zimniak et al., 2012].

1.2.1.2 *LxxPTPh motif*

The LxxPTPh motif mediated interaction with EBs were first described last year [Kumar et al., 2017]. It was first found in the budding yeast protein Kar9, which already binds Bim1 through two 'SxIP' motifs. Interestingly, although the LxxPTPh motif occupies very similar residues within EBH domains comparing to the 'SxIP' motif, and peptides containing the two different motifs compete with each other for binding the EBH domains, they interact with EBs with different mechanisms. Like 'SxIP', the 'LxxPTPh' motif is also widely present in other proteins. The authors demonstrated the 'LxxPTPh' motif:EB3-dependent plus-end tracking of human proteins SLAIN1, TACC1, and MACF1. The interaction between fission yeast TOG protein Dis1 and EB protein Mal3 is also mediated by a similar motif [Matsuo et al., 2016].

1.2.1.3 *CAP-Gly domain*

The third large group of 'hitchhikers' bind to the EEY/F tails of EBs through CAP-Gly domains. Like the CH domain, CAP-Gly domain is a highly conserved protein module. CAP-Gly domains contain a hydrophobic cavity with the signature motif 'GKNDG' that targets the C-terminal EEY/F motifs present in EBs, α-tubulins, human CLIP170, SLAIN2, and recently identified budding yeast TORC1 subunit Kog1 [Badin-Larcon et al., 2004, van der Vaart et al., 2017]. Cytoplasmic linker protein-170 (CLIP170) was the first CAP-Gly containing protein revealed to interact with microtubules [Pierre et al., 1992]. Its orthologue in budding yeast and fission yeast, Bik1 and Tip1, respectively, were shown later to bind microtubules through their CAP-Gly domains [Honnappa et al., 2006, Steinmetz and Akhmanova, 2008, Mishima et al., 2007, Gupta et al., 2010].

CLIP170 is composed of two CAP-Gly domains on its N-terminus, followed by coiled-coil and C-terminal metal binding domains, zinc fingers, and its own EEY/F motif. The C-terminal metal binding domains have been shown to bind CLIP170 to auto-inactivate its CAP-Gly domain [Lansbergen et al., 2004] as a mean to regulate CLIP170 interaction with microtubules. Another more sophisticated way of regulation is through the detyrosination

of α-tubulins. The C-terminal EEY tail of α-tubulins in many higher eukaryotic cells undergoes catalytic removal (detyrosination) and re-incorporation (retyrosination) of the tyrosine residue [ARCE et al., 1975, Raybin and Flavin, 1977, Hallak et al., 1977]. And interestingly the retyrosination was known to be mediated by tubulin-tyrosine ligase [Ersfeld et al., 1993], the enzymes responsible for detyrosination were only identified recently [Aillaud et al., 2017, Nieuwenhuis et al., 2017]. The C-terminal tyrosine residue appears to be very important for the interaction of CAP-Gly containing proteins with microtubules [Erck et al., 2005, Weisbrich et al., 2007]. The observation that tyrosinated microtubules bind more efficiently to CAP-Gly domain containing proteins CLIP170 and p150Glued suggests the tyrosination could be a way to regulate microtubule interactions with CAP-Gly domains [Peris et al., 2006, Bieling et al., 2008]. The CLIP170 orthologues Bik1 and Tip1 have only one CAP-Gly domain on the N-terminus, a long coiled-coil domain for assembling homodimers and a low complexity C-terminal tail. Yeast α-tubulins terminate with an EEF tail of which there is no regulation by de-tyrosination. Interestingly the structure of Bim1 CAP-Gly domain in complex with the Bim1 C-terminal ETF tail suggests that yeast CAP-Gly domains are similar to that of mammalians but specifically recognizes C-terminal phenylalanine [Stangier et al., 2018]. Both CLIP170 and Bik1 require the interaction with EBs to accumulate on plus-ends. All existing evidence suggests that CLIP170 family proteins can bind microtubules directly but require EBs to concentrate them at the plus-ends.

Despite the similar mechanism with which CLIP170 family proteins target microtubule plus-ends, their effects on microtubule dynamic instability are different. Loss of mammalian CLIP170 results in lower rescue frequency in vivo [Komarova et al., 2002a]. Further characterizations demonstrated that the CAP-Gly domains of CLIP170 strongly promote rescue and microtubule assembly in vitro [Arnal et al., 2004]. In contrast, fission yeast Tip1 mainly stabilizes microtubules by preventing catastrophe in vivo [Brunner and Nurse, 2000]. Loss of budding yeast Bik1 leads to short aMTs. Thus, Bik1 in general has a microtubule-stabilizing activity [Berlin et al., 1990]. However, how Bik1 stabilizes microtubules is unclear. One in vitro study reported that full length Bik1 in vitro not only fails to bind the free tubulin dimer but also inhibits microtubule assembly [Blake-Hodek et al., 2010].

1.2.2 *XMAP215 family proteins*

Another group of autonomous plus-end tracking proteins are the members of XMAP215 family proteins. XMAP215 was first purified from Xenopus eggs as a factor promoting microtubule assembly in vitro [Gard and Kirschner, 1987].

It turns out to be a very conserved microtubule polymerase from yeast to plant and humans. Its human homolog ch-TOG [Charrasse et al., 1995, Charrasse et al., 1998], budding yeast Stu2 [Wang and Huffaker, 1997], fission yeast Dis1 and Alp14 [Ohkura et al., 1988], Drosophila Msps [Cullen et al., 1999], and C.elegans Zyg9 [Matthews et al., 1998] are all featured with various number of tumor overexpressed gene (TOG) domains on their N-terminus. XMAP215 and human ch-TOG are monomeric proteins containing five TOG domains each. Yeast Stu2, Dis1, and Alp14 all form homodimers and each protein contains two TOG domains. Structural and cell biology studies of XMAP215 family proteins revealed two common features that are essential for their functions. The first is TOG domains preferably bind curved tubulin dimers in contrast to the straight tubulin within the microtubule shaft [Ayaz et al., 2012]. Second, in order to be fully functional as microtubule polymerases, their basic microtubule lattice binding regions located downstream of the TOG domains are required to facilitate binding to microtubules [Widlund et al., 2011]. TOG domains bind to free tubulins with high affinity, usually at nano-molar range [Ayaz et al., 2012, Geyer et al., 2015]. Multiple TOG domains are proposed to concentrate unpolymerized tubulins near growing plus-end through tethering to curved tubulins already bound at the plus-end [Ayaz et al., 2014]. Furthermore, it was shown recently that high local concentrations of XMAP215 homolog Zyg-9 in a protein condensate recruited tubulins and increased local tubulin concentration up to four fold [Woodruff et al., 2017]. Thus XMAP215 family proteins concentrate at microtubule plus-ends by recognizing the curved tubulins on the very tip, then polymerase microtubules either by bringing unpolymerized tubulin dimer one after another or simply by increasing the local free tubulin concentration.

Apart from binding to microtubule plus-ends, many XMAP215 family proteins have been shown to function at MTOCs by forming complexs with transforming acidic coiled-coil (TACC) proteins [Lee et al., 2001, Cullen and Ohkura, 2001, Sato et al., 2004, Kinoshita et al., 2005]. This feature is conserved from fission yeast to humans. Centrosomal or SPB component TACC or Apl7 proteins recruit XMAP215 proteins to MTOCs and contribute to the number and length of centrosomal microtubules. These complexes are activated by Aurora A kinase phosphorylation of TACC [Kinoshita et al., 2005, Barros et al., 2005, Peset et al., 2005] and by Ran-dependent nuclear import in fission yeast [Sato and Toda, 2007]. The same TACC:XMAP215 complex was not found in budding yeast, instead, budding yeast Stu2 was found to bind the SPB out plaque component Spc72 directly through its C-terminal tail in a microtubule independent manner [Wang and Huffaker, 1997, Chen et al., 1998, Usui et al., 2003], it was suggested that the Spc72-Stu2 interaction is

important for anchoring aMTs at the SPB. The functions of XMAP215 family proteins at MTOCs are still unclear.

1.2.3 *Kinesins*

Kinesins are a group of molecular motors that use the chemical energy from ATP hydrolysis to translocate along the microtubule and in some cases regulate the polymerization or depolymerization of microtubule plus-ends. Higher eukaryotes like mouse and human have more than 45 genes encoding kinesin superfamily proteins (KIFs), while budding yeast *Saccharomyces* encodes a much smaller number of only 6 kinesins (including the divergent kinesin Smy1) (reviewed in [Hildebrandt and Hoyt, 2000]). Similarly, fission yeast *Schizosaccharomyces pombe* also has only 8 kinesins [Chervitz et al., 1998]. This huge contrast of the number and complexity of kinesins is reflected by their functions. In eukaryotes, kinesins are tasked with regulating mitotic spindle and long range transport of cargos like membranous organelles and protein complexes, especially in polarized cells such as neurons and epithelial cells. In contrast, yeast kinesins function mainly in the mitotic spindle [Jacobs et al., 1988].

Despite the complexity of KIFs, analysis of their domain architecture groups them into three main types, based on the locations of their motor domain. Here I will focus on the kinesins that demonstrated activities in regulating microtubule dynamic instability.

1.2.3.1 *Non-motile kinesin-13*

Kinesin-13 such as MCAK (also named as Kif2C) in mammalian cells or XKCM1 in Xenopus are not motile, instead of hydrolyzing ATP to fuel the translocation along microtubules, they stabilize the curved conformation of tubulin dimers on microtubules plus-ends to promote catastrophe. Their activity is strong enough to dissociate tubulins from ends of taxol or GMPCPP stabilized microtubules. [Desai et al., 1999, Moores et al., 2002, Hunter et al., 2003, Asenjo et al., 2013, Burns et al., 2014]. A recent structure of Kif2C with a tubulin dimer revealed the structural elements required for stabilizing the curved conformation of tubulins [Wang et al., 2017]. Kinesin-13s target microtubule plus-ends directly [Wang et al., 2012a] or by diffusing along microtubules [Helenius et al., 2006]in vitro, but whether factors facilitate this process in vivo is unclear. Interestingly, a depolymerase active kinesin-13 only requires a monomeric motor domain downstream of a neck region [Wang et al., 2012a]. The current view is that ATP hydrolysis is not required for Kinesin-13s to depolymerize tubulins but for the recycling of the motor to

dissociate the kinesin from the detached tubulin [Friel and Howard, 2011, Wang et al., 2012a].

Moreover, their microtubule depolymerizing activities are regulated by their C-terminal tails. The C-terminal tail of MCAK interacts with its N-terminal motor domain in solution to facilitate the targeting of plus-ends instead of microtubule lattice. Upon interaction with microtubule, the C-terminal tail is displaced and MCAK is active as a depolymerase [Talapatra et al., 2015].

1.2.3.2 *Kinesin-8*

The next group of relatively well understood microtubule depolymerizing motors are Kinesin-8 family proteins. Differently from kinesin-13s, Kinesin-8s hydrolyze ATP to power the processive movement along microtubules toward plus-ends. All kinesin-8s studied so far are found to inhibit microtubule polymerization or promote depolymerization [Gupta et al., 2006, Varga et al., 2006, Su et al., 2011]. Kinesin-8 is a dimeric motor protein that consists of an N-terminal motor domain, a coiled-coil region, a flexible neck linker and a C-terminal tail region. It is widely accepted that Kinesin-8s target microtubule plus-ends by processive movement toward the plus-end, and that their C-terminal tail possess some affinity for microtubules to ensure the processive translocation [Stumpff et al., 2011, Su et al., 2013]. Experimental and modelling results suggest that the yeast Kinesin-8 Kip3 acts cooperatively to bump off previous Kip3 tubulin complex to remove tubulin dimers from microtubule plus-end. Also, Kip3 takes advantage of its high processivity and accumulates more on longer microtubules, such that Kip3 depolymerizes at a rate that increases with microtubule length. However, recently a new mechanism for how Kip3 promotes catastrophe was discovered [Arellano-Santoyo et al., 2017], in which its ATPase activity is suppressed when binding to curved tubulins, such that Kip3 binds plus-end longer and functions to stabilize the curved conformation of tubulin dimers to promote catastrophe.

Although Kinesin-8s are in general microtubule depolymerizing factors since cells lacking Kinesin-8s have long microtubules and Kip3 directly depolymerizes microtubules in vitro, Kinesin-8s demonstrate microtubule stabilizing activities in many cases. Chemical inhibition of Kif18a was not able to cause long microtubules similar to cases in Kif18a depletion assays [Catarinella et al., 2009]. Analysis of microtubule dynamics in *kip3*Δ cells suggests loss of KIP3 not only results in low catastrophe frequency but also slightly lower rescue frequency [Gupta et al., 2006, Fukuda et al., 2014]. These observations indicate a microtubule stabilizing activity of Kinesin-8s, the molecular mechanism and cellular regulation of which is still elusive.

1.2.3.3 *Kinesin-14*

Another group of kinesins promoting microtubule depolymerization is represented by budding yeast Kinesin-14 Kar3 and Drosophila Kinesin-14 Ncd. This group of kinesins are featured by a C-terminally localized motor domain and a minus-end directed motility [Endow et al., 1994, McDonald et al., 1990, Walker et al., 1990]. Stated by its name, KAR3 was one of the first factors found to be required for budding yeast karyogamy, or nuclear fusion upon mating[Meluh and Rose, 1990]. Subsequent studies revealed that Kar3 forms heterodimers with Cik1 or Vik1 to be targeted either to the cytoplasm or nucleus [Page and Snyder, 1992, Page et al., 1994, Manning et al., 1999, Barrett et al., 2000]. Although Cik1 do not have ATPase activity, the heterodimers with Kar3 are motile toward microtubule minus-ends and Cik1 target Kar3 to microtubule plus-ends. It is suggested that Kar3-Cik1 complex uses its minus-end directed motility to depolymerize microtubules from plus-end [Sproul et al., 2005].

1.2.3.4 *CENP-E*

CENP-E, the prototypical member of the kinesin-7 family, is a dimeric kinesin that localizes to centromeres and its roles in chromosome congression has been extensively studied. It is the first kinesin that was reported to promote microbule plus-end elongation in a ATP dependent manner [Sardar et al., 2010]. Interestingly, CENP-E is unlikely to do so by brining in new tubulin dimers because CENP-E fails to form a complex with the tubulin-dimer. The proposed model is that CENP-E continues to step on newly added tubulins to maintain a straight conformation. Later studies support the hypothesis of CENP-E mediating end-on attachment of polymerizing and depolymerizing microtubule plus-ends to kinetochores, and this behaviour relies on both of the motor domain and the C-terminal tail [Gudimchuk et al., 2013].

1.2.3.5 *Kip2 and its homolog Tea2*

Budding yeast kinesin Kip2 and its homolog in fission yeast Tea2 are plus-end directed kinesins that were referred to as Kinesin-7s in the past. In fact both of Kip2 and Tea2 have a fragment of low-complexity region upstream of their motor domains, and their coiled-coil domains are much smaller than human Kinesin-7 CENP-E. Importantly, Kip2 and Tea2 are both cytoplasmic proteins while CENP-E mainly functions at centromere.

There is accumulating evidence suggesting that Kip2 is a microtubule stabilizing factor in vivo [Huyett et al., 1998, Cottingham and Hoyt, 1997, Carvalho et al., 2004, Caudron et al., 2008], and it has been proposed that Kip2 stabi-

lizes microtubules by targeting and controlling the amount of Bik1 (Clip170 homolog), at the microtubule plus-end [Carvalho et al., 2004]. Recent observations demonstrate that Kip2 itself function as a microtubule polymerase independently of Bik1 [Hibbel et al., 2015]. Instead, Bik1 was observed to not only fail to bind but also destabilize microtubules in vitro. Moreover, full length Bik1 barely binds tubulin [Blake-Hodek et al., 2010]. Thus it is unlikely the current model describes how Kip2 and Bik1 functions together in cells. Meanwhile, it is also unclear how Kip2 polymerize microtubules.

1.3 AIM OF THIS WORK

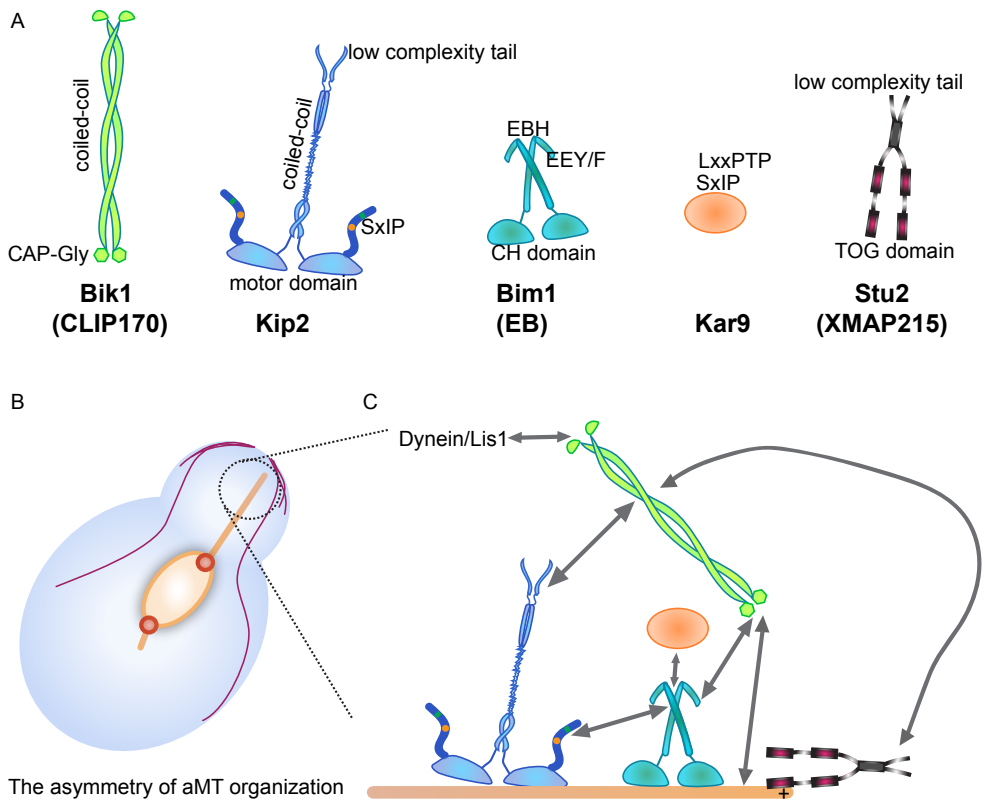

Figure 1.5 – Network of +TIPs on the budding yeast aMT plus-end. (A) Diagram of Bik1, Kip2, Bim1, Kar9, and Stu2 domain structure. (B) Asymmetric astral microtubule (aMT) organization in metaphase budding yeast. (C) Cartoon illustration of experimentally validated protein interactions forming complex networks.

It is an established fact that microtubule plus-ends are extremely crowded with +TIPs and interactions between them, not to mention the complexity of competition, synergistic, or hierarchy between these factors, as well as

regulation by post translational modifications. More than four decades of work using in vitro reconstitution, biophysical, and structural experiments has set the stage for us to begin to explore microtubule dynamic instability in living cells. Pioneering work using fluorescence recovery after photobleaching (FRAP) and fluorescence correlation spectroscopy (FCS) revealed the fast EBs and CLIP170 turnover on microtubule plus-ends both in vivo and in vitro [Bieling et al., 2007, Dragestein et al., 2008], suggesting the protein network on plus-ends is not only densely populated, prompt for regulation, but also extremely dynamic.

The central question in the field remains the molecular mechanisms of catastrophe and rescue. Building on current knowledge, the more precise question would be how is GTP hydrolysis coupled with the conformation change of the protofilament on the growing plus-ends. And under physiological conditions how rescue and catastrophe are regulated. But a far more pressing direction is how these small motifs mediated networks become relevant and how they are regulated during mitosis, cell polarizing, development, and eventually in human diseases.

One of the limiting step in understanding microtubule dynamics in living cells is to observe and record single microtubules from minus-ends to plus-ends with high spatiotemporal resolution, such that with the help of genetic tools we could manipulate the composition, even specific post-translational modifications on certain +TIPs to observe the response of the microtubule cytoskeleton. With that we can begin to explore the synergistic, antagonistic, or unknown pattern of relationships between microtubule polymerases, depolymerases, and kinases. Budding yeast cells are polarized and nucleate limited numbers of aMTs, thus it is an ideal case to study microtubule dynamics and its regulators in vivo. As summarized in Figure 1.5, majority of the classic +TIP interactions have been experimentally validated in vitro, with little knowledge of the stoichiometry, competition, regulation and functions of these interactions.

The goals of this work were to:

1. Establish an automatic or computer-assisted framework to quantify microtubule dynamics in living cells with high spatiotemporal resolution.
2. Document budding yeast aMT behaviour over the cell cycle.
3. Identify factors contributing to the establishment and maintenance of the asymmetric aMT organization in mitosis.
4. Investigate how the aMT destabilizing factor Kip3 antagonizes the stabilizing factor Kip2.

2

A COMPUTER-ASSISTED FRAMEWORK TO QUANTIFY MICROTUBULE DYNAMICS IN VIVO AT HIGH SPATIOTEMPORAL RESOLUTION

Microtubules in cells are characteristic for their nearly stochastic dynamic instability: their plus-end switch between growth and shrinkage phases. These two phases and the transitions between them, called rescue and catastrophe are targets of regulation to control the length of microtubules. Knowledge of their spatial and temporal distribution is crucial to understand the mechanism of the transitions and their functions in mitosis, cell polarization and directed movement.

The speed of growth and shrinkage, the frequencies of catastrophe and rescue are the four parameters to describe microtubule dynamics. It is rather easy to quantify them in in vitro systems with purified tubulins due to the constant growth and shrinkage speed, infrequent transitions and the two dimensional space in which the process is recorded. In live cells, however, aMT dynamics is regulated by numerous MAPs and interactions between them, thus are much more complex. The fact that aMTs pivot in a three dimensional space alone makes the task of studying them much harder. There are many attempts to quantify microtubule dynamics in live cells, fluorescently labeled tubulins are the firstly used probes to image microtubule dynamics in cells [Schulze and Kirschner, 1988, Sammak and Borisy, 1988, Rusan et al., 2001]. The major disadvantage of this method is the low intensity of fluorescence signal in the periphery [Gierke et al., 2010]. Although budding yeast assembles limited number of aMTs, due to the high density of tubulins in nucleus it is very challenging to define the location of minus ends and plus ends of aMTs (Figure 2.1A).

A complementary approach is to use fluorescently labeled plus-end-tracking proteins (+TIPs) to determine the location of plus ends [Akhmanova and Steinmetz, 2008]. Multiple methods have been developed to determine microtubule dynamics in mammalian cells [Salaycik et al., 2005, Mimori-Kiyosue et al., 2005, Matov et al., 2010, Neukirchen and Bradke, 2011], which take advantage of the almost flat periphery of the cell and strong +TIP signals. Budding yeast has a rigid cell wall so it is necessary to measure the microtubule length in three dimensions. Also, the endogenous levels of +TIPs are generally low when imaging with short exposure time in order to achieve high temporal resolution.

Here I describe a computer-assisted framework to assess aMT dynamics in budding yeast, employing the Lowlight tracking tool [Krull et al., 2014] to extract the 3D coordinates of minus ends and plus ends of aMTs from time-lapse image sequences with an acquisition frequency of one second per time point. All of the time series tracking results were analyzed with custom functions written in Matlab (MathWorks). Rescue and catastrophe events were annotated manually and recorded in Matlab (MathWorks), the speed of growth and shrinkage and the frequencies of transitions were computed based on the manual annotation.

2.1 VISUALIZATION OF ASTRAL MICROTUBULES IN VIVO

To observe aMTs in budding yeast, a SPB component and a +TIP were fused with fluorescent proteins to visualize the minus and plus ends of a microtubule respectively (Figure 2.1B). Since the spindle and the aMTs can be easily differentiated based on their dynamics, both of the minus and plus ends markers were fused with GFP to increase the time resolution by simplifying the image acquisition to a single channel. Among the four +TIPs tested, both Bik1 and Kip2 are ideal for the Low light tracker to follow the point-shaped objects. Bim1-3xsfGFP does not serve the purpose due to its high intensity in the nucleus, which tricks the Lowlight tracker to follow the centre of the spindle instead of SPBs. Kip3-3xsfGFP signal is extremely low on shrinking aMTs, especially on short aMTs, this results in failure of tracking shrinking aMTs. To test whether the C-terminal GFP fusion proteins are fully functional, a spot assay was performed to assess the growth and their synthetic lethality with *bim1*Δ. The result suggests that both Bik1-3xGFP and Kip2-3xsfGFP are functional for spindle alignment, except that Kip2-3xsfGFP cells demonstrated a slight growth defect (Figure 2.1C). Therefore, I used Bik1-3xGFP as plus end marker hereafter.

2.2 TIME-LAPSE SERIES ACQUISITION AND ANALYSIS

Cells expressing endogenous levels of Bik1-3GFP or Kip2-3xsfGFP together with Spc72-GFP were cultured in SC (synthetic medium) containing 2% glucose at 30°C. Log phase cells were collected and placed on an SC-medium agar patch for imaging. The glass coverslips were soaked in 100% ethanol and air-dried before using. An Nipkow spinning disk (Carl Zeiss) equipped with an incubator for temperature control was employed. Time-lapse movies were acquired using a back-illuminated EM-CCD camera Evolve 512 (Photometrics, Inc.) mounted on the spinning disk microscope with a motorized piezo

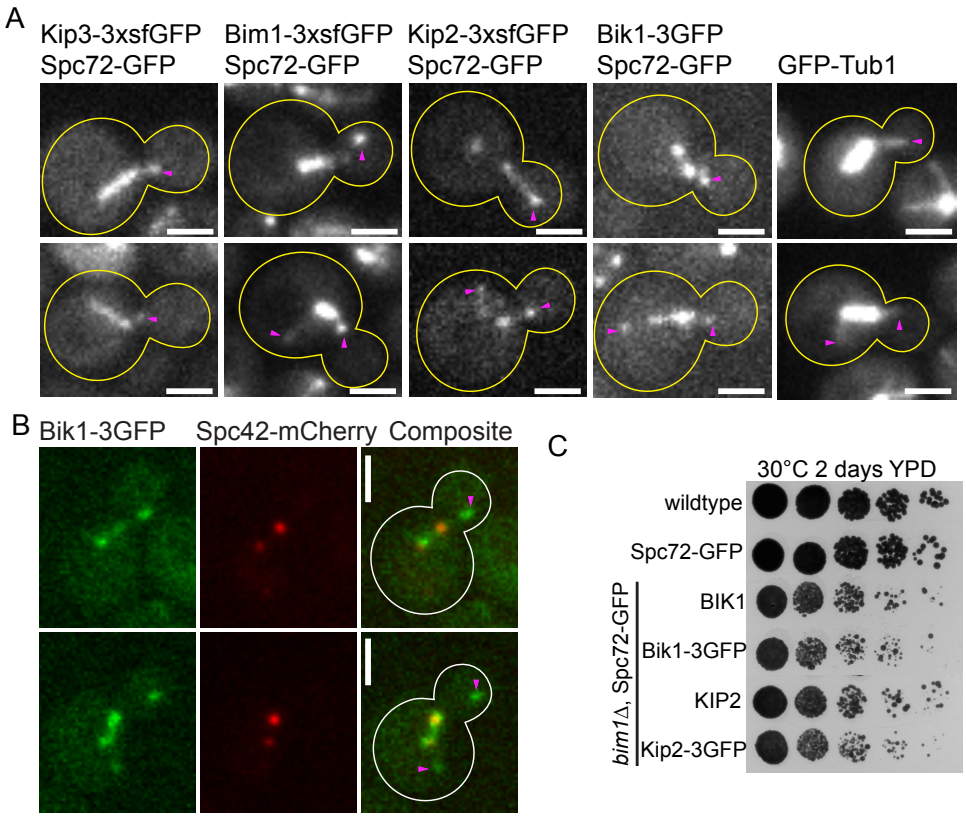

Figure 2.1 – Fluorescent markers to visualize aMTs. (A) Representative images of pre-anaphase wild-type yeast expressing various fluorescent markers for visualizing aMTs. (B) Representative images of cells expressing Bik1-3GFP (green) and SPB marker (red). (C) Expression of the Bik1-3xGFP and Kip2-3xsfGFP proteins do not cause synthetic growth lethality or defect with *bim1*Δ. 5-fold serial dilutions of indicated strains were plated on YPD plates. aMT plus ends are highlighted with magenta arrows. Scale bar: 2μm

stage (ASI MS-2000) and 100x 1.46 NA alpha Plan Apochromat oil immersion objective, driven by Metamorph based software VisiVIEW (Visitron Systems). 17 Z-section images separated by 0.24μm increments were captured with the exposure time of 30ms each, the whole stack took 1.07s. For recording aMT dynamics, 80 continuous repetitions were taken, the whole movie took 85.6s. The main focus of this study were metaphase cells, these cells were identified by their shape and spindle positioning and length.

INITIALIZATION OF TRACKING AND TRACKER PARAMETERS Low light Tracking Tool [Krull et al., 2014] is a maximum likelihood method based tracker specialised in tracking low intensity fluorescent objects. In addition to position information in x, y and z with time, the tracker also provides

the background-subtracted intensity of each object over time. To initiate tracking, the global options of the tracker were as following: Intensity Offset = 0; EMCCD gain: 800; Electrons per A/D count: 157 ; Δ Z (in pixels): 1.8. The point spread function parameters were the same as the default values. All of the tracking was performed on a Remote Desktop Server. All of the tracking was inspected by eye once finished to ensure no mistakes were made by the tracker, if there were, they were manually corrected. Mistakes were rare, except that of cells with low Bik1-3GFP intensity on microtubule plus-ends (e.g., *kip2*Δ cells). A typical case of mistake was that the tracker loses its target due to very rapid microtubule shrinkage. In the later case, since the microtubules are very short, an additional case of mistake is that the tracker mixes the identities of their objects. At least 300 individual aMTs were tracked and analyzed for each mutant, with 3 independent clones. Due to the limit of the microscope resolution and the fact that the tracker fails to distinguish microtubule plus ends and SPBs when the distance of the two objects is below 5 pixels, all of the aMTs shorter than 5 pixels (0.66 μm) are not quantified and are considered non-detectable.

TIME SERIES ANALYSIS OF THE TRACKING DATA All of the tracking data was analyzed with custom functions written in Matlab (MathWorks). In short, the 3D spindle length was computed according to the distance between the two SPBs, cells with spindles longer than 2 μm were considered anaphase cells and therefore excluded from this study. The growth phases, shrinkage phases and the transitions were annotated manually and recorded by Matlab functions (Figure 2.2). The catastrophe frequency was calculated by dividing the total number of catastrophe events by the total time the aMTs spent in growth, similarly, the rescue frequency was the result of total number of observed rescue events divided by total shrinkage time. The time an aMT was observed above the detection limit through the whole movie was defined as aMT lifetime.

2.3 TEMPORAL AND SPATIAL ORGANIZATION OF AMTS IN BUDDING YEAST

Budding yeast reorganises aMTs during the process of mitosis: it is widely observed and accepted that multiple aMTs are nucleated by the G1 phase SPB, while only one to two aMTs emanate from the pre-anaphase SPBs [Shaw et al., 1997, Shaw et al., 1998]. In pre-anaphase, aMT growth is mainly maintained for microtubules reaching toward the bud [Shaw et al., 1997]. With this framework we can for the first time thoroughly quantify and understand the temporal and spatial regulation of aMT in live cells. I assessed aMT dynamics with G1 and pre-anaphase cells. G1 phase aMTs are longest both

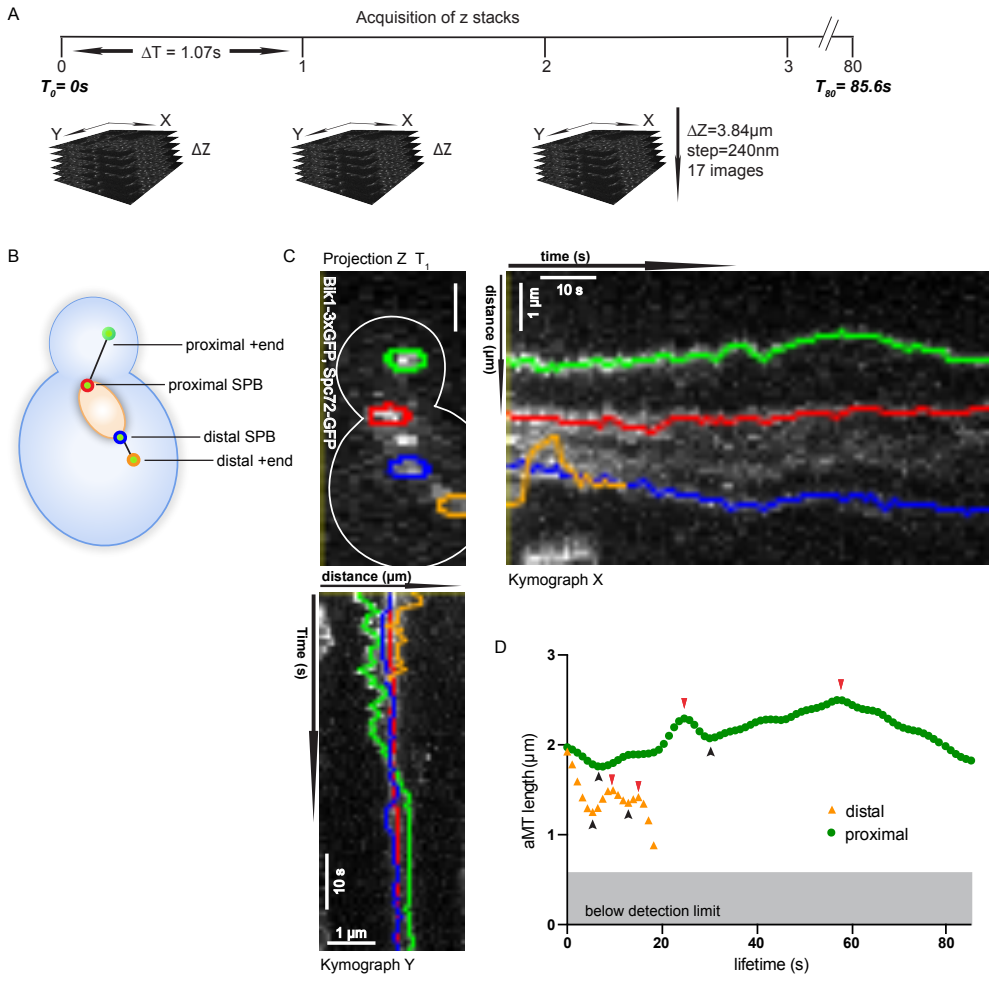

Figure 2.2 – Time-lapse series acquisition, tracking, and analysis. (A) Scheme of image acquisition. Scheme of pre-anaphase aMT organization (B) and a representative pre-anaphase cell expressing Bik1-3GFP and Spc72-GFP. (C) The maximum intensity projections on to the z-axis, y-axis and x-axis has been shown on the top left, top right and the bottom left. The traces of the proximal SPB, + end and the distal SPB, +ends are all clearly visible, they are colored in red, green, blue and yellow respectively. (D) The length of proximal (green) and distal (yellow) aMT overtime. The catastrophe and rescue events are indicated with red and black arrows respectively.

spatially (2.37 μm $\pm$ 0.87 μm; mean$\pm$s.d.) and in lifetime (54.04s $\pm$ 1.92 s; mean$\pm$s.e.m) (Figure 2.3B). After the separation of SPBs, the number of aMTs, as well as in the length and lifetime, desrease (Figure 2.3B). Not only temporally, distal aMTs are shorter (1.81 μm $\pm$ 0.72 μm; mean$\pm$s.d.) comparing to the proximal aMTs (2.08 μm $\pm$ 0.62 μm; mean$\pm$s.d.) in pre-anaphase (Figure 2.3B). To understand how the average length and lifetime of aMTs are controlled in different cell cycle stages and cellular compartments,

I quantified the speed of growth and shrinkage, and the frequencies of catastrophe and rescue of these aMTs. Surprisingly the speed of growth and shrinkage is very consistent, only the shrinkage speed of distal aMTs (2.76 μm/min $\pm$ 2.46 μm/min; mean$\pm$s.d.) is slightly slower than that of proximal aMTs (3.10 μm/min $\pm$ 1.21 μm/min; mean$\pm$s.d.) (Figure 2.3C), so it must be the frequencies of catastrophe or rescue that are regulated. Indeed, distal aMTs are the most dynamic, with the frequency of catastrophe at 4.59 event/min and the frequency of rescue at 2.99 events/min (Figure 2.3D). While the frequency of catastrophe of G1 phase aMTs (3.06 events/min) is similar to pre-anaphase proximal aMTs (2.81 events/min), G1 phase aMTs (2.27 event/min) have a much higher probability to encounter rescues(Figure 2.3D), this high frequency of rescue is the main factor leading to a long aMT population in G1 phase. In summary this in vivo imaging paradigm allows us to accurately measure the aMT behaviour in different cell cycle stages and compartments. We can conclude that aMT organization in budding yeast is temporally and spatially regulated, but the growth and shrinkage speeds are mostly stable. Instead, the frequencies of catastrophe and rescue are the main targets of regulation.

2.4 Temperature sensitivity of budding yeast aMTs

Microtubule polymerization is known to be temperature sensitive both in vitro [Collins and Vallee, 1987, Detrich et al., 2000] and in vivo [Velve-Casquillas et al., 2010]. Reconstituted microtubules depolymerize upon a temperature shift from 37°C to 4°C, it was suggested that this could be due to the increase of catastrophe events and the disappearance of rescue events at low temperature [Fygenson et al., 1994, Modig et al., 2000]. Temperature sensitive MAPs like MAP6 have been identified to bind and protect microtubules from cold-induced depolymerization in vertebrates [Delphin et al., 2012]. Budding yeast cells can survive for a very long time at 4°C, but no low temperature specific MAPs have been identified. As a proof of principle we examined whether a small change of temperature could alter aMT dynamics in live yeast cells, and whether our framework is sensitive enough to detect this change. We measured pre-anaphase proximal aMTs of yeast cells cultured and imaged under different temperature conditions: 25°C, 30°C, and 37°C. Except that cells grew at 37°C in synthetic medium overnight fail to form a bright Bik1-3xGFP focus on aMT plus end, so instead the cells were grew at 25°C then shifted to 37°C for 50 min before image acquisition. Indeed, a small increase in temperature (5 to 7 °C) is enough to remodel aMTs (Figure2.4A). The speed of growth increases with temperature, while the frequency of catastrophe decreases (Figure2.4B and D). This is not surprising since microtubule polymerization

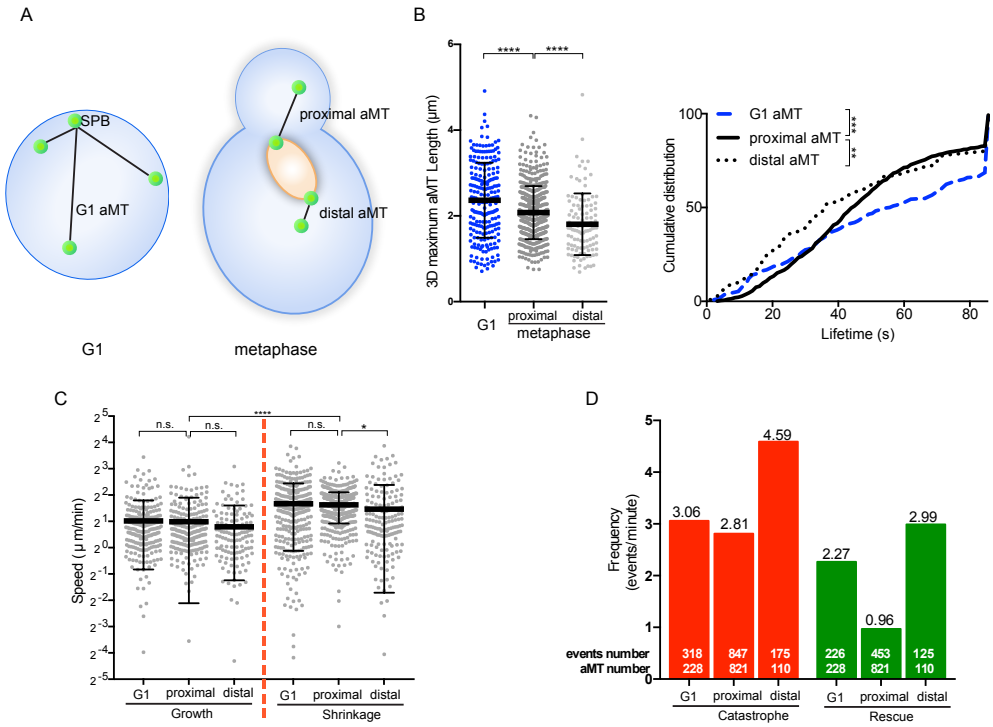

Figure 2.3 – Temporal and spatial organization of budding yeast aMTs. (A) Scheme of G1 phase and pre-anaphase aMT organization. (B) The experimentally observed length (left) and lifetime (right) of G1 phase (blue), pre-anaphase proximal (grey) and distal (light grey) aMTs are represented with scatter plot and cumulative distribution plot respectively. 92% of distal aMTs below detection limit are not accounted here. (C) Growth and shrinkage speed of G1 phase aMT, pre-anaphase proximal, and distal aMTs. (D) Catastrophe (red) and rescue (green) frequency of G1 phase aMT, pre-anaphase proximal, and distal aMTs. The number of microtubules and events quantified are marked in bold text. Statistical significances of panel C and aMT length (panel B left) were calculated using two-tailed student t-test, **** $p > 0.0001$. Statistical significance of lifetime (panel B right) was calculated with Kolmogorov-Smirnov test. Error bars show s.d. Cells are cultured and imaged at 30°C. In around 94% of metaphase cells, distal aMTs were below the detection limit of 666.67 nm, and those aMTs were not included in this figure.

is a process of hydrolysing GTP. On the other hand, microtubule depolymerization in vitro appears to be a passive process following catastrophe, but our experimental data suggests that microtubule shrinkage must be a regulated process in vivo (Figure2.4C). The growth speed of microtubules in in vitro TIRF experiments measured by different labs with either porcine brain tubulin or yeast tubulin is between 0.36 μm/min to 0.9 μm/min at room temperature depending on the free GTP-tubulin concentration, which is usually controlled between 7μM to 12 μM [Gardner et al., 2011b, Gudimchuk et al., 2013, Podolski et al., 2014]. In contrast, microtubules shrink at least 15

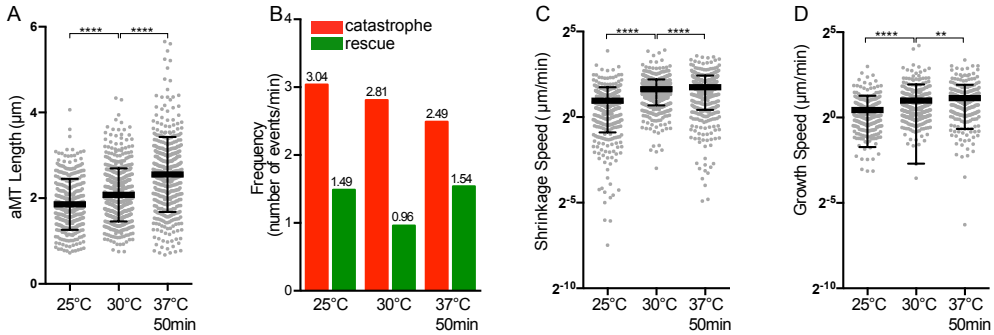

Figure 2.4 – Temperature sensitivity of aMTs in living cells. (A) Experimental data of measured pre-anaphase proximal aMT length at 25°C, 30°C, and 37°C (50min). (B) The catastrophe and rescue frequency of aMTs measured under different temperature conditions. The shrinkage speed (C) and the growth speed (D) of aMTs under different temperature conditions. Statistical significances were calculated using two-tailed student t-test, **** $p > 0.0001$, ** $p > 0.01$. Error bars show s.d.

times faster than they grow in reconstituted systems where rescues are barely observed [Gudimchuk et al., 2013, Bode et al., 2003]. The measured growth speed in vivo at 25°C (1.36 μm/min $\pm$ 1.05 μm/min; mean$\pm$s.d.) is quite close to what was observed in vitro. But the shrinkage speed is more than an order of magnitude slower than what was observed in vitro, implying that some factors counteract shrinkage in vivo. It is possible that the slow depolymerization is correlated with the high frequency of rescue. Taken together, microtubule dynamics is indeed temperature sensitive in yeast and our assay is robust enough to detect small alterations in aMT behaviour.

2.5 Revealing interplay between MAPs in vivo: Kip2 and Kip3

Extensive studies about individual MAPs have been conducted using reconstituted microtubules or high resolution cryo-EM reconstructions, yet how these MAPs interplay with each other is poorly understood. Thanks to the powerful genetic tools in yeast, we could begin to study these interplays in vivo. Here we choose the main aMT stabilizing factor Kip2 and the main aMT de-stabilizing factor Kip3 as examples. How Kip2 polymerizes or how Kip3 depolymerizes microtubules in vitro is somewhat known. In reconstituted systems Kip2 or Kip3 alone behaves as microtubule polymerase and depolymerase respectively, mainly by regulating catastrophe. How the kinesins regulate rescue is not well understood due to the extremely low frequency of rescues in vitro. To get an idea whether Kip2 and Kip3 in anyway counter play with each other, we created single deletions (*kip2*Δ and *kip3*Δ) of the kinesins, as well as the double deletion (*kip2*Δ*kip3*Δ), and compared aMT

behaviour in these cells. Consistent with previous studies, deletion of KIP2 resulted in short aMTs ((2.08 μm $\pm$ 0.62 μm [wt] to 1.40 μm $\pm$ 0.40 μm [*kip2*Δ]; mean$\pm$s.d.), loss of Kip3 instead lead to long aMTs(2.49 μm $\pm$ 0.85 μm; mean$\pm$s.d.). To be noted, around 85% of *kip2*Δ metaphase cells do not have measurable aMTs (longer than 666.66nm) and this portion of cells are not included here. Meanwhile, a small portion of *kip3*Δ cells assemble long and curved aMTs which are not included here either. So the actual differences of aMT length and lifetime between *kip2*Δ and *kip3*Δ cells is underestimated here (Figure2.5AB). Interestingly, deletion of both kinesins resulted in an intermediate aMT length (1.90 μm $\pm$ 0.62 μm; mean$\pm$s.d.), only slightly but significantly shorter comparing to wild-type cells. Importantly, although the difference in length is small, aMTs of *kip2*Δ*kip3*Δ cells are much shorter lived comparing to wild-type cells. These observations suggest a clear counteraction between the two kinesins, and aMTs in the double deletion cells are still less stable comparing to wild-type cells.

Reconstitutions suggested strong activities of Kip2 inhibiting and Kip3 promoting catastrophe. It is likely that the two kinesins counteract each other on controlling catastrophe. To test whether this is the case, we further annotated catastrophe and rescue events and computed their frequencies. As shown in Figure2.5C, loss of KIP2 leads to short aMTs mainly due to the extremely high catastrophe frequency (5.09 event/min), the long aMTs in *kip3*Δ cells mainly stems from the low catastrophe frequency (1.81 event/min). Agreeing with our hypothesis, deletion of both kinesins leads to an intermediate catastrophe frequency (2.97 event/min), which is very close to that of wild-type cells. Comparing catastrophe frequency of *kip2*Δ*kip3*Δ aMTs to that of *kip2*Δ or *kip3*Δ cells further reveals that although the two kinesins exert opposite effects on catastrophe, the two processes are largely independent, this is summarized in Figure2.5E (left).

Unexpectedly, we observed elevated rescue frequency in *kip2*Δ cells (1.68 events/min) and decreased rescue frequency in *kip3*Δ cells (0.73 event/min) (Figure2.5D). It is not a surprise for *kip3*Δ cells but these results clearly demonstrate that not only Kip3, but also Kip2 can regulate microtubule dynamics in opposite ways. So we wondered whether the two kinesins counter act each other in regulating rescues as well. To our surprise once again, deletion of KIP2 and KIP3 both did not give rise to a rescue frequency that is close to wild-type. Instead, rescue frequency is further decreased to 0.52 (events/min). Comparing rescue frequency of *kip2*Δ*kip3*Δ aMTs to that of *kip2*Δ or *kip3*Δ cells suggests loss of KIP3 in *kip2*Δ cells still lead to a strong decrease, but deletion of KIP2 in *kip3*Δ cells did not lead to an increase. This correlations suggest that Kip3 is capable of promoting rescue in the absence of Kip2, and that Kip2 strongly inhibit this activity of Kip3's. Our results

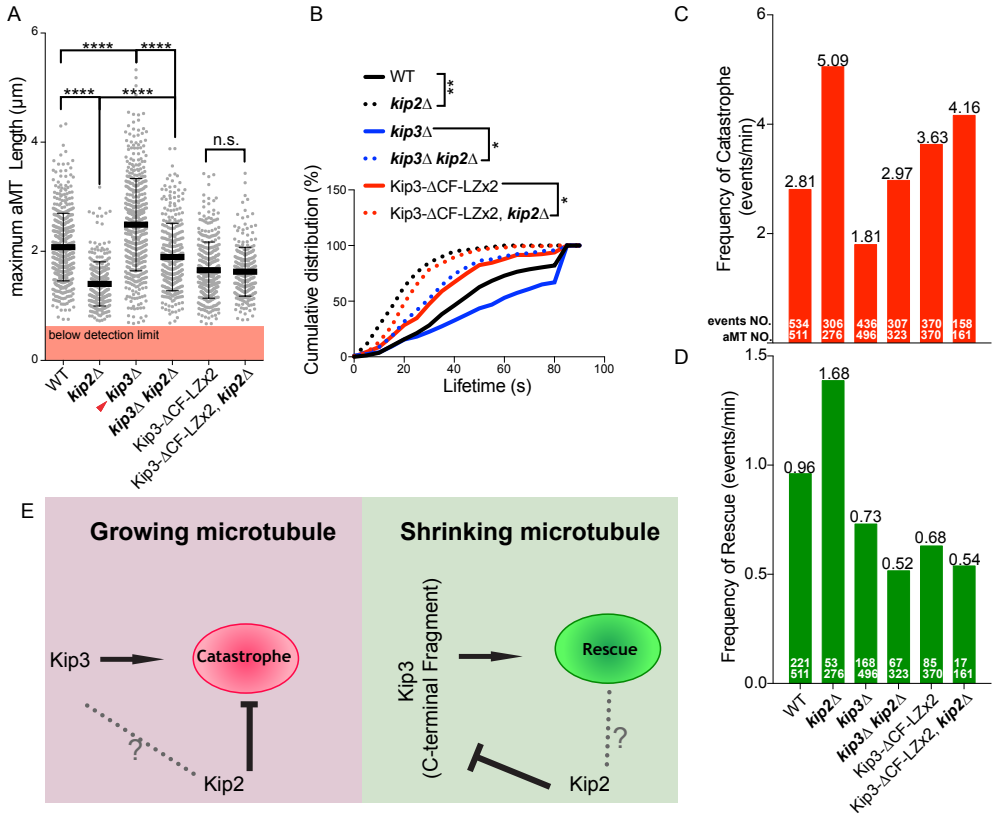

Figure 2.5 – Interplay between MAPs: Kip2 prevent rescues by inhibiting Kip3 on shrinking aMTs. (A)(B) Experimental data of measured pre-anaphase proximal aMT length (A) and lifetime (B) in indicated mutants. aMTs below the detection limit in *kip2*Δ, *kip2*Δ*kip3*Δ, and Kip3-ΔCF-LZx2,*kip2*Δ cells were not included. Red arrow: aMTs that were so long that started to curve in *kip3*Δ cells were not included. (C)(D) The catastrophe (C) and rescue (D) frequency of aMTs measured in indicated mutants. (E) Summary of genetic interactions between Kip2 and Kip3 on regulating growing and shrinking aMTs respectively. Statistical significances of aMT length were calculated using two-tailed student t-test. Differences among lifetime was demonstrated with cumulative distribution plot and assessed with Kolmogorov-Smirnov test. For all panels, **** $p > 0.0001$, ** $p > 0.01$, n.s., not significant. Error bars show s.d. Kip3-ΔCF-LZx2 represent the allele where two tandem copies of C-terminal-Fragment-less (481-805) Kip3 dimerized by Leucine-Zipper (Kip3(1-480)::Gcn5(250-281)) and driven by KIP3 promoter at the endogenous locus [Su et al., 2013, Fukuda et al., 2014]. Kip2-ΔT (1-645) and Kip2-ΔN (93-706) represent Kip2 C-terminal and N-terminal truncations respectively.

also suggest Kip2 may be able to promote rescues as well, this is particularly evident in the absence of Kip3. As mentioned earlier, it has been reported that the C-terminal fragment (CF) of Kip3 might mediate its microtubule stabilizing activity [Su et al., 2013, Fukuda et al., 2014], we obtained the duplicated Kip3-ΔCF allele dimerized by leucine zipper (LZ) (Kip3-ΔCF-LZx2) from the authors and tested whether it is indeed the case. The two

copies of Kip3-ΔCF-LZ expressed from the endogenous locus were not able to rescue the low rescue frequency of *kip3*Δ cells (0.73 event/min to 0.68 event/min). Again, deletion of KIP2 in these cells did not lead to an increase in rescue frequency. Altogether, these data demonstrate a Kip2 independent function of Kip3-CF to promote rescue, and this activity is inhibited by Kip2. Although Kip2 inhibit rescue through inhibiting Kip3-CF, it could still promote rescue weakly independently of Kip3. This is summarized in Figure2.5E (right).

Comparing the catastrophe frequency of Kip3-ΔCF-LZx2 cells (3.63 event/min) with wild-type cells (2.81 event/min), one can conclude that the dimerized motor domain of Kip3 still promote catastrophe. It would be an interesting idea to introduce a single copy of Kip3-ΔCF-LZ instead of the double copies.

2.6 COUPLING MULTIDIMENSIONAL DATA

This assay provides multidimensional data, including the microtubule length, lifetime, growth and shrinkage speeds, rescue and catastrophe frequencies, as well as background-subtracted intensity of tracked objects. One curious behaviour of microtubules is ageing, for which several hypothesis have been proposed. There have even been studies suggesting MAPs like Kip3 can accelerate this ageing process [Gardner et al., 2011a], which involves the ability of Kip3 accumulating on growing microtubule plus-ends in a length dependent manner. Despite decades of research, we still do not have a good understanding of whether other MAPs can accumulate on microtubule plus-ends length dependently. To address this question, we took the first time point of each movie and extracted the 3D aMT length along with the intensity of Bik1-3xGFP or Kip2-3xsfGFP on plus-ends. As shown in Figure2.6, Bik1 and Kip2 do not behave like Kip3, their plus-end accumulation must be regulated by other means.

The microtubule cytoskeleton plays critical roles, but how cells harness microtubule dynamics remains a huge challenge in cell biology partly due to the lack of tools with which we can quantify their dynamics in high temporal and spatial resolution. Here, we present a quantitative microscope based framework for assessing microtubule behaviour living budding yeast cells using computer-assisted tracking of a microtubule plus end marker such as Bik1-3xGFP and a minus end marker Spc72-GFP. Unlike its mammalian homolog CLIP-170, Bik1 binds both growing and shrinking microtubules, which allows us to follow the continuous trajectories regardless of the status of the aMTs. This framework is highly sensitive, providing comprehensive details of microtubule growth and shrinkage. These results are the first to extensively assess the behaviour of aMTs in three-dimensional, as previous

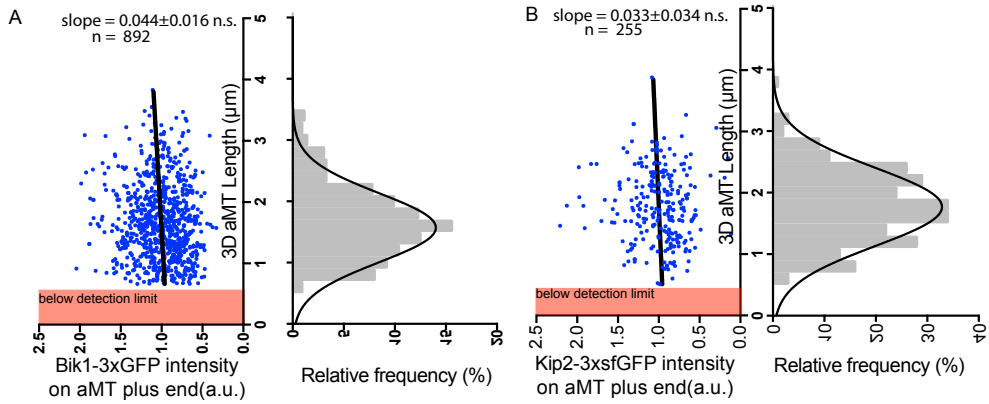

Figure 2.6 – Bik1-3xGFP and Kip2-3xsfGFP signals on aMT plus-ends are not correlated with aMT length. Scatter plot showing Bik1-3xGFP signal on aMT plus ends is not correlated with aMT length. Bik1-3xGFP (n=892) and Kip2-3xsfGFP (n=255) intensities were extracted from the first frame of the movies acquired at 30°C. The statistic significances were acquired by linear regression and further comparing the difference between acquired slope and zero.

approaches were either performing measurements with Z-projection, or not applying temporal resolution that is high enough [Vogel et al., 2001, Gupta et al., 2006, Fukuda et al., 2014, Fees et al., 2017]. We find that a complete growth phase or shrinkage phase can be as short as several seconds, so it is very likely that multiple catastrophe and rescue events were missed in previous works. Also microtubule pausing is rarely observed in budding yeast. aMT dynamics is not only regulated over the cell cycle but also differentially in different compartments. Our frame work would be a powerful tool to dissect the functions of individual MAPs but also the interplay between them. One of the most intriguing observation is the high frequency of rescues in cells, that is much higher than one would expect basing on the results acquired from in vitro systems. Meanwhile the aMT shrinkage speed in vivo is more than an order of magnitude smaller comparing to the values observed in vitro. This provides a platform and an entry point for studying the regulation of rescue events.

Our framework generates a lot more information that could answer many interesting questions. For example, microtubules have been reported to grow more slowly at the cell edge in mammalian cells [Komarova et al., 2002b, Kumar et al., 2009]. Coupling our current framework with an extra annotation of the cell geometry we will be able to answer whether any of the parameters describing aMT behaviour correlates with the geometry of the cells. Similarly, catastrophe is thought to be a consequence of microtubule ageing and factors like yeast Kinesin-8 Kip3 promotes this process [Gardner et al., 2011a]. Complete growth phases from one rescue till the next catastrophe

can be extracted, thus the ageing process can be studies with microtubules in physiological conditions. Most importantly, genetic perturbations like deletion of MAPs individually or in combination can be applied to dissect the mechanism. Not only for catastrophe, this is an ideal system to study the biochemical mechanisms for rescue events.

Although we took extreme care in the process of tracking initiation, tracking, and events annotation, we currently do not have a formal way to quantify the human introduced bias or errors. The tracking result of proximal aMTs in wildtype cells at 30°C were annotated by three different persons, the results were extremely similar (data not shown). It is also important to note that the measurement of curved microtubule is not possible with this method. More sophisticated time series analysis method will have to be developed to make the full use of the acquired data, also to further validate the manual annotation. On the other hand, these manually annotated time series data is a great resource to detect the hidden pattern of the trajectories.

3

A MECHANISM FOR THE CONTROL OF MICROTUBULE PLUS-END DYNAMICS FROM THE MINUS END

The microtubule cytoskeleton and the mitotic spindle are highly dynamic structure, yet their sizes are remarkably consistent, indicating that the polymerization and depolymerization of their constituent microtubules are well balanced. One typical case is the astral microtubules (aMTs) of budding yeast. This balance is partly achieved by microtubule destabilization factors (such as Kinesin-8 protein Kip3) and stabilization factors (such as kinesin Kip2). Loss of Kip3 results in long aMTs, oppositely, loss of Kip2 leads to very short aMTs. Depletion of both Kip2 and Kip3 allows cells to build intermediate length of aMTs again (shown in Chapter2 Figure2.5AB). Since these microtubule destabilization and stabilization factors execute their activities on plus-ends, a clear notion is that the amount of these factors on plus-ends can be a way to control microtubule length.

Extensive studies with reconstituted systems demonstrated that the Kip3 motor depolymerize long microtubules more efficiently than it does for short ones by accumulating on growing plus-end in a manner that depends on the length of the microtubule [Varga et al., 2006, Gardner et al., 2011a]. This is mainly achieved through three features of Kip3: its ability to processively move along microtubule toward plus-end over long distances, its moving speed being higher than that of microtubule growth [Varga et al., 2006, Su et al., 2011, Su et al., 2013], and its ability to stabilize microtubule protofilament curvature upon arrival at the plus-end [Arellano-Santoyo et al., 2017], thereby promoting catastrophe. As Kip3 molecules are recruited at random locations along the microtubule in vitro [Varga et al., 2006, Gardner et al., 2011a], the first two features cause Kip3 concentration on the microtubule to increase linearly from nearly undetectable levels at the minus to maximal levels at the plus end. In this model, the microtubule is thought to function as an antenna for the recruitment of Kip3, causing long microtubules to accumulate more Kip3 at their plus-ends than short ones and hence, destabilizing especially long microtubules. The length-dependent depolymerization has been proposed to be a mechanism for controlling the lengths of microtubules.

Intriguingly, recent characterization of Kip2 in vitro revealed similar abilities to move toward plus-end processively over a long distance with a speed exceeding microtubule growth [Hibbel et al., 2015], especially in the presence of its binding partners yeast EB1 (Bim1) and CLIP-170 (Bik1) [Roberts et al.,

2014]. Similarly, Kip2 molecules are expected to accumulate on microtubule plus-ends length-dependently. Indeed, Kip2 polymerizes long microtubules more efficiently than the short ones in vitro [Hibbel et al., 2015]. The preference over long microtubules for both polymerization and depolymerization does not appear to be the most logical way to harness the lengths of microtubules. Therefore, we set out to investigate the regulation of these motors in living cells and to understand how cells balance the activities of these motors to control the length of microtubules.

This part of work is conducted in collaboration with Lukas Widmer (PhD student with Prof. Jörg Stelling) and Marcel Stangier (PhD student with Prof. Michel Steinmetz). The methods and results regarding mathematical modelling and biophysical analysis of proteins will not be fully covered in this thesis.

3.1 Unlike Kip3, Kip2 does not accumulate on aMT plus-ends in MT length dependent manner

To investigate the relevance of these models in vivo, we visualized Kip3 and Kip2 in living yeast cells during metaphase by expressing either of these proteins as a 3xsfGFP fusion protein from their endogenous loci and under their native promoters. In these cells, the spindle pole bodies (SPBs, the yeast equivalent of the centrosome) from which the astral microtubules emanate and where microtubule minus-ends are anchored, were visualized through the expression of the SPB component Spc42 fused to mCherry. Plotting Kip3-3xsfGFP fluorescence along aMTs clearly revealed two features (Figure 3.1A). Firstly, the Kip3-3xsfGFP fluorescence at the plus-ends of aMTs significantly increased with the microtubule length (supplement Figure 1A). Secondly, the Kip3-3xsfGFP fluorescence increased linearly along the microtubule shaft to reach its maximal level at the plus-end, independently of the length class of the microtubules. Thus, Kip3 distribution in vivo fulfils the expectations of the antenna model.

Strikingly however, using the same microscopy setup Kip2-3xsfGFP fluorescence at aMT plus-ends correlated only very poorly with microtubule length, increasing only little if at all along aMTs (Figure 3.1B, supplement Figure 1B). The profile of its abundance was flat along microtubule shafts, showing only a distinct accumulation at microtubule plus-ends (Figure 3.1B). Clearly Kip2 does not behave as the antenna model predicted. To measure the assumed high processivity and moving speed of Kip2 in vivo, we recorded Kip2-3xsfGFP speckles movement along aMTs with time-lapse microscope. Spc72-GFP was used as the SPB marker to increase the temporal resolution. Kip2-3xsfGFP speckles moved with near constant speeds (6.26 $\pm$ 2.07

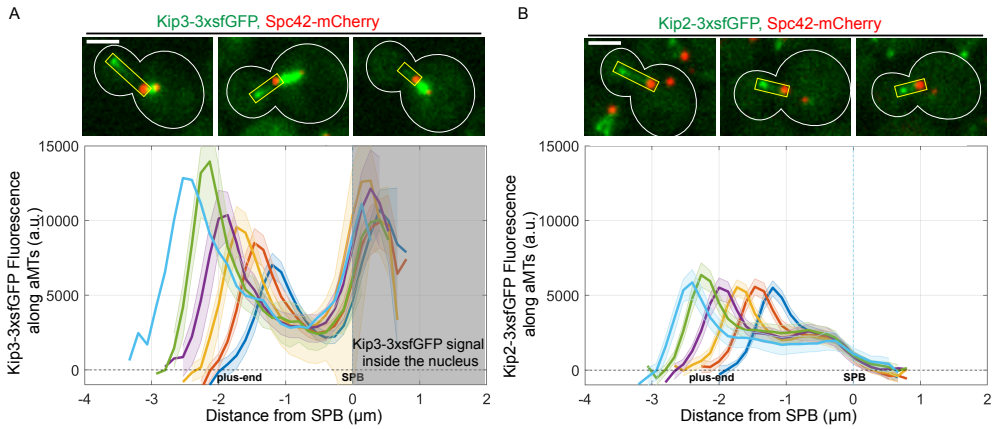

Figure 3.1 – Kip3 and Kip2 distribute along aMTs differently in vivo. (A) Kip3 binds along aMT length dependently. Representative images of metaphase cells expressing Kip3-3xsfGFP and SPB marker Spc42-mCherry with different lengths of aMTs (top) and line scan analysis of Kip3-3xsfGFP fluorescence profile along aMTs. (B) Kip2 accumulates on plus-ends in a length-independent manner. Representative images of metaphase cells expressing Kip2-3xsfGFP and Spc42-mCherry with different lengths of aMTs (top) and line scan analysis of Kip2-3xsfGFP fluorescence profile along aMTs. All profiles (n = 278 cells for Kip3, n = 505 cells for Kip2) were aligned toward SPB using the peak of Spc42-mCherry signal and binned according to their lengths with 266 nm (2 pixels) intervals. Horizontal dashed line, corrected background GFP signal in cytoplasm. Vertical dashed line, the centre of Spc42-mCherry signal. Shaded areas, 95% confidence intervals.

μm/min, mean $\pm$ s.d, n = 192 speckles, 2D, 25°C) that exceed the rate of microtubule growth (1.36 $\pm$ 1.01 μm/min, mean $\pm$ s.d, n = 250 growth phases, 3D, 25°C) by at least 4.6 folds (supplement Figure 2). Importantly, all observed speckles reached aMT plus-ends. These observations suggest that Kip2 distribution is regulated in a different manner comparing to Kip3 in living cells.

3.2 Kip2 is dominantly loaded from the SPB and not from the microtubule shaft

Modelling of motor localization along microtubules indicates that several profiles can be obtained, depending on solely three parameters, namely the on and off rates of cytoplasmic kinesin on microtubules, the step rate along microtubules and the rate of kinesin dissociation once at the microtubule end. Remarkably, whereas the accumulation of Kip2 at microtubule ends is easily explained by slow off rate at microtubule ends, no model based on these parameters could explain the non-null, flat distribution of the motor along the shaft. Instead, this flat distribution is reminiscent of the average

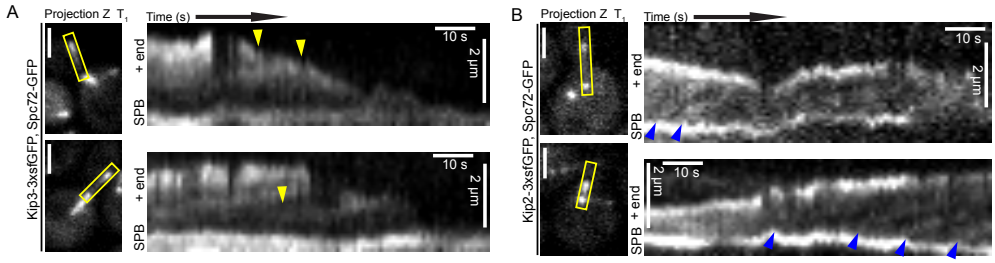

Figure 3.2 – Kip3 is loaded randomly along aMT while Kip2 is dominantly loaded from minus-end (SPB). Representative metaphase cells and kymographs of Kip3-3xsfGFP (A) or Kip2-3xsfGFP (B) associated aMTs. Z-sum-projection imaging of the boxed aMT is displayed as kymograph (right). The entire kymograph x-axis represents 85.6 s, with 1.07 s interval. Yellow arrow, emerging of a speckle along microtubule lattice. Blue arrow, emerging of a speckle at SPB.

distribution of vehicles on a track between entry and exit sites, at constant speed and entry rate. We therefore considered the possibility of an additional parameter, namely the possibility that in vivo the on-rate of Kip2 on microtubules would be different and much higher at the minus-end of the microtubule than anywhere else along the shaft. Obviously, such a model easily allows the emergence of profiles similar to that observed in our images. Therefore, we envisioned the possibility that Kip2 loading on microtubules could preferentially take place at the SPB.

As shown in Figure 3.2, kymographs of Kip3-3xsfGFP fluorescence using Spc72-GFP as the SPB marker demonstrated directional movement of Kip3 toward plus-ends. Importantly, majority of the Kip3-3xsfGFP speckles appeared along aMTs. In contrast, although Kip2-3xsfGFP speckles also moved toward plus-ends, a vast majority of them emerged from minus-ends, the SPB.

3.3 Bik1 prevents the random loading of Kip2 along microtubule shafts

Restricting the recruitment of a motor protein to the minus-end of a microtubule probably requires two distinct processes. First, the recruitment of the protein must be inhibited on the shaft of the microtubules. Second, some structure must efficiently recruit the motor protein near the minus end to facilitate its loading onto the microtubule. The motor protein Kip2 tightly interacts with the microtubule-binding protein Bik1, the ortholog of CLIP170 in higher eukaryotes [Carvalho et al., 2004]. Furthermore, former studies demonstrated that Bik1 is abundant at SPBs, which it binds even in the absence of microtubules [Carvalho et al., 2004]. Therefore, we investigated

the role of Bik1 in Kip2 behaviour. Remarkably, in cells lacking Bik1 the fluorescent signal of Kip2-3xsfGFP increased linearly along the microtubule, unlike in wild type cells (Figure 3.3AC). Furthermore, we identified a mutant Kip2-ΔT, which lacks the last 60 residues, fails to interact with Bik1 but is fully competent in forming homodimers (supplement Figure 3) and in motility (supplement Figure 2). Importantly, Kip2-ΔT-3xsfGFP fluorescence not only increased along microtubules but was also much higher comparing to wild type cells. The elevated fluorescence level can be partly accounted for by the increased Kip2-ΔT protein level (supplement Figure 9D).

Differently with Kip3-3xsfGFP distribution profiles, Kip2 fluorescence in cells deficient in Kip2-Bik1 interaction was already strong near SPB(Figure 3.3ABC). Mathematical modelling indicated that such a profile is best explained if Bik1 interaction with Kip2 inhibits Kip2 from being loaded onto microtubules along their shaft, but is not essential for Kip2 loading at SPBs. Close examination of Kip2-3xsfGFP kymographs in Kip2-ΔT and *bik1*Δ cells verified that in both cases Kip2 speckles still appeared from SPBs but even more started to appear along aMT shaft (Figure 3.3D).

To further investigate the loading of Kip2 at microtubule minus-ends, we generated a Kip2 allele that is deficient in hydrolyzing ATP (Kip2-G374A). The rationale is the following. Kip2 supplemented with non-hydrolyzable forms of ATP (e.g. AMP-PNP) can bind microtubules but not translocate, accumulate at the place where they are loaded [Hibbel et al., 2015]. We reasoned that if Kip2 is preferentially recruited at the minus-ends of microtubules, the ATPase deficient mutant of Kip2 that is not able to hydrolyze ATP should accumulate at the minus-ends of microtubules and less on the shaft. We therefore expressed Kip2-G374A-3xsfGFP from the endogenous KIP2 locus to investigate their localization. A caveat of this experiment is that the ATPase deficient form of Kip2 does not promote microtubule growth. Hence the corresponding mutant cells form only very short microtubules, making it difficult to resolve the microtubule minus and plus ends from each other by light microscopy. To overcome this problem, we restored microtubule length by expressing Kip2-G374A-3xsfGFP in diploid cells in which the other allele of Kip2 was fused with mCherry. In this setup, Kip2-G374A-3xsfGFP formed a focus and localized to the minus-end of aMTs. In contrast, Kip2-mCherry appeared along the microtubule and accumulated on the plus-end. Remarkably, the Kip2-G374A-3xsfGFP fluorescence was significantly stronger on the SPB oriented toward the bud (Figure 3.4A). These observations further supports the view that Kip2 is being dominantly loaded from the minus-ends of microtubules before starting to move along the shaft toward the plus-end. Using the Kip2 ATPase deficient allele, we can answer how Bik1 contributes to Kip2 loading at minus-ends quantitatively. As shown in Figure 3.4B, Kip2-

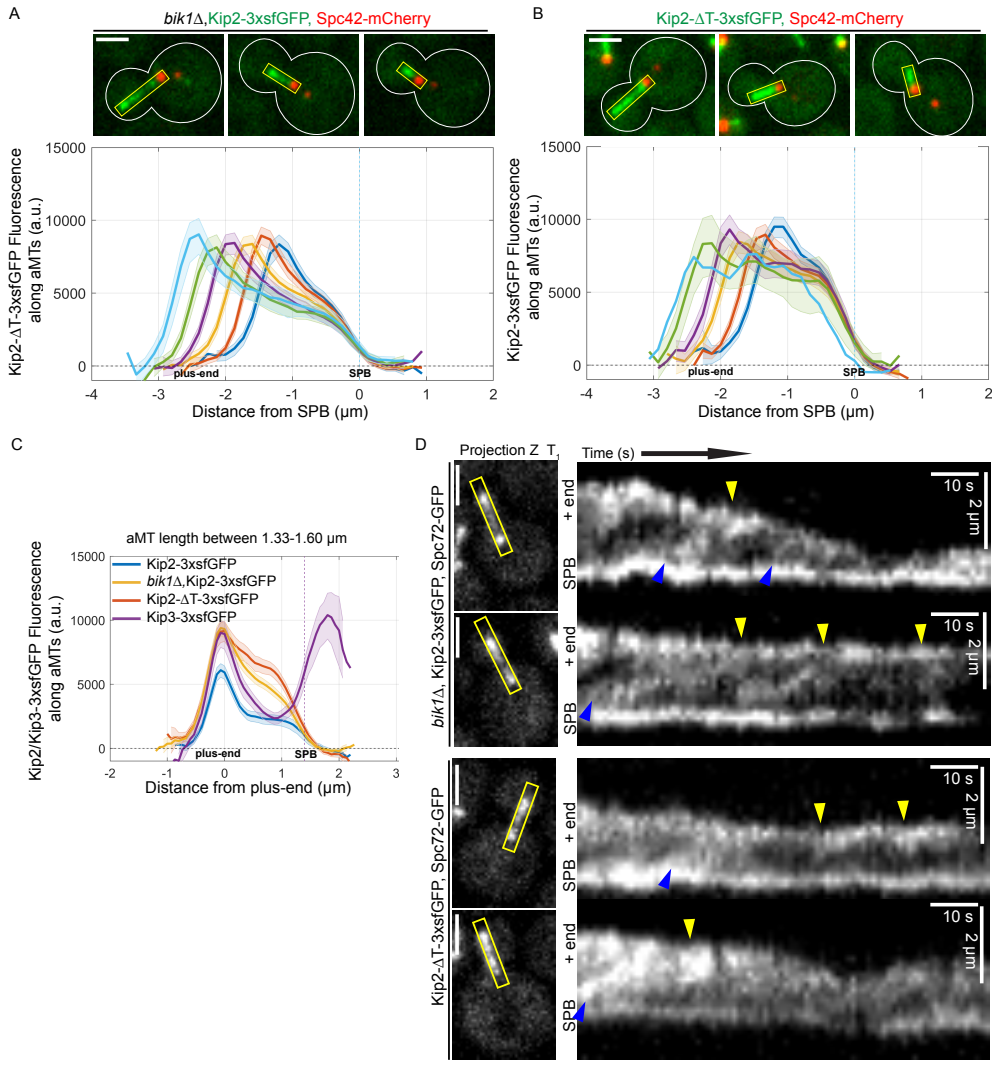

Figure 3.3 – Inhibition of Kip2 loading along microtubule is impaired in cells deficient of Bik1-Kip2 interaction. (A) Representative images of *bik1*Δ metaphase cells expressing Kip2-3xsfGFP and Spc42-mCherry with different lengths of aMTs (top) and line scan analysis of Kip2-3xsfGFP fluorescence profile along aMTs. (B) Representative images and line scan analysis of Kip2-ΔT-3xsfGFP fluorescence along aMTs. (C) GFP fluorescence distribution along aMTs of length between 1.22 to 1.60 μm in indicated mutants. All profiles (n = 588 cells for *bik1*Δ, n = 514 cells for Kip2-ΔT) were aligned toward SPB using the peak of Spc42-mCherry signal and binned according to their lengths with 266 nm (2 pixels) intervals. Horizontal dashed line, corrected background GFP signal in cytoplasm. Vertical dashed line, the centre of Spc42-mCherry signal. Shaded areas, 95% confidence intervals. (D) Representative kymographs of Kip2-3xsfGFP or Kip2-ΔT-3xsfGFP associated aMTs in metaphase cells of indicated genotype. Yellow arrow, emerging of a speckle along microtubule lattice. Blue arrow, emerging of a speckle at SPB.

G374A-3xsfGFP fluorescence on SPB was only reduced by about 20% in *bik1*Δ cells. Therefore, we concluded that Bik1 facilitates the recruitment of Kip2 at SPBs and inhibits its loading onto microtubules along their shaft.

3.4 Polo-like kinase Cdc5 mediated phosphorylation of Spc72 dominates the loading of Kip2 on bud-proximal SPBs

Next we investigated which molecules and structures near minus-ends or SPBs contribute to the efficient recruitment and loading of Kip2, especially near the bud-proximal SPBs, where Kip2 is dominantly loaded. aMTs are capped by γ-tubulin small complexes (comprised by γ-tubulin, Spc97, and Spc98) and then anchored onto the cytoplasmic side of SPBs by the transforming acidic coiled coil (TACC) family protein Spc72 (the yeast homolog of CDK5RAP2) [Knop and Schiebel, 1998], which is also a stable SPB outer-plaque component. Among these molecules, Spc72 became the most promising candidate for two reasons. It has been proposed to interact with Kip2 directly with its coiled-coil domain [Wang et al., 2012b]. In addition, Spc72 maintains a SPB localized pool of Stu2p [Usui et al., 2003], which in turn recruits Bik1 [Carvalho et al., 2004] that facilitates Kip2 recruitment. Culturing spc72-2 cells at restrictive temperature 37°C for 50 min was enough to strip the Kip ATPase deficient allele Kip2-G374A-3xsfGFP molecules off SPBs, however, the GFP fusion proteins started to form 'assemblies' in the cytoplasm. Therefore, we cultured spc72-2 cells at 30 °C for 2 hours instead. Again, inactivating Spc72 lead to a drastic reduction of Kip2-G374A accumulation at SPBs, especially the bud-proximal SPB (from 100 ± 3.70 a.u. [wt] to 28.39 ± 5.19 a.u. [*spc72-2*], mean ± s.d. of three clones, n > 80 cells per clone) (Figure 3.4B). These results lead to the conclusion that the SPB component Spc72 strongly contributes to the recruitment of Kip2 to minus-ends.

Equal amount of Spc72 molecules are stably assembled into each SPB. We reasoned that the dominance of Kip2 recruitment to the bud-proximal SPB is likely to be controlled by post-translational modifications subsequent to SPB assembly. Spc72 has been shown to be a substrate of yeast polo-like kinase Cdc5 [Snead et al., 2007]. Although at least one polo-box binding domain was identified in Spc72, the biological significance of Cdc5 mediated Spc72 phosphorylation is unknown. To test whether there is any relevance of Cdc5 mediated phosphorylation of Spc72 for Kip2 recruitment at the aMT minus-end, we generated strains where the known polo-box binding domain within Spc72 was compromised (Spc72-3A: Spc72-S231AS232AS236A) or where Cdc5 was inactivated owing to a temperature sensitive allele (*cdc5-2*). Inactivating Cdc5 lead to significant reduction of Kip2-G374A-3xsfGFP fluorescence (from 102.9 ± 5.87 a.u. [wt] to 52.81 ± 0.57 a.u. [*cdc5-2*], mean ± s.d. of three clones,

n > 80 cells per clone) from the bud-proximal SPB. Whereas not affecting its intensity on the other SPB. Similarly, in Spc72-3A cells, the Kip2-G374A-3xsfGFP intensity was not affected on the SPB distal to bud-neck. Whereas a substantial reduction was observed on the bud-proximal SPB (68.28 ± 17.83 a.u., mean ± s.d of three clones, n > 80 cells per clone). Thus, we conclude that Cdc5 mediated Spc72 phosphorylation promotes Kip2 motor recruitment on the bud-proximal SPB.

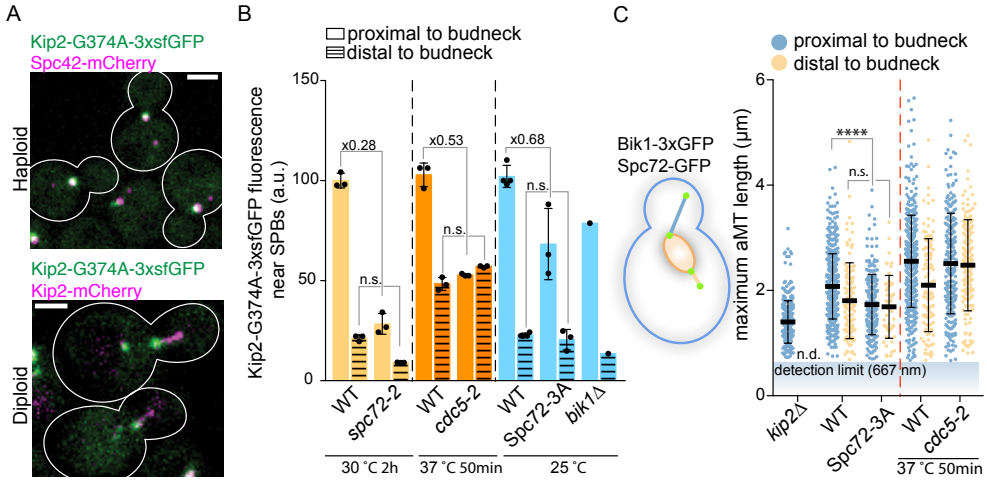

Figure 3.4 – Cdc5 mediated Spc72 phosphorylation promotes Kip2 motor loading on bud-proximal SPB. (A) Representative images of cells expressing the ATPase deficient mutant Kip2-G374A-3xsfGFP together with Spc42-mCherry in haploid cells or Kip2-mCherry in heterozygous diploid cells. Scale bar: 2 μm. (B) Quantification of Kip2-G374A-3xsfGFP intensity near SPBs in cells of indicated genotype and condition. Statistical significances were calculated using one-way ANOVAs test. (C) Measurements of maximum 3D aMT length within the 85.6s image acquisition window in metaphase cells of indicated genotype using Bik1-3xGFP and Spc72-GFP as the plus-end and minus-end marker respectively. n > 250 cells pooled from at least three independent clones for each mutant. Statistical significances for aMT length was calculated using student's t-test. For all panels, **** $p \leqslant 0.0001$, *** $p \leqslant 0.001$, ** $p \leqslant 0.01$, * $p \leqslant 0.05$, n.s. $p > 0.05$.

3.5 SPBs modulate their Kip2 recruitment activity to control microtubule dynamics at plus-ends

Kip2 is thought to stabilize aMTs by transporting Bik1 to plus-ends [Carvalho et al., 2004]. Indeed, monitoring Bik1-3xGFP fluorescence along microtubules revealed that like Kip2, Bik1-3xGFP speckles emerged from SPB and moved toward plus-end without falling off (supplement Figure 5B). Recent in vitro study suggested that Kip2 can function as a microtubule polymerase without Bik1 in vitro. Either way, *kip2*Δ cells only make very short aMTs [Carvalho

et al., 2004, Cottingham and Hoyt, 1997, Huyett et al., 1998], thus Kip2 is the major aMT stabilizing factor in budding yeast. Together, our data indicate that the microtubule stabilizing factor Kip2 is loaded onto microtubules at their minus-end and subsequently uses its motor activity to reach the plus-ends, where it is thought to promote microtubule growth. Furthermore, the two SPBs on each pole spindle differ in their activity to recruit Kip2, which in turn should rapidly impact the dynamics of the microtubules at their plus-ends. The bud-proximal SPB, which in wild-type cells always makes longer microtubules (Figure 6.1) [Lengefeld et al., 2017b], recruits about 5 times more Kip2 (Figure 3.4B).

To further validate the correlation between the Kip2 recruitment activity of SPBs and the dynamics of the aMTs they make, we asked whether Spc72-3A and cdc5-2 cells make shorter proximal aMTs without changing the lengths of distal aMTs. Using Bik1-3xGFP and Spc72-GFP as microtubule plus-end and minus-end markers, respectively, we measured the maximum 3D length and lifetime of individual astral microtubules over an image acquisition window of 85.6 seconds (Figure 3.4C). As anticipated, proximal aMTs in Spc72-3A cells (1.73 $\pm$ 0.57 μm, mean $\pm$ s.d, n = 244 aMTs) were shorter than that of wildtype cells (2.08 $\pm$ 0.62 μm, mean $\pm$ s.d, n = 509 aMTs, correlating with the lower activity of recruiting Kip2. Remarkably, in agreement with the unchanged Kip2 recruitment at distal SPB, distal aMTs of Spc72-3A cells (1.69 $\pm$ 0.60 μm, mean $\pm$ s.d, n = 51 aMTs, n.s.) stayed unchanged comparing to that of wildtype cells(1.80 $\pm$ 0.72 μm, mean $\pm$ s.d, n = 110 aMTs). Inactivating Cdc5 however did not shorten proximal aMT length, nevertheless, the length of proximal and distal aMTs became very symmetric. The complicated phenotype could be a collective output of the many Cdc5 substrates regulating aMT dynamics. Altogether, our results suggest that the activity of SPBs recruiting microtubule polymerase correlates with the length of the aMTs they carry.

4

YEAST CLIP-170 TURNS KINESIN KIP2 MOTOR DOMAIN INTO MICROTUBULE POLYMERASE AT PLUS-END

Microtubules are dynamic cytoskeletal filaments that undergo alternate growth and shrinkage phases by incorporating or disassembling the building blocks, $\alpha\beta$-tubulin dimers. This 'dynamic instability' [Mitchison et al., 1984] allows the microtubule cytoskeleton to be remodelled rapidly over the course of the cell cycle or upon external stimuli. It also allows polarized cells to organize asymmetric microtubules [Maddox et al., 2000]. Dynamic instability involves the transitions from growth to shrinkage, called catastrophe, and the transitions from shrinkage to growth, termed rescue. Various microtubule-associated proteins (MAPs) stabilize or destabilize microtubules by targeting catastrophe, rescue, growth speed, and shrinkage speed. Discovering how cells regulate and harness dynamic instability is a fundamental challenge in cell biology.

The mechanisms governing microtubule dynamics by individual MAPs have predominantly been tackled in two ways. One set of studies has employed purified components to reconstitute microtubule dynamics in vitro (e.g. [Gardner et al., 2011a, Podolski et al., 2014, Hibbel et al., 2015]). The second set of studies has accumulated high-resolution cryo-EM reconstructions of microtubules coupled to various MAP fragments (e.g. [Alushin et al., 2014, Howes et al., 2017], reviewed in [Nogales and Zhang, 2016]). These in vitro studies provided quantitative insights into the mechanism of individual MAPs, including atomic level details of tubulins together with MAPs, especially for microtubule destabilizing factors. Yet, the microtubule stabilizing factors and their interplay with other MAPs and regulators (like kinases and phosphatases) are understudied in vivo due to the difficulties in assessing microtubule dynamics in living cells with high spatio-temporal resolution.

Budding yeast cytoplasmic kinesin Kip2 is one of such examples. Kip2, together with its fission yeast homolog Tea2, has been considered a members of Kinesin-7 family [Wu et al., 2006, Verhey and Hammond, 2009, Miki et al., 2005]. However, Kip2 and Tea2 lack the two most common features of the Kinesin-7 family members: the long coiled-coil neck and the N-terminally located motor domain. In fact, one of the most intriguing features of Kip2 is the conserved low-complexity region upstream of its motor domain (supplement Figure 6), which is highly enriched in serines and threonines. They can

be heavily phosphorylated by the GSK3 homolog (Mck1) once the Ser63 is primed by kinases Dbf2 [Drechsler et al., 2015]. Interestingly, this same fragment enables the kinesin to bind to the yeast EB1 homolog (Bim1) [Drechsler et al., 2015]. Kip2 is a microtubule plus-end directed kinesin that transports the yeast homolog of CLIP-170 (Bik1) to plus-ends. It has been characterized as a microtubule stabilizing factor because deletion of KIP2 results in extremely short aMTs [Carvalho et al., 2004, Cottingham and Hoyt, 1997, Huyett et al., 1998]. The prevailing view is that Kip2 functions merely as a motor to target Bik1 to the plus-ends, while Bik1 can stabilize microtubules [Carvalho et al., 2004]. However recent reconstitution experiments [Hibbel et al., 2015] demonstrated that Kip2 alone stabilizes microtubules in vitro by polymerizing microtubules and inhibiting catastrophe. Thus, questions arise about whether Bik1 or Kip2 stabilizes microtubules in vivo and to why should Bik1 be required to hyper-elongate microtubules when Kip2 is overexpressed [Carvalho et al., 2004]. Intriguingly, another in vitro study [Blake-Hodek et al., 2010] suggests that Bik1 not only fails to stabilize microtubules, but also barely binds to free tubulins. Emerging data indicates that Bik1 not only hitchhikes on Kip2, but also promotes its motor processivity in the presence of Bim1 [Roberts et al., 2014]. It is evident that Kip2 is more than a transporter and Bik1 is more than a hitchhiker. The important unresolved issue is how the kinesin Kip2 converges the efforts of its own motility, microtubule stabilization activity, binding partners Bik1/Bim1, and kinases in living cells to achieve a certain average length of astral microtubules and their asymmetric organization between the bud and mom compartments.

4.1 Bik1-dependent accumulation of Kip2 on plus-end is indispensable for aMT polymerization

Kinesin Kip2 moves along aMT to reach the plus-end where it could polymerize microtubules. When studying the effect of Bik1 inhibiting Kip2 loading along the microtubule shaft (Chapter 3), we noticed a strong retention of Kip2 at microtubule plus-ends, which is Bik1-dependent. To investigate how Kip2 is retained at aMT plus-ends more systematically, we monitored Kip2-3xsfGFP distribution along aMTs in cells missing or having defect in direct Kip2 binding partners: *bim1*Δ, *bik1*Δ, and Kip2-ΔT cells. We performed three-dimensional (3D) time-lapse spinning-disk microscopy with an acquisition frequency of 1.07 sec per time point consisting of 17 images spanning 3.84 μm. Consistently with previous studies, Kip2-3xsfGFP speckles moved along aMTs but strongly accumulated on the plus-ends of aMTs independently of their growing or shrinking state (Figure 4.1A). Like reported by others [Caudron et al., 2008, Carvalho et al., 2004], the loss of Bim1 lead to increased

Kip2-3xsfGFP intensity on aMT plus-ends, without affecting the Kip2 protein level. Interestingly, deletion of BIK1 or abolishing the interaction between Kip2 and Bik1 instead resulted in a redistribution of Kip2-3xsfGFP from aMT plus-ends toward the lattice (Figure 4.1B). One more observation of the Kip2-ΔT cells was the elevated Kip2-ΔT-3xsfGFP protein level, which could be one of the reasons why excessive Kip2-ΔT-3xsfGFP molecules decorate aMT lattice comparing to that of the *bik1*Δ cells(Figure 4.1B). Therefore, we conclude that Bik1 is essential for retaining Kip2 at plus-ends.

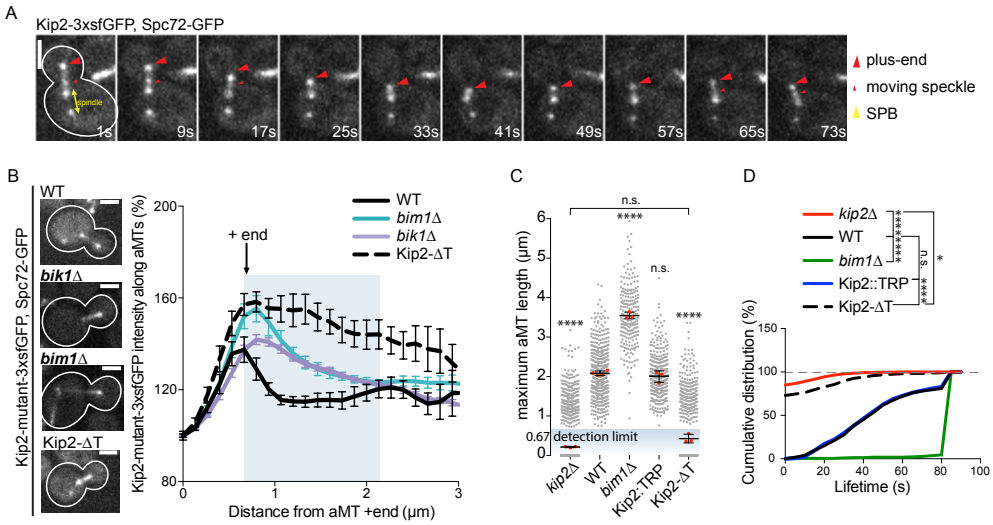

Figure 4.1 – Bik1 dependent accumulation of Kip2 on plus-ends is indispensable for microtubule polymerization. (A) Kip2 moves along aMT and accumulates on plus-end of both growing and shrinking aMT. The representative images depict the Z-sum-projection of one metaphase cell labeled with Kip2-3xsfGFP and a SPB marker Spc72-GFP. The movie has 1.07 s intervals, but only representative time points are shown here. (B) The representative images (left) and line scan analysis of Kip2-3xsfGFP fluorescence along aMTs from plus-end toward SPB in metaphase cells of indicated genotype. ($n > 50$ cells for each mutant, mean ± SEM). Measurements of maximum 3D aMT length (C) and lifetime (D) within the 85.6s image acquisition window in metaphase cells of indicated genotype using Bik1-3xGFP and Spc72-GFP as the plus-end and minus-end markers, respectively. All microtubules below detection limit (667 nm) were marked as 0 μm in length and 0 s in lifetime. $n > 250$ cells pooled from at least three independent clones for each mutant. In (C), grey dots are the aMT length in individual cells, red dots are the mean value of each clone, bars represent mean ± s.d., statistical significances for aMT length was calculated using one-way ANOVAs test. Differences among lifetime was demonstrated with cumulative distribution plot (D) and assessed with Kolmogorov-Smirnov test. Here after all aMT length and lifetime are represented in this same way. For all panels, **** $p \leqslant 0.0001$, *** $p \leqslant 0.001$, ** $p \leqslant 0.01$, * $p \leqslant 0.05$, n.s. $p > 0.05$. Scale bar: 2 μm.

Next, we asked whether the Bik1-dependent accumulation of Kip2 on plus-ends is of any significance to microtubule polymerization. To quantify

the 3D length of aMTs, we employed the 'low light tracking tool' [Krull et al., 2014] to follow the minus-end and plus-end of individual aMTs. This allows the extraction of 3D-coordinates of both the plus-end and the minus-end of each microtubule overtime. This microscopy-based assay worked well with wild-type cells in which Kip2-3xsfGFP molecules form a strong focus on the aMT plus-end (supplement Figure 7). However, it failed to detect plus-ends faithfully in *bik1*Δ cells and cells expressing Kip2-ΔT-3xsfGFP. The high intensity of the plus-end marker along aMT the lattice in these cells caused the maximum likelihood based 'low light tracking tool' to oscillate around the area near the plus-end, which lead to unreliable quantification of aMT length. We thus used Bik1-3xGFP as a plus-end marker. It is known that Kip2 is required for efficient targeting of Bik1 to aMT plus-ends [Carvalho et al., 2004]. As a proof of principle we knocked out the KIP2 gene to test whether the resulting low Bik1-3xGFP intensity (53.93 ± 24.14 % comparing to 100 ± 28.74 % in wt cells, mean ± s.d) on plus-ends was sufficient for faithful tracking. The tracking was successful and only around 15.09% (302 out of 2001) *kip2*Δ metaphase cells organized detectable aMTs (longer than 667 nm due to microscope resolution) in contrast to 100% (409 out of 409) of wild-type metaphase cells. Indeed, the loss of the microtubule polymerase Kip2 resulted in extremely short aMTs (0.21 ± 0.02 μm, mean ± s.d.) comparing to that of the wildtype cells (2.08 ± 0.06 μm, mean ± s.d.). Despite of the excessive amount of Kip2-ΔT proteins present along aMTs and on their plus-ends, Kip2-ΔT cells (0.42 ± 0.11 μm, mean ± s.d.) were not able to organize aMTs much longer than those of *kip2*Δ cells. This is exactly the case of the *bik1*Δ cells, in which Kip2 proteins heavily decorate aMTs and their plus-ends (Figure 4.1B), whereas only very short aMTs were formed [Carvalho et al., 2004]. These results demonstrate that the Bik1-dependent accumulation of Kip2 on aMT plus-end is essential for aMT polymerization.

4.2 KIP2 MOTOR DOMAIN BUT NOT THE REST OF THE KINESIN RECRUITS FREE TUBULIN DIMERS

Kip2 was the first kinesin found to be a microtubule polymerase, yet with which domain it recruits free tubulin dimers is unknown. Since the Kip2-ΔT cells phenocopy *kip2*Δ cells on aMT dynamics, we reasoned that the C-terminal tail of Kip2 could be essential for recruiting free tubulin dimers. To test this possibility, we purified the Kip2 C-terminal fragment (Kip2-CF: coiled-coil domain together with the C-terminal tail, illustrated in Figure 4.2A) from bacteria and subjected it to an isothermal titration calorimetry (ITC) experiment to monitor its interaction with free tubulin dimers. As shown in Figure 4.2B, Kip2-CF does not bind free tubulin dimers. Furthermore, using

a pelleting assay with Taxol-stabilized microtubules, we found that Kip2-CF failed to bind microtubules (Figure 4.2C). Together, these data ruled out the possibility of Kip2 C-terminal tail and the coiled-coil domain binding free tubulin dimers and mediating microtubule polymerization directly. These data also demonstrated that the inability of Kip2-ΔT to polymerize microtubules stems from its dissociation from Bik1, and not from losing the ability to bind free tubulin dimers.

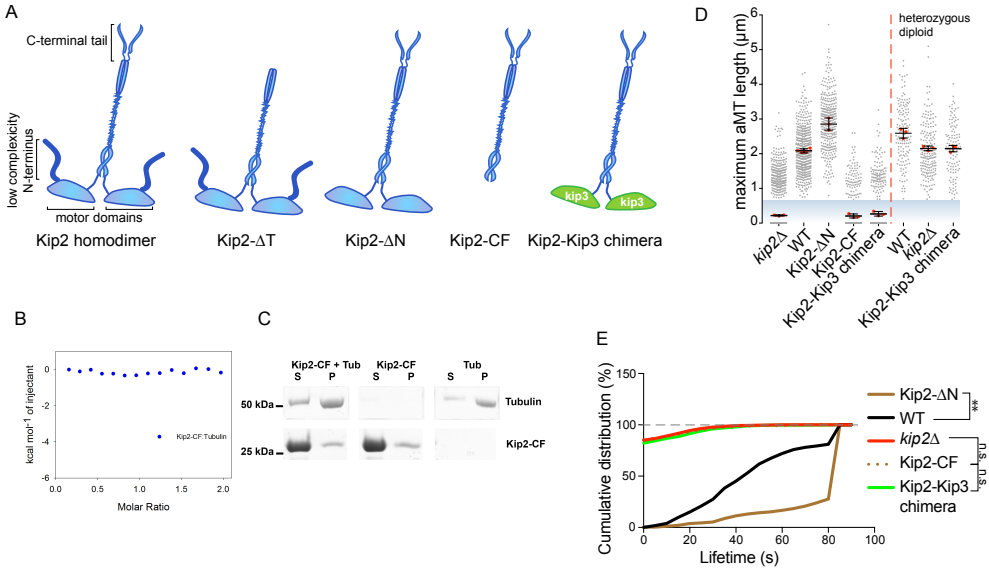

Figure 4.2 – Kip2 motor domain has to recruit free tubulin dimers, not the rest of the kinesin. (A) Diagrams of Kip2 mutants. (B) Kip2-CF does not bind free tubulins. ITC experiment for Kip2-CF:free tubulins. (C) Kip2-CF does not bind microtubule. Coomassie-Blue-stained gel of microtubule sedimentation assay of Kip2-CF with taxol stabilized microtubules. S, supernatant; P, pellet. Measurements of maximum 3D aMT length (D) and lifetime (E) using Bik1-3xGFP and Spc72-GFP as the plus-end and minus-end marker respectively. All microtubules below detection limit (667 nm) were marked as 0 μm in length and 0 s in lifetime. For all panels, **** $p \leqslant 0.0001$, *** $p \leqslant 0.001$, ** $p \leqslant 0.01$, * $p \leqslant 0.05$, n.s. $p > 0.05$.

To determine whether the low-complexity N-terminal fragment mediates microtubule polymerization, we generated the Kip2-ΔN mutant, which lacks the N-terminal fragment (residues 2-89) (illustrated in Figure 4.2A) and measured aMT dynamics in these cells. Interestingly, aMTs were not only longer in length (2.86 $\pm$ 0.18 μm, mean $\pm$ s.d.) but also longer in lifetime (Figure 4.2DE), suggesting that the N-terminal fragment acts as an inhibitor of microtubule polymerization and is not directly involved in polymerization itself. We conclude that the motor domain itself might recruit free tubulin dimers and polymerize microtubules. Indeed, removal of Kip2 motor domain (Kip2-CF) rendered Kip2 inactive in microtubule polymerization (Figure

4.2DE). One downside of the Kip2-CF mutant is that the Kip2-CF proteins are non-motile and have no affinity to microtubules, thus are unlikely to reach aMT plus-ends as efficiently. Remarkably, we found that the Kip2-CF-mNeonGreen fusion protein tracked both growing and shrinking microtubule plus-ends by binding to Bik1 (supplement Figure 8AB). To overcome this issue, we replaced the Kip2 motor domain with the Kip3 motor domain, which is known to depolymerize microtubule. The motor domain of Kip3 powers motility by hydrolyzing ATP and depolymerizes microtubule by stabilizing curved tubulin dimer conformation at plus-ends [Arellano-Santoyo et al., 2017]. The Kip2-Kip3 chimera mutant was created by fusing the Kip3 motor domain upstream of Kip2-CF (illustrated in Figure 4.2A). Unlike Kip3, the Kip2-Kip3 chimera is present only in cytoplasm and binds both growing and shrinking microtubules (supplement Figure 8C). This functional Kip2-Kip3 chimera construct expressed from KIP2 locus was not able to rescue microtubule length and lifetime of *kip2*Δ cells (Figure 4.2DE). The failure of Kip2-Kip3 chimera restoring aMT dynamics defect in heterozygous diploid cells (Figure 4.2DE) further suggests that Kip2 motor domain is dominantly involved in microtubule polymerization. These results present a dual-function motor domain powering kinesin motility along microtubule lattice and microtubule polymerization at plus-ends.

4.3 Distinct free tubulin dimer interface within Kip2 motor domain confers its microtubule polymerization activity

Motile kinesins bind to microtubules with their motor domain at high and low affinity in the course of ATP hydrolysis. The alternating 'strongly bound' and 'weakly bound' states allow kinesins to translocate along microtubules. We wondered whether Kip2 utilizes the same interface to bind microtubules and to recruit free tubulin dimers, or whether that interface specialized in recognizing and recruiting free tubulin dimers has appeared in evolution. To differentiate between these possibilities, we developed a homology model of the Kip2 motor domain bound to tubulin, basing on a Kif2C-tubulin complex structure [Wang et al., 2017]. Three potential tubulin interfaces within the Kip2 motor domain were predicted by the homology model and each of which is featured with positively charged residues: Lys294Arg296, Arg384Arg385, and Arg446 (Figure 4.3A). We introduced alanine substitutions of these residues to perturb the three potential tubulin interfaces individually and monitored the ability of the mutated Kip2-3xsfGFP protein keep to bind microtubules, reach microtubule plus-ends, and polymerize microtubules in cells. As shown in Figure 4.3C, Kip2 bearing mutation in Arg384Arg385 diffused in the cytoplasm and barely interacted with microtubules. In par-

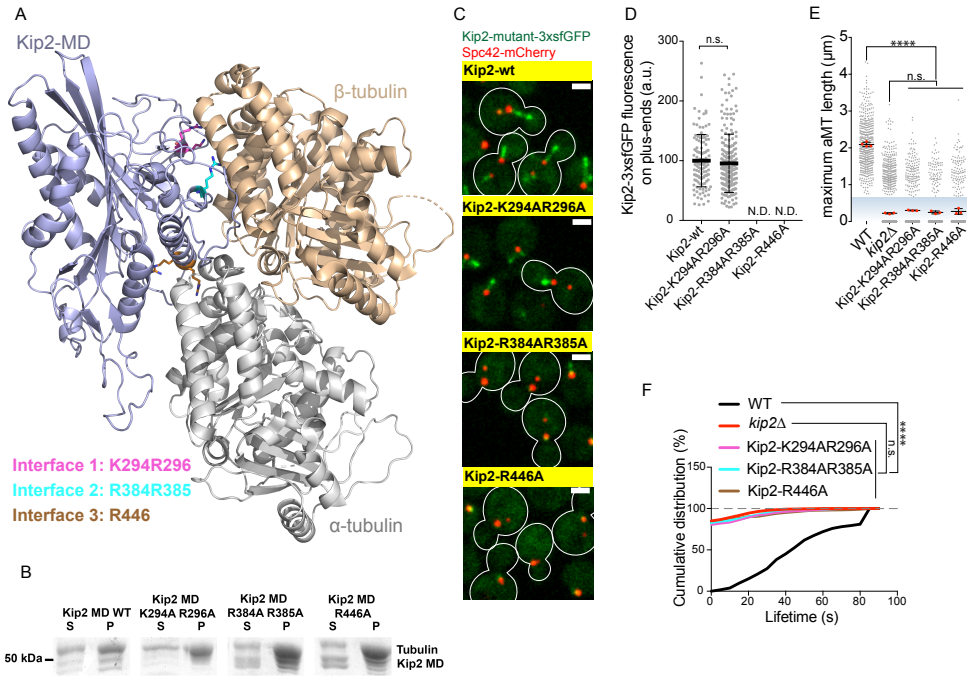

Figure 4.3 – Distinct tubulin interface within Kip2 motor domain mediates interaction with free tubulins specifically. (A) Overview of the Kip2 motor domain-tubulin complex structural model and the three highlighted tubulin interfaces of Kip2 motor domain featured by critical amino acids. (B) Coomassie-Blue-stained gel of microtubule sedimentation assay of Kip2 motor domain (Kip2-MD) and tubulin interface mutants with taxol stabilized microtubules. S, supernatant; P, pellet. (C) Representative images of yeast cells expressing Spc42-mCherry and wildtype Kip2-3xsfGFP or Kip2 containing mutations in three tubulin interfaces respectively. Scale bar, 2μm. (D) Quantification of Kip2-3xsfGFP fluorescence levels at metaphase aMT plus-ends from cells shown in (B), N.D., not detectable. Kip2-3xsfGFP levels in wildtype control were set to 100%. Bars represent mean $\pm$ s.d. pooled from three independent clones with n=125 cells for Kip2-wt and n=212 cells for Kip2-K294AR296A. Measurements of maximum 3D aMT length (E) and lifetime (F) using Bik1-3xGFP and Spc72-GFP as the plus-end and minus-end marker respectively. All microtubules below detection limit (667 nm) were marked as 0 μm in length and 0 s in lifetime. For all panels, **** $p \leqslant 0.0001$, *** $p \leqslant 0.001$, ** $p \leqslant 0.01$, * $p \leqslant 0.05$, n.s. $p > 0.05$.

ticular, Kip2 containing mutation in Arg446 did not bind to any structure specifically. Moreover, these mutations destabilized aMTs just like in the *kip2*Δ mutant (Figure 4.3EF). In contrast, mutations in Lys294Arg296 did not affect Kip2-binding microtubules and its ability to reach plus-ends (Figure 4.3D). Strikingly, although equal amount of Kip2, thus motor domains, were present at aMT plus-ends, Kip2-K294AR296A was not competent in microtubule polymerization (Figure 4.3EF). These results predict that the potential tubulin interface featured by Lys294Arg296 is essential for polymerizing microtubules

but dispensable for binding and walking along microtubules. Whereas the other two interfaces are likely involved in translocating along microtubule.

A

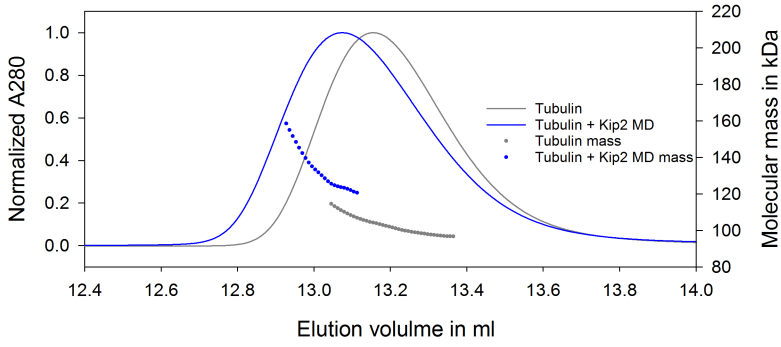

B

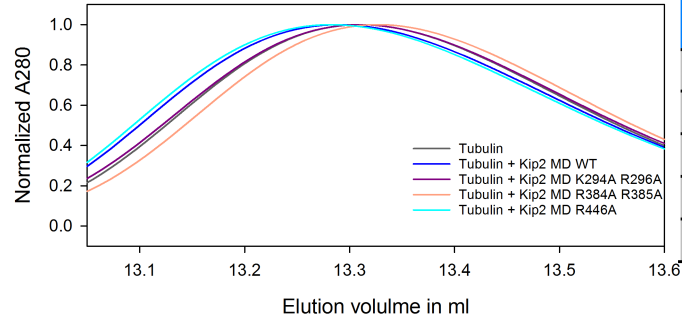

Protein	Mass in kDa
Tublin alone	109
Kip2 MD WT	147
Kip2 MD K294A R296A	127
Kip2 MD R384A R385A	141
Kip2 MD R446A	139

Figure 4.4 – Kip2-K294R296 featured tubulin interface strongly contribute to free tubulin binding. (A) Kip2 motor domain (Kip2-MD) and free tubulins co-elute as a complex (blue trace). Analysis of complex formation by SEC-MALS (size-exclusion chromatography with multi-angle light scattering analysis). The differential refractive index (left axis) and molecular mass (right axis) are plotted as a function of the column elution volume. The derived masses from the static light-scattering are about 147 kDa for Kip2-MD and tubulin complex (blue peak) and 109 kDa for tubulin alone (grey peak). (B) SEC-MALS analysis of complex formation between Kip2-MD tubulin interface mutants with free tubulins. The derived mass are listed on the right side.

To test this hypothesis, we expressed and purified variants of the Kip2 motor domains bearing these mutations from bacteria. None of the mutations affected the folding of the motor domain, which suggested that the effects of these mutations in yeast cells were not an artifact of protein misfolding. Using a pelleting assay with Taxol-stabilized microtubules, we confirmed that Arg384Arg385 and Arg446 mediated interaction with microtubule, and that mutation in Lys294Arg296 does not affect microtubule affinity of the motor domain significantly (Figure 4.3B).

Next, we tested whether Kip2 motor domain can indeed bind to free tubulin dimers and whether this interaction is mediated by Lys294Arg296. SEC-MALS analysis (size exclusion chromotography coupled to multi-angle light scattering) of complex formation between wildtype Kip2 motor domain (Kip2-MD) with free tubulins yielded a molecular mass of 147kDa, higher than that of free tubulin alone (109 kDa) (Figure 4.4A). It is important to note that Kip2-MD purified in the presence of ATP triggered free tubulins to form 'assemblies' quickly, and we are still characterizing the nature of these 'assemblies'. Interestingly, Kip2-MD purified in the presence of ADP does so much less efficiently. Strikingly, introduction of Kip2-K294AR296A substitutions decreased the mass of Kip2-MD/tubulin complex to 127 kDa, whereas mutations in the other two interfaces only weakly affected the complex formation. Thus, these studies identified two interfaces required for Kip2 motor domain to bind microtubules and one (K294R296) is mainly contributing to recognizing and binding free tubulin dimers. Also, the ATP triggered formation of tubulin 'assemblies' imply that ATP hydrolyzation could be involved in microtubule polymerization.

4.4 Phosphorylation of Kip2 N-terminus dampens AMT polymerization by releasing Kip2 from Bik1 on plus-ends

The low-complexity N-terminal fragment of Kip2 is phosphorylated by Cdk1, Dbf2/Dbf20, and Mck1 [Drechsler et al., 2015]. It has been shown that Kip2 phosphorylation decreases the intrinsic microtubule affinity of Kip2, and thus destabilizes microtubules. In light of the essential function of Bik1 at plus-ends for Kip2 to make the transition from motor protein to microtubule polymerase, we decided to investigate again the effects of Kip2 phosphorylation.

We manipulated Kip2 phosphorylation by substituting Ser63 with alanine (Kip2-S63A) to reduce phosphorylation or substituting sixteen relevant serines on N-terminus (highlighted in red in supplement Figure 6A) with aspartic acid (Kip2-allD) to mimic phosphorylation, like previously reported. Close analysis of Kip2 phosphorylation by the phos-tag PAGE suggested that the removal of Kip2 N-terminus (Kip2-ΔN) further reduced its phosphorylation level comparing to that of Kip2-S63A (supplement Figure 9AB). Thus, we have a set of Kip2 phospho-mutants of which the phosphorylation levels gradually decrease from Kip2-allD, to Kip2-wt, and Kip2-S63A (Figure 4.5B). Although all of the Kip2 variants were expressed from the native promotor, the protein level of Kip2-allD is substantially higher than that of the other mutants. (supplement Figure 9C).

To validate that Kip2 phosphorylation destabilizes aMTs, metaphase aMT dynamics of *mck1*Δ, *clb4*Δ, and *dbf20*Δ *dbf2-2* cells at 30°C were quantified. Indeed, inactivating Mck1, Cdk1/Clb4, or inhibiting Dbf20/Dbf2 activity using the temperature sensitive allele *dbf2-2* was sufficient to stabilize aMTs significantly (Figure 4.5A). Most importantly, this stabilization effect was largely Kip2 dependent: further deletion of KIP2 gene in the kinase mutants set the aMTs to the same length of *kip2*Δ cells (Figure 4.5A). The slight remaining increase of aMT length in *clb4*Δ *kip2*Δ cells (0.51 ± 0.20 μm, mean ± s.d.) comparing to *kip2*Δ cells (0.21 ± 0.02 μm, mean ± s.d.) indicates that Cdk1/Clb4 regulates targets other than Kip2 affecting microtubule dynamics. Analysis of metaphase aMT dynamics in Kip2 phospho-mutants further supported this notion. Kip2 phosphorylation level inversely correlated with the resulting average aMT length (Figure 4.5A). These data establish that phosphorylation of Kip2 destabilize aMTs by inhibiting the microtubule polymerase activity of Kip2.

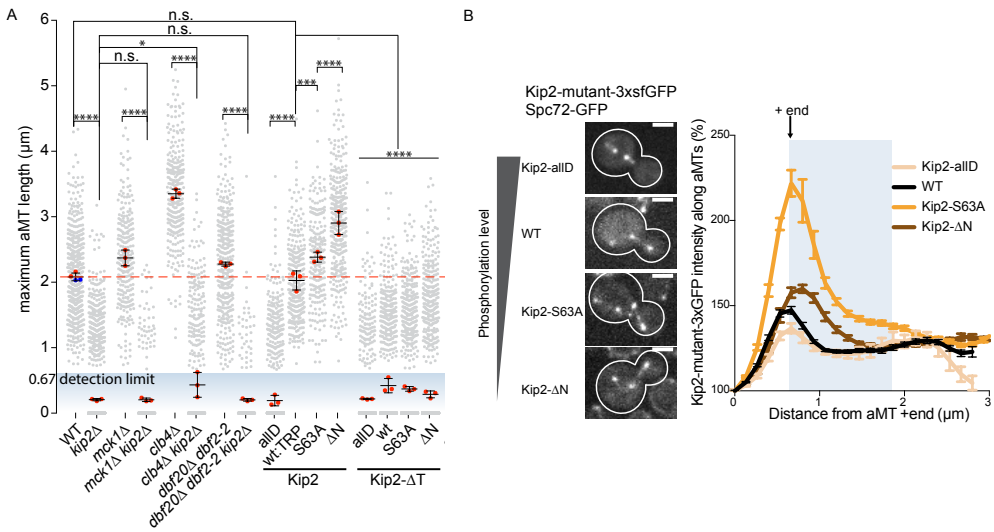

Figure 4.5 – Phosphorylation of Kip2 de-stabilize aMTs by inactivating the microtubule polymerase activity of Kip2. (A) Measurements of maximum 3D aMT length using Bik1-3xGFP and Spc72-GFP as the plus-end and minus-end marker respectively. All microtubules below detection limit (667 nm) were marked as 0 μm in length. (B) Representative images (left) of and line scan analysis of Kip2-3xsfGFP fluorescence along aMTs from plus-end toward SPB in metaphase cells of indicated genotype. (n > 50 cells for each mutant, mean ± SEM). For all panels, **** $p \leqslant 0.0001$, *** $p \leqslant 0.001$, ** $p \leqslant 0.01$, * $p \leqslant 0.05$, n.s. $p > 0.05$. Scale bar, 2μm.

Line scan analysis of Kip2 phosphomutants fused to 3xsfGFP along aMTs revealed that phosphorylation reduced Kip2 accumulation on plus-ends (Figure 4.5B). This dramatic change of Kip2 quantity on aMT plus-ends prompted us to investigate an alternative mechanism with which phosphorylation inac-

tivate Kip2 as a microtubule polymerase. Instead of reducing Kip2 affinity to microtubules, phosphorylation could reduce Kip2 affinity to Bik1p that is present on aMT plus-ends. To test this hypothesis, we investigated whether phosphorylation can still destabilize aMTs in the Kip2-ΔT context where Kip2 no longer binds Bik1. As shown in Figure 4.5A, comparing to the full length Kip2 phosphomutants, Kip2 phosphorylation barely affected the aMT dynamics in the context of Kip2-ΔT. These results clearly demonstrate that the phosphorylation controls Kip2 activity mainly in a Bik1 dependent manner.

To specifically study how phosphorylation and Bik1 regulate Kip2 activity, we developed the 'Δmotor' system where Kip2-Δmotor no longer possesses affinity to microtubules, and only tracks microtubule plus-ends by binding to Bik1. The 'Δmotor' system was developed in light of the mutant Kip2-ΔN-Δmotor (same as Kip2-CF: Figure 4.2AB, supplement Figure 3 and 8A). Kip2-ΔN-Δmotor (Kip2-CF) binds neither to free tubulins nor to microtbules, in contrast it binds to Bik1 with extremely high affinity and tracks both growing and shrinking aMT plus-ends (supplement Figure 3). To verify the 'Δmotor' system, we clarified the following two questions. Firstly, Kip2-ΔN-Δmotor tracks aMT plus-ends in a Bik1, and only Bik1, not any other MAP (e.g. Kip3, Kar3) dependent manner (Figure 4.6A). Secondly, introducing mutations in Kip2 N-terminus still allows us to manipulate phosphorylation levels (Figure 4.6D). Next, we fused the Kip2-Δmotor phospho-mutants with 3xsfGFP and monitored how phosphorylation affected the quantity of Kip2-Δmotor proteins on aMT plus-ends. As shown in Figure 4.6B, the majority of the Δmotor proteins diffused in the cytoplasm. Interestingly, a portion of the Kip2-Δmotor and Kip2-S63A-Δmotor proteins entered nucleus and appeared on spindles. Importantly, the fluorescence intensities of various Kip2-Δmotor-3xsfGFP phospho-mutants on plus-ends inversely correlated with their phosphorylation levels (Figure 4.6C). To test whether the increased accumulation of Kip2-Δmotor proteins upon reduction of phosphorylation is still Bik1 dependent, we further deleted the C-terminal tails from all Δmotor mutants, which abolished their accumulation on aMT plus-ends in all cases. The fluorescence of Bik1-3xGFP on aMT plus-ends in Kip2-Δmotor mutants did not change between cells with different Kip2 phosphorylation levels (supplement Figure 11B). Altogether, we conclude that phosphorylation inactivates Kip2 microtubule polymerase activity mainly by releasing Kip2 from Bik1 on plus-ends.

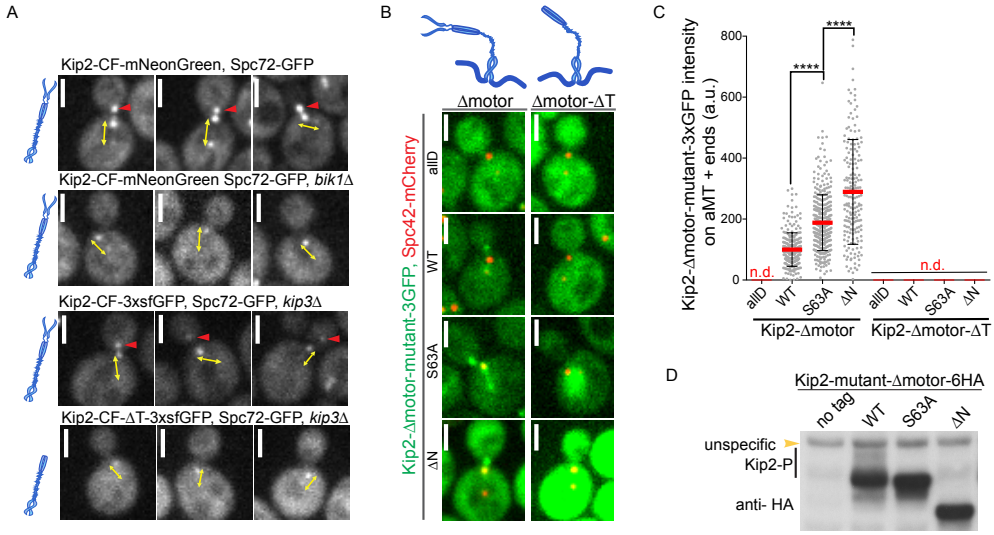

Figure 4.6 – Phosphorylation of the Kip2 N-terminus releases Kip2 from aMT plus-end. (A) The Kip2-CF protein accumulates on aMT plus-end in a Bik1 dependent manner. Representative images of metaphase cells expressing Kip2-CF fused with mNeonGreen or 3xsfGFP in indicated mutants. (B) Diagrams of the Kip2-Δmotor mutants and representative images of metaphase cells expressing Spc42-mCherry together with indicated Kip2-Δmotor mutants fused with 3xsfGFP. (C) Quantification of GFP fluorescence levels at metaphase aMT plus-ends from the cells shown in (B), n.d., not detectable. The GFP levels in Kip2-WT-Δmotor control were set to 100%. Bars represent mean ± s.d. pooled from three independent clones with n=258 cells for WT-Δmotor, n = 362 cells for S63A-Δmotor, and n=188 cells for ΔN-Δmotor. (D) WB detection of Kip2-Δmotor mutants fused with 6xHA in cycling cells. **** $p \leqslant 0.0001$. Scale bar, 2μm.

4.5 PHOSPHORYLATION TRIGGERS THE INTERACTION BETWEEN KIP2 N-TERMINI AND C-TERMINI

Next, we asked how the phosphorylation-dependent release of Kip2 is achieved. It is clear that this process requires phosphorylated N-termini, the C-termini that bind to Bik1, but not the motor domain. One possible scenario is that the phosphorylated N-termini bind to Kip2-CF, which perturbs its interaction with Bik1, and causes the release of Kip2. We tested the potential phosphorylation-triggered interaction between Kip2 N-termini and C-termini with the bimolecular fluorescence complementation (BIFC) assay, which enables trapping and visualization of even transient interactions. The fluorescent protein Venus is split into N-terminal (VN) and C-terminal (VC) fragments. Only when fused to a pair of interacting proteins, they form intact Venus irreversibly and become fluorescent. Initially, we simply split Kip2 into two halves. The first half N-terminal fragment (Kip2-NF) containing the motor domain was fused downstream of VN. To ensure cytoplasmic

localization and dimerization, a classical NES (Nuclear export signal) present in the viral protein Rev and a leucine zipper were fused downstream of the motor domain. In light of the observation that microtubule is required for Kip2 phosphorylation, the motor domain was preserved to ensure proper phosphorylation of the N-terminus. Again, we introduced mutations into the N-terminus to manipulate phosphorylatin level. The resulting chimeric protein VN-Kip2-NF-NES-LZ was co-expressed with Kip2-CF-VC (illustrated in supplement Figure 12) in *kip2*Δ cells. To our surprise, co-expression of VN-Kip2-ΔN-NF-NES-LZ with Kip2-CF-VC already reconstituted Venus (supplement Figure 12), suggesting an interaction between the Kip2 motor domain and the C-terminal fragment. Intriguingly, the reintroduction of either wild-type or S63A N-terminus (residues: 1-92) upstream of the motor domain abolished Venus restoration. These observations indicate a function of the low complexity N-terminus to free its motor domain from being bound by the C-terminal fragment of the protein.

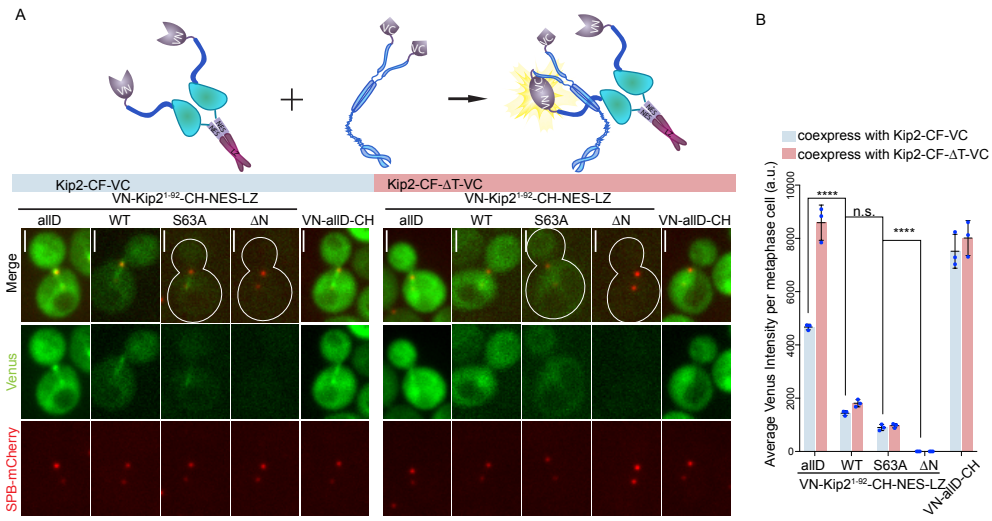

Figure 4.7 – Phosphorylated Kip2 N-terminus interacts with Kip2-CF in a BiFC Assay. (A) Diagrams of the VN and VC fusion proteins (top) and representative images of *kip2*Δ metaphase cells expressing SPB marker Spc42-mCherry and the indicated VN/VC fusion proteins. (B) Quantification of Venus fluorescence per metaphase cell (made using a developed Fiji macro; see chapter 8 for details). Bars represent mean ± s.d. obtained from three independent clones, statistical significance was calculated using one-way ANOVAs test. **** $p \leqslant 0.0001$, *** $p \leqslant 0.001$, ** $p \leqslant 0.01$, * $p \leqslant 0.05$, n.s. $p > 0.05$. Scale bar: 2 μm.

To simplify the system, we redesign the experiment by replacing the Kip2 motor domain with a microtubule binding domain that was unlikely to interact with Kip2-CF. The calponin homology (CH) domain from Bim1 was chosen because of its affinity to microtubule and not to Kip2 or Bik1. As

expected, replacing the motor domain with the CH domain provided us a background in which no basal Venus restoration was observed. As shown in Figure 4.7A, co-expressing VN-CH-NES-LZ with Kip2-CF-VC in *kip2*Δ cells was not able to restore Venus at all. In this context, introducing Kip2 N-terminus with various phosphorylation status upstream of the CH domain promoted Venus restoration to different extent, as quantified in Figure 4.7A. The Venus fluorescence was most profound in the phospho-mimetic situation where VN-allD-CH-NES-LZ was co-expressed with Kip2-CF-VC. Regardless of the Kip2 phosphorylation level and of the NES engineered in the chimeric proteins, we noticed that Venus fluorescence appeared both in the cytoplasm and in the nucleus, and that the Venus signal is enriched on mitotic spindle. We reasoned that the Kip2-N-termini could override the Rev NES. Indeed, Kip2(1-92)-mNeonGreen fusion protein demonstrated a similar distribution pattern and enriched in nucleus (supplement Figure 13). These results suggest that phosphorylated Kip2 N-termini and Kip2-CF can form a complex.

To further test whether this phosphorylation dependent Venus restoration requires Bik1, we co-expressed the VN fusion proteins with Kip2-CF-ΔT-VC, which does not bind to Bik1. Loss of the Kip2 C-terminal tail, as well as its interaction with Bik1, did not affect Venus restoration, except that the restored Venus signal fails to concentrate on mitotic spindle. Altogether, we conclude that phosphorylation of Kip2 N-termini triggers its interaction with Kip2-CF.

4.6 Phosphorylated Kip2 N-termini may be a prerequisite for the Kip2 recruitment to SPBs

In Chapter 3, we showed that in living cells the recruitment and loading of Kip2 onto microtubules is a controlled process and that it is inhibited along microtubule and promoted at SPB. We wondered whether the phosphoregulation of Kip2 affects its recruitment at SPB. To monitor the distribution profile of Kip2-S63A-3xsfGFP and Kip2-ΔN-3xsfGFP along aMTs, again we used Spc42-mCherry as the SPB marker and performed line scan analysis of GFP fluorescence distribution along aMTs. As shown in Figure 4.8A, strikingly, reducing Kip2 phosphorylation by substituting Ser63 with alanine strongly reduced Kip2-S63A intensity near SPB. Meanwhile, Kip2-S63A-3xsfGFP intensity along microtubule increased linearly. Furthermore, its intensity at plus-ends increased with the length of microtubules. All the changes suggested that Kip2-S63A, like Kip3, is recruited and loaded along the microtubule shaft randomly. Interestingly, Kip2-ΔN-3xsfGFP distributed along microtubule very similarly with wildtype molecules, except for the increased background GFP intensity in cytoplasm, which is due to the elevated protein level (sup-

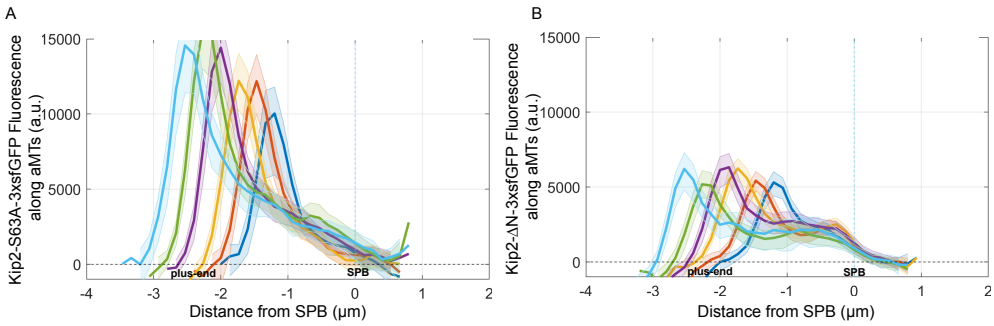

Figure 4.8 – Unphosphorylated Kip2 N-termini compromises the inhibition of Kip2 loading along the microtubule shaft and prevents its recruitment at the SPB. (A) Kip2-S63A-3xsfGFP binds along aMT length dependently and is absent near SPB. Line scan analysis of Kip2-S63A-3xsfGFP fluorescence profile along aMTs. (B) Kip2-S63A-3xsfGFP accumulates aMTs in a similar pattern with Kip2-wt-3xsfGFP (Figure 3.1B). All profiles (n = 263 cells for Kip2-S63A-3xsfGFP, n = 376 cells for Kip2-S63A-3xsfGFP) were aligned toward SPB using the peak of Spc42-mCherry signal and binned according to their lengths with 266 nm (2 pixels) intervals. Horizontal dashed line, corrected background GFP signal in cytoplasm. Vertical dashed line, the centre of Spc42-mCherry signal. Shaded areas, 95% confidence intervals.

plement Figure 9CD). Next, we plan to check the amount of Kip2-S63A and Kip2-ΔN being recruited at SPB in the context of ATPase deficient and *kip3*Δ. These preliminary results strongly indicate that the unphosphorylated Kip2 N-terminus overrides the regulation of SPB. However, the loss of N-terminus again allows the SPB to control the recruitment and loading of Kip2. Thus, the unphosphorylated N-terminus actively inhibits SPB based recruitment with mechanisms that are yet to be revealed.

5

MULTIFUNCTIONAL C-TERMINAL TAIL CONFERS KIP3 DUAL-MODE REGULATION ON MICROTUBULE

Budding yeast Kinesin-8 Kip3 is one of the first motors that demonstrated the dual-mode regulation on microtubule dynamics[Su et al., 2011, Fukuda et al., 2014], these motors de-stabilize growing microtubules but stabilize shrinking microtubules. This part of work was initially inspired by the observation that Kip3 motor domain can promote catastrophe (Chapter 2 Figure2.5), and that its C-terminal fragment downstream of the motor domain is indispensable for microtubule stabilization. This suggests that distinct domains within one kinesin execute opposite effects on microtubules, which poses a very interesting question: how do Kip3 proteins or cells regulate the two opposing activities and whether the two activities are independent from each other.

In this chapter, we first dissect the functions of various domains of Kip3 genetically and biochemically, then present preliminary results on how the stabilizing and de-stabilizing activities of Kinesin-8 can be united and regulated.

5.1 KIP3 BINDS TO BOTH GROWING AND SHRINKING AMT PLUS-ENDS

Kip3 proteins have been reported to be processive plus-end directed motors, that bind only growing but not shrinking microtubule plus-ends[Gupta et al., 2006, Varga et al., 2006, Su et al., 2011]. The reported localization of Kip3 does not support the idea that Kip3 stabilizes shrinking microtubules. To investigate this issue in detail, we fused Kip3 with 3xsfGFP or mNeonGreen and subjected these cells to high spatial-temporal resolution microscopy with a spinning disk. With the interval of 1.07 s, we observed a strong accumulation of Kip3-3xsfGFP on growing MT plus-ends. Immediately after catastrophe, the intensity of Kip3-3xsfGFP decreases but is still quite abundant on shrinking aMT plus-ends (Figure 5.1A). Several more representative kymographs of growing and shrinking aMTs are shown in Figure 5.1B to demonstrate the presence of Kip3 on shrinking aMTs.

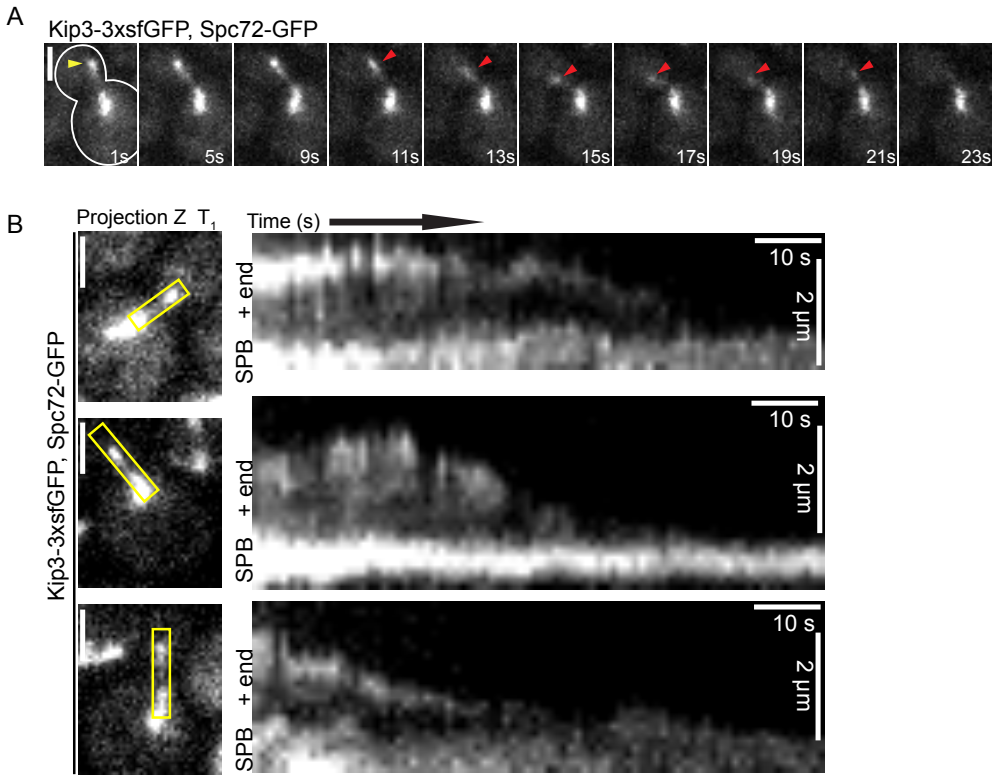

Figure 5.1 – Kinesin-8 Kip3 binds to both growing and shrinking aMT plus-ends. (A) Kip3-3xsfGFP binds along aMTs and accumulates on plus-ends of both growing (yellow arrow) and shrinking (red arrow) aMTs. Representative images depict the Z-sum-projection of one metaphase cell labeled with Kip3-3xsfGFP and a SPB marker Spc72-GFP. The movie has 1.07 s intervals, but only representative time points are shown here. (B) Further representative metaphase cells (left) and kymographs of Kip3-3xsfGFP associated aMTs. Z-sum-projection imaging of the boxed aMT is displayed as kymograph (right). Kip3-3xsfGFP proteins remain accumulate on shrinking aMT plus-ends with weaker intensity. The entire kymograph x-axis represents 85.6 s, with 1.07 s interval.

5.2 Identification of a novel tubulin binding domain resides within Kip3 C-terminal fragment

Knowing the Kip3 C-terminal fragment (445-806) is indispensable for promoting rescue, we took an biochemical approach to characterize this fragment. All of the used constructs in this work are illustrated in Figure 5.2A. Our collaborator Marcel at PSI purified the Kip3 805 fragment from bacteria and set out to crystallize it. Interestingly, he was able to solve the structure of the fragment up to amino acid number 693 and the C-terminus tail appeared to be too flexible to be determined (unpublished data from Marcel). To test whether the Kip3 693 fragment was able to interact with tubulins directly,

Kip3 693 and tubulin dimers were subjected to ITC analysis, the data shown in Figure 5.2F revealed that Kip3 C-terminal domain (CTD: 445-693) is a strong tubulin binding partner with a Kd at around 500nM. We reasoned that this strong interaction with free tubulins could be the main reason that Kip3-CF is required for promoting rescues. Yet, the functional significance of the flexible tail (694-806) remains a mystery. We decided to go back to living yeast cells and dissect the functions of Kip3-ΔCF-LZ and Kip3-ΔT genetically.

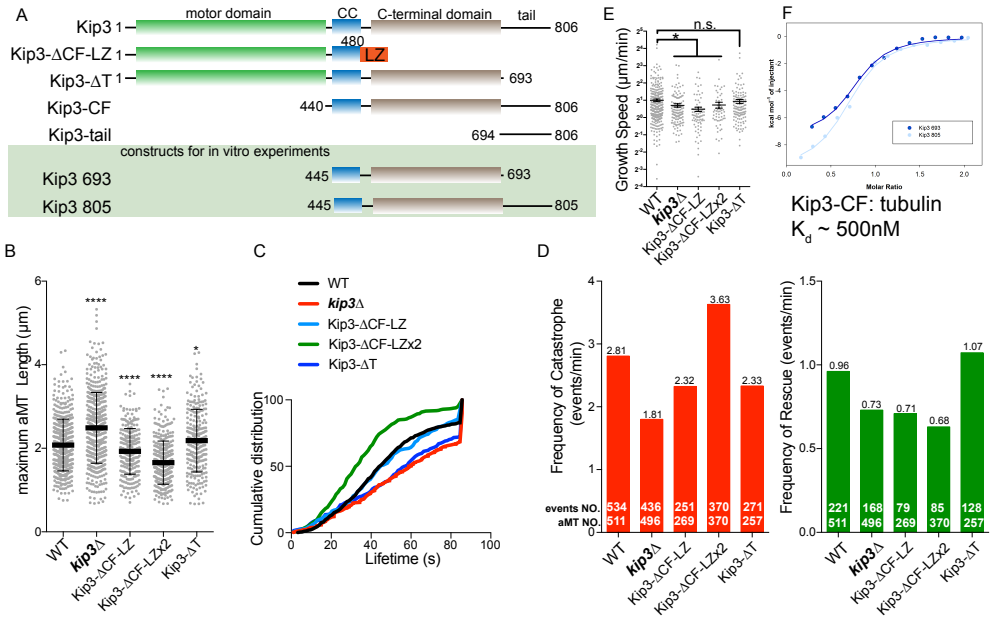

Figure 5.2 – Kip3-CF is essential for promoting resuce and facilitate the motor domain to promote catastrophe. (A) Schematic of the constructs used in this part of work. Kip3 contains a motor domain (green), followed by a short neck consisting of 4-5 coiled-coil heptads (CC, blue), a C-terminal domain (brown), and a flexible tail. The leucine zipper (orange) was added to maintain the dimeric state of Kip3-ΔCF-LZ, which was originally constructed by Xiaolei Su[Su et al., 2013]. Deletion of Kip3 tail (Kip3-ΔT was obtained by CRISPR-Cas system.) All of the Kip3 mutants were expressed from the endogenous KIP3 locus. Constructs for in vitro experiments are highlighted in green box (design and conducted by Marcel Stangier (PSI). (B-F) Experimental data of measured aMT dynamics in indicated mutants. Maximum length (B) and lifetime (C) of individual pre-anaphase proximal aMTs within the 85.6 s image acquisition window are represented with column scatter plot (mean ± s.d.) and cumulative distribution plot respectively. The catastrophe and rescue (D) frequency of aMTs are computed by dividing the total number of annotated catastrophe or rescue events with total time spend in growth or shrinkage respectively. The number of annotated events and aMTs are marked within corresponding columns. The speed of aMT growth (E) is demonstrated with column scatter plot (mean ± SEM). Statistical significance was calculated using two-tailed Student t-test on measurable dataset. **** $p < 0.0001$, *** $p < 0.001$, ** $p < 0.01$, n.s. = not significant. (F) ITC experiments for Kip3 693:tubulin (dark blue closed circles) and Kip3 805:tubulin (light blue closed circles). Solid lines are the fits that were obtained by using the monomeric concentrations of the proteins.

5.3 THE C-TERMINAL TUBULIN BINDING DOMAIN IS ESSENTIAL FOR PROMOTING RESCUE

To test the functions of Kip3 tail and CF in regulating microtubule dynamics, we created yeast strains missing these domains and quantified their aMT behaviour. A defect in aMT regulation after the insertion of a selection marker downstream of KIP3 was observed (see Figure 6.6B), thus the strains in need were obtained either by CRISPR (Kip3-ΔT) or 5-FOA mediated excision of the URA marker (Kip3-ΔCF-LZ). The Kip3-ΔCF-LZx2 allele was a gift from Dr. Mohan L. Gupta. As shown in Figure 5.2BCD, the loss of Kip3 tail did not compromise rescue frequency (0.96 event/min (wt) to 1.07 event/min). Instead, further removal of the C-terminal tubulin binding domain decreased the rescue frequency to the similar level of *kip3*Δ cells (0.71 event/min). Increase the Kip3-ΔCF-LZ protein level by expressing two copies of the gene did not rescue the defect (0.68 event/min). Consistent with the high affinity to free tubulins demonstrated by ITC (Figure 5.2F), loss of the C-terminal domain and not the flexible tail lead to significantly smaller growth speed (Figure 5.2E). These results revealed the essential function of the C-terminal tubulin binding domain in promoting rescue. Also, they suggest an active microtubule growth promoting activity of the C-terminal tubulin binding domain, thus the aMT stabilization activity is likely to be active regardless of growth or shrinkage status. The flexible tail does not promote rescue, if anything, it could inhibit rescue events.

5.4 THE TAIL OF KIP3 FACILITATES ITS MOTOR DOMAIN TO PROMOTE CATASTROPHE

There was strong indication that Kip3 motor domain could promote catastrophe (Chapter 2 Figure2.5). To compare Kip3 mutants expressing the same level of proteins, we computed catastrophe frequency of Kip3-ΔCF-LZ cells. Removal of Kip3 CF did decrease the catastrophe frequency from 2.81 (event/min, wt) to 2.32 (event/min), but not as low as 1.81 (event/min) of *kip3*Δ cells. Furthermore, increase of Kip3-ΔCF-LZ protein level pushed the catastrophe frequency to 3.63 (event/min, Kip3-ΔCF-LZx2). These data reveal three important messages: Firstly, the dimerized Kip3 motor domains posses the ability to promote catastrophe. Secondly, the C-terminal tubulin binding domain is unlikely involved in regulating catastrophe. Thirdly, Kip3 flexible tail promotes catastrophe, either by facilitating its motor domain or by acting as a catastrophe promoting factor on its own.

The tail itself, regardless the dimeric status, fails to interact with microtubules in living cells (Figure 5.3), indicating the tail itself has no or very weak

affinity to microtubules. It has been shown by in vitro microtubule pelleting assay that Kip3-CF binds to microtubules at an affinity around 5.9±0.6 μM. We went on to express Kip3-CF-3xsfGFP at the endogenous locus to see whether this fragment could bind microtubules in vivo. Interestingly, both Kip3-CF-3xsfGFP and LZ-Kip3-CF-3xsfGFP were expressed at extremely low levels (confirmed by WB in Figure 5.6A elution panel). And these low levels of GFP fused proteins did not appear to bind microtubules. Basing on these observations, Kip3 tail is unlikely to promote catastrophe on its own. The only feasible possibility left is that Kip3 tail facilitate it motors to promote catastrophe.

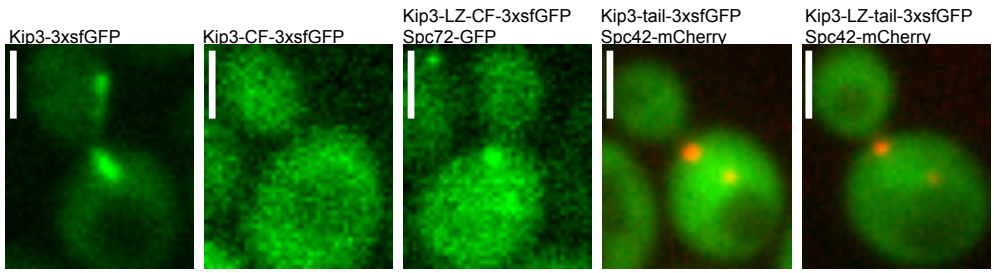

Figure 5.3 – The C-terminal fragment (Kip3-CF: 440-806) or tail (Kip3-tail: 694-806) of Kip3 does not bind microtubules regardless of dimerization status in living cells. Representative images of metaphase cells expressing indicated fusion proteins from endogenous loci. Leucine Zipper (LZ: Gcn5 (250-281) was added for maintaining the dimerization state. White boxes represent scale bars. The low Kip3-CF-3xsfGFP protein level is verified by WB in figure5.6

5.5 PHOSPHORYLATION OF KIP3 TAIL MAY REGULATE ITS MOTOR PROCESSIVITY

Next we asked how would the flexible tail facilitate its motor domains. We have reached this conclusion by an genetic approach, interestingly this was also an idea proposed basing on biochemical and biophysical experiments [Su et al., 2011], in which the authors demonstrated that Kip3-CF facilitates a microtubule binding fragment (KHC_{560}) that is not able to concentrate on microtubule plus-ends to appear on plus-ends in reconstituted system. Unfortunately the authors of this work did not test whether the Kip3-CF itself was able to bind to microtubule plus-ends. Nevertheless, the authors demonstrated that the CF was promoting Kip3 processivity and plus-end dwell time in their system. In addition, the C-terminal fragment of human Kinesin-8 Kif18A has also been shown to heighten Kif18A processivity. Only that the C-terminal fragment of Kif18A can bind to microtubules in vivo[Mayr et al., 2011]. It is an appealing idea that Kip3 tail promotes the motor

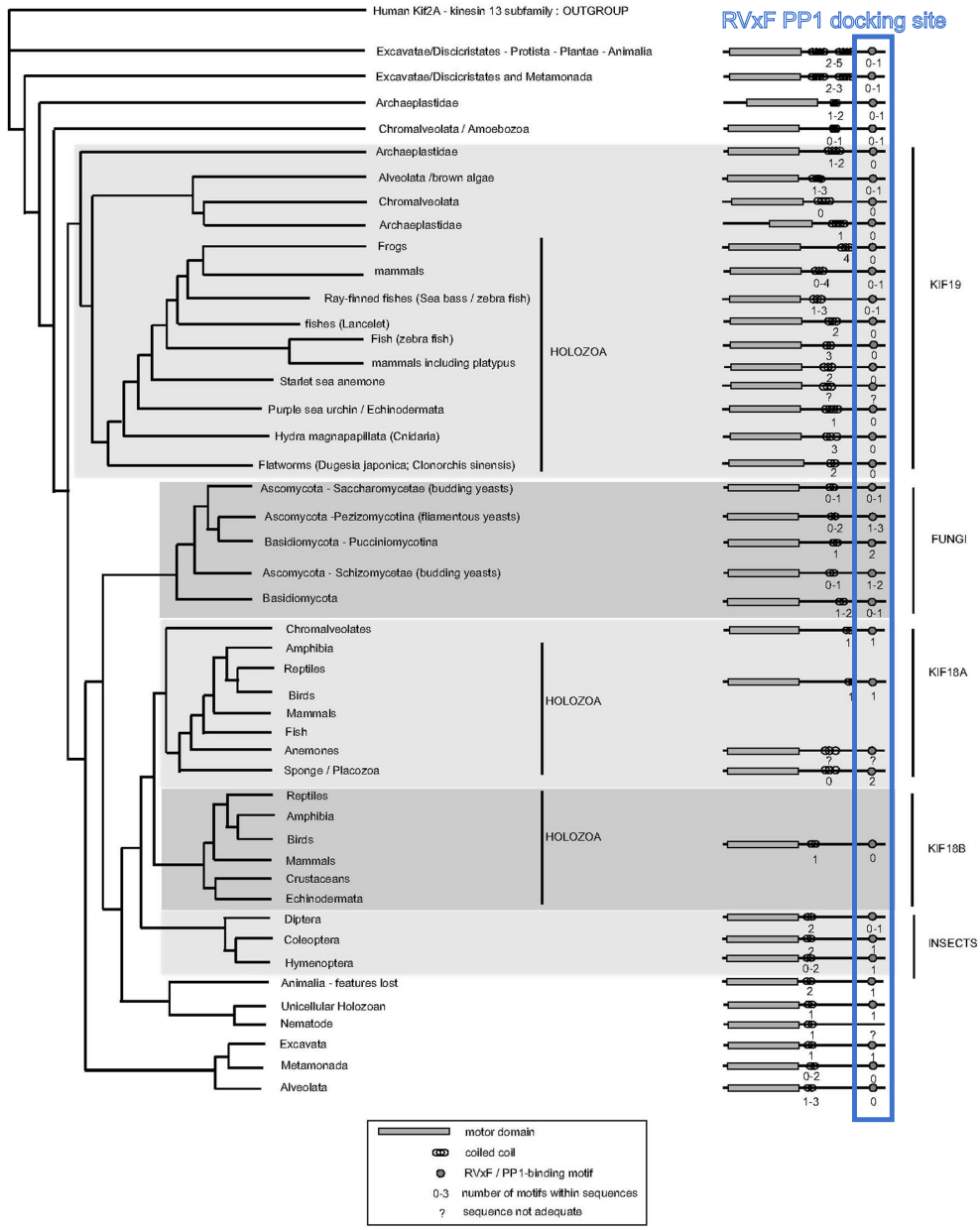

Figure 5.4 – Figure adapted from [De Wever et al., 2014] demonstrating the highly conserved RVxF PP1 docking site at the C-termini of Kinesin-8 family motors. Numbers underneath reflect the numbers of motifs identified. Question marks indicate a lack of publicly available sequences.

processivity thus facilitates in promoting catastrophe. An immediate next step will be to fuse full length Kip3, Kip3-ΔCF-LZ, and Kip3-ΔT with 3xsfGFP to test whether the loss of Kip3 tail causes defects on the motor processivity.

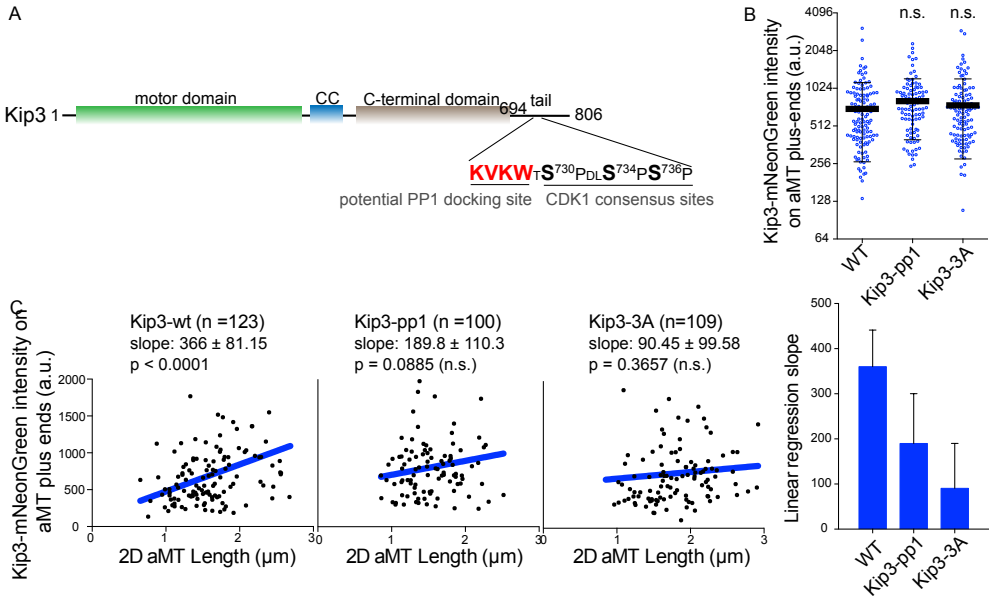

Figure 5.5 – The Kip3 tail could regulate kinesin processivity. (A) Schematic of the potential PP1 docking site and three consecutive CDK1 consensus phosphorylation sites on Kip3 tail. (B) Intensity of wild-type Kip3-mNeonGreen (WT) and mutants with disrupted potential PP1 docking site (Kip3-pp1) or disrupted CDK1 consensus sites (Kip3-3A) on metaphase proximal aMT plus-ends. (Shown as mean ± s.d., statistical significance was calculated using two-tailed Student t-test on measurable dataset. n.s. = not significant.) (C) Scatter plot of indicated Kip3-mutant-mNeonGreen intensity on plus-ends as a function of aMT length. Linear regression results are shown as the blue solid line. The p value represents whether the slope is significantly non-zero. The slopes obtained from linear regression are plotted on the right. The quantification was done on metaphase proximal aMTs. These results were quantified by block course students Jannik Hugener and Christian Doerig.

When trying to identify biological relevant features of Kip3 tail basing on its amino acid sequence, a RVxF motif followed by three consecutive CDK1 consensus sites came into the focus (Figure 5.5A). RVxF motif is a general group of sequences that binds to a hydrophobic groove of protein phosphatase-1 (PP1)[Egloff et al., 1997, Bollen, 2001, Cohen, 2002], such that to provide substract specificity for PP1. Remarkably, this potential PP1 docking site in Kip3 C-terminus is highly conserved within the Kinesin-8 family[De Wever et al., 2014]. In particular, the direct interaction between human Kinesin-8 Kif8 and PP1 is experimentally validated[De Wever et al., 2014]. However, the functions of the RVxF motif mediated interaction with PP1 is not known. One idea will be the PP1 docking motif regulates Kip3 phosphorylation status, which in turn regulates the processivity of Kip3. Yeast strains baring mutations in the potential PP1 docking motif (Kip3-pp1) and in the following Cdk1 consensus sites (Kip3-3A) were generated, and

the intensities of these proteins fused to mNeonGreen on aMT plus-ends in metaphase were quantified. As shown in Figure 5.5B, disruption of the PP1 docking site or prevention of potential phosphorylation on Kip3 tail via alanine substitution did not change the amount of Kip3 protein on plus-ends.

Next, we employed the length dependent distribution of Kip3 as a mean to reflect the motor processivity. This assay would only be valid under the condition that Kip3 moves faster than microtubule growth. Luckily, this is likely the case for Kip3 in vivo. [Varga et al., 2006] estimated that the Kip3 speckles move along microtubules at a speed of 2.8±1.0 μm/min (mean±s.d., 2D projection) without mentioning the temperature in which they cultured and imaged yeast cells. This is certainly faster than the microtubule growth speed either at 25°C (1.36±1.05 μm/min, mean±s.d., 3D) or at 30°C (1.98±1.73 μm/min, mean±s.d., 3D). Theoretically, high motor processivity leads to length dependent accumulation of the motor on plus-ends, whereas low processivity would dampen this length dependency (well documented for Kip3 in reconstituted system[Varga et al., 2006]). Unexpectedly, the length dependency of Kip3-mNeonGreen intensity on plus-ends in vivo has not been reported. Among metaphase aMTs, we observed a significant dependency between aMT length and Kip3-mNeonGreen intensity on plus-ends (slope=366±81.5, n=123, p<0.0001), which suggests that indeed Kip3 full length proteins are rather processive when moving along aMTs. Upon disruption of the potential PP1 docking site (slope=189.8±110.3, n=100, p=0.0885, n.s.) or the prevention of potential Kip3 tail phosphorylation on three serine (slope=90.45±99.58, n=109, p=0.3657, n.s.), this dependency is largely weakened. These results are preliminary but strongly indicate that one of the functions of the flexible tail could be regulating Kip3 processivity. Furthermore, this activity could be regulated by the phosphorylation status of Kip3 tail.

5.6 Kip2 interacts with the tail of Kip3 to inhibit its rescue promoting activity

Here I would like to update some preliminary results regarding the physical interaction between Kip2 and the tail of Kip3 (Figure 5.6AB). As described earlier in Figure 2.5F, Kip2 physically interact with Kip3 in a Kip2 N-terminus, C-terminus, and Bik1 independent manner. This interaction may mediate the inhibition of Kip2 toward Kip3's rescue promoting activity. To test whether Kip3 CF or tail is sufficient to interact with Kip2, we expressed Kip3-CF-3xsfGFP and Kip3-tail-3xsfGFP from endogenous locus. Using GFP-trap (Chromo Tek) to precipitate Kip3 proteins fused to 3xsfGFP, we were able to enrich Kip2-6HA proteins with Kip3-tail-3xsfGFP. This observation indicates

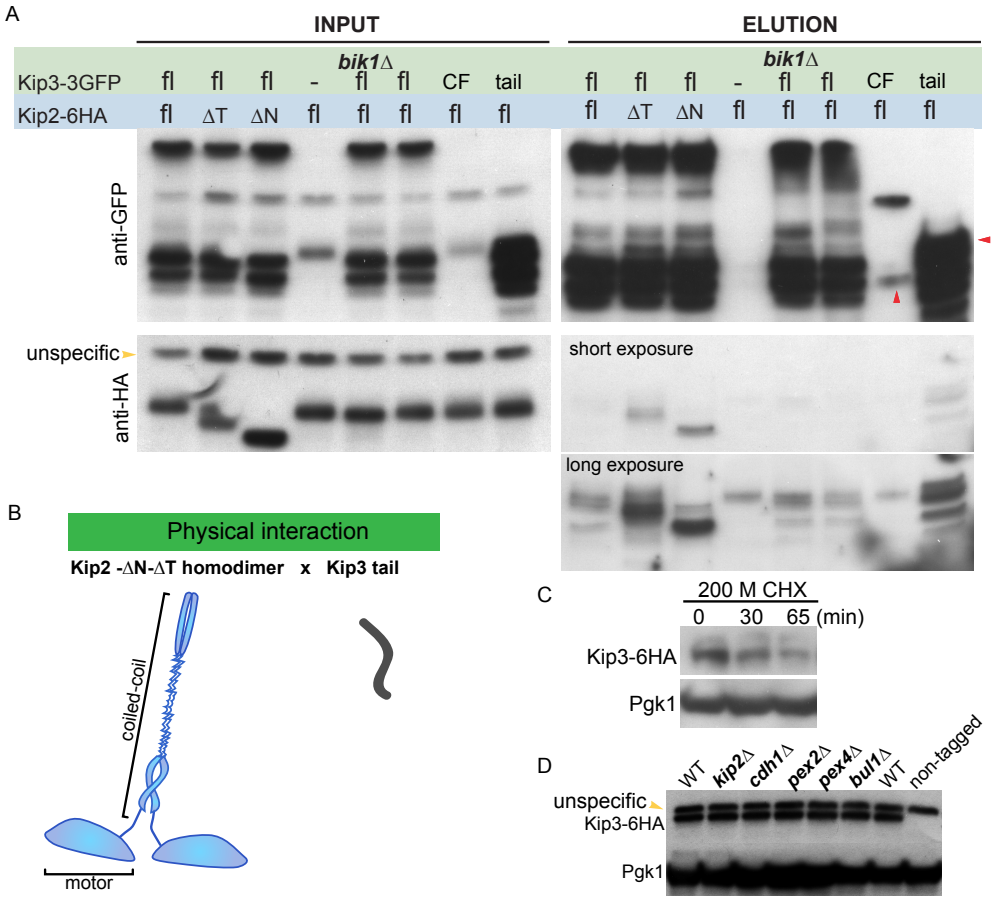

Figure 5.6 – Kip3 tail interacts with Kip2 independently of Bik1. (A) Endogenously expressed 3xsfGFP tagged Kip3 mutants coprecipitate with endogenously expressed 6xHA tagged Kip2 mutants. Lysates from cells expressing the indicated epitope-tagged proteins were immunoprecipitated with GFP-trap to precipitate Kip3 mutants and blotted with anti-HA mAb to detect Kip2 mutants. (preliminary result) (B) Illustration of current understanding of protein domians involved in Kip2-Kip3 interaction. (C) WB analysis for endogenously expressed Kip3-6HA 0 min, 30 min, and 65 min after the addition of 200 μM CHX. (D) WB analysis for endogenously expressed Kip3-6HA in indicated mutants. Pgk1 serves as loading control.

that the Kip3 tail was sufficient to bind Kip2. Although the Kip3 tail is dispensable for promoting rescue (Figure 5.2BCD), it may still be the target of Kip2 inhibition.

6

ASTRAL MICROTUBULE NETWORK ASYMMETRY IN MITOTIC BUDDING YEAST

Microtubules (MTs) establish a wide range of spatial patterns corresponding to their functions, the arrangement of which is specific to cell types. Microtubule patterning does not occur randomly, instead is primarily determined by distinct sub-cellular sites called microtubule-organizing centers (MTOCs), which are centrosomes in majority of eukaryotes, except plants and early mammalian embryos. In many epithelial cells, MTOC function enriches apically, generating MTs organized along the apical-basal axis. In contrast, MTs in neurons are distributed all along the lengths of axons and dendrites. Axonal MTs are uniformly arranged with their plus-ends toward the tip, whereas dendrite MTs have mixed polarity in most cases. Thus, the two co-existing MTOCs in asymmetrically dividing cells pose an interesting asymmetrical pattern of MTs.

MTs, among others, are asymmetrically organized in asymmetrically dividing cells. The alignment of the mitotic spindle with the cell polarity axis is achieved to ensure proper DNA segregation to both mother and daughter cells [Siller and Doe, 2009]. As a result, the two MTOCs on the two ends of mitotic spindles are spatially designated, one eventually is segregated into daughter cell and the other goes to mother cell. Interestingly, the spatial organization of MT arrays emanated by the two MTOCs is not random [Lerit et al., 2013]. For example, the MTOC proximal to the niche of *Drosophila* male germline stem cells (mGSCs) often associates with many MTs, whereas the distal MTOC usually associates with very few MTs [Yamashita et al., 2007]. Similarly, in *Drosophila* neural stem cells (NBs), MTs emanated from the MTOC designated to the future NB are more abundant, instead the MT cluster made by the MTOC proximal to the ganglion mother cell (GMC) is less abundant and shorter [Januschke and Gonzalez, 2010, Januschke et al., 2013]. The theme of asymmetric MTs continues in the most studied model system budding yeast. Similarly, one of the two budding yeast SPBs (yeast centrosomes) is positioned proximal to the bud neck (proximal SPB) and the other SPB is located distal to the bud neck (distal SPB). Consequently, two arrays of astral microtubules (aMTs) are nucleated by the two SPBs respectively, one facing the bud compartment and the other facing the bottom of the mom compartment (Figure 2.2B). These two arrays of aMTs have been observed to be morphologically distinct: the array nucleated by proximal SPB is usually

longer and more abundant than the array nucleated by the distal SPB [Shaw et al., 1997, Shaw et al., 1998, Segal and Bloom, 2001, Grava et al., 2006]. An obvious pattern is that MT arrays are consistently longer and more abundant toward the progeny with high proliferation potency in all these cases, which poses several fundamental questions: 1- How do polarized cells establish the asymmetric organization of MT arrays? 2- What are the functions of this asymmetric organization? 3- Why do polarized cells need asymmetrically organized MTs?

To begin to answer these questions, we work with *Saccharomyces cerevisiae*, frequently compared to stem cell divisions. Using the computer-assisted framework described in chapter 2, we compared the asymmetrical pattern of aMTs in various mutants, aiming to dissect and understand the establishment of this asymmetry.

6.1 The asymmetric organization of aMTs is independent of SPB history

In many eukaryotes, MTOCs are produced through conservative or semi-conservative duplication [Bornens and Piel, 2002, Barral and Liakopoulos, 2009]. In either case, this results in two co-existing MTOCs with different history: a pre-existing MTOC inherited from previous cell division and a newly assembled MTOC.

Like the MT arrays, MTOCs are segregated non-randomly. The coincidence of the pre-existing MTOC being segregated into the future stem cell progeny and it being associated with more abundant MTs has prompted a prevailing view of the history of MTOCs drives MT asymmetry. This view is based on the idea that MTOCs mature overtime and therefore the pre-existing MTOCs carry more abundant pericentriolar material (PCM) thus nucleate more MTs than the newly assembled MTOCs. While this is apparently true in the case of *Drosophila* mGSCs, the opposite has been observed in *Drosophila* NBs, where the newly assembled MTOC is associated with abundant and stabilized MTs. The correlation of the SPB history and aMT asymmetry has not been characterized in budding yeast.

To distinguish whether the new SPB is indeed not mature enough to nucleate aMTs or aMTs are simply destabilized in the mom compartment, we tested whether inverted spindles, i.e., spindles that oriented the new SPB toward the bud instead of the pre-existing one, still failed organizing long aMTs from the new SPB. We took advantage of the 'conservative' manner of incorporation for Spc72 [Lengefeld et al., 2017b]. Due to the relatively slow folding of yeGFP, the pre-existing SPB constituted of mature Spc72-yeGFP appears brighter comparing to the new SPB (Figure 6.1A). Using

Bik1-3GFP as aMT plus-end marker, we observed a measurable aMT (3D length $>$ 666.6 nm) on virtually all SPBs localized proximally to the bud neck, irrespectively of whether it was the pre-existing (92.1% of the cells) or the new (7.9% of the cells) SPB (Figure 6.1A). Very few cells formed a measurable aMT emanating from the distal SPB regardless of its history. Importantly, the length and lifetime of aMTs emanating from the proximal SPB exhibited undistinguishable distributions between pre-exisitng and new SPBs (Figure 6.1B).

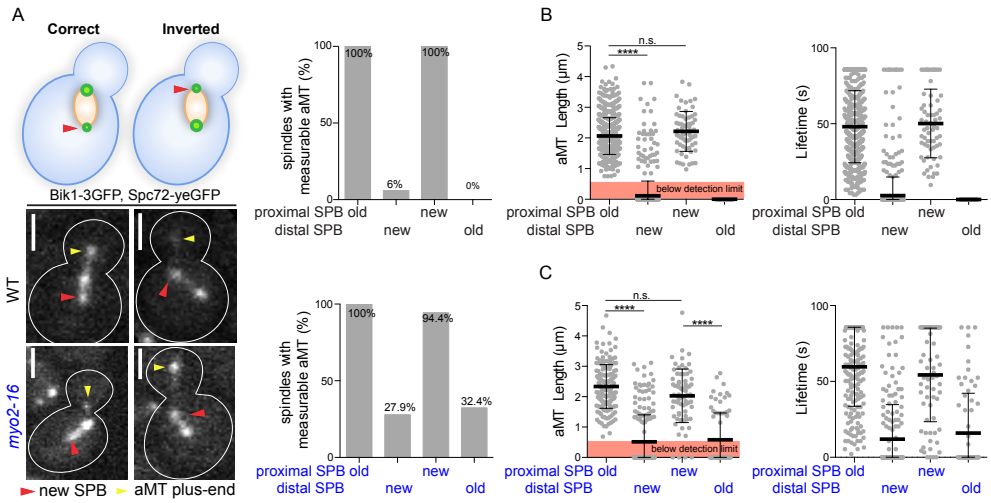

Figure 6.1 – Proximal SPB organizes long aMT regardless of its history. (A) Representative images and schemes of correctly oriented and inverted spindles with Spc72-yeGFP as SPB history marker and Bik1-3xGFP as MT plus-end marker. Due to the resolution limit of the microscope, an aMT was defined as measurable when its length was above 666.6 nm. Quantification of measurable aMTs from pre-existing or new SPB of correctly oriented or inverted spindles (%) in wild-type or *myo2-16* mutant cells (n $\geq$ 500 measured cells from 3 independent clones, mean $\pm$ s.d.) (B) (C) Average length (μm) and lifetime (s) of aMTs organized from pre-existing or new SPB of correctly oriented or inverted spindles in wild-type or *myo2-16* mutant cells. If the aMT length was below the detection limit, the point was counted as 0 (n $\geq$ 500 measured cells from 3 independent clones, mean $\pm$ s.d.). Statistical significance was calculated using two-tailed Student t-test on measurable dataset. **** $p <$ 0.0001, n.s. = none significant. Scale bars represent 2 μm. The new SPB is marked with a red arrow. The aMT plus-end is marked with a yellow arrow. *myo2-16* mutant cells were shifted from 25 °C to 30 °C for 2 h before imaging at 30 °C.

The 7.9% of inverted spindles may carry a inappropriately mature new SPB on the proximal side. To investigate this possibility, we asked whether artificially disorienting spindles cause the same behaviour. We made use of the *myo2-16* mutant, which lost the interaction between Kar9 and actin cables when grown at restrictive temperature and hence randomised spindle orientation [Schott et al., 1999, Yin et al., 2000]. Interestingly, all correctly

oriented and 94.4% of inverted spindles in *myo2-16* mutant cells organized measurable aMTs on the proximal SPB and much fewer on the distal SPB (Figure 6.1A). In the *myo2-16* mutant cells, the occupancy of aMT at distal SPB was higher compared to wild-type cells, but this effect was independent of the history of distal SPB. Again, the history of proximal SPB did not affect the distribution of aMT length and lifetime in the *myo2-16* mutant cells (Figure 6.1C). Altogether, these data strongly suggest that in metaphase, the new SPB is as competent as the pre-existing SPB in organizing aMTs. The asymmetrical aMT organization is independent of SPB history.

Two more pieces of data to strengthen this view. Firstly, the previous student Jette from the lab tested whether the aMTs emanated from the proximal SPB of the inverted spindles are fully functional in positioning and aligning spindles. She did not observe any difference between correctly oriented and inverted spindles, this result was published [Lengefeld et al., 2017b]. Secondly, the group of Prof. Jackie Vogel employed super-resolution microscopy to compare the amount of γ-tubulin complexes and their receptors Spc72 on the outer plaque of pre-existing and new SPBs, again no difference was observed [Lengefeld et al., 2017b]. All these results strongly suggest that the pre-existing and new SPBs in budding yeast are structurally and functionally equivalent to organize aMTs. In other words, aMT asymmetry is a regulated process and not simply determined by SPB history.

6.2 Spatial phosphoregulation of Kip2 contributes to aMT asymmetry organization

Since aMTs are consistently longer on the bud proximal side, it is natural to assume that either spatial cues exist in the bud or near the bud neck to stabilize proximal aMTs, or oppositely aMTs emanated on the distal side are de-stabilized, or both. One scenario will be one or several MAP's activities in stabilizing or de-stabilizing aMTs are spatially regulated. To narrow down the responsible MAPs, we performed a small scale screen covering the known budding yeast MAPs: Kip2, Kip3, Kar3, Dyn1, and Bim1 (Figure 6.2) by deleting the MAPs one by one and quantifying aMT behaviours. Here I define occupancy as the percentage of SPBs carrying measurable aMTs. Among all mutants quantified, occupancy of distal SPBs are always below 15%. Except that of the kinase mutants, which can reach 35%. Another exception is the *bfa1*Δ*bub2*Δ cells, the distal aMT occupancy reached 37.3% (140/375). In this aspect, I was not able to identify any mutant that could break the asymmetry of aMT occupancy. Since the distal occupancy is very low, hereafter I will focus on the asymmetry of aMT length and lifetime. Also, I will refer to the aMT length asymmetry as aMT asymmetry hereafter.

Bim1 stood out from the screen. Loss of Bim1 lead to even more asymmetric aMTs. Bim1 proteins strongly accumulate on proximal aMT plus-ends, thus it is not a surprise that Bim1 exhibited a stronger de-stabilizing activity on the proximal side. The other tested MAPs did affect aMT length in their own ways but did not have a large impact on aMT asymmetry. When tested in combinations, aMTs in *kip2*Δ *kip3*Δ cells were still very asymmetric, aMTs in *kip2*Δ *kar3*Δ cells were more symmetric, with a small number of quantified aMTs. A preliminary attempt to change tubulin composition of MTs by deleting TUB3 also did not demonstrate a strong effect on aMT asymmetry. So this screen was not able to identify a single MAP that dictates aMT asymmetry, however it is possible that not a single one MAP but two or more MAPs are involved to antagonize each other.

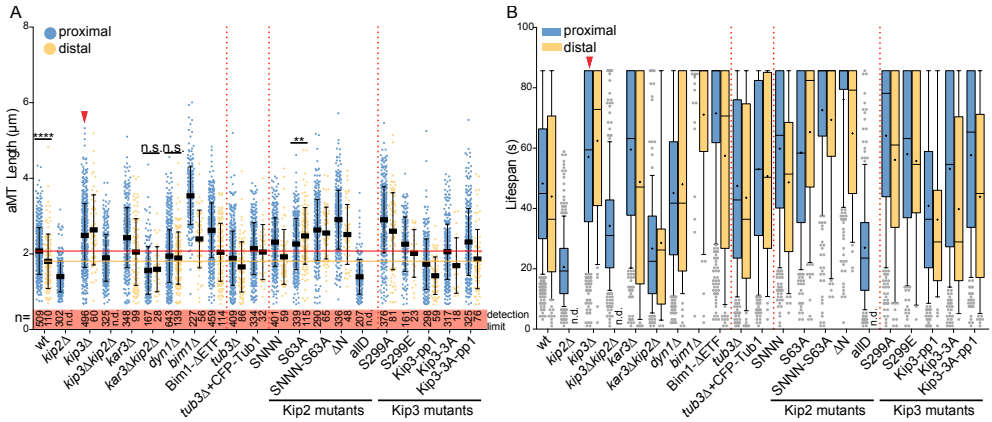

Figure 6.2 – Manipulations of the Microtubule Associated Proteins affect aMT asymmetry organization. (A, B) Quantification of the maximum 3D length (A) and lifetime (B) of metaphase proximal (blue) and distal (yellow) aMTs in indicated mutants. aMT length is represented with a scatter plot, each mutant comprises $\geq$ 200 metaphase cells from 3 independent clones, mean $\pm$ s.d. Statistical significance was calculated using two-tailed Student t-test on measurable dataset. **** $p < 0.0001$, n.s. = not significant. Lifetime of aMTs is represented with a box plot, the whiskers mark the 10-90 percentile, the bar in the middle of box represents median, the symbol + represents mean, the outliers are shown as grey dots. aMTs below detection limit are not represented here. For the following mutants, extra movies were acquired and with which only distal aMTs were quantified: wild-type, *dyn1*Δ, and Kip2-SNNN. The populations of which long and curved aMTs were not quantified are marked with red arrows. All mutants were cultured and imaged at 30 °C in synthetic media. The Kip3 mutants were acquired through CRISPR-cas9 system. n.d., not detected.

While being unproductive with the screen, a Kip2 mutant Kip2-S63A demonstrated extremely strong phenotype by reverting the asymmetry. Proximal aMTs were both longer in length and lifetime comparing to the distal aMTs in Kip2-S63A cells (Figure 6.2A,B). In addition, this strong phenotype was independent of Kip3 (data not shown) and the neighbouring 'SXIP' mo-

tif involved in potential interaction with Bim1. As described in chapter 3 and 4, the hypo-phosphorylated Kip2-S63A are recruited along the aMT shaft, therefore contributes stabilizing distal aMTs. Indeed, the reduction of Kip2 phosphorylation in Kip2-S63A cells stabilized aMTs on both proximal (2.08±0.62 μm to 2.26±0.68 μm, mean ± s.d., $p < 0.0001$) and distal (1.81±0.71 μm to 2.48±0.75 μm, mean ± s.d., $p < 0.0001$) sides, but with a much stronger effect on the distal side(Figure 6.2A,B). Consistent with the observation that Kip2-ΔN is not dominantly recruited along the microtubule shaft, aMTs in Kip2-ΔN cells are asymmetric with the proximal aMTs (2.91±0.77 μm, mean ± s.d.) being much longer than that of the distal aMTs (2.52±0.79 μm, mean ± s.d.). A comparison of aMT asymmetry between Kip2-S63A and Kip2-ΔN cells revealed that the regained asymmetry can be accounted for by the increased proximal aMT length (2.26±0.68 μm versus 2.91±0.77 μm, mean ± s.d., $p < 0.0001$) but no difference on the distal side (2.48±0.75 μm versus 2.52±0.79 μm, mean ± s.d., $p = 0.769$, n.s.) (Figure 6.2A,B). We reasoned that the interaction with Bim1 could specifically destabilize aMTs on the proximal side due to the highly asymmetric localization of Bim1 to the proximal plus-ends. To test whether Kip2-Bim1 interaction preferably destabilize proximal aMTs, we introduced mutations into the 'SXIP' motif (Kip2-SNNN) on Kip2 N-terminus to weaken its interaction with Bim1. Indeed, the disruption of the 'SXIP' motif prolonged proximal aMT (2.31±0.64 μm, mean ± s.d., $p < 0.0001$) but not distal aMTs (1.92±0.73 μm, mean ± s.d., $p = 0.318$, n.s.). Similarly, the disruption of 'SXIP' motif in Kip2-S63A cells (Kip2-SNNN-S63A) prolonged proximal aMTs (2.26±0.68 μm to 2.64±0.81 μm, mean ± s.d., $p < 0.0001$) but not distal aMTs (2.48±0.75 μm to 2.55±0.69 μm, mean ± s.d., $p = 0.497$, n.s.). With these data, we establish that Kip2-Bim1 interaction specifically destabilize proximal aMTs (Figure 6.3B left).

The loss of aMT length asymmetry in Kip2-S63A cells was largely a consequence of Kip2-S63A being recruited along aMT shafts. A second possibility causing very minor effect could derive from a slightly higher Kip2 phosphorylation level in the mom compartment (Figure 6.3B right). To test the hypothesis of higher Kip2 phosphorylation level in mom compartment, we made use of the Kip2-Δmotor mutants described earlier (Chapter 4). Kip2-Δmotor-3xsfGFP fusion proteins binds to aMT plus and minus ends by interacting with Bik1, high phosphorylation level on Kip2 N-terminus dissociates the fusion proteins from Bik1 thus off aMT plus and minus ends (Figure 4.6). If a gradient of Kip2 phosphorylation being higher on the distal side does exist, prevention or mimicking of Kip2 N-terminus phosphorylation should lead to more symmetric distribution of the fusion proteins bound to aMT plus and minus ends comparing to Kip2-wt-Δmotor-3xsfGFP. We quantified

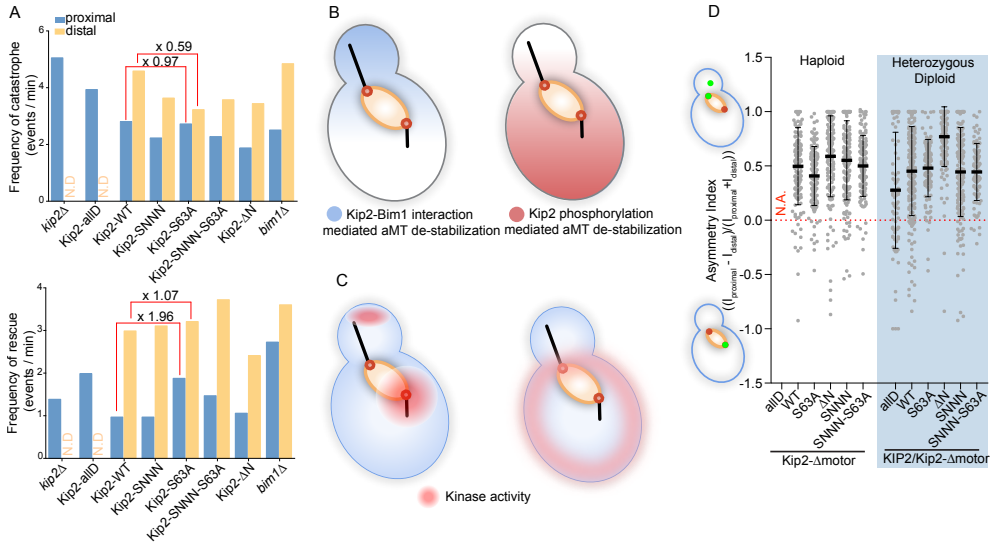

Figure 6.3 – Spatial phosphoregulation of Kip2 and Kip2-Bim1 interaction contribute to aMT asymmetry. (A) Quantification of the catastrophe and rescue frequencies of proximal (blue) and distal (yellow) aMTs in indicated mutants. (B) Graphic illustration of the effects of Kip2-Bim1 interaction and Kip2 phosphorylation on aMT dynamics in mitotic cells. (C) Quantification of asymmetry index $(((FI_{proximalplus-end} + FI_{proximalSPB}) - (FI_{distalSPB} + FI_{distalplus-end}))/(FI_{total}))$ of Kip2-Δmotor-3xsfGFP mutants in metaphase haploid and heterozygous diploid cells. n > 100 cells pooled from two independent experiments, mean ± s.d., Figure 6.2A)

the asymmetry index by dividing the difference between the fluorescence intensity of proximal and distal aMT bound Kip2-Δmotor-3xsfGFP fusion proteins by the total fluorescence intensity of aMT bound fusion proteins. Theoretically, this asymmetry index reaches the value of 1 when all of the aMT bound Kip2-Δmotor-3xsfGFP fusion proteins are on the proximal side and -1 when all of the aMT bound fusion proteins are on the distal side. The value would be 0 when it is perfectly symmetric. Introduction of Kip2-S63A did reduce the asymmetry index slightly (0.50±0.36 to 0.41±0.27, mean ± s.d.). Unfortunately the phosphor-mimic mutant Kip2-allD-Δmotor-3xsfGFP failed to bind aMTs, thus no asymmetry index was acquired. However, the phosphor-mimic mutant was able to bind aMTs in heterozygous diploid cells, in which the asymmetry index was reduced from 0.45±0.41 (Kip2-wt-Δmotor) to 0.28±0.53 (mean ± s.d.). These results suggest that indeed Kip2 phosphorylation level is higher in the mom compartment.

To identify the upstream kinases of Kip2 regulating aMT asymmetry organization, we took two approaches. First I tested all of the known kinases of Kip2, including Dbf2/Dbf20, Cdk1/Clb4, and Mck1. It has been suggested that Dbf2/Dbf20 primes the phosphorylation of Kip2-S63, subsequently Mck1 spreads the phosphorylation toward the upstream of the protein [Drechsler et al., 2015]. Although inactivating Cdk1 with the *cdc28-as1* strain [Ubersax et al., 2003] or by deleting the cyclins did not change Kip2 phosphorylation level in vivo, Cdk1 was able to phosphorylate Kip2 in vitro [Drechsler et al., 2015]. As predicted, depletion of these kinases individually resulted in longer aMTs, but the stabilization effect was strong on both proximal and distal sides (Figure 6.4). If anything, deletion of CLB4 even had a stronger effect on proximal aMTs comparing to distal aMTs. Being the main Kip2 kinase, inactivation of Dbf2/Dbf20 both at 30°C or at 37°C for 50 minutes did not weaken the aMT length asymmetry like the Kip2-S63A mutant did. We reasoned that Kip2 is unlikely the only Dbf2/Dbf20 substrate that contributes to aMT asymmetry, thus the unchanged asymmetry upon inactivation of Dbf2/Dbf20 could be a collective behaviour of phosphor-regulation of various MAPs down stream of Dbf2/Dbf20. Dbf2/Dbf20 is a central component of the Mitotic Exit Network (MEN), which has been established to be active already during metaphase to regulate the asymmetry of Kar9 localization and the history-dependent SPB segregation [Hotz et al., 2012]. We next tested whether another MEN kinase Cdc15 could affect aMT asymmetry. Similarly, inactivation of the *cdc15-1* allele by growing cells at restrictive temperature (37°C) for 50 minutes stabilized aMT on both sides but no effect on aMT asymmetry was observed. In the same line, we tested two more SPB inheritance network (SPIN) kinases Swe1 and Kin3 [Lengefeld et al., 2017a], these kinases ensure the faithful segregation of pre-existing SPBs into the bud. Consistent with the observation that SPB history does not control aMT asymmetry, loss of Swe1 or Kin3 had no impact on aMT behaviour and asymmetry(Figure 6.4). My attempt of screening through the classical networks involved in SPB or Kar9 asymmetry finishes with a Kar9 mutant baring an Alanine substitution on Ser197 (Kar9-S197A). Like Kip2-Ser63, Kar9-Ser197 resides in a tandem Dbf2/Cdk1 consensus site (RFAS[197]PIR). Also, Dbf2/Dbf20 dependent phosphorylation of Kar9 on Ser197 and two other serines has been shown to be important for the Kar9 asymmetry. Inhibition of Kar9 phosphorylation by S197A substitution lead to more symmetric Kar9 [Hotz et al., 2012]. Furthermore, Kar9 has been reported to interact with Kip2 basing on yeast two-hybrid experiments (Y2H) [Maekawa et al., 2003]. The similarities of Kar9 and Kip2 phosphor-regulation together with the potential physical interaction between the two make Kar9

a promising candidate of driving aMT asymmetry. Disappointingly, S197A substitution on Kar9 prolonged proximal aMT much more than distal aMTs (Figure 6.4).

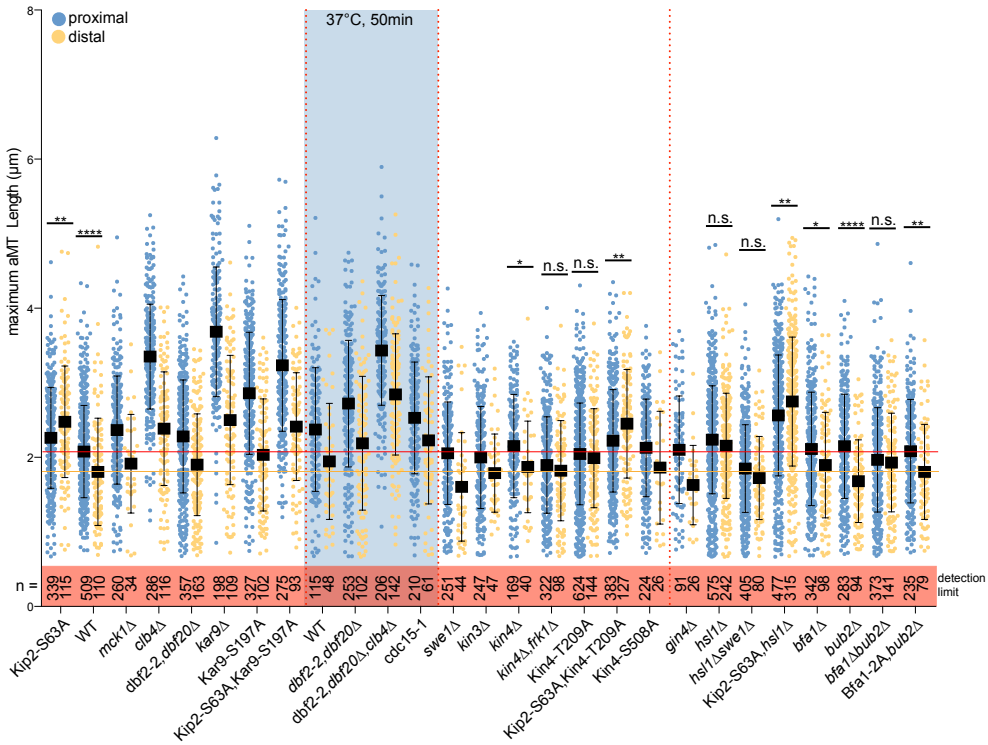

Figure 6.4 – Screening of potential kinases regulating aMT length asymmetry. Quantification of the maximum 3D length of metaphase proximal (blue) and distal (yellow) aMTs in indicated mutants. All mutants were cultured and imaged at 30 °C in synthetic media except those highlighted in a light box. aMT length is represented with a scatter plot, mean ± s.d. Statistical significance was calculated using two-tailed Student t-test on measurable dataset. **** $p < 0.0001$, *** $p < 0.001$, ** $p < 0.01$, n.s. = not significant.

It is clear that deletion of kinases is not the ideal way to narrow down the upstream factors, mainly due to the broad range of substrates of each kinase and the poorly understood kinase specificity. So we took another approach by further studying the consequences of Kip2 phosphoregulation. We quantified and compared the frequencies of catastrophe and rescue among several relevant Kip2 mutants. The frequencies of catastrophe and rescue were computed with events manually annotated and recorded with custom functions written in Matlab (MathWorks). Importantly, the slight but significant increase of proximal aMT length (2.08±0.62 μm to 2.26±0.68 μm, mean ± s.d.) in Kip2-S63A cells was mainly due to the almost doubled frequency of rescue (x1.96) and unchanged frequency of catastrophe(x0.97). Oppositely,

the rather large increase of distal aMT length (1.81±0.71 μm to 2.48±0.75 μm, mean ± s.d.) stems from the decrease of catastrophe frequency (x0.59) and unchanged frequency of rescue (x0.97). Kip2-S63A stabilizes proximal aMTs by increasing the frequency of rescue, whereas stabilizes distal aMTs by decreasing the frequency of catastrophe. There are two ways to interpret these observations, which will lead to two different predictions regarding where Kip2 should be highly phosphorylated.

The first way is to focus on the fact that rescue events always occur on shrinking MTs while catastrophe events only on growing MTs. Then the observation of spatial regulation of catastrophe and rescue can be translated: the reduction of Kip2 phosphorylation only affects rescue on proximal aMTs, suggesting Kip2 should be phosphorylated on shrinking aMTs; oppositely Kip2 should be phosphorylated on growing aMTs. The prediction will be the kinase activity source in the bud should be on proximal aMT plus-end or cortex, whereas the kinase activity in mom should be at the distal SPB (Figure 6.3C left). Cdk1/Clb4 and Dbf2/Dbf20 fall into this category. Both non-over-expressed Cdk1 and Clb4 proteins have been observed prominently on proximal aMT plus-ends in a Kar9 dependent way [Maekawa et al., 2003], which suggests that Cdk1/Clb4 could be more active on the proximal aMT plus-ends comparing to distal aMTs and that deletion of KAR9 or CLB4 should result in consistent aMT behaviour regarding asymmetry. When compared the aMT length and asymmetry between *clb4*Δ and *kar9*Δ cells, indeed in both cases aMTs are globally stabilized and the degrees of asymmetry were higher than wildtype cells. I devised a simple ratio to evaluate the degrees of aMT length asymmetry by dividing the proximal aMT average length by that of distal aMT, deletion of CLB4 or KAR9 increased this ratio from 1.15 (WT) to 1.41 and 1.47 (*clb4*Δ and *kar9*Δ respectively). Importantly, Kar9-S197A substitution was enough to increase the ratio to 1.41. Furthermore, depletion of the direct Kar9 interacting partner Bim1 increased the ratio to 1.48 (*bim1*Δ) as well(Figure 6.5A). These results demonstrate that Cdk1/Clb4 activity destabilizes aMTs globally, that this aMT destabilization is mostly executed via Kip2, and that this activity is much stronger on the proximal side (Figure 4.5). Also, the stronger Cdk1/Clb4 kinase activity on Kip2 relies on the proximal plus-end binding proteins Bim1 and Kar9.

Another way is to consider that rescue events tend to occur on short MTs while catastrophe events on long MTs. This allows one to speculate that Kip2 is phosphorylated on short aMTs close to bud neck on the proximal side; on the distal side, Kip2 is instead phosphorylated on long aMTs, for instance near mom cortex (Figure 6.3C right). This unique localization of kinase activity source does not imply a long list of candidates: kinases active on the bud neck and mom cortex during metaphase.

For the kinases active on the bud neck, we mainly tested the ones known to be involved in the septin cytoskeleton formation and stabilization: Cla4, Nim-related kinases Gin4, Kcc4, and Hsl1, also Eml1. These kinases localize at the bud-neck in a septin dependent manner and their activities contribute to the septin cytoskeleton organization. Extensive work on the septins have established the fundamental functions of septins in polarizing membranes and cell division ([Barral et al., 1999], reviewed in [Longtine and Bi, 2003, Spiliotis and Nelson, 2006, Bridges and Gladfelter, 2015]), so it is not a farfetched idea that these kinases could drive the asymmetry of aMTs as well, allowing the cooperation of septin cytoskeleton and MTs. Three of these kinases were eliminated by eye inspection: Cla4, Kcc4, and Elm1. Deletion of CLA4 or KCC4 did not lead to obvious change on aMT length. Similar with its paralog KCC4, loss of GIN4 did not perturb aMT organization (Figure 6.4). *elm1*Δ cells exhibited a strong phenotype of long buds due to the failure of transitioning from apical bud growth to isotropic bud growth, among the metaphase cells inspected, all of which had a extremely long proximal aMT accompanying the long buds, which leads to extremely asymmetric aMTs. Knowing the essential function of Nim-related kinases (Gin4, Kcc4, and Hsl1) and Swe1 in coordinating cell cycle progression and septin cytoskeleton [Barral et al., 1999], while none of the *gin4*Δ, *kcc4*Δ, and *swe1*Δ cells exhibited a weaker aMT asymmetry, it is a surprise to observe a strong reduction of aMT asymmetry both in length (ratio of proximal aMT length to distal aMT length from 1.15 to 1.03) and occupancy (distal aMT occupancy from 6.0% to 42.1%) in *hsl1*Δ cells (Figure 6.4). Taken together, the screen of bud-neck localized kinases gave rise to one single hit Hsl1.

Next, we continued to test kinases enriched on mom cortex during metaphase. One such well known kinase is Kin4, which localizes to mom cortex throughout the cell cycle and at the distal SPB during mid-anaphase, a player of the spindle position checkpoint (SPOC), which monitors spindle alignment and prevents cells with disoriented spindles from exiting mitosis by inhibiting MEN activity (reviewed in [Caydasi et al., 2010a, Caydasi and Pereira, 2012]). SPOC activity is only required in anaphase but Kin4 has been shown to be active throughout the cell cycle [Caydasi et al., 2010b]. So we went on to test whether the active Kin4 during metaphase could contribute to aMT asymmetry. To our disappointment, aMT length and asymmetry were not disturbed at all in *kin4*Δ cells (Figure 6.4). Since Kin4 was such an appealing candidate, we created a double mutant of Kin4 and its paralog Frk1 (*kin4*Δ*frk1*Δ) before giving up, of which the aMTs are more symmetric in length (proximal/distal length ratio from 1.15 to 1.04). In light of this observation, we reasoned that Frk1 could still be active in *kin4*Δ cells and if the kinase activity was essential for aMT asymmetry, a Kin4 kinase dead mutant should exhibit more

symmetric aMTs. Indeed, upon inactivating the kinase activity of Kin4 by substituting Thr209 to Ala (Kin4-T209A) [Chan and Amon, 2009], the distal aMTs were stabilized whereas proximal aMTs stayed un-disturbed (Figure 6.4). This biased stabilization of distal aMTs reduced the ratio of proximal to distal average length from 1.15 (wt) to 1.03 (*kin4*Δ)(Figure 6.5A). To dissect whether the restriction of Kin4 on mom cortex was important for its activity in aMT asymmetry, we introduced a Ser508 to Ala substitution (Kin4-S508A) to allow its spreading onto bud cortex while maintaining kinase activity [Chan and Amon, 2010]. Interestingly, no aMT behaviour changes were observed in these cells (Figure 6.4). With these results, we conclude that Kin4 is another kinase contributing to the aMT length asymmetry. Importantly, its kinase activity but not the distinct mom cortex localization is essential for its ability to establish or maintain aMT asymmetry. All of the known functions of Kin4 have focused on its critical role in surveillancing spindle position, on which its downstream factors are Bfa1 and Bub2. To test whether Kin4 employs the same signalling cascade for promoting aMT asymmetry, strains with single and double deletions of BFA1 and BUB2 were created. Interestingly, absence of Bfa1 or Bub2 alone was not sufficient to achieve symmetrical aMTs, only in *bfa1*Δ*bub2*Δ cells, aMTs were highly symmetric in length (mean proximal/distal ratio from 1.15 to 1.02)(Figure 6.46.5AB) and occupancy (distal aMT occupancy from 6% to 37.2%).

Taken together, the screen of kinases with two approaches was limited by the small number of candidates and the complicated output of each kinase mutant, but did shed light on several potential relevant kinases, including the known Kip2 kinases Cdk1/Clb4, Dbf2/Dbf20, the bud neck kinase Hsl1, Kin4 and its downstream factors Bfa1/Bub2.

6.4 DESTABILIZATION OF DISTAL AMTS DRIVEN BY HSL1 AND SPOC COMPONENTS

The screen did not allow me to pinpoint one or two kinases driving the process of aMT asymmetry explicitly, but revealed a pattern of spatial preference in regulating aMT length. For instance the Cdk1/Clb4, Bim1, and Kar9 mutants exhibited a stronger effect on proximal aMTs, MEN and SPIN related mutants did not demonstrate strong preference over proximal and distal aMTs. Importantly, loss of Hsl1, Kin4 kinase activity (Kin4-T209A) or its downstream factors Bfa1/Bub2 specifically stabilized distal aMTs whereas proximal aMTs were not disturbed, resulting in lower ratio of mean proximal to distal length (from 1.15 (wt) to 1.04 (*hsl1*Δ), 1.03(Kin4-T209A), and 1.02 (*bfa1*Δ*bub2*Δ) respectively)(Figure 6.5AB). Despite the slight stabilizing effect of proximal aMTs in Kip2-S63A cells, the S63A substitution lead to similar

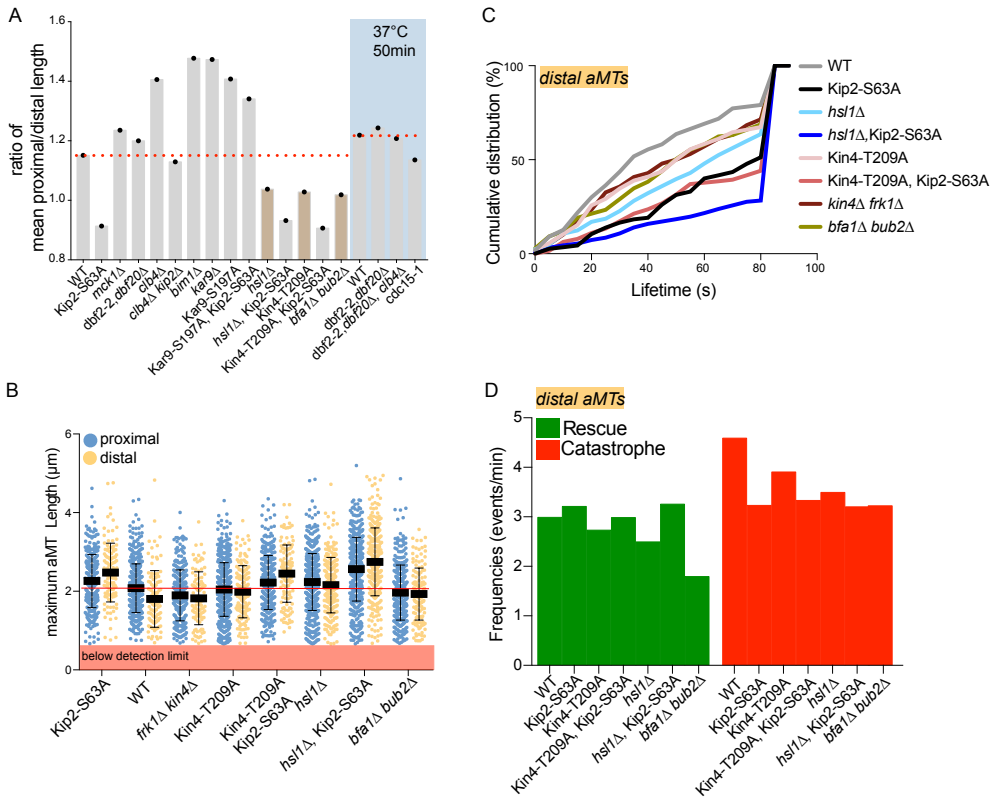

Figure 6.5 – Active de-stabilization of distal aMTs by Hsl1 and SPOC components in metaphase. (A) Ratio of the average proximal to distal aMT length in indicated mutants. (B) Quantification of the maximum 3D length of metaphase proximal (blue) and distal (yellow) aMTs in indicated mutants. All mutants were cultured and imaged at 30 °C in synthetic media. aMT length is represented with a scatter plot, mean ± s.d. Statistical significance was calculated using two-tailed Student t-test on measurable dataset. **** $p < 0.0001$, *** $p < 0.001$, ** $p < 0.01$, n.s. = not significant. (C) Quantification of the lifetime of distal aMTs in the indicated mutants, the lifetimes are represented in cumulative distribution plot. (D) Quantification of the frequencies of catastrophe and rescue of the distal aMTs in indicated mutants.

distal aMT biased stabilization (ratio of mean proximal/distal length to 0.91). To understand whether the bias toward distal aMTs in Hsl1 and SPOC mutants is mediated by Kip2 phosphorylation, we introduced Kip2-S63A in addition, and the degree of aMT length asymmetry was further reverted like in Kip2-S63A cells(Figure 6.5AB). Further comparison of distal aMT length and lifetime suggests the effect of Hsl1 and Kip2-S63A is mostly additive but Kin4 and Kip2-S63A seems to act through the same pathway (Figure 6.5BC). As described earlier, Kip2-S63A stabilizes distal aMTs mainly by inhibiting catastrophe (catastrophe frequency reduced from 4.59 (wt) to 3.23 (Kip2-S63A)) (Figure 6.3A). Interestingly, the Kin4 kinase-dead allele only decreased

the catastrophe frequency of distal aMTs to 3.91 (events/min); combination of Kin4-T209A and Kip2-S63A further reduced the catastrophe frequency to 3.33(events/min). These results suggest Kip2 as a downstream target of Kin4 in mom compartment. Together, Hsl1, Kin4 and Bfa1/Bub2 specifically destabilize distal aMTs to promote aMT length asymmetry. Phosphorylation of Kip2 could be one of the downstream event of Kin4.

6.5 Spatial phosphoregulation of other MAPs: Kip3 and Stu2

A more direct approach to identify aMT asymmetry promoting factors is to work with MAPs, more specifically to manipulate phosphorylation status of MAPs. To this stage, it is clear that aMT asymmetry is not driven by one or two kinases but several being distinctly active at various cellular locations. We came up with several criteria to make use of the information we have gathered. 1- The MAP should be one of the major aMT stabilizing or de-stabilizaing factors: Kip2, Stu2, Kip3, and Kar3; 2- The MAP should have potential or verified phosphorylation sites of Cdk1, Dbf2/Dbf20, Hsl1, or Kin4; 3- It is ideal that the MAP contains the signature Cdk1/Dbf2 tandem consensus site like that of Kip2-S63. Following these criteria, no such potential phosphorylation sites on Kar3 were found. However, interesting sites were found on both Kip3 and Stu2.

Kip3 is the main aMT de-stabilizing factor and counteracts with Kip2. Both Thr254 and Ser299 of Kip3 reside within the classical Cdk1/Dbf2 tandem consensus site (Figure 6.6A). To test whether T254 and S299 mediate spatial phosphor-regulation, alanine substitution of the two amino acids were generated on a plasmid and inserted into the endogenous locus. Unexpectedly, insertion of a selection marker (TRP or NatMX) downstream of KIP3 locus already affect aMT length and lifetime (Figure 6.6B). Nevertheless, a strong effect of Kip3-T254AS299A on reverting aMT length asymmetry is evident (Figure 6.6B). To avoid the insertion of any selection marker, CRISPR-Cas9 system [Laughery et al., 2015a] was employed to create the double alanine substitution strain. I was not able to successfully obtain the T254A substitution. Kip3-S299A alone resulted in long aMTs on both sides without changing asymmetry (Figure 6.2AB). Using the CRISPR-Cas9 system, I was able to obtain several more Kip3 mutants and none of which affected aMT asymmetry (Figure 6.2AB). With these preliminary results, Kip3-T254 becomes a promising site for spatial phosphor-regulation. A recent study identified the ability of Kip3 motor domain recognising and stabilising curved conformation of tubulin dimers to de-stabilize MTs [Arellano-Santoyo et al., 2017], a phosphorylation initiated switch within the motor domain to manage this activity will not be impossible.

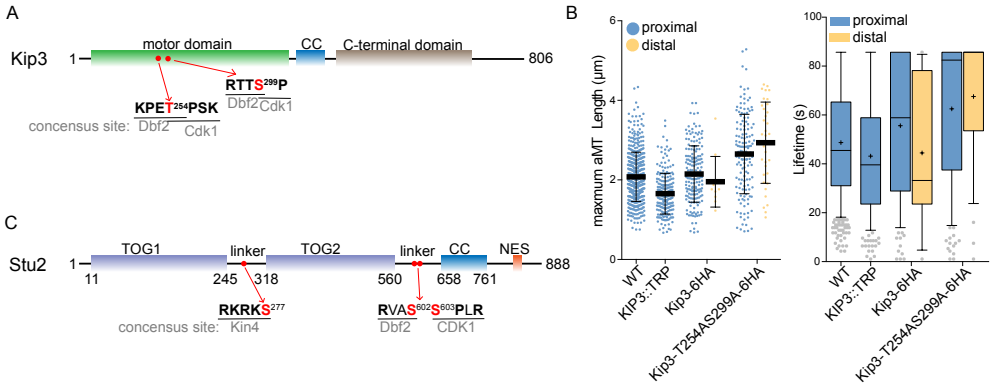

Figure 6.6 – Other potential MAPs as targets of spatial phosphoregulation. (A,C) Schematic drawing of domain organization and potential phosphorylation sites of Kip3 (A) and Stu2 (C). (B) Quantification of the maximum 3D length and lifetime of metaphase proximal (blue) and distal (yellow) aMTs in indicated mutants. Kip3::TRP represents the negative control of the insertion of a TRP cassette about 500bp downstream of KIP3 ORF. Kip3-6HA represents the negative control of fusing 6HA downstream of Kip3.

Stu2 is a MT stabilising factor for which plenty structural, biophysical, and cell biology data are available. However, how Stu2 affects and regulates aMT dynamics and organization in living cells is poorly understood. Structural studies propose that Stu2 employs its two TOG domains to recognize curved tubulin dimers and to recruit free tubulin dimers. Interestingly, a Kin4 consensus site (RKRKS-277) is found on the flexible linker between the two TOG domains (Figure 6.6C). In addition, two consecutive serines (RVAS-602S-603PLR) on the linker between the second TOG domain and its coiled-coil domain are consensus sites of Dbf2 and Cdk1 respectively (Figure 6.6C). Moreover, all of these three sites have been reported to be phosphorylated.

These potential spatially regulated phosphorylation sites on Kip3 and Stu2 are extremely interesting and worthy to follow up.

7 DISCUSSION

7.1 THE UNEXPECTED FUNCTION OF SPBS IN REGULATING MICROTUBULE PLUS-END DYNAMICS

The microtubule organizing centers (MTOCs), such as the mammalian centrosome or the yeast spindle pole body (SPB), have indispensable functions in organizing, nucleating, and anchoring microtubule arrays. Despite the remarkable progress made over the decades, no direct evidence ever demonstrated whether and how MTOCs can regulate the dynamics of microtubule plus-ends. We discovered that the budding yeast SPB controls the dynamics of plus-ends by recruiting and deploying Kip2 from minus-ends, which are anchored to SPBs. The high processivity of Kip2 allows all motors to reach plus-ends, thus the activity of SPBs recruiting Kip2 is transmitted to the amount of Kip2 on plus-ends, which in turn regulates the dynamics of plus-ends.

The anchorage of microtubules to MTOCs requires the γ-tubulin complex, which is further bound to γ-tubulin complex receptors. Interestingly enough, the receptors are a diverse group of proteins that could also function as γ-tubulin complex activators. In flies and worms, receptor proteins SAS-4/CPAP recruits not only γ-tubulin complexes, but also other PCM components [Kirkham et al., 2003, Gopalakrishnan et al., 2012]. In budding yeast, two different receptors (Spc72 and Spc110) anchor γ-tubulin complexes to the cytoplasmic and nuclear surface of SPB respectively, indicating that one MTOC can organize two different types of anchorage sites. Moreover, the XMAP215 homolog Stu2 interacts with Spc72 to contribute to the anchorage of microtubules at SPBs [Usui et al., 2003]. Such a pool of Stu2 has not been found on the nuclear surface of SPBs. What is the biological significance of such categorization? Our results show that the γ-tubulin complex receptor Spc72 indeed provides a 'microenvironment' on the cytoplasmic surface of SPBs, enabling the regulation of the plus-end dynamics from SPBs. The successful regulation relies on the following conditions.

Firstly, the recruitment of the kinesin to microtubule shaft must be prohibited. Kinesins are motor proteins hydrolyzing ATP to translocate along microtubules or depolymerize microtubules at plus-ends. Their moving direction, moving speed, processivity, and their forces generated by moving have been always in the spotlight of studies. However, the location from

which they are recruited and loaded onto microtubules was never an interest because so far none of the known kinesins demonstrated any preference, both in vivo and in vitro. We found that although Kip2, like others, can be loaded anywhere along the microtubule shaft in vitro [Hibbel et al., 2015], its loading along the shaft is mostly absent in vivo. This is strongly supported by the length independent accumulation of Kip2 molecules on plus-ends (supplement Figure 1B), as well as the flat, non null distribution of Kip2 between minus-ends and plus-ends (Figure 3.1B). The absence of Kip2 loading along the shaft in kymograph analysis further supports this notion (Figure 3.2B). Furthermore, the accumulation of Kip2 molecules that are deficient in ATP hydrolyzation near the SPB instead of along the microtubule shaft (Figure 3.4A). In contrast, Kip3 behaves consistently with what was observed in vitro. The Kip3 molecules accumulate along the microtubule shaft linearly from nearly undetectable near SPB to highly abundant in a length dependent manner (Figure 3.1A, supplement Figure 1A). The Kymograph analysis further validates that Kip3 is loaded randomly along the microtubule shaft (Figure 3.2A). It will be interesting to monitor whether the ATPase deficient version of Kip3 starts to appear all along the shaft. We further show that the inhibition of Kip2 loading along shaft is achieved by binding to its cargo Bik1. The paradox is that Kip2 transports Bik1 toward plus-ends by moving along microtubule shaft, whereas Bik1 inhibits its recruitment or association with shaft. This is still to be understood and will be further discussed later regarding the functions of Bik1.

Secondly, microtubule minus-ends or structures near minus-ends must be efficiently recruiting and loading the kinesin. In budding yeast, Spc97, Spc98, and Tub4 constitute the small γ-tubulin complex, which is recruited to the nuclear and cytoplasmic sides of SPB by Spc110 and Spc72, respectively (Figure 7.1). Defects in Spc72 and γ-tubulin complex interaction, in Spc72 and outer plaque SPB components (Nud1) interaction, and in Tub4 phosphorylation all eventually cause some degree of detachment of aMTs from SPBs, which is in agreement with the function of SPB anchoring aMTs. We found that Spc72 is not only important for the anchorage but also essential for the efficient recruitment of Kip2 to aMT minus-ends. More importantly, reducing the yeast polo-like kinase Cdc5 mediated phosphorylation on Spc72 by blocking its polo-box binding motif or inactivating Cdc5 substantially reduced the recruitment of Kip2 to SPBs (Figure 3.4B). Importantly, in *S. cerevisae*, Spc72 is stably incorporated into SPBs once it is recruited and organizes aMTs throughout the cell cycle. Thus the phosphorylation-based regulation fully coincides with its context. Furthermore, mass spectrometry based analysis of Spc72 phosphorylation revealed that phosphorylated Ser349Ser350 are also localized within a polo box binding motif [Keck et al., 2011]. It will

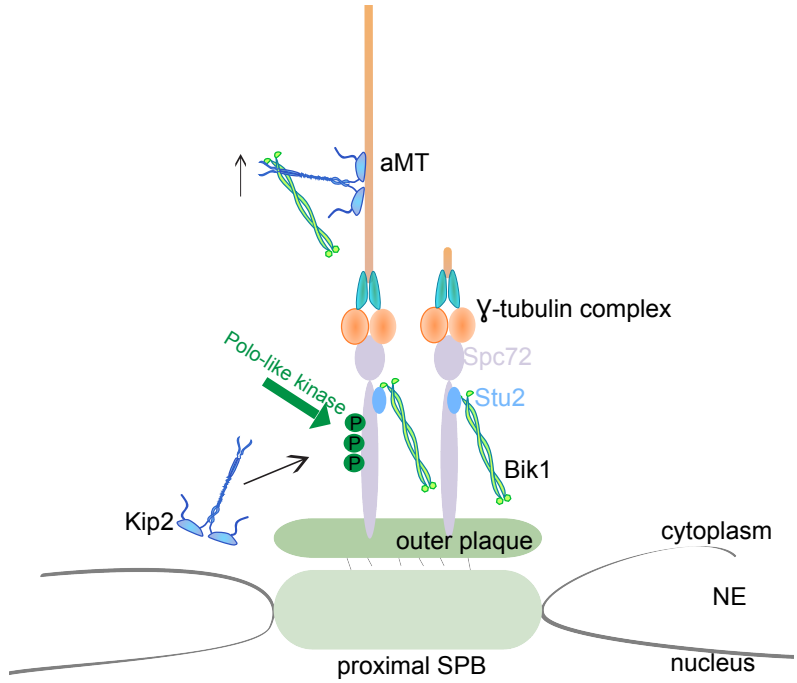

Figure 7.1 – Model of Polo-like kinase promoted Kip2 recruitment at the proximal SPB during metaphase. See discussion for details.

be important to test whether further substituting Ser349Ser350 with alanine will further dampen the Kip2 recruitment to SPBs. Finally, the ability of Spc72 to interact with Stu2 may facilitate the Kip2 recruitment. Stu2 binds to Spc72 even in the absence of microtubules: this is also the reason that Stu2 being considered as a SPB component. Although no direct interaction has been reported between Kip2 and Stu2, Stu2 has strong affinity toward Bik1, and their interaction does not compete with Kip2 for binding sites on Bik1 (unpublished, Marcel). Consistently, a stable pool of Bik1 has been shown to be present near SPBs and is dependent on Stu2. With these observations, one possible scenario is that the SPB pool of Bik1 facilitate Kip2 recruitment and deployment.

Thirdly, the kinesin must be processive and moves faster than the microtubule growth, ensuring the kinesin to reach the plus-end once deployed. Only then the amount of kinesins left the SPB will be equivalent to the amount that arrived at the plus-end. The activity of a SPB to recruit kinesin will be reflected by the dynamics of plus-ends. In vivo, Kip2 speckles (3.48 μm/min) move much faster than the microtubule growth at the same temperature (1.36 μm/min). Previous studies reported 6.6 [Carvalho et al., 2004] and 2.3 μm/min [Caudron et al., 2008] respectively, which is in the same range as our

measurement. Two independent in vitro studies reported that the run length of a single Kip2 dimer is about 4 μm [Hibbel et al., 2015] on its own or at about 4 μm in the presence of Bik1 and Bim1 [Roberts et al., 2014]. In either case, both Bik1 and Bim1 are present in wild-type cells and we observed high processivity for Kip2 even in *bim1*Δ cells where aMTs are very long. These features of Kip2 both in vitro and in vivo ensure its arrival at plus-ends once loaded from SPB.

In conclusion, we have shown that the processive motor and polymerase Kip2 is deployed from SPBs, thus the amount of Kip2 on plus-ends is dictated by the activity of SPBs recruiting and loading Kip2. The regulation of the Kip2 recruitment at SPBs reveals a novel mechanism with which cells harness microtubule dynamics. A length dependent depolymerase like Kip3 is expected to lead to a length dependent catastrophe frequency as well as a corresponding decrease in the relative spread of the length distribution. We have not been able to quantify the catastrophe frequency as a function of length in vivo, but the loss of Kip3 did lead to a broader spread of aMT length (Figure 2.5A). A polymerase with length insensitive activity instead is expected to maintain a minimum level of aMT length, and should not interfere with the length dependent catastrophe frequency. So in a wild-type population of cells, we should still expect a length dependent catastrophe frequency.

Further studies are required to reveal how Bik1 prevents Kip2 from associating with the microtubule shaft, and how Cdc5 mediated phosphorylation promotes the Kip2 recruitment to minus-ends. A good starting point is to ask where would Kip2 be associating with Bik1, where it will dissociate, or will Kip2 be dissociating with Bik1 at all? In the same line, is Kip2 recruited to minus-ends together with Bik1? or Kip2 assembles with Bik1 at minus-ends before its departure? Meanwhile, our results demonstrated that the Cdc5 mediated phosphorylation affected the bud-proximal Kip2 recruitment strongly, but not so much for the distal side. This indicates that either Cdc5 activity is much stronger on the proximal side or the kinase(s) priming for Cdc5 possesses stronger activity on the proximal side.

7.2 KIP2 MOTOR DOMAIN AS A MICROTUBULE POLYMERASE

Fast growth of microtubules is essential for the rapid assembly of the microtubule cytoskeleton during the cell division. Cytoplasmic kinesin Kip2 and the CLIP-170 homolog have long been implicated in polymerizing astral microtubules (aMTs). For a very long time, the accepted model was that Kip2 transports Bik1 as a cargo to microtubule plus-ends, such that Bik1 can stabilize microtubules. We revisited the topic and found that the motor

domain of Kip2 can both hydrolyze ATP to translocate along microtubules and also recruit free tubulin dimers to polymerize microtubule at plus-ends. Strikingly, Bik1 is indispensable for Kip2 to make the transition from motor protein to microtubule polymerase at plus-ends. These results explain the facts that both Bik1 and Kip2 are required to polymerize microtubules in vivo, and that over-expression of Kip2 alone in the absence of Bik1 does not promote microtubule polymerization at all.

7.2.1 *One motor, two functions, three tubulin interfaces*

Kinesin couples the cycle of ATP hydrolysis to its mechanical changes to carry out various cellular functions. The majority of the kinesins actively move along microtubules to transport cellular cargos. Another group like kinesin-13 family members, are not motile but depolymerize microtubules. A unique subfamily of kinesin superfamily, kinesin-8 members have been well known to possess both the microtubule based motility and the ability to depolymerize microtubules at plus-ends. Here we report the first kinesin motor domain that can both move along microtubules and polymerize microtubule at plus-ends.

To achieve the dual functions, Kip2 motor domain should meet the following two requirements: (1) the ability to adopt two different interfaces for straight microtubules and curved free tubulin dimers, and (2) the ability to recruit and concentrate free tubulin dimers at plus-end with high efficiency. The well studied kinesin-8 family members follow similar principles to coordinate their motility and depolymerase activity. Except that instead of recruiting free tubulin dimers, their motor domains stabilize the curved conformation of plus-ends to destabilize the microtubules [Ogawa et al., 2004, Shipley et al., 2004, Arellano-Santoyo et al., 2017]. To fulfill these requirements, we found that the Kip2 motor domain has developed distinct tubulin interfaces to differentiate free tubulin dimers from microtubules. Meanwhile, two of the tubulin interfaces confer its affinity to microtubule. Tubulin curvature is a simple structural mechanism by which kinesins can discriminate unpolymerized from polymerized-tubulin. Proteins that recognize curved $\alpha\beta$-tubulin tend to make long interfaces that span both α-tubulin and β-tubulin. So it will be very interesting to study whether the three tubulin interfaces of Kip2 make contact with the regions on $\alpha\beta$-tubulins that differ between curved and straight conformations. And whether the Kip2 motor domain was able to recognize the curved tubulins on plus-ends. Cooperative structural changes upon the interaction with curved tubulin dimers in not uncommom. For instance, kinesin-8 KIF19A put all three tubulin interfaces in use when on plus-ends, the retraction of one of the interfaces stabilizes the tubulin curvature [Wang et al., 2016]. To understand better how Kip2 coordinates the three

tubulin interfaces, a detailed structure of Kip2 together with tubulin will be helpful.

7.2.2 *How does a motor domain polymerize microtubules?*

Microtubule polymerization is achieved by accelerating growth to counteract depolymerization. Depolymerization usually involves the direct removal of tubulin dimers or the stabilization of tubulin curvature at plus-ends. In contrast, polymerization can be the result of the direct addition of tubulin dimers or the straightening of tubulin dimers on plus-ends. Kip2 motor domain forms a complex with free tubulin dimers in vitro (Figure 4.4), supplementing ATP during the motor domain purification promoted the tubulin and ATP bound motor domains to form 'assemblies' quickly. We are still in the process of understanding the nature of these 'assemblies' using electron microscopy. One possible scenario is ATP bound motor domain binds to free tubulins with very high affinity and concentrates them. Locally concentrating tubulins is a very effective way of polymerizing or even nucleating microtubules. For instance, Stu2/XMAP215 proteins use multiple free tubulin interacting TOG domains to tether and concentrate $\alpha\beta$-tubulin near plus-ends [Ayaz et al., 2014]. More recently, the centrosome of *C.elegans* has been shown to be able to nucleate microtubule aster in the absence of γ-tubulin by concentrating tubulins to be above the critical concentration for self-assembling [Woodruff et al., 2017]. Another intriguing observation is that like the nucleation factor XMAP215 [Wieczorek et al., 2015], Kip2 facilitates microtubule nucleation by lowering the nucleation critical concentration from 10 μM to 4 μM in their reconstituted system [Hibbel et al., 2015]. Basing on the nature of the motor domain and the absolute requirement of ATP for Kip2 to polymerize microtubules in vitro [Hibbel et al., 2015], we propose that ATP bound motor domain recruits and concentrates free tubulin dimers, whereas hydrolysis of ATP might reduce its affinity to tubulins, thus allowing the motor domain to efficiently repeat this cycle to boost the tubulin concentration near plus-ends.

Is Kip2 motor domain able to straighten the curved tubulins on plus-ends? To do this the motor domain has to be able to recognize microtubule plus-ends. In vitro the full length Kip2 resides at plus-ends for up to 30 $\pm$ 26 s before dissociating, which leads to the accumulation of Kip2 at plus-ends [Hibbel et al., 2015]. Since the rest of Kip2 protein has no affinity toward microtubules (Figure 4.2), we conclude that the motor domain does have a slightly increased affinity toward the plus-end comparing to the microtubule lattice. In vivo, cells defective in Kip2 and Bik1 interaction still accumulate a small amount of motors on plus-ends (Figure 3.3ABD), supporting the

notion that the motor domain can recognize plus-ends. However, those Kip2 motors seems to be incompetent in polymerizing microtubules (Figure 4.5). Altogether, it is unclear whether the Kip2 motor domain contributes to microtubule growth by changing tubulin curvature in vitro. Even if it does, its effect in vivo is minor.

7.2.3 *Phosphorylation mediated Kip2 inhibition*

When the cargo-binding domain of a motor protein is empty, often the kinesin auto-inhibits itself by blocking its motor domain with the cargo-binding domain [Hackney, 1995, Friedman and Vale, 1999, Coy et al., 1999, Liu et al., 2006, Torisawa et al., 2014, Cheng et al., 2014]. We found that the N-terminal low complexity fragment of Kip2 exactly prevents the autoinhibition like this to happen (supplement Figure 12). Instead, phosphorylated N-terminus occupies the C-terminal fragment of kip2 and prevents its interaction with Bik1, probably by introducing conformational changes of Kip2 or by occupying part of the region in Kip2-CF that is essential for Bik1 binding (Figure 4.7). Kip2 molecules with phosphorylated N-terminus have no affinity to Bik1 and lower affinity to microtubule [Drechsler et al., 2015]. Consistently, phosphomimetic Kip2 (Kip2-allD) is inactive in polymerizing microtubules (Figure 4.5A) and is less abundant on plus-ends (supplement Figure 11B).

Remarkably, the serine/threonine enriched low-complexity N-terminus of Kip2 is highly conserved among Saccharomycetales and with fission yeast Tea2 (supplement Figure 6). It is possible that these kinesin or kinesin-like proteins utilize similar mechanisms to control their activities.

7.2.4 *The multifaceted functions of Bik1*

The third requirement for a motor to polymerize microtubule is the ability to reside on plus-ends for some time. As discussed earlier, without interacting with Bik1, the majority of Kip2 molecules fail to be retained on plus-ends and fail to polymerize microtubule. Thus the central function of Bik1 in microtubule polymerization is to retain Kip2 on plus-end thus allow Kip2 motor domain to polymerize microtubules. Together with the results presented in Chapter 3 and earlier studies, I will discuss the multifaceted functions of Bik1.

FACILITATE THE LOADING OF KIP2 ON SPB A population of Bik1 has been reported to associate with SPB in a Stu2 dependent manner, and this population (halftime of recovery after FRAP 521 s, mean, range from 285

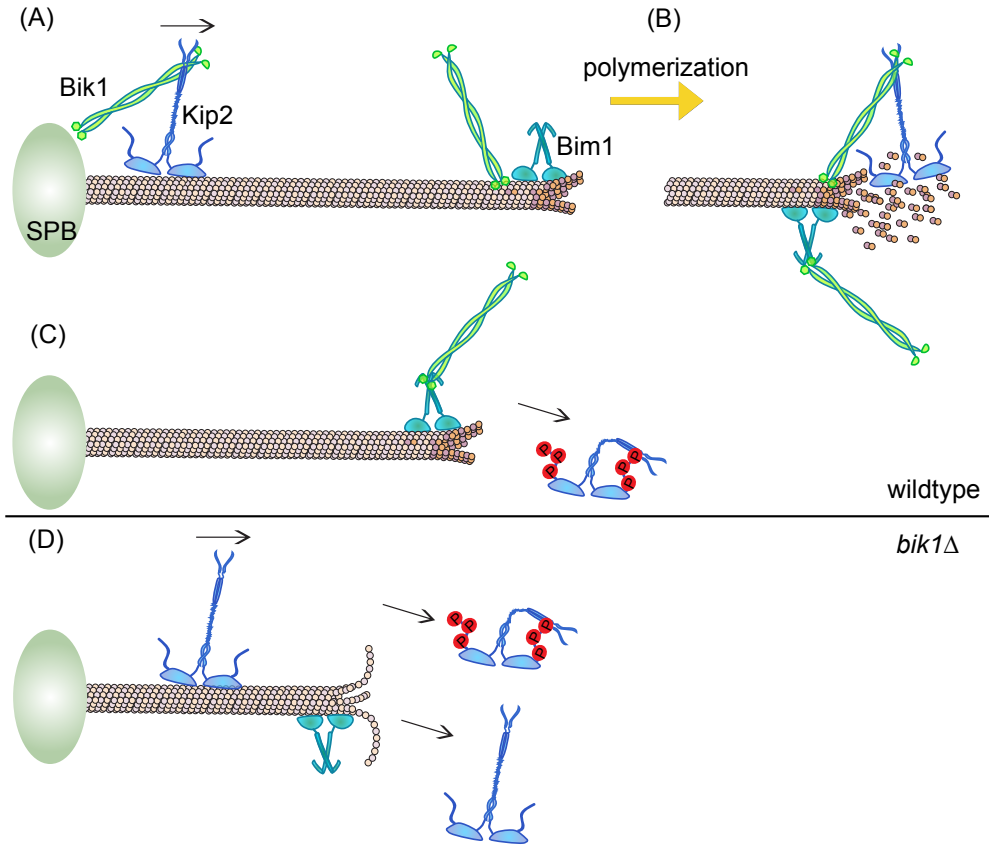

Figure 7.2 – Model illustrating the potential events underlying Kip2 and Bik1 mediated microtubule polymerization. Yellow arrow, microtubule growing and shrinkage status. Black arrow, the flow of Kip2 translocating along microtubules and dissociating from plus-ends. (A) Based on results from this study and earlier work. Kip2 departs from the microtubule minus-end together with Bik1 to travel toward the plus-end. Bik1 may increase the processivity of Kip2 together with Bim1. (B) Upon arrival at the plus-end, Bik1 binds to microtubules or Bim1 in the vicinity with its CAP-Gly domain, freeing the Kip2 motor domain from microtubules to recruit free tubulin dimers. (C) Accumulated phosphorylation on Kip2 N-terminus releases Kip2 from Bik1 and plus-ends, rendering Kip2 inactive. (D) In the absence of Bik1, Kip2 motors reach plus-ends and quickly fall off regardless of its phosphorylation state, thus fail to polymerize microtubules.

s to 864 s) of Bik1 turns over very slowly comparing to the pool on aMT plus-ends (halftime of recovery after FRAP 19.2 ± 12.9 s) [Carvalho et al., 2004]. Moreover, the abundant Stu2 that associates with SPBs by binding to Spc72 directly [Usui et al., 2003] maintains the SPB associated pool of Bik1. The function of this SPB associated pool of Bik1 is unknown. Both published data [Carvalho et al., 2004] and our own observation (supplement Figure 5) strongly demonstrate that indeed Bik1 travels with Kip2 along microtubules

to reach plus-ends. Remarkably, all of the observed Kip2-3xsfGFP and Bik1-3xGFP speckles depart from SPBs. We propose that this pool of Bik1 could be a storage with which Kip2 can assemble into complex with before the departure. [Carvalho et al., 2004] demonstrated that the SPB associated Bik1 is not essential for targeting Bik1 to plus-ends. Consistently, using the Kip2 ATPase deficient allele, we also show that they are not essential for Kip2 recruitment at SPBs.

RETAIN AND TIME THE RELEASING OF KIP2 ON PLUS-END Kip2 pre-assemble with Bik1 before departing at SPBs, which targets Bik1 to plus-ends. A change of perspective is in order here because all of the results indicate that Kip2 transports Bik1 for its own benefits. First, Bik1 may promote Kip2 processivity along aMTs. Second, Bik1 is required for Kip2 to be retained on plus-ends. The second point together with the Kip2 phosphoregulation proposes a model in which Bik1 gates the release of Kip2 at plus-ends. The strong interaction between Kip2 C-termini and Bik1 coiled-coil domain prevents Kip2 to dissociate from plus-ends. Only when Kip2 N-termini accumulate sufficient amount of phosphorylation, it will be allowed to dissociate from plus-ends. This model is supported by the following evidences. Kip2-CF (same as Kip2-ΔN-Δmotor) binds to Bik1 strongly both in vivo and in vitro, and the phosphorylated N-termini was sufficient to dissociate Kip2-CF from Bik1. Furthermore, the restoration of Venus intensity by phosphorylated Kip2 N-termini and Kip2-CF-ΔT was successful, indicating that the phosphorylation driven N-termini and C-termini interaction did not require Bik1. This also implies that phosphorylated Kip2 is unlikely to be in a complex with Bik1.

In *bik1*Δ cells, the release of Kip2 from plus-end is no longer controlled. They randomly associate along the microtubule shaft and move toward the plus-end. Upon arrival in living cells, the Kip2 motor domain itself only has very weak ability to stay on plus-ends, if at all. Thus Kip2 molecules quickly dissociate regardless of their phosphorylation state. One consequence is Kip2 is no longer active as a polymerase without being retained on plus-ends. A second consequence is unphosphorylated Kip2 released into cytoplasm may associate with microtubule shaft randomly, thus causing the uncontrolled loading in locations other than SPBs.

DOES BIK1 DIRECTLY CONTRIBUTE TO MICROTUBULE POLYMERIZATION? Differently with Bik1, its mammalian homolog CLIP-170 targets microtubule plus-ends by binding to EB proteins and uses the two CAP-gly domains to stabilize microtubule by copolymerizing with tubulins and promoting rescue [Komarova et al., 2002a, Arnal et al., 2004]. One study reported that full length

Bik1 in vitro not only fails to bind free tubulins but also inhibits microtubule assembly [Blake-Hodek et al., 2010]. However, the activities of Bik1 CAP-gly domain has not been tested in vitro so far. In our studies, we observed low Bik1-3xGFP intensity on plus-ends (around half of wildtype cells) in multiple cases where Kip2 molecules are still very abundant at plus-ends, including all of the Kip2-ΔT mutants and the Kip2-K294AR296A cells (supplement Figure 11B). The failure of interacting with Kip2 and being targeted to plus-ends in Kip2-ΔT cells can account for the low Bik1-3xGFP intensity. But not for Kip2-K294AR296A cells, in which Kip2-K294AR296A molecules still possess the domain that is involved in binding Bik1 and accumulate on plus-ends as efficient as wildtype Kip2 (Figure 4.3C). The nice retention on plus-ends also indicates that Kip2-K294AR296A still binds Bik1. Thus, targeting Bik1 to plus-ends with Kip2 motility is not sufficient for maintaining the abundance of Bik1 molecules, and yet another factor has to be involved.

One common feature of the Kip2-ΔT and Kip2-K294AR296A cells is that aMTs are not efficiently polymerized. We can imagine that very likely Bik1 is only accumulated during active incorporation of tubulin dimers. Although full length Bik1 did not show any affinity to free tubulins in vitro [Blake-Hodek et al., 2010], its CAP-gly domain intrinsically binds microtubule by recognizing the EEY/F motifs of Bim1 and α-tubulin. It could be that Bik1 faciliates microtubule polymerization by binding to the freshly incorporated tubulins and stabilize them. Intriguingly, when we were studying the in vivo functions of Bik1 CAP-gly mediated interaction with Bim1 and α-tubulin, we found that the interaction with Bim1 is important for Bim1 to remove Bik1 from the lattice and accumulate them on the plus-end, and that the interaction with α-tubulin is far more important, being essential for Bik1 functions (supplement Figure 14). Together, we speculate that Bik1 mostly interacts with microtubules directly in order to stabilize the transient feature after tubulin addition. Subsequent encounters with Bim1 allows Bim1 to collect Bik1 together with Kip2 to follow the dynamic plus-ends. Finally, the homologs of Kip2, Bim1, and Bik1 function as an efficient plus-end tracking system in fission yest [Bieling et al., 2007]. The dynamic interactions within these factors and with microtubule may be important for efficient tip-tracking.

7.3 A MODEL FOR REGULATING THE FLOW OF KIP2 AT THE MICROTUBULE MINUS-END AND PLUS-END

We have shown that Kip2 phosphorylation regulates both its loading at SPB and its dissociation at plus-end. When and where Kip2 gets phosphorylated or dephosphorylated is at the core to understand Kip2 regulation. To summarize the relevant knowledge about Kip2 phosphorylation: (1) in living cells,

Kip2 phosphorylation is mainly primed by Dbf2/Dbf20 and subsequently spread by yeast GSK3 (Mck1) [Drechsler et al., 2015]; (2) phosphorylation on N-terminus decreases the binding of Kip2 to microtubule [Drechsler et al., 2015]; (3) phosphorylation dissociates Kip2 from Bik1 (Figure 4.6 and 4.7); (4) unphosphorylated N-terminus prevents the recruitment of Kip2 at SPB (Figure 4.8). We propose the following model basing on these observations (Figure 7.3).

Kip2 must be phosphorylated in order to be recruited to SPB. Hence, prior to assemble with Bik1 and to translocate onto microtubule, Kip2 must be dephosphorylated. Next, Kip2 and Bik1 travel together till plus-end, where Kip2 is retained on plus-end by Bik1. Only when the low complexity N-terminus of Kip2 accumulates phosphorylation, Kip2 dissociates itself from Bik1, hence from the plus-end, by interacting with the coiled-coil domain of Kip2. We propose that Kip2 stays phosphorylated in cytoplasm for the following two reasons. One is that phosphorylation reduces Kip2 affinity to microtubule, which reduces the probability of random loading of Kip2 on microtubule shaft. The other is that phosphorylation benefits the recruitment of Kip2 to SPB. In this scenario, Bik1 fulfils the important role of gating unphosphorylated Kip2 at plus-end, where only phosphorylated Kip2 is released into cytoplasm. Furthermore, this model explains the random Kip2 loading along aMT shaft in *bik1*Δ cells due to the failure of retaining unphosphorylated Kip2 at plus-end, without affecting total Kip2 phosphorylation level (supplement Figure 9D). The unphosphorylated Kip2 diffusing in cytoplasm will bind to microtubule shaft with their motor domains, whereas the phosphorylated Kip2 will be recruited to SPB to enter the next cycle (model illustrated in Figure 7.3).

This model predicts that Kip2 is to be dephosphorylated at SPB before assembling with Bik1 and stepping onto microtubule. Also, Kip2 phosphorylation, or at least the 'amplification' of Kip2 phosphorylation should occur after the departure from the minus-end. Extensive cell based experiments suggested that the LATS-related kinase Dbf2 primes for yeast GSK-3 (Mck1) on Kip2 N-terminus [Drechsler et al., 2015]. Dbf2 kinase is a part of mitotic exit network (MEN) that is active already in metaphase and is required for correct spindle orientation [Hotz et al., 2012]. In contrast to the accumulation of Dbf2 at the bud-neck and SPBs, majority of the Dbf2 molecules diffuse in cytoplasm during metaphase. Thus it is unclear whether Dbf2 primes Kip2 phosphorylation near SPBs, along microtubules, or at plus-ends. Interestingly however, the potential Bim1 (EB1 homolog) binding site of Dbf2 (SxIP motif, residue 487-490) is essential for its activities in Kar9 asymmetry, spindle orientation, and mitotic exit (unpublished data, Manual Hotz, Barral lab). SxIP motif mediated interactions are usually relatively weak with the K_d value

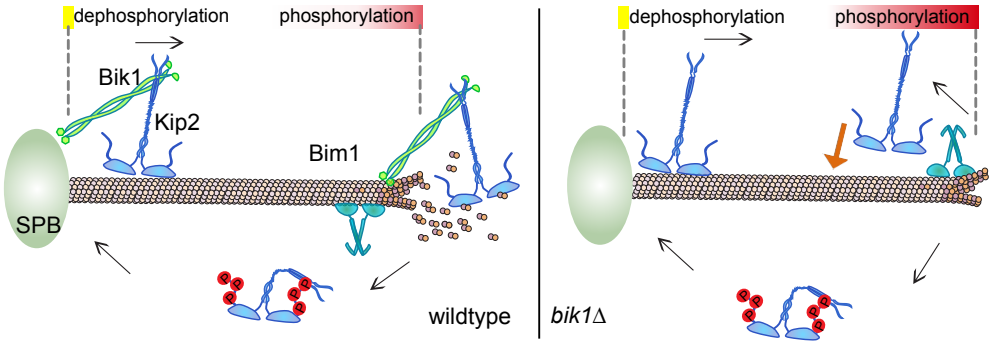

Figure 7.3 – Model illustrating the potential events underlying the Kip2 flow driven by the SPB and phosphorylation. Black arrow: the flow of Kip2 translocating along microtubules and dissociating from plus-ends. Orange arrow: aberrant loading of Kip2 along the microtubule lattice. In wildtype cells (left), Kip2 and Bik1 is deployed from the SPB where microtubule minus-end is anchored. Bik1 may increase the processivity of Kip2 together with Bim1. Upon arrival, Bik1 gates the release of Kip2 from plus-ends by binding tightly to unphosphorylated Kip2. In turn, phosphorylated Kip2 has low affinity to microtubule and is strongly recruited to SPBs. Dephosphorylation of Kip2 at SPBs might be required in order to start moving along microtubule. In *bik1Δ* cells, Kip2 can be released from plus-end quickly regardless of its phosphorylation status. Phosphorylated Kip2 can be recruited to SPB, while unphosphorylated Kip2 will bind the microtubule lattice randomly (orange arrow).

above 10 μM, thus it is possible that Dbf2 requires the dynamic interaction with Bim1 in order to be active. At this point the exact location at which Kip2 is phosphorylated is unclear, but our model predicts that it has to be on the microtubules. This prediction is supported by the fact that nocodazole induced microtubule polymerization abolishes Kip2 phosphorylation as quick as 20 min [Drechsler et al., 2015].

Although this model explains the majority of the observations we have made, the recruitment of Kip2-ΔN molecules to SPBs again is out of the picture. Overall, the unphosphorylated N-terminus antagonizes the SPB based regulation of Kip2 recruitment. Basing on current knowledge, we can only speculate that yet more factors may be involved.

7.4 The asymmetric organization of aMTs in metaphase

7.4.1 *The history of SPBs does not determine aMT asymmetry*

A prevailing model in the field proposes that the asymmetric aMT organization between the two mitotic MTOCs is driven by one of them being mature and fully active, whereas the other one is still immature [Lerit et al., 2013]. We tested this model in budding yeast and found it is not the case, rather it

is the result of regulations based on the spatial location of SPBs. We came to this conclusion for the following reasons.

First, analysis of the amounts of γ-tubulin complex and its receptor Spc72 on the outer plaques of the pre-existing and new SPBs establishes that very early on into the metaphase these structural components are already equivalent between the two SPBs [Lengefeld et al., 2017b]. Second, Spc72 is a stable component of the outer plaque and exchanges little between the two SPBs [Lengefeld et al., 2017b]. Third, having clarified that the two SPBs are equivalent structurally, comparing the dynamics of proximal aMTs nucleated by pre-existing and new SPBs further validates that the history or maturation of the SPBs does not determine aMT asymmetry. These results indicate that the proximal SPB is positioned in a microtubule stabilizing area, its MTOC activity is higher independently of its history.

Kar9 asymmetrically associates with proximal SPB and bridges the aMT plus-ends with actin cytoskeleton to ensure the positioning of mitotic spindles [Theesfeld et al., 1999, Beach et al., 2000, Yin et al., 2000, Hwang et al., 2003, Liakopoulos et al., 2003]. One possible way of regulation is the signalling pathways driving Kar9 asymmetry also determines aMT asymmetry. Both the MEN pathway [Valerio-Santiago and Monje-Casas, 2011, Rock et al., 2013] and the SPIN [Hotz et al., 2012, Lengefeld et al., 2017a] contribute to control Kar9 asymmetry. However, aMTs in *kar9*Δ cells and MEN pathway mutants are even more asymmetric. In the same line, none of the tested SPIN mutants demonstrated significant defect in aMT asymmetry. Consistently, in *myo2-16* mutant cells, the two SPBs show an equal probability of being proximal to the bud and are equally competent to organize aMTs. Yet, Kar9 still preferentially associates with the pre-existing SPB [Lengefeld et al., 2017b]. Thus it is unlikely that Kar9 drives aMT asymmetry. However, we can not exclude the possibility of the MEN or SPIN components contributing to aMT asymmetry due to their broad range of substrates.

7.4.2 *Potential spatial imbalance of kinase activities*

The compositions of +TIPs decorating the two aMT arrays are vastly different. For instance Kar9 and Bim1 are much more abundant on proximal aMT plus-ends [Maekawa et al., 2003, Liakopoulos et al., 2003]. Another layer of the differences could originate from the differential post-translational modifications of those factors. It has been shown that the cyclin dependent kinase Cdc28, in complex with cyclin Clb4, only associates with the SPB and aMT projected into the bud [Maekawa and Schiebel, 2004]. Although the proximal side dominant localization of Cdc28/Clb4 relies on one of its substrates Kar9, the phosphorylation it introduces on Kar9 instead takes Kar9

off the distal side [Hotz et al., 2012]. At this stage it is unclear whether the activity of Cdc28/Clb4 is stronger on one side of the mitotic spindle, however evidently, the phosphorylation of +TIPs can be differentially regulated on the two sides of mitotic spindles.

Our observation that the Kip2 phosphoablative mutant (Kip2-S63A) causes a much stronger effect on the distal aMT length and lifetime further supports this idea. We have found a situation in which the SPBs have no direct control over the Kip2 recruitment to aMTs by removing the motor domain completely (Kip2-Δmotor). Using the Kip2-Δmotor system, we found that the distribution of phosphomimetic Kip2-allD-Δmotor is more symmetric whereas Kip2-S63A-Δmotor is more asymmetric. One plausible interpretation is that the Kip2 phosphorylation level is slightly higher in the mom compartment. GSK-3 (Mck1) accumulates on bud cortex in early metaphase [Drechsler et al., 2015]. Thus, the prediction is the Dbf2 activity in the mom compartment is higher than that in the bud. Nevertheless, the inactivation of Dbf2 is not able to abolish the aMT asymmetry. One scenario is that Dbf2 ensures the distal aMTs are short, while another or several other kinases might be involved in stabilizing proximal aMTs. It is important to note that, Kip2 phosphorylation level is not changed in Cdc15 mutants [Drechsler et al., 2015]. Furthermore, the reduction of Kip3 phosphorylation by substituting the potential Dbf2 sites Thr245 and Ser299 with alanine (Kip3-T245AS299A) prolonged distal aMTs more than that of proximal aMTs, resulting in reverted asymmetry (preliminary results, Figure 6.6). Thus, Dbf2 could act on multiple MAPs, especially microtubule polymerases and depolymerases, to ensure the destabilization of distal aMTs.

The most well studied function of Dbf2 is its involvement in the mitotic exit, which is required in the late stage of the mitosis and its functions are SPB based [Bardin and Amon, 2001, Queralt and Uhlmann, 2008]. Also, it has been found to be active already during early mitosis [Hotz et al., 2012] for the correct spindle positioning when the majority of Dbf2 is still diffusing in the cytoplasm. Interestingly, Dbf2 activity is also required for mild acid stress response. It does so by phosphorylating V-ATPase subunits Vma1 and Vma2 to regulate the V-ATPase activity[Valerio-Santiago and Monje-Casas, 2011]. It would be interesting to test whether the V-ATPases in the mom compartment responds better or faster to acid stress. Another interesting aspect is testing whether Dbf2 is involved in other stress responses, ageing and memory formation. The potential asymmetry of the Dbf2 activity could have broad implications on these cellular processes.

7.4.3 *SPBs based regulation of aMT asymmetry*

Since the maturation or history of the budding yeast MTOCs does not control aMT asymmetry and their γ-tubulin complex receptor Spc72 is stably incorporated [Lengefeld et al., 2017b], SPBs provide a perfect platform to carry information that could further be transmitted to differential lengths of aMTs that they nucleate. We described such a mechanism in Chapter 3, which relies on the polo-like kinase Cdc5 mediated phosphorylation of Spc72 to recruit microtubule polymerase Kip2. Remarkably, the proximal SPB has much stronger activity in recruiting Kip2 compared to the distal SPB. Also, the proximal SPB makes a long aMT whereas the distal SPB only makes a very short one (Figure 3.4). This strong correlation indicates that the important function of SPBs in dictating aMT asymmetry. Moreover, failing the SPB based recruitment of Kip2 by the phosphoablative mutant Kip2-S63A (Figure 4.8A) drastically reduces the SPB biased aMT asymmetry. Now that the potential events on the proximal SPB is better understood, further work is required in order to understand whether the distal SPB recruit Kip2 with a similar mechanism, and whether more kinases or more layers of regulations are in play.

Among the hits from the aMT asymmetry screen, mutants like Kin4-T209A (kinase-inactive) and *bfa1*Δ*bub2*Δ establish symmetric aMTs mostly by stabilizing distal aMTs (Figure 6.5). It is unclear whether this is achieved through SPB-based regulation, but Bfa1 and Bub2 are both SPB associated proteins through out the cell cycle. Similarly, although Cdc5 inactivation caused a strong reduction of Kip2 recruitment specifically at proximal SPB (Figure 3.4), the symmetry of aMTs is the result of the stabilization of distal aMTs. Interestingly, all of these molecules have been shown to bind to Spc72 and Spc72 serves as a scaffold to transmit spindle positioning signals [Snead et al., 2007, Gryaznova et al., 2016, Caydasi et al., 2010a]. This network might be active early in metaphase and contributes to aMT asymmetry.

Although we found that unlike Drosophila NBs and mGSCs, the maturation of yeast MTOC does not determine aMT asymmetry, a common central player is the polo-like kinase. Both the localization and activity of polo-like kinase is strongly correlated with the abundant aMT array in Drosophila NBs [Rusan and Peifer, 2007, Singh et al., 2014]. Do higher eukaryotes also promote MTOCs based recruitment of polymerases to stabilize one of aMT arrays with bias? The current model proposes that polo kinase both phosphorylates centrobin (CNB) [Januschke et al., 2011] and recruits γ-tubulin complexes [Glover, 2005], which explains the biased occupancy but not the length of aMTs. Thus, further work is required to test this hypothesis in higher eukaryotes.

8

MATERIALS AND METHODS

8.1 STRAINS AND PLASMIDS

Yeast strains and plasmids used in this study are listed in the supplement tables. All strains are isogenic to S288C, more specifically, they are all derived from the Barral lab yYB384, unless specified otherwise. All gene deletions were created using the PCR-based integration system [Janke et al., 2004] and gene deletions were verified by PCR analysis. Fluorescent or HA-tagged proteins were tagged at endogenous loci [Knop et al., 1999]. Specific Kip2 mutations were introduced on a pRS314-Kip2-3xsfGFP:KanMX plasmid or a pRS304-Kip2 plasmid via site-directed mutagenesis (pfu-Turbo, Stratagene). Kip2 locus was then amplified and integrated in a *kip2*Δ strain and the correct integration was verified by PCR and sequencing. Same methods were applied for Kip3 mutants. Some strains were created with CRISPR-Cas9 system as indicated [Laughery et al., 2015b], the oligonucleotides and plasmids used are in the supplement material of this thesis. Plasmids for Bimolecular Fluorescence Complementation(BiFC) assay were a gift from S. Michnick. Kip2 fragments, BIK1 and BIM1 ORFs were amplified from the genome, integrated in to the BiFC plasmids by homologous recombination and the plasmid sequences verified by sequencing.

8.2 MEDIA AND GROWTH CONDITIONS

Cells were cultured in YEPD (yeast extract peptone) or SC (synthetic medium) containing 2% dextrose. Cells for BiFC assay were obtained fresh by transformation and cultured in SC-Leu-His medium. Temperature sensitive mutant strains were diluted to OD_{600} 0.15 and cultivated at 25°C for 4 hours then shifted to 37°C for 50min before analysis. For live cell imaging, overnight cultures in SC were diluted to OD_{600} 0.15 and cultivated for 4 more hours before placed on an SC-medium agar patch for microscopy imaging.

8.3 FLUORESCENCE MICROSCOPY

An Nipkow spinning disk (Carl Zeiss) equipped with an incubator for temperature was employed. Time-lapse movies were acquired using a back-

illuminated EM-CCD camera Evolve 512 (Photometrics, Inc.) mounted on the spinning disk microscope with a motorized piezo stage (ASI MS-2000) and 100x 1.46 NA alpha Plan Apochromat oil immersion objective, driven by Metamorph based software VisiVIEW (Visitron Systems). 17 Z-section images separated by 0.24 μm increments were captured with the exposure time of 30ms each, the whole stack took 1.07s. For imaging aMT dynamics, 80 continuous repetitions were taken. For imaging strains with both GFP and mCherry signals, the GFP channel was always set to 30ms exposure time and the mCherry channel with 50ms exposure time. For diploids cells expressing Kip2-mCherry, the exposure time was set at 100ms for mCherry channel. Images in figures represent sum fluorescence intensity Z-projections. Scale bars represent 2 μm.

8.4 IMAGE AND DATA ANALYSIS

Pre-anaphase cells were manually collected based on the shape of cells and the size of spindles. To determine the length of astral microtubules, three-dimensional coordinates of microtubule +ends and the corresponding SPB were extracted with the Low Light Tracking Tool [Krull et al., 2014]. The distance between an aMT plus-end and the corresponding SPB represents the length of microtubule, the distance between the proximal and distal SPBs is the spindle length. Cells with spindles longer than 2 μm were excluded. All of the time series tracking results were analyzed with custom functions written in Matlab (MathWorks).

For fluorescence intensity, a Region Of Interest (ROI) was drawn around the area of interest (AOI) and the integrated density was quantified. An identically sized ROI was put next to the AOI to determine the background signal. The background intensity was subtracted from the ROI intensity to yield the fluorescent intensity (AU). For every experiment that was performed for quantification of fluorescent intensity (AU), corresponding wild type cells were imaged and analysed for comparison to mutant cells. Average values of wild type cells of different experiments were used for normalisation and comparison between experiments.

For analyzing the profiles of GFP fusion proteins along aMTs, the sum intensity projection of the images was used. A 5 pixel (666.7 nm) width line was used to scan aMTs from plus-ends toward SPBs.

For analyzing the BiFC experiment images, regions of interest of Venus signals were created as the following: the max intensity projection of the

image was duplicated and smoothed with different Gaussian blurs (sigma 3 and sigma 4), then subtracted from each other. The result image was converted to a binary mask applying the same threshold for all images. 'Analyze Particles' function was used to create regions of interest of the original max intensity projection image. The sum of all mean intensities of individual metaphase cells was divided by the total number of metaphase cells (which includes cells that displayed no Venus signal) to obtain the average Venus intensity per metaphase cell.

8.5 WESTERN BLOTS

For protein extraction, 2 OD_{600} log phase cell cultures were spun down and pellets were washed once with ice cold PBS, then lysed with Zirconia-Silicate beads in lysis buffer (50mM Tris pH 7.5, 150mM NaCl, 0.5mM EDTA, 1mM MgCl2, Roche Complete Protease and phosphatase inhibitors and 0.2% NP-40) on a FastPrep-24 homogenizer. Lysate was cleared by centrifugation at 5000 x *g*, 4°C for 5min. For phosphatase treatment, phosphatase inhibitor was excluded from the lysis buffer, samples were incubated at 30°C for 30min with λ -phosphatase (New England Biolabs). For western blot, samples were separated on a 6% SDS-polyacrylamide gel (SDS-PAGE), wet-transferred on a polyvinylidene fluoride (PVDF) membrane for western blotting. Antibodies used were primary antibodies anti-GFP (1:1000, mouse monoclonal, Roche), anti-HA (1:1000, mouse monoclonal, Covance Inc.), anti-Pgk1 (1:4000, mouse monoclonal, Invitrogen), anti-Puf6 (1:1000, Rabbit polyclonal, a gift from Prof. Vikram Panse, UZH) and secondary antibodies goat anti-Rabbit IgG conjugated to horseradish peroxidase (1:5000, Bio-Rad) and goat anti-Mouse IgG conjugated to horseradish peroxidase (1:5000, Bio-Rad).

8.6 MN^{2+}-PHOS-TAG SDS-PAGE

For whole cell lysate samples of Mn^{2+}-Phos-tag SDS-PAGE, EDTA was excluded from the lysis buffer. Phos-tag Acrylamide (WaKo Pure Chemical Industries Ltd.) concentration was optimized to 25μM. Samples were separated on a 6% Mn^{2+}-Phos-tag SDS-PAGE. For optimal separation of phosphorylated and non-phosphorylated protein species, the power supply was set to be at 20mA/gel constant current and electrophoresis required around 5 hours for completion. For transfer of gel separated proteins to PVDF membranes, gels were washed 3 x 10min with transfer buffer containing 10mM EDTA. The rest of the procedure was consistent with usual western blot.

8.7 CO-IMMUNOPRECIPITATIONS

Extracts were prepared from 30 OD_{600} cells as described above. Equal volumes of extracts from equal OD_{600} cells were immunoprecipitated with 25μl equilibrated GFP-Trap_A (Chromotek) beads for 3 hours at 4°C. After washing the beads 5 x 5min with wash buffer (10mM Tris pH7.5, 400mM NaCl, 0.5mM EDTA), proteins were eluted by boiling beads in Laemmli buffer.

8.8 STATISTICS

Each experiment was repeated with three or more independent clones (biological replicates). The standard deviation (s.d.) of independent clones is shown in the graphs, or as indicated. n.s. (not significant) or asterisks indicate P values from Student's t-test or one-way ANOVA as indicated. Except that the differences of cumulative distributions were evaluated by Kolmogorov-Smirnov test. No statistical method was used to predetermine sample distribution.

BIBLIOGRAPHY

[Aillaud et al., 2017] Aillaud, C., Bosc, C., Peris, L., Bosson, A., Heemeryck, P., Van Dijk, J., Le Friec, J., Boulan, B., Vossier, F., Sanman, L. E., et al. (2017). Vasohibins/svbp are tubulin carboxypeptidases (tcp) that regulate neuron differentiation. *Science*, page eaao4165.

[Akhmanova and Steinmetz, 2008] Akhmanova, A. and Steinmetz, M. O. (2008). Tracking the ends: a dynamic protein network controls the fate of microtubule tips. *Nature reviews Molecular cell biology*, 9(4):309–322.

[Alushin et al., 2014] Alushin, G. M., Lander, G. C., Kellogg, E. H., Zhang, R., Baker, D., and Nogales, E. (2014). High-resolution microtubule structures reveal the structural transitions in $\alpha\beta$-tubulin upon gtp hydrolysis. *Cell*, 157(5):1117–1129.

[ARCE et al., 1975] ARCE, C. A., RODRIGUEZ, J. A., BARRA, H. S., and CAPUTTO, R. (1975). Incorporation of l-tyrosine, l-phenylalanine and l-3, 4-dihydroxyphenylalanine as single units into rat brain tubulin. *The FEBS Journal*, 59(1):145–149.

[Arellano-Santoyo et al., 2017] Arellano-Santoyo, H., Geyer, E. A., Stokasimov, E., Chen, G.-Y., Su, X., Hancock, W., Rice, L. M., and Pellman, D. (2017). A tubulin binding switch underlies kip3/kinesin-8 depolymerase activity. *Developmental cell*, 42(1):37–51.

[Arnal et al., 2004] Arnal, I., Heichette, C., Diamantopoulos, G. S., and Chrétien, D. (2004). Clip-170/tubulin-curved oligomers coassemble at microtubule ends and promote rescues. *Current biology*, 14(23):2086–2095.

[Asenjo et al., 2013] Asenjo, A. B., Chatterjee, C., Tan, D., DePaoli, V., Rice, W. J., Diaz-Avalos, R., Silvestry, M., and Sosa, H. (2013). Structural model for tubulin recognition and deformation by kinesin-13 microtubule depolymerases. *Cell reports*, 3(3):759–768.

[Aumeier et al., 2016] Aumeier, C., Schaedel, L., Gaillard, J., John, K., Blanchoin, L., and Théry, M. (2016). Self-repair promotes microtubule rescue. *Nature cell biology*, 18(10):1054–1064.

[Ayaz et al., 2014] Ayaz, P., Munyoki, S., Geyer, E. A., Piedra, F.-A., Vu, E. S., Bromberg, R., Otwinowski, Z., Grishin, N. V., Brautigam, C. A., and Rice,

L. M. (2014). A tethered delivery mechanism explains the catalytic action of a microtubule polymerase. *Elife*, 3:e03069.

[Ayaz et al., 2012] Ayaz, P., Ye, X., Huddleston, P., Brautigam, C. A., and Rice, L. M. (2012). A tog: $\alpha\beta$-tubulin complex structure reveals conformation-based mechanisms for a microtubule polymerase. *Science*, 337(6096):857–860.

[Badin-Larcon et al., 2004] Badin-Larcon, A., Boscheron, C., Soleilhac, J., Piel, M., Mann, C., Denarier, E., Fourest-Lieuvin, A., Lafanechere, L., Bornens, M., and Job, D. (2004). Suppression of nuclear oscillations in saccharomyces cerevisiae expressing glu tubulin. *Proceedings of the National Academy of Sciences of the United States of America*, 101(15):5577–5582.

[Bardin and Amon, 2001] Bardin, A. J. and Amon, A. (2001). Men and sin: what's the difference? *Nature Reviews Molecular Cell Biology*, 2(11):815.

[Barral and Liakopoulos, 2009] Barral, Y. and Liakopoulos, D. (2009). Role of spindle asymmetry in cellular dynamics. *International review of cell and molecular biology*, 278:149–213.

[Barral et al., 1999] Barral, Y., Parra, M., Bidlingmaier, S., and Snyder, M. (1999). Nim1-related kinases coordinate cell cycle progression with the organization of the peripheral cytoskeleton in yeast. *Genes & Development*, 13(2):176–187.

[Barrett et al., 2000] Barrett, J. G., Manning, B. D., and Snyder, M. (2000). The kar3p kinesin-related protein forms a novel heterodimeric structure with its associated protein cik1p. *Molecular biology of the cell*, 11(7):2373–2385.

[Barros et al., 2005] Barros, T. P., Kinoshita, K., Hyman, A. A., and Raff, J. W. (2005). Aurora a activates d-tacc–msps complexes exclusively at centrosomes to stabilize centrosomal microtubules. *J Cell Biol*, 170(7):1039–1046.

[Beach et al., 2000] Beach, D. L., Thibodeaux, J., Maddox, P., Yeh, E., and Bloom, K. (2000). The role of the proteins kar9 and myo2 in orienting the mitotic spindle of budding yeast. *Current Biology*, 10(23):1497–1506.

[Berlin et al., 1990] Berlin, V., Styles, C. A., and Fink, G. R. (1990). Bik1, a protein required for microtubule function during mating and mitosis in saccharomyces cerevisiae, colocalizes with tubulin. *The Journal of Cell Biology*, 111(6):2573–2586.

[Bhattacharya et al., 2011] Bhattacharya, R., Yang, H., and Cabral, F. (2011). Class v β-tubulin alters dynamic instability and stimulates microtubule detachment from centrosomes. *Molecular biology of the cell*, 22(7):1025–1034.

[Bieling et al., 2008] Bieling, P., Kandels-Lewis, S., Telley, I. A., van Dijk, J., Janke, C., and Surrey, T. (2008). Clip-170 tracks growing microtubule ends by dynamically recognizing composite eb1/tubulin-binding sites. *J Cell Biol*, 183(7):1223–1233.

[Bieling et al., 2007] Bieling, P., Laan, L., Schek, H., Munteanu, E. L., Sandblad, L., Dogterom, M., Brunner, D., and Surrey, T. (2007). Reconstitution of a microtubule plus-end tracking system in vitro. *Nature*, 450(7172):1100.

[Blake-Hodek et al., 2010] Blake-Hodek, K. A., Cassimeris, L., and Huffaker, T. C. (2010). Regulation of microtubule dynamics by bim1 and bik1, the budding yeast members of the eb1 and clip-170 families of plus-end tracking proteins. *Molecular biology of the cell*, 21(12):2013–2023.

[Bode et al., 2003] Bode, C. J., Gupta, M. L., Suprenant, K. A., and Himes, R. H. (2003). The two α-tubulin isotypes in budding yeast have opposing effects on microtubule dynamics in vitro. *EMBO reports*, 4(1):94–99.

[Bollen, 2001] Bollen, M. (2001). Combinatorial control of protein phosphatase-1. *Trends in biochemical sciences*, 26(7):426–431.

[Bornens and Piel, 2002] Bornens, M. and Piel, M. (2002). Centrosome inheritance: birthright or the privilege of maturity? *Current biology*, 12(2):R71–R73.

[Bowne-Anderson et al., 2013] Bowne-Anderson, H., Zanic, M., Kauer, M., and Howard, J. (2013). Microtubule dynamic instability: a new model with coupled gtp hydrolysis and multistep catastrophe. *Bioessays*, 35(5):452–461.

[Bridges and Gladfelter, 2015] Bridges, A. A. and Gladfelter, A. S. (2015). Septin form and function at the cell cortex. *Journal of Biological Chemistry*, 290(28):17173–17180.

[Brouhard and Rice, 2014] Brouhard, G. J. and Rice, L. M. (2014). The contribution of $\alpha\beta$-tubulin curvature to microtubule dynamics. *J Cell Biol*, 207(3):323–334.

[Brunner and Nurse, 2000] Brunner, D. and Nurse, P. (2000). Clip170-like tip1p spatially organizes microtubular dynamics in fission yeast. *Cell*, 102(5):695–704.

[Buey et al., 2006] Buey, R. M., Díaz, J. F., and Andreu, J. M. (2006). The nucleotide switch of tubulin and microtubule assembly: a polymerization-driven structural change. *Biochemistry*, 45(19):5933–5938.

[Burns et al., 2014] Burns, K. M., Wagenbach, M., Wordeman, L., and Schriemer, D. C. (2014). Nucleotide exchange in dimeric mcak induces longitudinal and lateral stress at microtubule ends to support depolymerization. *Structure*, 22(8):1173–1183.

[Carvalho et al., 2004] Carvalho, P., Gupta, M. L., Hoyt, M. A., and Pellman, D. (2004). Cell cycle control of kinesin-mediated transport of bik1 (clip-170) regulates microtubule stability and dynein activation. *Developmental cell*, 6(6):815–829.

[Catarinella et al., 2009] Catarinella, M., Grüner, T., Strittmatter, T., Marx, A., and Mayer, T. U. (2009). Btb-1: a small molecule inhibitor of the mitotic motor protein kif18a. *Angewandte Chemie International Edition*, 48(48):9072–9076.

[Caudron et al., 2008] Caudron, F., Andrieux, A., Job, D., and Boscheron, C. (2008). A new role for kinesin-directed transport of bik1p (clip-170) in saccharomyces cerevisiae. *Journal of cell science*, 121(9):1506–1513.

[Caydasi et al., 2010a] Caydasi, A. K., Ibrahim, B., and Pereira, G. (2010a). Monitoring spindle orientation: Spindle position checkpoint in charge. *Cell division*, 5(1):28.

[Caydasi et al., 2010b] Caydasi, A. K., Kurtulmus, B., Orrico, M. I., Hofmann, A., Ibrahim, B., and Pereira, G. (2010b). Elm1 kinase activates the spindle position checkpoint kinase kin4. *The Journal of cell biology*, 190(6):975–989.

[Caydasi and Pereira, 2012] Caydasi, A. K. and Pereira, G. (2012). Spoc alert—when chromosomes get the wrong direction. *Experimental cell research*, 318(12):1421–1427.

[Chan and Amon, 2009] Chan, L. Y. and Amon, A. (2009). The protein phosphatase 2a functions in the spindle position checkpoint by regulating the checkpoint kinase kin4. *Genes & development*, 23(14):1639–1649.

[Chan and Amon, 2010] Chan, L. Y. and Amon, A. (2010). Spindle position is coordinated with cell-cycle progression through establishment of mitotic exit-activating and-inhibitory zones. *Molecular cell*, 39(3):444–454.

[Charrasse et al., 1995] Charrasse, S., Mazel, M., Taviaux, S., Berta, P., Chow, T., and Larroque, C. (1995). Characterization of the cdna and pattern of

expression of a new gene over-expressed in human hepatomas and colonic tumors. *The FEBS Journal*, 234(2):406–413.

[Charrasse et al., 1998] Charrasse, S., Schroeder, M., Gauthier-Rouviere, C., Ango, F., Cassimeris, L., Gard, D. L., and Larroque, C. (1998). The togp protein is a new human microtubule-associated protein homologous to the xenopus xmap215. *Journal of cell science*, 111(10):1371–1383.

[Chen et al., 1998] Chen, X. P., Yin, H., and Huffaker, T. C. (1998). The yeast spindle pole body component spc72p interacts with stu2p and is required for proper microtubule assembly. *The Journal of cell biology*, 141(5):1169–1179.

[Cheng et al., 2014] Cheng, L., Desai, J., Miranda, C. J., Duncan, J. S., Qiu, W., Nugent, A. A., Kolpak, A. L., Wu, C. C., Drokhlyansky, E., Delisle, M. M., et al. (2014). Human cfeom1 mutations attenuate kif21a autoinhibition and cause oculomotor axon stalling. *Neuron*, 82(2):334–349.

[Chervitz et al., 1998] Chervitz, S. A., Aravind, L., Sherlock, G., Ball, C. A., Koonin, E. V., Dwight, S. S., Harris, M. A., Dolinski, K., Mohr, S., Smith, T., et al. (1998). Comparison of the complete protein sets of worm and yeast: orthology and divergence. *Science*, 282(5396):2022–2028.

[Chrétien et al., 1995] Chrétien, D., Fuller, S. D., and Karsenti, E. (1995). Structure of growing microtubule ends: two-dimensional sheets close into tubes at variable rates. *The Journal of cell biology*, 129(5):1311–1328.

[Cohen, 2002] Cohen, P. T. (2002). Protein phosphatase 1–targeted in many directions. *Journal of cell science*, 115(2):241–256.

[Collins and Vallee, 1987] Collins, C. A. and Vallee, R. B. (1987). Temperature-dependent reversible assembly of taxol-treated microtubules. *The Journal of cell biology*, 105(6):2847–2854.

[Coombes et al., 2013] Coombes, C. E., Yamamoto, A., Kenzie, M. R., Odde, D. J., and Gardner, M. K. (2013). Evolving tip structures can explain age-dependent microtubule catastrophe. *Current Biology*, 23(14):1342–1348.

[Cottingham and Hoyt, 1997] Cottingham, F. R. and Hoyt, M. A. (1997). Mitotic spindle positioning in saccharomyces cerevisiae is accomplished by antagonistically acting microtubule motor proteins. *The Journal of cell biology*, 138(5):1041–1053.

[Coy et al., 1999] Coy, D. L., Hancock, W. O., Wagenbach, M., and Howard, J. (1999). Kinesin's tail domain is an inhibitory regulator of the motor domain. *Nature cell biology*, 1(5):288.

[Cullen et al., 1999] Cullen, C. F., Deák, P., Glover, D. M., and Ohkura, H. (1999). Mini spindles. *The Journal of cell biology*, 146(5):1005–1018.

[Cullen and Ohkura, 2001] Cullen, C. F. and Ohkura, H. (2001). Msps protein is localized to acentrosomal poles to ensure bipolarity of drosophila meiotic spindles. *Nature cell biology*, 3(7):637–642.

[Davidson and Wood, 2016] Davidson, A. J. and Wood, W. (2016). Unravelling the actin cytoskeleton: a new competitive edge? *Trends in cell biology*, 26(8):569–576.

[Davis et al., 1993] Davis, A., Sage, C. R., Wilson, L., and Farrell, K. W. (1993). Purification and biochemical characterization of tubulin from the budding yeast saccharomyces cerevisiae. *Biochemistry*, 32(34):8823–8835.

[De Wever et al., 2014] De Wever, V., Nasa, I., Chamousset, D., Lloyd, D., Nimick, M., Xu, H., Trinkle-Mulcahy, L., and Moorhead, G. B. (2014). The human mitotic kinesin kif18a binds protein phosphatase 1 (pp1) through a highly conserved docking motif. *Biochemical and biophysical research communications*, 453(3):432–437.

[Delphin et al., 2012] Delphin, C., Bouvier, D., Seggio, M., Couriol, E., Saoudi, Y., Denarier, E., Bosc, C., Valiron, O., Bisbal, M., Arnal, I., et al. (2012). Map6-f is a temperature sensor that directly binds to and protects microtubules from cold-induced depolymerization. *Journal of Biological Chemistry*, 287(42):35127–35138.

[Desai and Mitchison, 1997] Desai, A. and Mitchison, T. J. (1997). Microtubule polymerization dynamics. *Annual review of cell and developmental biology*, 13(1):83–117.

[Desai et al., 1999] Desai, A., Verma, S., Mitchison, T. J., and Walczak, C. E. (1999). Kin i kinesins are microtubule-destabilizing enzymes. *Cell*, 96(1):69–78.

[Detrich et al., 2000] Detrich, H. W., Parker, S. K., Williams, R. C., Nogales, E., and Downing, K. H. (2000). Cold adaptation of microtubule assembly and dynamics structural interpretation of primary sequence changes present in the α-and β-tubulins of antarctic fishes. *Journal of Biological Chemistry*, 275(47):37038–37047.

[Dimitrov et al., 2008] Dimitrov, A., Quesnoit, M., Moutel, S., Cantaloube, I., Poüs, C., and Perez, F. (2008). Detection of gtp-tubulin conformation in vivo reveals a role for gtp remnants in microtubule rescues. *science*, 322(5906):1353–1356.

[Dragestein et al., 2008] Dragestein, K. A., van Cappellen, W. A., van Haren, J., Tsibidis, G. D., Akhmanova, A., Knoch, T. A., Grosveld, F., and Galjart, N. (2008). Dynamic behavior of gfp–clip-170 reveals fast protein turnover on microtubule plus ends. *J Cell Biol*, 180(4):729–737.

[Drechsler et al., 2015] Drechsler, H., Tan, A. N., and Liakopoulos, D. (2015). Yeast gsk-3 kinase regulates astral microtubule function through phosphorylation of the microtubule-stabilizing kinesin kip2. *J Cell Sci*, 128(21):3910–3921.

[Duellberg et al., 2016] Duellberg, C., Cade, N. I., Holmes, D., and Surrey, T. (2016). The size of the eb cap determines instantaneous microtubule stability. *Elife*, 5:e13470.

[Dumontet and Jordan, 2010] Dumontet, C. and Jordan, M. A. (2010). Microtubule-binding agents: a dynamic field of cancer therapeutics. *Nature reviews Drug discovery*, 9(10):790–803.

[Egloff et al., 1997] Egloff, M.-P., Johnson, D. F., Moorhead, G., Cohen, P. T., Cohen, P., and Barford, D. (1997). Structural basis for the recognition of regulatory subunits by the catalytic subunit of protein phosphatase 1. *The EMBO journal*, 16(8):1876–1887.

[Endow et al., 1994] Endow, S. A., Kang, S. J., Satterwhite, L. L., Rose, M. D., Skeen, V. P., and Salmon, E. D. (1994). Yeast kar3 is a minus-end microtubule motor protein that destabilizes microtubules preferentially at the minus ends. *The EMBO journal*, 13(11):2708.

[Erck et al., 2005] Erck, C., Peris, L., Andrieux, A., Meissirel, C., Gruber, A. D., Vernet, M., Schweitzer, A., Saoudi, Y., Pointu, H., Bosc, C., et al. (2005). A vital role of tubulin-tyrosine-ligase for neuronal organization. *Proceedings of the National Academy of Sciences*, 102(22):7853–7858.

[Erickson and O'Brien, 1992] Erickson, H. P. and O'Brien, E. T. (1992). Microtubule dynamic instability and gtp hydrolysis. *Annual review of biophysics and biomolecular structure*, 21(1):145–166.

[Ersfeld et al., 1993] Ersfeld, K., Wehland, J., Plessmann, U., Dodemont, H., Gerke, V., and Weber, K. (1993). Characterization of the tubulin-tyrosine ligase. *The Journal of cell biology*, 120(3):725–732.

[Evans et al., 1985] Evans, L., Mitchison, T., and Kirschner, M. (1985). Influence of the centrosome on the structure of nucleated microtubules. *The Journal of Cell Biology*, 100(4):1185–1191.

[Fees et al., 2017] Fees, C. P., Estrem, C., and Moore, J. K. (2017). High-resolution imaging and analysis of individual astral microtubule dynamics in budding yeast. *JoVE (Journal of Visualized Experiments)*, (122):e55610–e55610.

[Friedman and Vale, 1999] Friedman, D. S. and Vale, R. D. (1999). Single-molecule analysis of kinesin motility reveals regulation by the cargo-binding tail domain. *Nature cell biology*, 1(5):293.

[Friel and Howard, 2011] Friel, C. T. and Howard, J. (2011). The kinesin-13 mcak has an unconventional atpase cycle adapted for microtubule depolymerization. *The EMBO journal*, 30(19):3928–3939.

[Fukuda et al., 2014] Fukuda, Y., Luchniak, A., Murphy, E. R., and Gupta, M. L. (2014). Spatial control of microtubule length and lifetime by opposing stabilizing and destabilizing functions of kinesin-8. *Current Biology*, 24(16):1826–1835.

[Fygenson et al., 1994] Fygenson, D. K., Braun, E., and Libchaber, A. (1994). Phase diagram of microtubules. *Physical Review E*, 50(2):1579.

[Gard and Kirschner, 1987] Gard, D. L. and Kirschner, M. W. (1987). A microtubule-associated protein from xenopus eggs that specifically promotes assembly at the plus-end. *The Journal of cell biology*, 105(5):2203–2215.

[Gardner et al., 2011a] Gardner, M. K., Zanic, M., Gell, C., Bormuth, V., and Howard, J. (2011a). Depolymerizing kinesins kip3 and mcak shape cellular microtubule architecture by differential control of catastrophe. *Cell*, 147(5):1092–1103.

[Gardner et al., 2011b] Gardner, M. K., Zanic, M., Gell, C., Bormuth, V., and Howard, J. (2011b). Depolymerizing kinesins kip3 and mcak shape cellular microtubule architecture by differential control of catastrophe. *Cell*, 147(5):1092–1103.

[Geyer et al., 2015] Geyer, E. A., Burns, A., Lalonde, B. A., Ye, X., Piedra, F.-A., Huffaker, T. C., and Rice, L. M. (2015). A mutation uncouples the tubulin conformational and gtpase cycles, revealing allosteric control of microtubule dynamics. *Elife*, page e10113.

[Ghaemmaghami et al., 2003] Ghaemmaghami, S., Huh, W.-K., Bower, K., Howson, R. W., Belle, A., Dephoure, N., O'shea, E. K., and Weissman, J. S. (2003). Global analysis of protein expression in yeast. *Nature*, 425(6959):737–741.

[Gierke et al., 2010] Gierke, S., Kumar, P., and Wittmann, T. (2010). Analysis of microtubule polymerization dynamics in live cells. *Methods in cell biology*, 97:15–33.

[Gigant et al., 2000] Gigant, B., Curmi, P. A., Martin-Barbey, C., Charbaut, E., Lachkar, S., Lebeau, L., Siavoshian, S., Sobel, A., and Knossow, M. (2000). The 4 å x-ray structure of a tubulin: stathmin-like domain complex. *Cell*, 102(6):809–816.

[Glover, 2005] Glover, D. M. (2005). Polo kinase and progression through m phase in drosophila: a perspective from the spindle poles. *Oncogene*, 24(2):230.

[Godsel et al., 2008] Godsel, L. M., Hobbs, R. P., and Green, K. J. (2008). Intermediate filament assembly: dynamics to disease. *Trends in cell biology*, 18(1):28–37.

[Gopalakrishnan et al., 2012] Gopalakrishnan, J., Chim, Y.-C. F., Ha, A., Basiri, M. L., Lerit, D. A., Rusan, N. M., and Avidor-Reiss, T. (2012). Tubulin nucleotide status controls sas-4-dependent pericentriolar material recruitment. *Nature cell biology*, 14(8):865.

[Grava et al., 2006] Grava, S., Schaerer, F., Faty, M., Philippsen, P., and Barral, Y. (2006). Asymmetric recruitment of dynein to spindle poles and microtubules promotes proper spindle orientation in yeast. *Developmental cell*, 10(4):425–439.

[Gryaznova et al., 2016] Gryaznova, Y., Caydasi, A. K., Malengo, G., Sourjik, V., and Pereira, G. (2016). A fret-based study reveals site-specific regulation of spindle position checkpoint proteins at yeast centrosomes. *Elife*, 5.

[Gudimchuk et al., 2013] Gudimchuk, N., Vitre, B., Kim, Y., Kiyatkin, A., Cleveland, D. W., Ataullakhanov, F. I., and Grishchuk, E. L. (2013). Kinetochore kinesin cenp-e is a processive bi-directional tracker of dynamic microtubule tips. *Nature cell biology*, 15(9):1079–1088.

[Guesdon et al., 2016] Guesdon, A., Bazile, F., Buey, R. M., Mohan, R., Monier, S., García, R. R., Angevin, M., Heichette, C., Wieneke, R., Tampé, R., et al. (2016). Eb1 interacts with outwardly curved and straight regions of the microtubule lattice. *Nature cell biology*, 18(10):1102–1108.

[Gupta et al., 2010] Gupta, K. K., Joyce, M. V., Slabbekoorn, A. R., Zhu, Z. C., Paulson, B. A., Boggess, B., and Goodson, H. V. (2010). Probing interactions between clip-170, eb1, and microtubules. *Journal of molecular biology*, 395(5):1049–1062.

[Gupta et al., 2006] Gupta, M. L., Carvalho, P., Roof, D. M., and Pellman, D. (2006). Plus end-specific depolymerase activity of kip3, a kinesin-8 protein, explains its role in positioning the yeast mitotic spindle. *Nature cell biology*, 8(9):913–923.

[Hackney, 1995] Hackney, D. D. (1995). Highly processive microtubule-stimulated atp hydrolysis by dimeric kinesin head domains. *Nature*, 377(6548):448.

[Hallak et al., 1977] Hallak, M. E., Rodriguez, J., Barra, H., and Caputto, R. (1977). Release of tyrosine from tyrosinated tubulin. some common factors that affect this process and the assembly of tubulin. *FEBS letters*, 73(2):147–150.

[Helenius et al., 2006] Helenius, J., Brouhard, G., Kalaidzidis, Y., Diez, S., and Howard, J. (2006). The depolymerizing kinesin mcak uses lattice diffusion to rapidly target microtubule ends. *Nature*, 441(7089):115–119.

[Hernández-Vega et al., 2017] Hernández-Vega, A., Braun, M., Scharrel, L., Jahnel, M., Wegmann, S., Hyman, B. T., Alberti, S., Diez, S., and Hyman, A. A. (2017). Local nucleation of microtubule bundles through tubulin concentration into a condensed tau phase. *bioRxiv*, page 119800.

[Herrmann et al., 2007] Herrmann, H., Bär, H., Kreplak, L., Strelkov, S. V., and Aebi, U. (2007). Intermediate filaments: from cell architecture to nanomechanics. *Nature Reviews Molecular Cell Biology*, 8(7):562–573.

[Hibbel et al., 2015] Hibbel, A., Bogdanova, A., Mahamdeh, M., Jannasch, A., Storch, M., Schäffer, E., Liakopoulos, D., and Howard, J. (2015). Kinesin kip2 enhances microtubule growth in vitro through length-dependent feedback on polymerization and catastrophe. *eLife*, 4:e10542.

[Hildebrandt and Hoyt, 2000] Hildebrandt, E. R. and Hoyt, M. A. (2000). Mitotic motors in saccharomyces cerevisiae. *Biochimica et Biophysica Acta (BBA)-Molecular Cell Research*, 1496(1):99–116.

[Honnappa et al., 2009] Honnappa, S., Gouveia, S. M., Weisbrich, A., Damberger, F. F., Bhavesh, N. S., Jawhari, H., Grigoriev, I., van Rijssel, F. J., Buey, R. M., Lawera, A., et al. (2009). An eb1-binding motif acts as a microtubule tip localization signal. *Cell*, 138(2):366–376.

[Honnappa et al., 2005] Honnappa, S., John, C. M., Kostrewa, D., Winkler, F. K., and Steinmetz, M. O. (2005). Structural insights into the eb1–apc interaction. *The EMBO journal*, 24(2):261–269.

[Honnappa et al., 2006] Honnappa, S., Okhrimenko, O., Jaussi, R., Jawhari, H., Jelesarov, I., Winkler, F. K., and Steinmetz, M. O. (2006). Key interaction modes of dynamic+ tip networks. *Molecular cell*, 23(5):663–671.

[Hotz et al., 2012] Hotz, M., Leisner, C., Chen, D., Manatschal, C., Wegleiter, T., Ouellet, J., Lindstrom, D., Gottschling, D. E., Vogel, J., and Barral, Y. (2012). Spindle pole bodies exploit the mitotic exit network in metaphase to drive their age-dependent segregation. *Cell*, 148(5):958–972.

[Howes et al., 2017] Howes, S. C., Geyer, E. A., LaFrance, B., Zhang, R., Kellogg, E. H., Westermann, S., Rice, L. M., and Nogales, E. (2017). Structural differences between yeast and mammalian microtubules revealed by cryo-em. *J Cell Biol*, pages jcb–201612195.

[Hunter et al., 2003] Hunter, A. W., Caplow, M., Coy, D. L., Hancock, W. O., Diez, S., Wordeman, L., and Howard, J. (2003). The kinesin-related protein mcak is a microtubule depolymerase that forms an atp-hydrolyzing complex at microtubule ends. *Molecular cell*, 11(2):445–457.

[Hussmann et al., 2016] Hussmann, F., Drummond, D. R., Peet, D. R., Martin, D. S., and Cross, R. A. (2016). Alp7/tacc-alp14/tog generates long-lived, fast-growing mts by an unconventional mechanism. *Scientific reports*, 6:20653.

[Huyett et al., 1998] Huyett, A., Kahana, J., Silver, P., Zeng, X., and Saunders, W. S. (1998). The kar3p and kip2p motors function antagonistically at the spindle poles to influence cytoplasmic microtubule numbers. *Journal of Cell Science*, 111(3):295–301.

[Hwang et al., 2003] Hwang, E., Kusch, J., Barral, Y., and Huffaker, T. C. (2003). Spindle orientation in saccharomyces cerevisiae depends on the transport of microtubule ends along polarized actin cables. *The Journal of cell biology*, 161(3):483–488.

[Hyman et al., 1992] Hyman, A. A., Salser, S., Drechsel, D., Unwin, N., and Mitchison, T. J. (1992). Role of gtp hydrolysis in microtubule dynamics: information from a slowly hydrolyzable analogue, gmpcpp. *Molecular biology of the cell*, 3(10):1155–1167.

[Jacobs et al., 1988] Jacobs, C. W., Adams, A., Szaniszlo, P. J., and Pringle, J. R. (1988). Functions of microtubules in the saccharomyces cerevisiae cell cycle. *The Journal of cell biology*, 107(4):1409–1426.

[Janke et al., 2004] Janke, C., Magiera, M. M., Rathfelder, N., Taxis, C., Reber, S., Maekawa, H., Moreno-Borchart, A., Doenges, G., Schwob, E., Schiebel,

E., et al. (2004). A versatile toolbox for pcr-based tagging of yeast genes: new fluorescent proteins, more markers and promoter substitution cassettes. *Yeast*, 21(11):947–962.

[Jánosi et al., 1998] Jánosi, I. M., Chrétien, D., and Flyvbjerg, H. (1998). Modeling elastic properties of microtubule tips and walls. *European biophysics journal*, 27(5):501–513.

[Januschke and Gonzalez, 2010] Januschke, J. and Gonzalez, C. (2010). The interphase microtubule aster is a determinant of asymmetric division orientation in drosophila neuroblasts. *The Journal of cell biology*, pages jcb–200905024.

[Januschke et al., 2011] Januschke, J., Llamazares, S., Reina, J., and Gonzalez, C. (2011). Drosophila neuroblasts retain the daughter centrosome. *Nature communications*, 2:243.

[Januschke et al., 2013] Januschke, J., Reina, J., Llamazares, S., Bertran, T., Rossi, F., Roig, J., and Gonzalez, C. (2013). Centrobin controls mother–daughter centriole asymmetry in drosophila neuroblasts. *Nature Cell Biology*, 15(3):241–248.

[Keck et al., 2011] Keck, J. M., Jones, M. H., Wong, C. C., Binkley, J., Chen, D., Jaspersen, S. L., Holinger, E. P., Xu, T., Niepel, M., Rout, M. P., et al. (2011). A cell cycle phosphoproteome of the yeast centrosome. *Science*, 332(6037):1557–1561.

[Kinoshita et al., 2005] Kinoshita, K., Noetzel, T. L., Pelletier, L., Mechtler, K., Drechsel, D. N., Schwager, A., Lee, M., Raff, J. W., and Hyman, A. A. (2005). Aurora a phosphorylation of tacc3/maskin is required for centrosome-dependent microtubule assembly in mitosis. *J Cell Biol*, 170(7):1047–1055.

[Kirkham et al., 2003] Kirkham, M., Müller-Reichert, T., Oegema, K., Grill, S., and Hyman, A. A. (2003). Sas-4 is a c. elegans centriolar protein that controls centrosome size. *Cell*, 112(4):575–587.

[Knop and Schiebel, 1998] Knop, M. and Schiebel, E. (1998). Receptors determine the cellular localization of a γ-tubulin complex and thereby the site of microtubule formation. *The EMBO Journal*, 17(14):3952–3967.

[Knop et al., 1999] Knop, M., Siegers, K., Pereira, G., Zachariae, W., Winsor, B., Nasmyth, K., and Schiebel, E. (1999). Epitope tagging of yeast genes using a pcr-based strategy: more tags and improved practical routines. *Yeast*, 15(10B):963–972.

[Komarova et al., 2002a] Komarova, Y. A., Akhmanova, A. S., Kojima, S.-i., Galjart, N., and Borisy, G. G. (2002a). Cytoplasmic linker proteins promote microtubule rescue in vivo. *J Cell Biol*, 159(4):589–599.

[Komarova et al., 2002b] Komarova, Y. A., Vorobjev, I. A., and Borisy, G. G. (2002b). Life cycle of mts: persistent growth in the cell interior, asymmetric transition frequencies and effects of the cell boundary. *Journal of cell science*, 115(17):3527–3539.

[Krull et al., 2014] Krull, A., Steinborn, A., Ananthanarayanan, V., Ramunno-Johnson, D., Petersohn, U., and Tolić-Nørrelykke, I. M. (2014). A divide and conquer strategy for the maximum likelihood localization of low intensity objects. *Opt. Express*, 22(1):210–228.

[Kumar et al., 2017] Kumar, A., Manatschal, C., Rai, A., Grigoriev, I., Degen, M. S., Jaussi, R., Kretzschmar, I., Prota, A. E., Volkmer, R., Kammerer, R. A., et al. (2017). Short linear sequence motif lxxptph targets diverse proteins to growing microtubule ends. *Structure*.

[Kumar et al., 2012] Kumar, P., Chimenti, M. S., Pemble, H., Schönichen, A., Thompson, O., Jacobson, M. P., and Wittmann, T. (2012). Multisite phosphorylation disrupts arginine-glutamate salt bridge networks required for binding of cytoplasmic linker-associated protein 2 (clasp2) to end-binding protein 1 (eb1). *Journal of Biological Chemistry*, 287(21):17050–17064.

[Kumar et al., 2009] Kumar, P., Lyle, K. S., Gierke, S., Matov, A., Danuser, G., and Wittmann, T. (2009). Gsk3β phosphorylation modulates clasp–microtubule association and lamella microtubule attachment. *The Journal of cell biology*, 184(6):895–908.

[Kumar and Wittmann, 2012] Kumar, P. and Wittmann, T. (2012). + tips: Sxipping along microtubule ends. *Trends in cell biology*, 22(8):418–428.

[Lansbergen and Akhmanova, 2006] Lansbergen, G. and Akhmanova, A. (2006). Microtubule plus end: a hub of cellular activities. *Traffic*, 7(5):499–507.

[Lansbergen et al., 2004] Lansbergen, G., Komarova, Y., Modesti, M., Wyman, C., Hoogenraad, C. C., Goodson, H. V., Lemaitre, R. P., Drechsel, D. N., Van Munster, E., Gadella, T. W., et al. (2004). Conformational changes in clip-170 regulate its binding to microtubules and dynactin localization. *The Journal of cell biology*, 166(7):1003–1014.

[Laughery et al., 2015a] Laughery, M. F., Hunter, T., Brown, A., Hoopes, J., Ostbye, T., Shumaker, T., and Wyrick, J. J. (2015a). New vectors for simple

and streamlined crispr–cas9 genome editing in saccharomyces cerevisiae. *Yeast*, 32(12):711–720.

[Laughery et al., 2015b] Laughery, M. F., Hunter, T., Brown, A., Hoopes, J., Ostbye, T., Shumaker, T., and Wyrick, J. J. (2015b). New vectors for simple and streamlined crispr–cas9 genome editing in saccharomyces cerevisiae. *Yeast*, 32(12):711–720.

[Lee et al., 2001] Lee, M. J., Gergely, F., Jeffers, K., Peak-Chew, S. Y., and Raff, J. W. (2001). Msps/xmap215 interacts with the centrosomal protein d-tacc to regulate microtubule behaviour. *Nature cell biology*, 3(7):643–649.

[Lengefeld et al., 2017a] Lengefeld, J., Hotz, M., Rollins, M., Baetz, K., and Barral, Y. (2017a). Budding yeast wee1 distinguishes spindle pole bodies to guide their pattern of age-dependent segregation. *Nature cell biology*, 19(8):941.

[Lengefeld et al., 2017b] Lengefeld, J., Yen, E., Chen, X., Leary, A., Vogel, J., and Barral, Y. (2017b). Spatial cues and not spindle pole maturation drive the asymmetry of astral microtubules between new and pre-existing spindle poles. *Molecular Biology of the Cell*, pages mbc–E16.

[Lerit et al., 2013] Lerit, D. A., Smyth, J. T., and Rusan, N. M. (2013). Organelle asymmetry for proper fitness, function, and fate. *Chromosome research*, 21(3):271–286.

[Liakopoulos et al., 2003] Liakopoulos, D., Kusch, J., Grava, S., Vogel, J., and Barral, Y. (2003). Asymmetric loading of kar9 onto spindle poles and microtubules ensures proper spindle alignment. *cell*, 112(4):561–574.

[Liu et al., 2006] Liu, J., Taylor, D. W., Krementsova, E. B., Trybus, K. M., and Taylor, K. A. (2006). Three-dimensional structure of the myosin v inhibited state by cryoelectron tomography. *Nature*, 442(7099):208.

[Longtine and Bi, 2003] Longtine, M. S. and Bi, E. (2003). Regulation of septin organization and function in yeast. *Trends in cell biology*, 13(8):403–409.

[Lu et al., 2007] Lu, P., Vogel, C., Wang, R., Yao, X., and Marcotte, E. M. (2007). Absolute protein expression profiling estimates the relative contributions of transcriptional and translational regulation. *Nature biotechnology*, 25(1):117–124.

[Ludueña, 1997] Ludueña, R. F. (1997). Multiple forms of tubulin: different gene products and covalent modifications. *International review of cytology*, 178:207–275.

[Maddox et al., 2000] Maddox, P. S., Bloom, K. S., and Salmon, E. (2000). The polarity and dynamics of microtubule assembly in the budding yeast saccharomyces cerevisiae. *Nature cell biology*, 2(1):36–41.

[Maekawa and Schiebel, 2004] Maekawa, H. and Schiebel, E. (2004). Cdk1-clb4 controls the interaction of astral microtubule plus ends with subdomains of the daughter cell cortex. *Genes & development*, 18(14):1709–1724.

[Maekawa et al., 2003] Maekawa, H., Usui, T., Knop, M., and Schiebel, E. (2003). Yeast cdk1 translocates to the plus end of cytoplasmic microtubules to regulate bud cortex interactions. *The EMBO Journal*, 22(3):438–449.

[Manning et al., 1999] Manning, B. D., Barrett, J. G., Wallace, J. A., Granok, H., and Snyder, M. (1999). Differential regulation of the kar3p kinesin-related protein by two associated proteins, cik1p and vik1p. *The Journal of cell biology*, 144(6):1219–1233.

[Matov et al., 2010] Matov, A., Applegate, K., Kumar, P., Thoma, C., Krek, W., Danuser, G., and Wittmann, T. (2010). Analysis of microtubule dynamic instability using a plus-end growth marker. *Nature methods*, 7(9):761–768.

[Matsuo et al., 2016] Matsuo, Y., Maurer, S. P., Yukawa, M., Zakian, S., Singleton, M. R., Surrey, T., and Toda, T. (2016). An unconventional interaction between dis1/tog and mal3/eb1 in fission yeast promotes the fidelity of chromosome segregation. *J Cell Sci*, 129(24):4592–4606.

[Matthews et al., 1998] Matthews, L. R., Carter, P., Thierry-Mieg, D., and Kemphues, K. (1998). Zyg-9, a caenorhabditis elegans protein required for microtubule organization and function, is a component of meiotic and mitotic spindle poles. *The Journal of cell biology*, 141(5):1159–1168.

[Maurer et al., 2011] Maurer, S. P., Bieling, P., Cope, J., Hoenger, A., and Surrey, T. (2011). Gtpγs microtubules mimic the growing microtubule end structure recognized by end-binding proteins (ebs). *Proceedings of the National Academy of Sciences*, 108(10):3988–3993.

[Maurer et al., 2014] Maurer, S. P., Cade, N. I., Bohner, G., Gustafsson, N., Boutant, E., and Surrey, T. (2014). Eb1 accelerates two conformational transitions important for microtubule maturation and dynamics. *Current Biology*, 24(4):372–384.

[Mayr et al., 2011] Mayr, M. I., Storch, M., Howard, J., and Mayer, T. U. (2011). A non-motor microtubule binding site is essential for the high processivity and mitotic function of kinesin-8 kif18a. *PLoS One*, 6(11):e27471.

[McDonald et al., 1990] McDonald, H. B., Stewart, R. J., and Goldstein, L. S. (1990). The kinesin-like ncd protein of drosophila is a minus end-directed microtubule motor. *Cell*, 63(6):1159–1165.

[Meluh and Rose, 1990] Meluh, P. B. and Rose, M. D. (1990). Kar3, a kinesin-related gene required for yeast nuclear fusion. *Cell*, 60(6):1029–1041.

[Mickey and Howard, 1995] Mickey, B. and Howard, J. (1995). Rigidity of microtubules is increased by stabilizing agents. *The Journal of cell biology*, 130(4):909–917.

[Miki et al., 2005] Miki, H., Okada, Y., and Hirokawa, N. (2005). Analysis of the kinesin superfamily: insights into structure and function. *Trends in cell biology*, 15(9):467–476.

[Mimori-Kiyosue et al., 2005] Mimori-Kiyosue, Y., Grigoriev, I., Lansbergen, G., Sasaki, H., Matsui, C., Severin, F., Galjart, N., Grosveld, F., Vorobjev, I., Tsukita, S., et al. (2005). Clasp1 and clasp2 bind to eb1 and regulate microtubule plus-end dynamics at the cell cortex. *The Journal of cell biology*, 168(1):141–153.

[Mishima et al., 2007] Mishima, M., Maesaki, R., Kasa, M., Watanabe, T., Fukata, M., Kaibuchi, K., and Hakoshima, T. (2007). Structural basis for tubulin recognition by cytoplasmic linker protein 170 and its autoinhibition. *Proceedings of the National Academy of Sciences*, 104(25):10346–10351.

[Mitchison, 1993] Mitchison, T. (1993). Localization of an exchangeable gtp binding site at the plus end of microtubules. *Science*, 261(5124):1044–1048.

[Mitchison et al., 1984] Mitchison, T., Kirschner, M., et al. (1984). Dynamic instability of microtubule growth. *nature*, 312(5991):237–242.

[Modig et al., 2000] Modig, C., Wallin, M., and Olsson, P.-E. (2000). Expression of cold-adapted β-tubulins confer cold-tolerance to human cellular microtubules. *Biochemical and biophysical research communications*, 269(3):787–791.

[Moores et al., 2002] Moores, C. A., Yu, M., Guo, J., Beraud, C., Sakowicz, R., and Milligan, R. A. (2002). A mechanism for microtubule depolymerization by kini kinesins. *Molecular cell*, 9(4):903–909.

[Nakata et al., 2011] Nakata, T., Niwa, S., Okada, Y., Perez, F., and Hirokawa, N. (2011). Preferential binding of a kinesin-1 motor to gtp-tubulin–rich microtubules underlies polarized vesicle transport. *The Journal of cell biology*, 194(2):245–255.

[Nawrotek et al., 2011] Nawrotek, A., Knossow, M., and Gigant, B. (2011). The determinants that govern microtubule assembly from the atomic structure of gtp-tubulin. *Journal of molecular biology*, 412(1):35–42.

[Neff et al., 1983] Neff, N. F., Thomas, J. H., Grisafi, P., and Botstein, D. (1983). Isolation of the β-tubulin gene from yeast and demonstration of its essential function in vivo. *Cell*, 33(1):211–219.

[Neukirchen and Bradke, 2011] Neukirchen, D. and Bradke, F. (2011). Cytoplasmic linker proteins regulate neuronal polarization through microtubule and growth cone dynamics. *Journal of Neuroscience*, 31(4):1528–1538.

[Nieuwenhuis et al., 2017] Nieuwenhuis, J., Adamopoulos, A., Bleijerveld, O. B., Mazouzi, A., Stickel, E., Celie, P., Altelaar, M., Knipscheer, P., Perrakis, A., Blomen, V. A., et al. (2017). Vasohibins encode tubulin detyrosinating activity. *Science*, page eaao5676.

[Nogales, 2000] Nogales, E. (2000). Structural insights into microtubule function. *Annual review of biochemistry*, 69(1):277–302.

[Nogales et al., 1998] Nogales, E., Wolf, S. G., and Downing, K. H. (1998). Structure of the $\alpha\beta$ tubulin dimer by electron crystallography. *Nature*, 391(6663):199–203.

[Nogales and Zhang, 2016] Nogales, E. and Zhang, R. (2016). Visualizing microtubule structural transitions and interactions with associated proteins. *Current opinion in structural biology*, 37:90–96.

[Ogawa et al., 2004] Ogawa, T., Nitta, R., Okada, Y., and Hirokawa, N. (2004). A common mechanism for microtubule destabilizers—m type kinesins stabilize curling of the protofilament using the class-specific neck and loops. *Cell*, 116(4):591–602.

[Ohkura et al., 1988] Ohkura, H., Adachi, Y., Kinoshita, N., Niwa, O., Toda, T., and Yanagida, M. (1988). Cold-sensitive and caffeine-supersensitive mutants of the schizosaccharomyces pombe dis genes implicated in sister chromatid separation during mitosis. *The EMBO journal*, 7(5):1465.

[Ohta et al., 2002] Ohta, T., Essner, R., Ryu, J.-H., Palazzo, R. E., Uetake, Y., and Kuriyama, R. (2002). Characterization of cep135, a novel coiled-coil centrosomal protein involved in microtubule organization in mammalian cells. *J Cell Biol*, 156(1):87–100.

[Page et al., 1994] Page, B. D., Satterwhite, L. L., Rose, M. D., and Snyder, M. (1994). Localization of the kar3 kinesin heavy chain-related protein requires the cik1 interacting protein. *The Journal of Cell Biology*, 124(4):507–519.

[Page and Snyder, 1992] Page, B. D. and Snyder, M. (1992). Cik1: a developmentally regulated spindle pole body-associated protein important for microtubule functions in saccharomyces cerevisiae. *Genes & development*, 6(8):1414–1429.

[Pecqueur et al., 2012] Pecqueur, L., Duellberg, C., Dreier, B., Jiang, Q., Wang, C., Plückthun, A., Surrey, T., Gigant, B., and Knossow, M. (2012). A designed ankyrin repeat protein selected to bind to tubulin caps the microtubule plus end. *Proceedings of the National Academy of Sciences*, 109(30):12011–12016.

[Peris et al., 2006] Peris, L., Thery, M., Fauré, J., Saoudi, Y., Lafanechère, L., Chilton, J. K., Gordon-Weeks, P., Galjart, N., Bornens, M., Wordeman, L., et al. (2006). Tubulin tyrosination is a major factor affecting the recruitment of cap-gly proteins at microtubule plus ends. *J Cell Biol*, 174(6):839–849.

[Peset et al., 2005] Peset, I., Seiler, J., Sardon, T., Bejarano, L. A., Rybina, S., and Vernos, I. (2005). Function and regulation of maskin, a tacc family protein, in microtubule growth during mitosis. *J Cell Biol*, 170(7):1057–1066.

[Pierre et al., 1992] Pierre, P., Scheel, J., Rickard, J. E., and Kreis, T. E. (1992). Clip-170 links endocytic vesicles to microtubules. *Cell*, 70(6):887–900.

[Podolski et al., 2014] Podolski, M., Mahamdeh, M., and Howard, J. (2014). Stu2, the budding yeast xmap215/dis1 homolog, promotes assembly of yeast microtubules by increasing growth rate and decreasing catastrophe frequency. *Journal of Biological Chemistry*, 289(41):28087–28093.

[Queralt and Uhlmann, 2008] Queralt, E. and Uhlmann, F. (2008). Cdk-counteracting phosphatases unlock mitotic exit. *Current opinion in cell biology*, 20(6):661–668.

[Ravelli et al., 2004] Ravelli, R. B., Gigant, B., Curmi, P. A., Jourdain, I., Lachkar, S., Sobel, A., and Knossow, M. (2004). Insight into tubulin regulation from a complex with colchicine and a stathmin-like domain. *Nature*, 428(6979):198–202.

[Raybin and Flavin, 1977] Raybin, D. and Flavin, M. (1977). Modification of tubulin by tyrosylation in cells and extracts and its effect on assembly in vitro. *The Journal of cell biology*, 73(2):492–504.

[Rice et al., 2008] Rice, L. M., Montabana, E. A., and Agard, D. A. (2008). The lattice as allosteric effector: structural studies of $\alpha\beta$-and γ-tubulin clarify the role of gtp in microtubule assembly. *Proceedings of the National Academy of Sciences*, 105(14):5378–5383.

[Roberts et al., 2014] Roberts, A. J., Goodman, B. S., and Reck-Peterson, S. L. (2014). Reconstitution of dynein transport to the microtubule plus end by kinesin. *eLife*, 3:e02641.

[Rock et al., 2013] Rock, J. M., Lim, D., Stach, L., Ogrodowicz, R. W., Keck, J. M., Jones, M. H., Wong, C. C., Yates, J. R., Winey, M., Smerdon, S. J., et al. (2013). Activation of the yeast hippo pathway by phosphorylation-dependent assembly of signaling complexes. *Science*, page 1235822.

[Rusan et al., 2001] Rusan, N. M., Fagerstrom, C. J., Yvon, A.-M. C., and Wadsworth, P. (2001). Cell cycle-dependent changes in microtubule dynamics in living cells expressing green fluorescent protein-α tubulin. *Molecular biology of the cell*, 12(4):971–980.

[Rusan and Peifer, 2007] Rusan, N. M. and Peifer, M. (2007). A role for a novel centrosome cycle in asymmetric cell division. *The Journal of cell biology*, 177(1):13–20.

[Salaycik et al., 2005] Salaycik, K. J., Fagerstrom, C. J., Murthy, K., Tulu, U. S., and Wadsworth, P. (2005). Quantification of microtubule nucleation, growth and dynamics in wound-edge cells. *Journal of cell science*, 118(18):4113–4122.

[Sammak and Borisy, 1988] Sammak, P. J. and Borisy, G. G. (1988). Direct observation of microtubule dynamics in living cells. *Nature*, 332(6166):724–726.

[Sardar et al., 2010] Sardar, H. S., Luczak, V. G., Lopez, M. M., Lister, B. C., and Gilbert, S. P. (2010). Mitotic kinesin cenp-e promotes microtubule plus-end elongation. *Current Biology*, 20(18):1648–1653.

[Sato and Toda, 2007] Sato, M. and Toda, T. (2007). Alp7/tacc is a crucial target in ran-gtpase-dependent spindle formation in fission yeast. *Nature*, 447(7142):334–337.

[Sato et al., 2004] Sato, M., Vardy, L., Garcia, M. A., Koonrugsa, N., and Toda, T. (2004). Interdependency of fission yeast alp14/tog and coiled coil protein alp7 in microtubule localization and bipolar spindle formation. *Molecular biology of the cell*, 15(4):1609–1622.

[Schatz et al., 1986] Schatz, P., Pillus, L., Grisafi, P., Solomon, F., and Botstein, D. (1986). Two functional alpha-tubulin genes of the yeast saccharomyces cerevisiae encode divergent proteins. *Molecular and cellular biology*, 6(11):3711–3721.

[Schott et al., 1999] Schott, D., Ho, J., Pruyne, D., and Bretscher, A. (1999). The cooh-terminal domain of myo2p, a yeast myosin v, has a direct role in secretory vesicle targeting. *The Journal of cell biology*, 147(4):791–808.

[Schulze and Kirschner, 1988] Schulze, E. and Kirschner, M. (1988). New features of microtubule behaviour observed in vivo.

[Seetapun et al., 2012] Seetapun, D., Castle, B. T., McIntyre, A. J., Tran, P. T., and Odde, D. J. (2012). Estimating the microtubule gtp cap size in vivo. *Current Biology*, 22(18):1681–1687.

[Segal and Bloom, 2001] Segal, M. and Bloom, K. (2001). Control of spindle polarity and orientation in saccharomyces cerevisiae. *Trends in cell biology*, 11(4):160–166.

[Shaw et al., 1998] Shaw, S. L., Maddox, P., Skibbens, R. V., Yeh, E., Salmon, E., and Bloom, K. (1998). Nuclear and spindle dynamics in budding yeast. *Molecular biology of the cell*, 9(7):1627–1631.

[Shaw et al., 1997] Shaw, S. L., Yeh, E., Maddox, P., Salmon, E. D., and Bloom, K. (1997). Astral microtubule dynamics in yeast: a microtubule-based searching mechanism for spindle orientation and nuclear migration into the bud. *The Journal of cell biology*, 139(4):985–994.

[Shelanski and Taylor, 1968] Shelanski, M. L. and Taylor, E. W. (1968). Properties of the protein subunit of central-pair and outer-doublet microtubules of sea urchin flagella. *The Journal of cell biology*, 38(2):304–315.

[Shipley et al., 2004] Shipley, K., Hekmat-Nejad, M., Turner, J., Moores, C., Anderson, R., Milligan, R., Sakowicz, R., and Fletterick, R. (2004). Structure of a kinesin microtubule depolymerization machine. *The EMBO journal*, 23(7):1422–1432.

[Siller and Doe, 2009] Siller, K. H. and Doe, C. Q. (2009). Spindle orientation during asymmetric cell division. *Nature cell biology*, 11(4):365–374.

[Singh et al., 2014] Singh, P., Nair, A. R., and Cabernard, C. (2014). The centriolar protein bld10/cep135 is required to establish centrosome asymmetry in drosophila neuroblasts. *Current biology*, 24(13):1548–1555.

[Slep et al., 2005] Slep, K. C., Rogers, S. L., Elliott, S. L., Ohkura, H., Kolodziej, P. A., and Vale, R. D. (2005). Structural determinants for eb1-mediated recruitment of apc and spectraplakins to the microtubule plus end. *The Journal of cell biology*, 168(4):587–598.

[Slep and Vale, 2007] Slep, K. C. and Vale, R. D. (2007). Structural basis of microtubule plus end tracking by xmap215, clip-170, and eb1. *Molecular cell*, 27(6):976–991.

[Snead et al., 2007] Snead, J. L., Sullivan, M., Lowery, D. M., Cohen, M. S., Zhang, C., Randle, D. H., Taunton, J., Yaffe, M. B., Morgan, D. O., and Shokat, K. M. (2007). A coupled chemical-genetic and bioinformatic approach to polo-like kinase pathway exploration. *Chemistry & biology*, 14(11):1261–1272.

[Spiliotis and Nelson, 2006] Spiliotis, E. T. and Nelson, W. J. (2006). Here come the septins: novel polymers that coordinate intracellular functions and organization. *Journal of Cell Science*, 119(1):4–10.

[Sproul et al., 2005] Sproul, L. R., Anderson, D. J., Mackey, A. T., Saunders, W. S., and Gilbert, S. P. (2005). Cik1 targets the minus-end kinesin depolymerase kar3 to microtubule plus ends. *Current biology*, 15(15):1420–1427.

[Stangier et al., 2018] Stangier, M. M., Kumar, A., Chen, X., Farcas, A.-M., Barral, Y., and Steinmetz, M. O. (2018). Structure-function relationship of the bik1-bim1 complex. *Structure*.

[Steinmetz and Akhmanova, 2008] Steinmetz, M. O. and Akhmanova, A. (2008). Capturing protein tails by cap-gly domains. *Trends in biochemical sciences*, 33(11):535–545.

[Stumpff et al., 2011] Stumpff, J., Du, Y., English, C. A., Maliga, Z., Wagenbach, M., Asbury, C. L., Wordeman, L., and Ohi, R. (2011). A tethering mechanism controls the processivity and kinetochore-microtubule plus-end enrichment of the kinesin-8 kif18a. *Molecular cell*, 43(5):764–775.

[Su and Qi, 2001] Su, L.-K. and Qi, Y. (2001). Characterization of human mapre genes and their proteins. *Genomics*, 71(2):142–149.

[Su et al., 2013] Su, X., Arellano-Santoyo, H., Portran, D., Gaillard, J., Vantard, M., Thery, M., and Pellman, D. (2013). Microtubule-sliding activity of a kinesin-8 promotes spindle assembly and spindle-length control. *Nature cell biology*, 15(8):948–957.

[Su et al., 2011] Su, X., Qiu, W., Gupta, M. L., Pereira-Leal, J. B., Reck-Peterson, S. L., and Pellman, D. (2011). Mechanisms underlying the dual-mode regulation of microtubule dynamics by kip3/kinesin-8. *Molecular cell*, 43(5):751–763.

[Suarez and Kovar, 2016] Suarez, C. and Kovar, D. R. (2016). Internetwork competition for monomers governs actin cytoskeleton organization. *Nature Reviews Molecular Cell Biology*, 17(12):799–810.

[Talapatra et al., 2015] Talapatra, S. K., Harker, B., and Welburn, J. P. (2015). The c-terminal region of the motor protein mcak controls its structure and activity through a conformational switch. *Elife*, 4:e06421.

[Theesfeld et al., 1999] Theesfeld, C. L., Irazoqui, J. E., Bloom, K., and Lew, D. J. (1999). The role of actin in spindle orientation changes during the saccharomyces cerevisiae cell cycle. *The Journal of cell biology*, 146(5):1019–1032.

[Thoma et al., 2010] Thoma, C. R., Matov, A., Gutbrodt, K. L., Hoerner, C. R., Smole, Z., Krek, W., and Danuser, G. (2010). Quantitative image analysis identifies pvhl as a key regulator of microtubule dynamic instability. *The Journal of cell biology*, 190(6):991–1003.

[Torisawa et al., 2014] Torisawa, T., Ichikawa, M., Furuta, A., Saito, K., Oiwa, K., Kojima, H., Toyoshima, Y. Y., and Furuta, K. (2014). Autoinhibition and cooperative activation mechanisms of cytoplasmic dynein. *Nature cell biology*, 16(11):1118.

[Tropini et al., 2012] Tropini, C., Roth, E. A., Zanic, M., Gardner, M. K., and Howard, J. (2012). Islands containing slowly hydrolyzable gtp analogs promote microtubule rescues. *PloS one*, 7(1):e30103.

[Ubersax et al., 2003] Ubersax, J. A., Woodbury, E. L., Quang, P. N., Paraz, M., Blethrow, J. D., Shah, K., Shokat, K. M., and Morgan, D. O. (2003). Targets of the cyclin-dependent kinase cdk1. *Nature*, 425(6960):859–864.

[Usui et al., 2003] Usui, T., Maekawa, H., Pereira, G., and Schiebel, E. (2003). The xmap215 homologue stu2 at yeast spindle pole bodies regulates microtubule dynamics and anchorage. *The EMBO Journal*, 22(18):4779–4793.

[Valerio-Santiago and Monje-Casas, 2011] Valerio-Santiago, M. and Monje-Casas, F. (2011). Tem1 localization to the spindle pole bodies is essential for mitotic exit and impairs spindle checkpoint function. *The Journal of Cell Biology*, 192(4):599–614.

[van der Vaart et al., 2017] van der Vaart, B., Fischböck, J., Mieck, C., Pichler, P., Mechtler, K., Medema, R. H., and Westermann, S. (2017). Torc1 signaling exerts spatial control over microtubule dynamics by promoting nuclear export of stu2. *J Cell Biol*, 216(11):3471–3484.

[Vandecandelaere et al., 1999] Vandecandelaere, A., Brune, M., Webb, M. R., Martin, S. R., and Bayley, P. M. (1999). Phosphate release during microtubule assembly: what stabilizes growing microtubules? *Biochemistry*, 38(25):8179–8188.

[Varga et al., 2006] Varga, V., Helenius, J., Tanaka, K., Hyman, A. A., Tanaka, T. U., and Howard, J. (2006). Yeast kinesin-8 depolymerizes microtubules in a length-dependent manner. *Nature cell biology*, 8(9):957–962.

[Velve-Casquillas et al., 2010] Velve-Casquillas, G., Costa, J., Carlier-Grynkorn, F., Mayeux, A., and Tran, P. T. (2010). A fast microfluidic temperature control device for studying microtubule dynamics in fission yeast. *Methods in cell biology*, 97:185–201.

[Verhey and Hammond, 2009] Verhey, K. J. and Hammond, J. W. (2009). Traffic control: regulation of kinesin motors. *Nature Reviews Molecular Cell Biology*, 10(11):765–777.

[Vogel et al., 2001] Vogel, J., Drapkin, B., Oomen, J., Beach, D., Bloom, K., and Snyder, M. (2001). Phosphorylation of γ-tubulin regulates microtubule organization in budding yeast. *Developmental cell*, 1(5):621–631.

[Wade, 2009] Wade, R. H. (2009). On and around microtubules: an overview. *Molecular biotechnology*, 43(2):177–191.

[Walker et al., 1988] Walker, R., O'brien, E., Pryer, N., Soboeiro, M., Voter, W., Erickson, H., and Salmon, E. (1988). Dynamic instability of individual microtubules analyzed by video light microscopy: rate constants and transition frequencies. *The Journal of cell biology*, 107(4):1437–1448.

[Walker et al., 1990] Walker, R. A., Salmon, E. D., and Endow, S. A. (1990). The drosophila claret segregation protein is a minus-end directed motor molecule. *Nature*, 347(6295):780.

[Wang et al., 2016] Wang, D., Nitta, R., Morikawa, M., Yajima, H., Inoue, S., Shigematsu, H., Kikkawa, M., and Hirokawa, N. (2016). Motility and microtubule depolymerization mechanisms of the kinesin-8 motor, kif19a. *Elife*, 5.

[Wang and Huffaker, 1997] Wang, P. J. and Huffaker, T. C. (1997). Stu2p: A microtubule-binding protein that is an essential component of the yeast spindle pole body. *The Journal of cell biology*, 139(5):1271–1280.

[Wang et al., 2017] Wang, W., Cantos-Fernandes, S., Lv, Y., Kuerban, H., Ahmad, S., Wang, C., and Gigant, B. (2017). Insight into microtubule

disassembly by kinesin-13s from the structure of kif2c bound to tubulin. *Nature communications*, 8(1):70.

[Wang et al., 2012a] Wang, W., Jiang, Q., Argentini, M., Cornu, D., Gigant, B., Knossow, M., and Wang, C. (2012a). Kif2c minimal functional domain has unusual nucleotide binding properties that are adapted to microtubule depolymerization. *Journal of Biological Chemistry*, 287(18):15143–15153.

[Wang et al., 2012b] Wang, Y., Zhang, X., Zhang, H., Lu, Y., Huang, H., Dong, X., Chen, J., Dong, J., Yang, X., Hang, H., et al. (2012b). Coiled-coil networking shapes cell molecular machinery. *Molecular biology of the cell*, 23(19):3911–3922.

[Watanabe et al., 2009] Watanabe, T., Noritake, J., Kakeno, M., Matsui, T., Harada, T., Wang, S., Itoh, N., Sato, K., Matsuzawa, K., Iwamatsu, A., et al. (2009). Phosphorylation of clasp2 by gsk-3β regulates its interaction with iqgap1, eb1 and microtubules. *Journal of cell science*, 122(16):2969–2979.

[Weisbrich et al., 2007] Weisbrich, A., Honnappa, S., Jaussi, R., Okhrimenko, O., Frey, D., Jelesarov, I., Akhmanova, A., and Steinmetz, M. O. (2007). Structure-function relationship of cap-gly domains. *Nature structural & molecular biology*, 14(10):959–967.

[Weisenberg et al., 1968] Weisenberg, R. C., Broisy, G. G., and Taylor, E. W. (1968). Colchicine-binding protein of mammalian brain and its relation to microtubules. *Biochemistry*, 7(12):4466–4479.

[Widlund et al., 2011] Widlund, P. O., Stear, J. H., Pozniakovsky, A., Zanic, M., Reber, S., Brouhard, G. J., Hyman, A. A., and Howard, J. (2011). Xmap215 polymerase activity is built by combining multiple tubulin-binding tog domains and a basic lattice-binding region. *Proceedings of the National Academy of Sciences*, 108(7):2741–2746.

[Wieczorek et al., 2015] Wieczorek, M., Bechstedt, S., Chaaban, S., and Brouhard, G. J. (2015). Microtubule-associated proteins control the kinetics of microtubule nucleation. *Nature cell biology*, 17(7):907.

[Woodruff et al., 2017] Woodruff, J. B., Gomes, B. F., Widlund, P. O., Mahamid, J., Honigmann, A., and Hyman, A. A. (2017). The centrosome is a selective condensate that nucleates microtubules by concentrating tubulin. *Cell*, 169(6):1066–1077.

[Wu et al., 2006] Wu, X., Xiang, X., and Hammer, J. A. (2006). Motor proteins at the microtubule plus-end. *Trends in cell biology*, 16(3):135–143.

[Xia et al., 2014] Xia, P., Liu, X., Wu, B., Zhang, S., Song, X., Yao, P. Y., Lippincott-Schwartz, J., and Yao, X. (2014). Superresolution imaging reveals structural features of eb1 in microtubule plus-end tracking. *Molecular biology of the cell*, 25(25):4166–4173.

[Yamashita et al., 2007] Yamashita, Y. M., Mahowald, A. P., Perlin, J. R., and Fuller, M. T. (2007). Asymmetric inheritance of mother versus daughter centrosome in stem cell division. *Science*, 315(5811):518–521.

[Yin et al., 2000] Yin, H., Pruyne, D., Huffaker, T. C., and Bretscher, A. (2000). Myosin v orientates the mitotic spindle in yeast. *Nature*, 406(6799):1013–1015.

[Zhang et al., 2015] Zhang, R., Alushin, G. M., Brown, A., and Nogales, E. (2015). Mechanistic origin of microtubule dynamic instability and its modulation by eb proteins. *Cell*, 162(4):849–859.

[Zimniak et al., 2012] Zimniak, T., Fitz, V., Zhou, H., Lampert, F., Opravil, S., Mechtler, K., Stolt-Bergner, P., and Westermann, S. (2012). Spatiotemporal regulation of ipl1/aurora activity by direct cdk1 phosphorylation. *Current Biology*, 22(9):787–793.

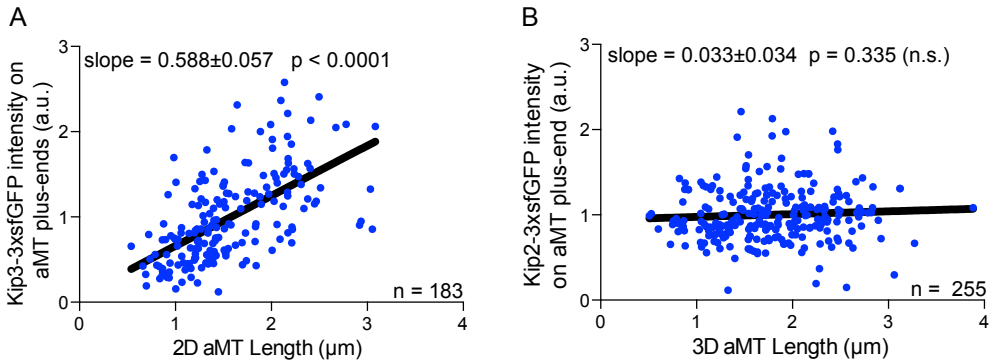

Figure 1 – The amount of Kip3 on plus-end increases with microtubule length, whereas Kip2 amount on plus-end does not change with microtubule length. Scatterplot of Kip3-3xsfGFP (A) or Kip2-3xsfGFP (B) intensity on plus-ends and microtubule length (μm) with linear regression line in black.

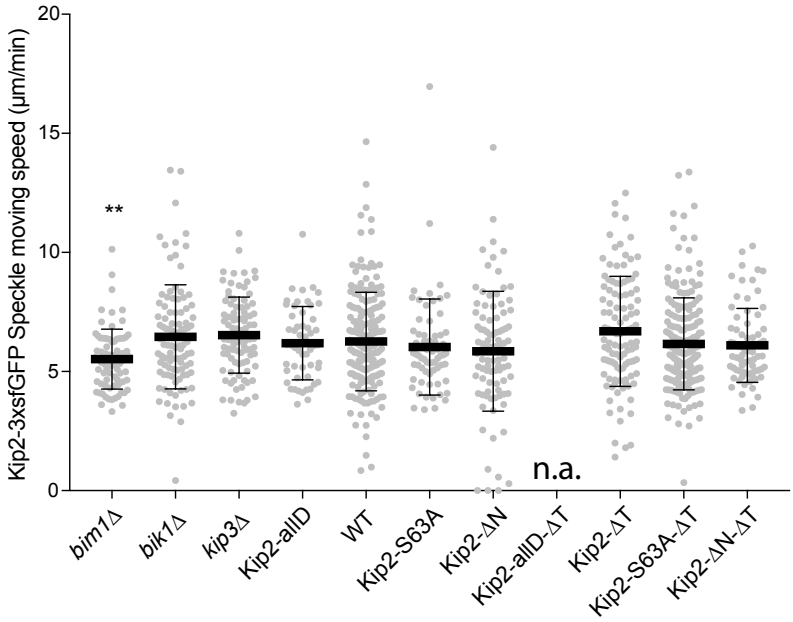

Figure 2 – Measurements of Kip2-3xsfGFP speckle moving speed along proximal aMT of metaphase cells with z-sum-projection of images acquired with 1.07 s intervals at 25°C. Statistical significances were calculated using student's t-test, **** $p \leqslant 0.0001$, *** $p \leqslant 0.001$, ** $p \leqslant 0.01$, * $p \leqslant 0.05$, n.s. $p > 0.05$. Only significant changes are shown. n.a., not available.

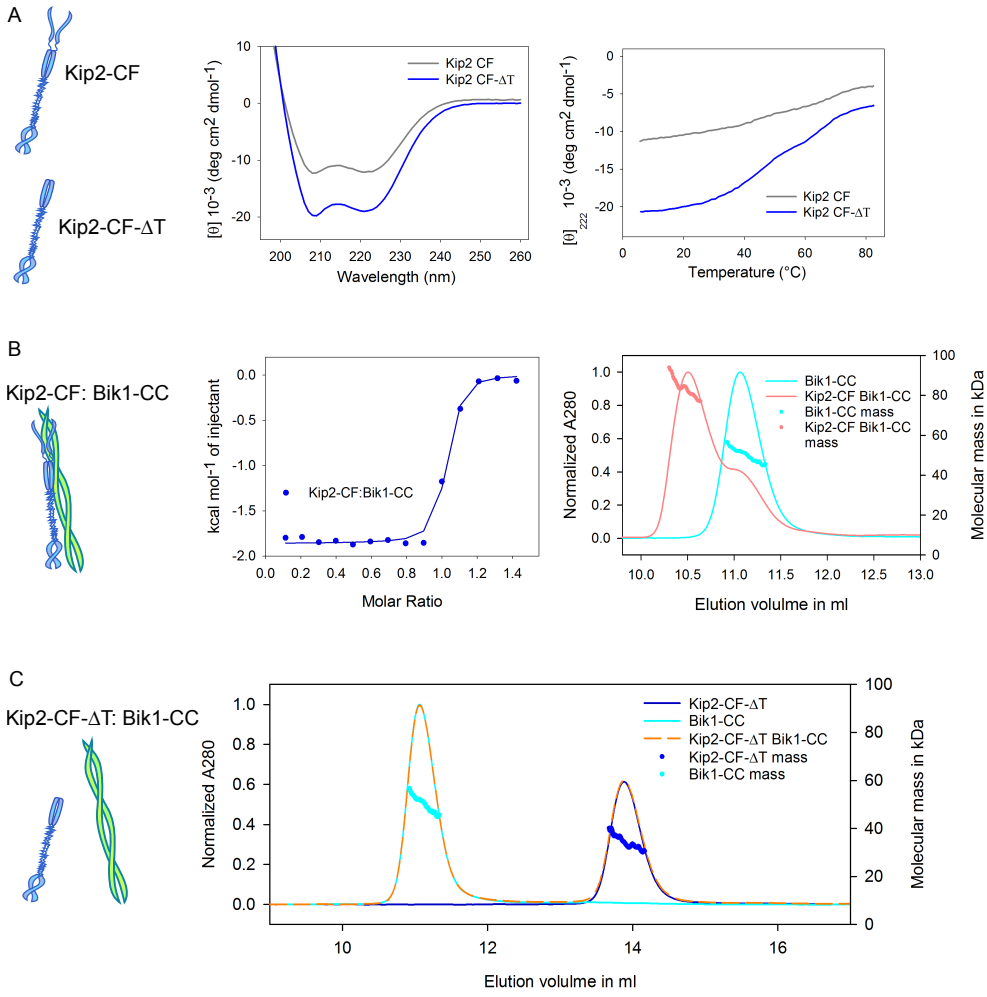

Figure 3 – Biophysical characterization of Kip2-CF and Bik1-CC interactions. (A)Both Kip2-CF and Kip2-CF-ΔT are well folded and dimerized. CD spectra (left) and thermal unfolding profiles (right) of Kip2-CF and Kip2-CF-ΔT. The spectra were recorded at 5 °C in PBS at a protein concentration of 0.2 mg/ml. The thermal unfolding profiles were recorded at 222nm. (B) ITC experiment (left) for Kip2-CF:Bik1-CC (closed circles). The solid line represents the fit that was obtained by using the monomeric concentrations of Bik1-CC and Kip2-CF. SEC-MALS experiments (right) of Bik1-CC alone (cyan) and Bik1-CC together with Kip2-CF (salmon) demonstrates the complex formation of Kip2-CF with Bik1-CC. Kip2-CF describes the C-terminal fragment of Kip2 (residues: 504-706) and Bik1-CC consists of the coiled-coil domian of Bik1 (residues 182-396). The UV absorption as 280nm and the molecular masses across the peaks determined by MALS are plotted. (C) SEC-MALS experiments of indicated proteins: The UV absorption as 280 nm of Bik1-CC alone (cyan), Kip2-CF-ΔT alone (blue) and Bik1-CC together with Kip2-CF-ΔT (orange) and the molecular masses across the peaks of Bik1-CC and Kip2-CF-ΔT determined by MALS are plotted. Kip2-CF-ΔT represents the C-terminal fragment of Kip2 (residues: 504-645).

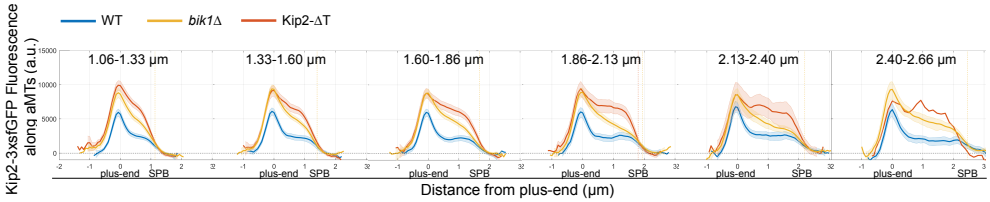

Figure 4 – Kip2-3xsfGFP distribution profiles along aMTs in metaphase cells of indicated genotype.

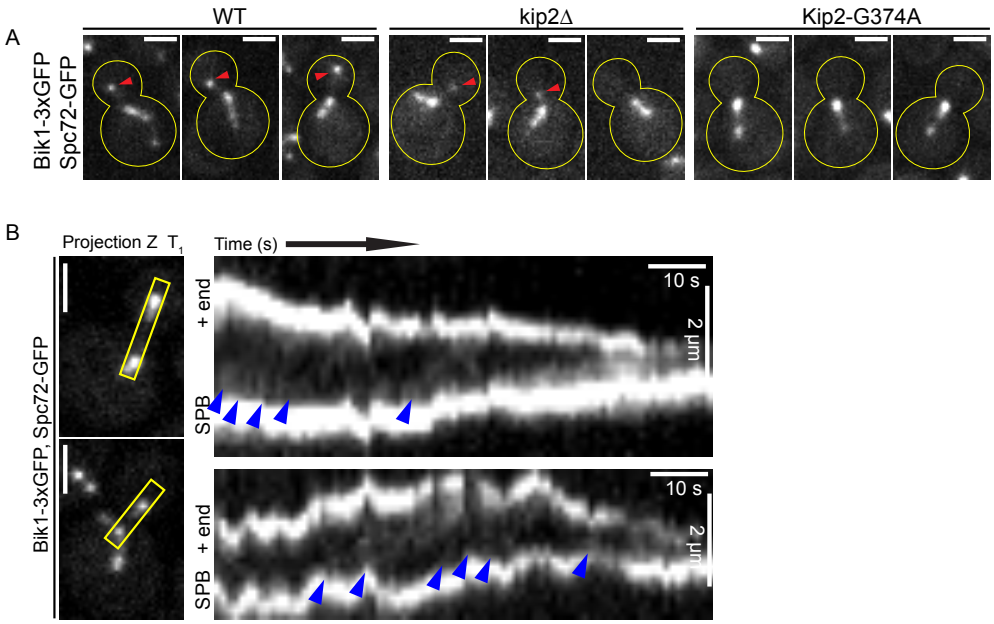

Figure 5 – Bik1 travels with Kip2 processively from microtubule minus-end to plus-end. (A) Representative images of cells expressing Bik1-3xGFP and Spc72-GFP in various context. Bik1-3xGFP is targeted to microtubule plus-end less efficiently in *kip2*Δ cells. ATP deficient Kip2 even traps Bik1-3xGFP at minus-ends where they are recruited. (B) Representative metaphase cells and kymographs of Bik1-3xGFP associated aMTs. Z-sum-projection imaging of the boxed aMT is displayed as kymograph (right). The entire kymograph x-axis represents 85.6 s, with 1.07 s interval. Blue arrow, emerging of a speckle at SPB. Scale bar, 2μm.

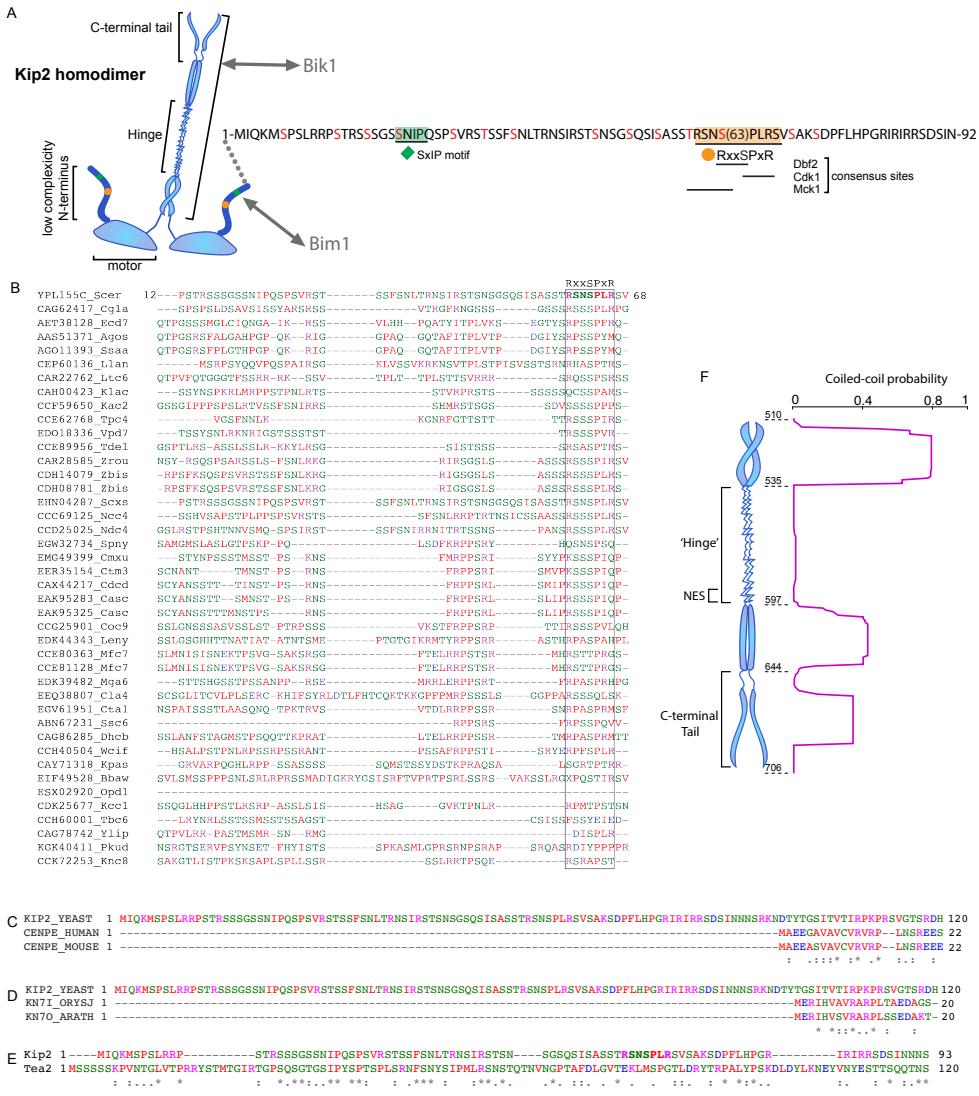

Figure 6 – Analysis of Kip2 features basing on its sequence. (A) Graphical representation of Kip2 domain organization. All of the serines and threonines mutated to aspartic acid in the Kip2-allD mutant are highlighted by red colour. Alignment of the N-terminal extensions of Kip2 and its homologs among Saccharomycetales(B), mammalian kinesin-7 CENP-E in human and mouse (C), plant kinesin-7s (D), and fission yeast Tea2 (E). (F) Analysis of the Kip2 sequence using a coiled-coil-prediction server (http://cb.csail.mit.edu/cb/multicoil/cgi-bin/multicoil.cgi/), with a cut-off of 0.5.

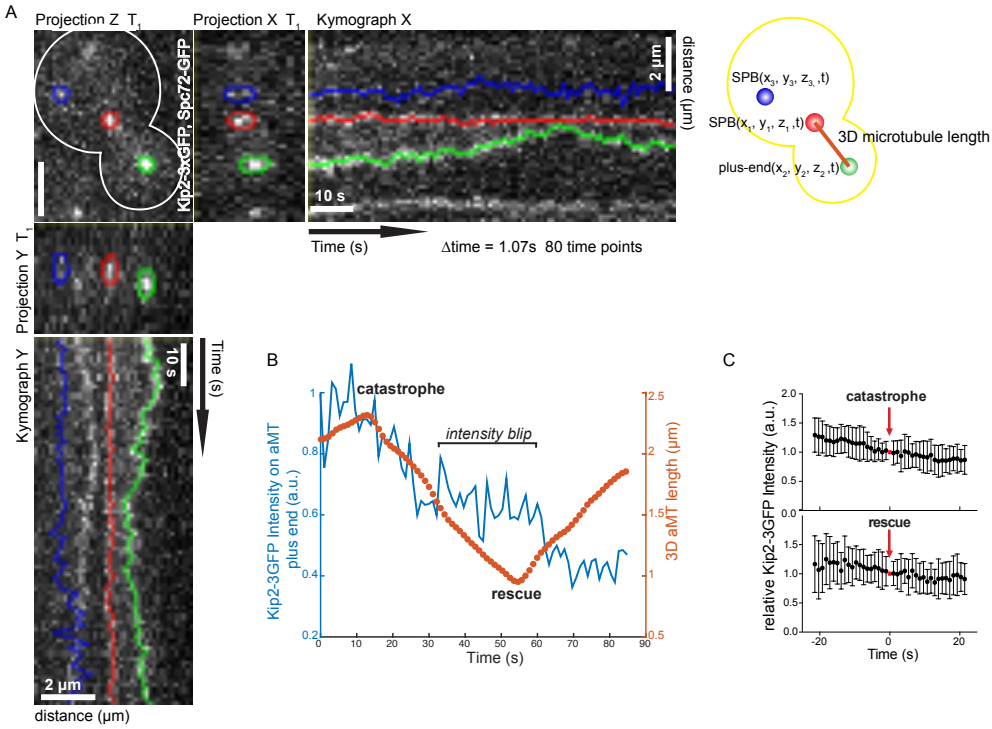

Figure 7 – Tracking aMT minus-end and plus-end using Spc72-GFP and Kip2-3xsfGFP as markers respectively. (A) Representative metaphase cell expressing Kip2-3xsfGFP and Spc72-GFP. The maximum intensity projections on to the z-axis, y-axis and x-axis has been shown on the top left, top right and the bottom left. The traces of the proximal SPB, + end and the distal SPB, +ends are all clearly visible, they are colored in red, green, blue and yellow respectively. Scale bar, 2μm. (B) The length of proximal aMT (orange) and background subtracted intensity of Kip2-3xsfGFP on plus-end (blue) overtime. (C) Kip2-3xsfGFP intensity on plus-end is not correlated with catastrophe or rescue event. Only events having no co-occurring catastrophe and resue events are counted. n = 29 events for catastrophe, n = 14 events for rescue.

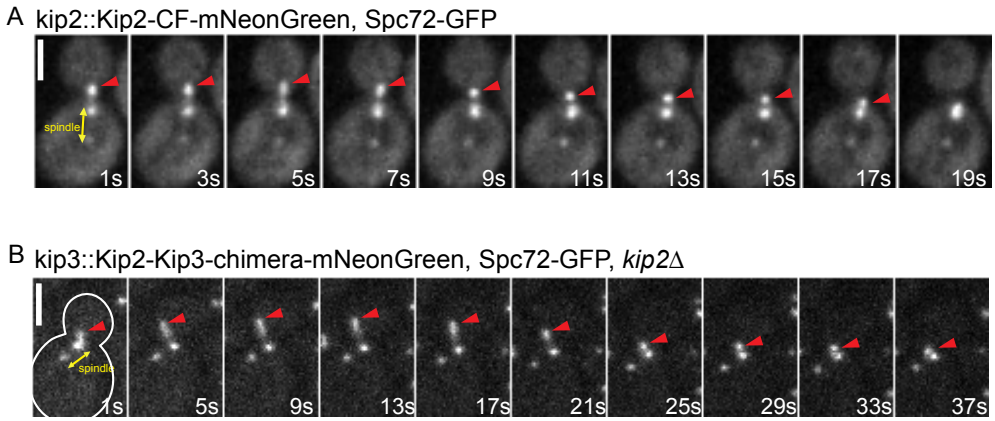

Figure 8 – Kip2-CF tracks microtubule plus-ends independently of Kip2 motor domian. (A) Kip2-CF-mNeonGreen accumulates on plus-end of both growing and shrinking aMT. Representative images depict the Z-sum-projection of one metaphase cell expressing Kip2-CF-mNeonGreen and a SPB marker Spc72-GFP. (B) The chimera protein composed of Kip3 motor domain and Kip2-CF accumulates on plus-end of both growing and shrinking aMT. The movies have 1.07 s intervals, but only representative time points are shown here. Scale bar, 2μm.

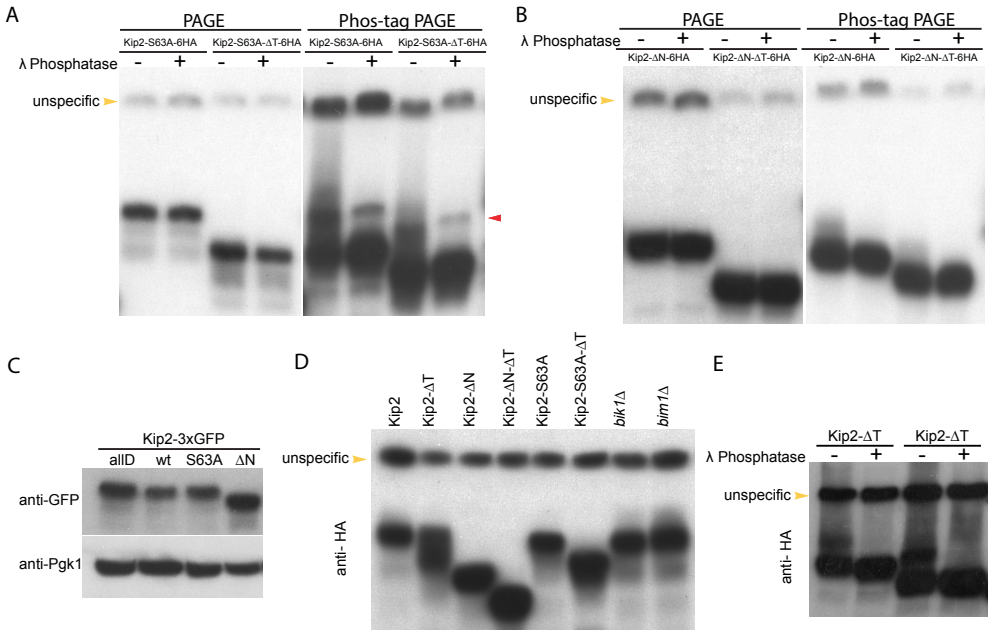

Figure 9 – Analysis of the abundance and phosphorylation level of Kip2 mutants with Western blotting. (A, B, E) Lysate prepared from cycling cells of indicated genotype were treated with or without λ-phosphatase and subjected to SDS-PAGE in the presence (right) or absence (left) of Mn^{2+}-Phos-tag followed by immunoblotting with anti-HA. Lysate prepared from cycling cells of indicated genotype were blotted with anti-GFP (C) or anti-HA (D). Pgk1 was used as a loading control.

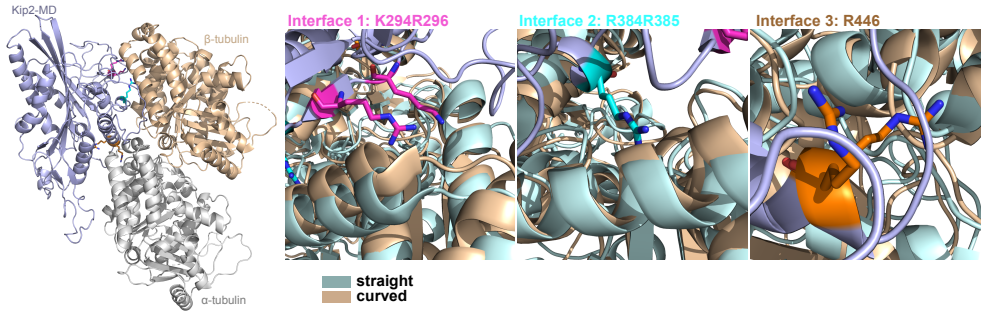

Figure 10 – The tubulin interface 1 might differentiate free tubulin dimers from microtubules by recognizing the different curvature conformations of the two.

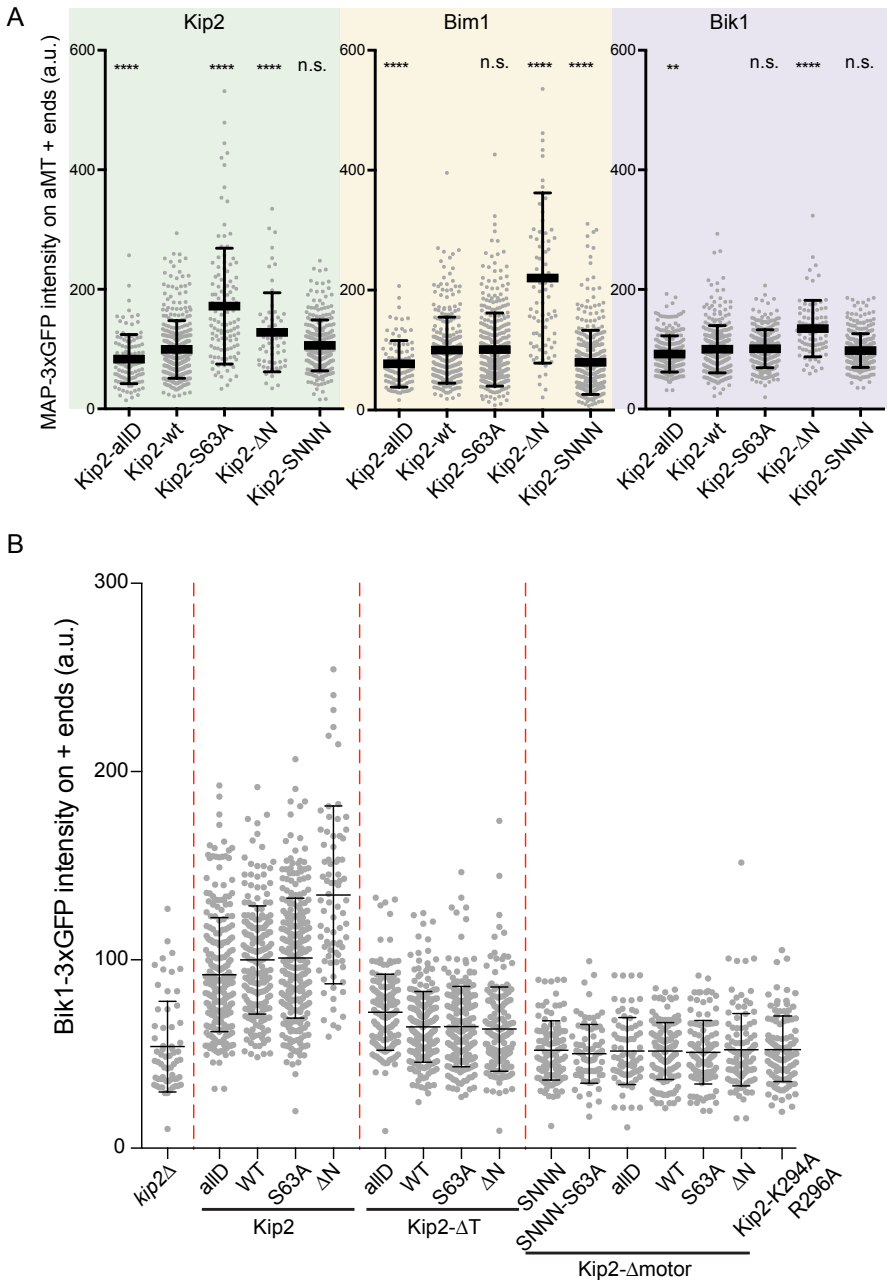

Figure 11 – (A) Analysis of Kip2 (left), Bim1 (middle), and Bik1 (right) abundance on aMT plus-ends in indicated Kip2 mutants. (B) Analysis of Bik1-3xGFP fluorescence on aMT plus-ends in the indicated Kip2 mutants. Statistical significances were calculated using student's t-test, **** $p \leqslant 0.0001$, *** $p \leqslant 0.001$, ** $p \leqslant 0.01$, * $p \leqslant 0.05$, n.s. $p > 0.05$.

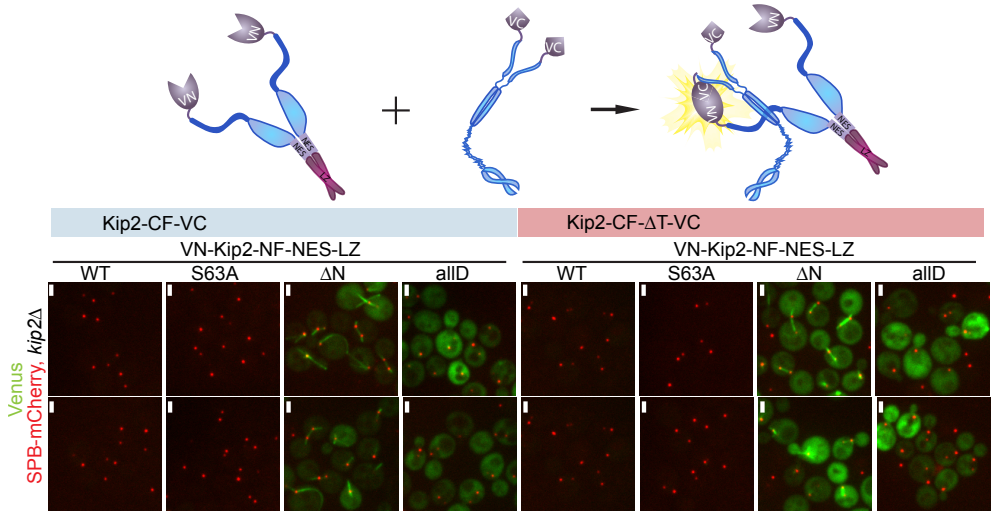

Figure 12 – Kip2 N-terminus prevents Kip2-CF from interacting with Kip2 motor domian in a BiFC Assay. Diagrams of the VN and VC fusion proteins (top) and representative images (bottom) of *kip2*Δ metaphase cells expressing SPB marker Spc42-mCherry and the indicated VN/VC fusion proteins. Scale bar: 2 μm.

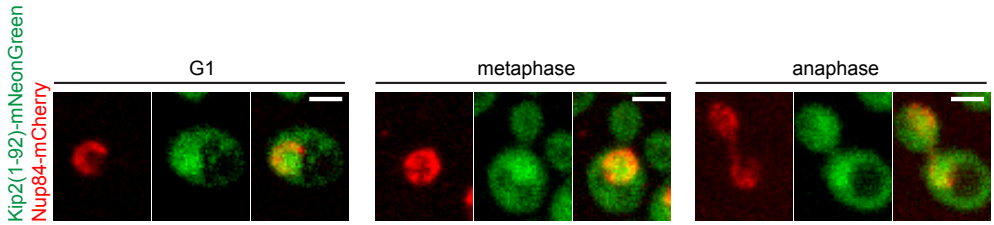

Figure 13 – In contrast to the exclusive cytosolic localization of full length Kip2p, the N-terminus of Kip2 fused to mNeonGreen is more abundant in nucleus. Representative images of G1 phase (left), metaphase (middle), and anaphase (right) cells expressing Kip2(1-92)-mNeonGreen and Nup84-mCherry. Scale bar: 2 μm.

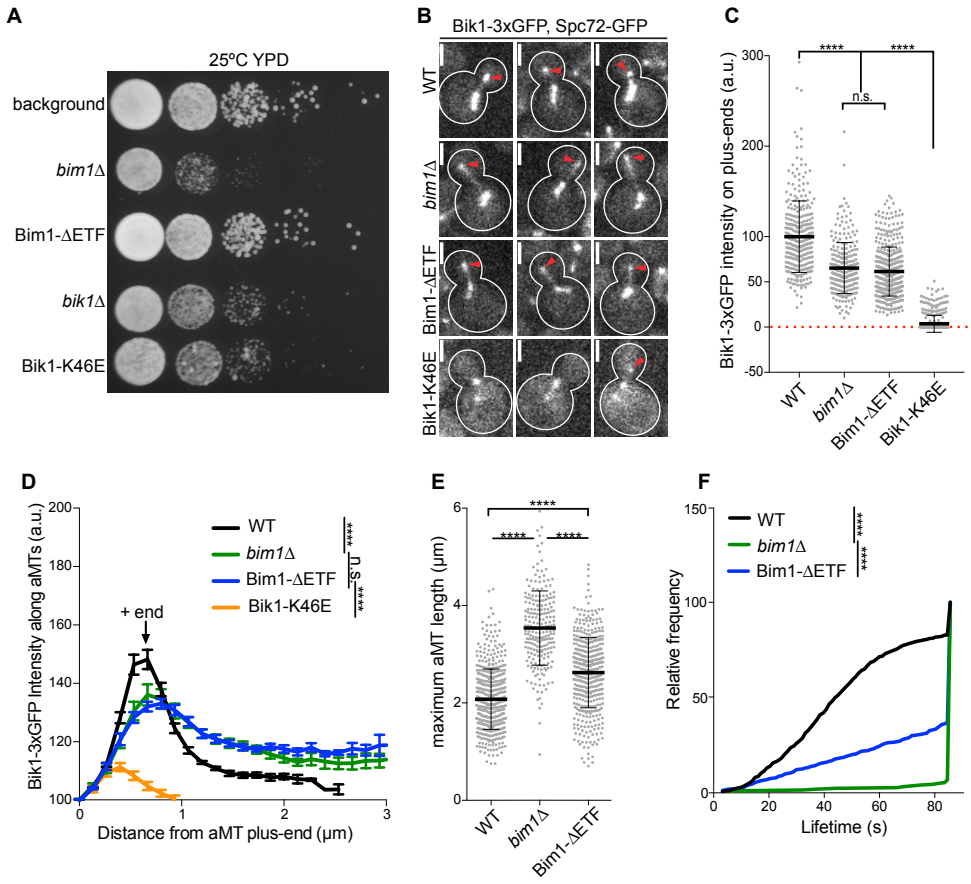

Figure 14 – Localization of Bik1 proteins on aMTs and the dynamics of aMTs in metaphase is altered in cells deficient in Bik1 CAP-Gly domain-mediated interactions. (A) Spot growth assay of background (Bik1-3xGFP, Spc72-GFP), *bim1*Δ, Bim1-ΔETF, and Bik1-K46E cells grown for 2 days on solid YPD agar at 25 °C. Spots are from logphase growing cell samples that was sequentially diluted tenfold. (B)Representative images of wild type, *bim1*Δ, Bim1-ΔETF metaphase cells expressing Bik1-3xGFP or Bik1-K46E-3xGFP and Spc72-GFP. Red arrowhead marks aMT plus-end. White box represents scale bar. (C) and (D) Quantification of Bik1-3xGFP fluorescence intensity (a.u.) on aMT plus-ends ($n > 250$ cells pooled from 3 independent clones for each mutant, mean ± s.d.) or Bik1-3xGFP distribution along aMTs by line scanning ($n > 30$ for each mutant, mean ± SEM, only cells positive with Bik1 K46E-3xGFP signal on plus-ends were used in line scanning analysis) in wild type, *bim1*Δ, Bim1-ΔETF, and Bik1-K46E metaphase cells. Statistical significance was calculated using two-tailed student t-test. (E) and (F) Measurements of maximum three-dimensional aMT length and lifetime within the 85.6s image acquisition window in wild type, *bim1*Δ, Bim1-ΔETF, and Bik1-K46E metaphase cells using Bik1-3xGFP and Spc72-GFP as the plus-end marker and minus-end marker respectively ($n > 250$ cells pooled from 3 independent clones for each mutant, mean ± s.d.). Statistical significances for aMT length was calculated using two-tailed student t-test. Differences among lifetime was demonstrated with cumulative distribution plot and assessed with Kolmogorov-Smirnov test. For all panels, **** $p > 0.0001$; n.s., not significant. N.D., not determined. (Bik1 K46E not shown because MT length was not measurable.) Scale bar: 2 μm.

ABBREVIATIONS

Abbreviation	Full Meaning
aMT	astral microtubule, or cytoplasmic microtubule
+TIP	plus-end tracking protein
CHO cells	Chinese hamster ovary cells
CAP-Gly domain	Cytoskeleton associated Protein Glycine-rich domain
CLIP	Cytoplasmic linker protein
EBs	End Binding proteins
CH domain	Calponin homology domain
EBH domain	EB homology domain
TOG domain	named after the human protein ch-TOG
yeGFP	yeast enhanced green fluorescent protein
sfGFP	superfolder green fluorescent protein
EM-CCD	Electron-multiplying charge-coupled device
MAP	Microtubule associated protein
SxIP	Consensus sequence that mediate interaction with EBs
LxxPTPh	Consensus sequence that mediate interaction with EBs
CENP-E	centromere protein E
cryoEM	Cryoeletron microscopy
MTOC	Microtubule-organizing center
SPB	Spindle pole body, yeast centrosome
GTP	Guanosine triphosphate
GDP	Guanosine diphosphate
GMPCPP	A slowly hydrolyzable GTP analog
GTPγS	A slowly hydrolyzable GTP analog
GDP-Pi	Guanosine diphosphate-γ-phosphate
TIRF	Total internal reflection fluorescence microscope
ER	endoplasmic reticulum
TACC	transforming acidic coiled-coil protein
KIF	kineisn superfamily proteins
FRAP	fluorescence recovery after photobleaching
FCS	fluorescence correlation spectroscopy
MEN	Mitotic Exit Network, Hippo pathway in metazoans
SPIN	SPB inheritance network

Metaphase aMT dynamics in Kip2 mutants

Haploids @ 30 ℃	kip2Δ-proximal	kip2Δ-distal	allD-proximal	allD-distal	WT-proximal	WT-distal	SNNN-proximal	SNNN-distal
total number of aMTs	301	n.a.	200	n.a.	511	110	399	57
total time spent in growth (s)	3605	n.a.	3263	n.a.	11364	2286	10967	1699
speed of grwoth (μm/min, mean±s.d.)	1.463±0.9164	n.a.	2.052±1.467	n.a.	1.994±1.839	1.754±1.304	1.944±1.702	1.889±1.608
total time spent in shrinkage (s)	2609.5	n.a.	2322.9	n.a.	13312	2547.2	13021	1171.6
mean speed of shrinkage (μm/min, mean±s.d.)	4.183±2.081	n.a.	3.586±2.307	n.a.	3.101±1.496	2.763±2.458	2.807±1.566	3.334±3.422
total number of catastrophe events	306	n.a.	214	n.a.	531	175	408	88
total number of rescue events	73	n.a.	77	n.a.	216	127	211	71
frequency of catastrophe (event/min)	5.0929	n.a.	3.935	n.a.	2.8036	4.5932	2.2322	3.1077
frequency of rescue (event/min)	1.6785	n.a.	1.9889	n.a.	0.97357	2.9915	0.97224	3.6361

table continues	S63A-proximal	S63A-distal	SNNN-S63A-proximal	SNNN-S63A-distal	ΔN-proximal	ΔN-distal	bim1Δ-proximal	bim1Δ-distal
total number of aMTs	266	115	290	65	336	48	227	56
total time spent in growth (s)	7620	3998	9745	2332	11082	1396	10015	1783
speed of grwoth (μm/min, mean±s.d.)	2.072±1.516	2.169±1.719	1.748±1.615	1.725±1.601	1.825±1.532	1.837±1.277	1.675±1.294	1.646±1.493
total time spent in shrinkage (s)	7953.6	3514.2	11309	2175.7	14505	1718.7	9129.5	2197.9
mean speed of shrinkage (μm/min, mean±s.d.)	2.652±2.693	2.198±1.745	2.026±1.68	2.317±2.36	2.314±1.513	2.826±2.198	1.715±1.398	2.403±2.542
total number of catastrophe events	346	215	370	139	348	80	419	144
total number of rescue events	266	188	277	135	237	69	415	132
frequency of catastrophe (event/min)	2.7244	3.2266	2.2781	3.5763	1.8841	3.4384	2.5102	4.8458
frequency of rescue (event/min)	1.8784	3.2099	1.4697	3.7229	1.0631	2.4088	2.7274	3.6034

List of plasmids used in this study

Plasmid (pYB) number	Genotype	Source
2256	p413-Adh1-ATG-linker-VN HIS AmpR	This study
2258	p415-Adh1-ATG-linker-VC LEU AmpR	This study
2263	p415-Adh1-Kip2(510-706)-CF-linker-VC LEU AmpR	This study
2264	p415-Adh1-Kip2(510-644)-CF-ΔT-linker-VC LEU AmpR	This study
2281	p413-Adh1-VN-Kip2-allD(1-92)-Bim1(1-210) HIS AmpR	This study
2286	p413-Adh1-VN-Kip2-wt(1-92)-Bim1(1-210)-NES-linker-LZ HIS AmpR	This study
2284	p413-Adh1-VN-Kip2-S63A(1-92)-Bim1(1-210)-NES-linker-LZ HIS	This study
2282	p413-Adh1-VN-Bim1(1-210)-NES-linker-LZ HIS AmpR	This study
2285	p413-Adh1-VN-Kip2-allD(1-92)-Bim1(1-210)-NES-linker-LZ HIS AmpR	This study
2275	p413-Adh1-VN-Kip2-wt-NF(1-509)-NES-linker-LZ HIS AmpR	This study
2276	p413-Adh1-VN-Kip2-S63A-NF(1-509)-NES-linker-LZ HIS AmpR	This study
2277	p413-Adh1-VN-Kip2-ΔN-NF(93-509)-NES-linker-LZ HIS AmpR	This study
2278	p413-Adh1-VN-Kip2-allD-NF(1-509)-NES-linker-LZ HIS AmpR	This study

List of oligonucleotides used in CRISPR

Bim1-ΔETF	gRNA target	5′-CAACAACTTGATCATCGACGAGG-3′
	Repair template F p1438	5′-GGTGAGGTTGGCGTGAGCAACAACTTGATCATCGACGAGTAAGTTGAGAACTAAAAAGCAGTATTGTTTTCGAATATGT-3′
	Repair template R p1439	5′-ACATATTCGAAAACAATACTGCTTTTTAGTTCTCAACTTACTCGTCGATGATCAAGTTGTTGCTCACGCCAACCTCACC- 3′
Kip3-ΔT	gRNA target	5′-TGTGTTTGTAAAATTGCTATCGG-3′ pYB2325
	Repair template F p1440	5′-GTTTGAATCTTTTGCCAGAACTTTTATCGCCAATCCtGATAGCAATTAACATACATATCCTACGTAAACTATCGAATATA-3′
	Repair template F p1441	5′-TATATTCGATAGTTTACGTAGGATATGTATGTTAATTGCTATCaGGATTGGCGATAAAAGTTCTGGCAAAAGATTCAAAC-3′
Kip2-S63A	gRNA target	5′-GGCTGATACGGATCTTAGTGGGG -3′ pYB2320
	Repair template F p1442	5′-GGTTCTCAGTCGATTTCTGCATCTTCCACTAGAAGTAACgcaCCACTAAGATCCGTATCAGCCAAATCCGATCCCTTCCT-3′
	Repair template R p1437	5′-AGGAAGGGATCGGATTTGGCTGATACGGATCTTAGTGGtgcGTTACTTCTAGTGGAAGATGCAGAAATCGACTGAGAACC-3′
Stu2-S277A	gRNA target	5′- TAATATGGACTTTCTTTTCCTGG-3′ pYB2291
	Repair template F p1443	5′- TTGGAAAAGAAAAGAAGCCAAGAGGAGGAAGCgAGGAAAAGAAAGgCCATATTATCGAATGATGAGGGGGAATATCAG -3′
	Repair template R p1444	5′- CTGATATTCCCCCTCATCATTCGATAATATGGcCTTTCTTTTCCTcGCTTCCTCCTCTTGGCTTCTTTTCTTTTCCAA -3′
Stu2-S602AS603A	gRNA target	5′- CGGTGAAGATGCCACTCTCTTGG-3′ pYB2292
	Repair template F p1445	5′- TCTCCTGAAAAAAAGTTCTGTACTTCCCTCaAAGAGAGTGGCAgCTgCACCGCTGAGAAATGATAACAAAAGTAAAGTGA -3′
	Repair template R p1446	5′- TCACTTTACTTTTGTTATCATTTCTCAGCGGTGcAGcTGCCACTCTCTTtGAGGGAAGTACAGAACTTTTTTTCAGGAGA -3′
Kin4-T209A	gRNA target	5′- TAGTTCTGGTGCTGCATAACAGG-3′ pYB2321

	Repair template F p1447	5′- GAAGATAACGAATTAATGAAAgCTTCTTGTGGTTCGCCaTGTTATGCAGCACCAGAACTAGTTGTTAGTACCAAGGCATA -3′
	Repair template R p1448	5′- TATGCCTTGGTACTAACAACTAGTTCTGGTGCTGCATAACAtGGCGAACCACAAGAAGcTTTCATTAATTCGTTATCTTC -3′
Kin4-S508A	gRNA target	5′- ACGTGCCTCGCAGTAGACCTAGG-3′ pYB2322
	Repair template F p1450	5′- CCACCGTATTGGTAATTATCACGTGCCTCGCAGTAGACCTAGaCCAACTgCATATTATCCTGGACTCAGTCGTAACACCG-3′
	Repair template R p1449	5′- CGGTGTTACGACTGAGTCCAGGATAATATGcAGTTGGtCTAGGTCTACTGCGAGGCACGTGATAATTACCAATACGGTGG-3′
Bfa1-S180A	gRNA target	5′- GCGTCACTTCAAGAAACTTAAGG-3′ pYB2323
	Repair template F p1451	5′- CTATCAAATAGCGTCACTTCAAGAAACTTAagaTCTGGTAATTCTGTAAGATTTAAGAAAgCTATGCCTAACTTAGCTTTAGTTAATCCA-3′
	Repair template R p1452	5′- TGGATTAACTAAAGCTAAGTTAGGCATAGcTTTCTTAAATCTTACAGAATTACCAGAtctTAAGTTTCTTGAAGTGACGCTATTTGATAG-3′
Bfa1-S150A	gRNA target	5′- TGAGTTTGGAAGATAAACCAAGG-3′ pYB2326
	Repair template F p1453	5′- GATAGAAAACTGAGTTTGGAAGATAAACCAAGACTAAAGCAACCTAGAGCAATGATGGAATTGAAACCAAAAAGAAAAC -3′
	Repair template R p1454	5′- GTTTTCTTTTTGGTTTCAATTCCATCATTGCTCTAGGTTGCTTTAGTCTTGGTTTATCTTCCAAACTCAGTTTTCTATC-3′
Bik1-K46E	gRNA target	5′- TCCATCGTTCTTACCAATGTTGG-3′ pYB2324
	Repair template F	5′-GCTGGAATGTTTGCTGGTGTAGACTTACTTGCCAACATTGGTGAGAACGATGGATCATTCATGGGGAAGAAGTATTTTCAAACGGAGTATCCTC-3′
	Repair template R	5′-GAGGATACTCCGTTTGAAAATACTTCTTCCCCATGAATGATCCATCGTTCTCACCAATGTTGGCAAGTAAGTCTACACCAGCAAACATTCCAGC-3′
Kip3-K125R	gRNA target	5′-GATGCGTGCAAGGGCCACTAAGG-3′ pYB2327
	Repair template F p1455	5′-GTGATCAGGTCCTGAACTCGATGCGTGCAAGGGCCACTAgaGCCACTGCGTCCTCTATCAATAACAGCAATGCTACGAAC-3′
	Repair template R p1456	5′-GTTCGTAGCATTGCTGTTATTGATAGAGGACGCAGTGGCtcTAGTGGCCCTTGCACGCATCGAGTTCAGGACCTGATCAC-3′

Kip3-pp1	gRNA target	5′-CATAGGGCTGGGACTAAGGTCGG-3′ pYB2328
	Repair template F p1457	5′-CCTACAACGGCAAAATTTTTCCCAAAAAAAAGcAAAGgcGACGAGTCCaGACCTTAGTCCCAGCCCTATGATTGAACCACAACCGGAGCTAGAACCAGAA-3′
	Repair template R p1458	5′-TTCTGGTTCTAGCTCCGGTTGTGGTTCAATCATAGGGCTGGGACTAAGGTCtGGACTCGTCgcCTTTgCTTTTTTTTGGGAAAAATTTTGCCGTTGTAGG-3′
Kip3-3A	Repair template F p1488	TTTTTCCCAAAAAAAAGTAAAGTGGACGgcTCCCGAtCTTgcTCCCgcCCCTATGATTGAACCACAACCGGAGCTAGAAC
	Repair template R p1489	GTTCTAGCTCCGGTTGTGGTTCAATCATAGGGgcGGGAgcAAGaTCGGGAgcCGTCCACTTTACTTTTTTTTGGGAAAAA
Kip3-3A-pp1	Repair template F P1490	CGGCAAAATTTTTCCCAAAAAAAAGcAAAGgcGACGgcTCCCGAtCTTgcTCCCgcCCCTATGATTGAACCACAACCGGA
	Repair template R p1491	TCCGGTTGTGGTTCAATCATAGGGgcGGGAgcAAGaTCGGGAgcCGTCgcCTTTgCTTTTTTTTGGGAAAAATTTTGCCG
Spc72-Δstu2	gRNA target	5′-TAACTGTGATCCTGCTGGTGAGG-3′ pYB2295
	Repair template F p1459	5′-GAGCAAGATGAAAATGCCCATCTTCTTGATAAAGAAagtTCACCAGCAGGATCACAGTTAGAAAGTAGGGACTCACCATC-3′
	Repair template R p1460	5′-GATGGTGAGTCCCTACTTTCTAACTGTGATCCTGCTGGTGAactTTCTTTATCAAGAAGATGGGCATTTTCATCTTGCTC-3′
Spc72-S236A	Repair template F p1461	5′-CAAAGCAGGATAAGGAAGAATTTCTTTCACTGGCCCAGagtTCACCAGCAGGAgCACAGTTAGAAAGTAGGGACTCACCATCAAGTAAAGAGG-3′
	Repair template R p1462	5′-CCTCTTTACTTGATGGTGAGTCCCTACTTTCTAACTGTGcTCCTGCTGGTGAactCTGGGCCAGTGAAAGAAATTCTTCCTTATCCTGCTTTG-3′
Spc72-S231AS232A	Repair template F p1463	5′-AAGCAGGATAAGGAAGAATTTCTTTCACTGGCCCAGgctgCACCAGCAGGATCACAGTTAGAAAGTAGGGACTCACCATC-3′
	Repair template R p1464	5′-GATGGTGAGTCCCTACTTTCTAACTGTGATCCTGCTGGTGcagcCTGGGCCAGTGAAAGAAATTCTTCCTTATCCTGCTT-3′
Spc72-S231AS232A S236A	Repair template F p1465	5′-CAAAGCAGGATAAGGAAGAATTTCTTTCACTGGCCCAGgcagCACCAGCAGGAgCACAGTTAGAAAGTAGGGACTCACCATCAAGTAAAGAGG-3′
	Repair template R p1466	5′-CCTCTTTACTTGATGGTGAGTCCCTACTTTCTAACTGTGcTCCTGCTGGTGctgcCTGGGCCAGTGAAAGAAATTCTTCCTTATCCTGCTTTG-3′

List of strains used in this study

Yeast (yYB) Strain number	Mating type	Genotype	background	source
9733 (WT)	a	*ura3-52 his3Δ200 leu2 lys2-801 trp1Δ63 Ade2+*	S288C	this study
10377 (WT)	alpha	*ura3-52 his3Δ200 leu2 lys2-801 trp1Δ63 Ade2+*	S288C	this study
11068	alpha	*Bik1-3xGFP:HYG Spc72-GFP:His3MX* *ura3-52 his3Δ200 leu2 lys2-801 trp1Δ63 Ade2+*	S288C	this study
11069	a	*Bik1-3xGFP:HYG Spc72-GFP:His3MX* *ura3-52 his3Δ200 leu2 lys2-801 trp1Δ63 Ade2+*	S288C	this study
9806	a	*Kip2-3xsfGFP:KanMX4 Spc72-GFP:His3MX* *ura3-52 his3Δ200 leu2 lys2-801 trp1Δ63 Ade2+*	S288C	this study
11045	alpha	*Bim1-3xsfGFP:KanMX4* *ura3-52 his3Δ200 leu2 lys2-801 trp1Δ63 Ade2+*	S288C	this study
10414	a	*Kip3-3xsfGFP:KanMX4 Spc72-GFP:His3MX* *ura3-52 his3Δ200 leu2 lys2-801 trp1Δ63 Ade2+*	S288C	this study
14702	a	*Bik1-3xGFP:HYG Spc42-mCherry:NatMX* *ura3-52 his3Δ200 leu2 lys2-801 trp1Δ63 Ade2+*	S288C	this study
12090	a	*GFP-TUB1:LEU2* *ura3-52 his3-Δ200 trp1-Δ63*	S288C	Su et al., 2013
11076	a	*bim1Δ::hphNT1 Spc72-GFP:His3MX* *ura3-52 his3Δ200 leu2 lys2-801 trp1Δ63 Ade2+*	S288C	this study
10795	a	*Kip2-ΔT-3xsfGFP:KanMX4 Spc72-GFP:His3MX* *ura3-52 his3Δ200 leu2 lys2-801 trp1Δ63 Ade2+*	S288C	this study
10792	a	*Kip2-SNNN1-3xsfGFP:KanMX4 Spc72-GFP:His3MX* *ura3-52 his3Δ200 leu2 lys2-801 trp1Δ63 Ade2+*	S288C	this study
11046	a	*Kip2-3xsfGFP:KanMX4 Spc72-GFP:His3MX bik1Δ::hphNT1* *ura3-52 his3Δ200 leu2 lys2-801 trp1Δ63 Ade2+*	S288C	this study
11048	a	*Kip2-3xsfGFP:KanMX4 Spc72-GFP:His3MX bim1Δ::hphNT1* *ura3-52 his3Δ200 leu2 lys2-801 trp1Δ63 Ade2+*	S288C	this study
10676	a	*Kip2-S63A-3xsfGFP:KanMX4 Spc72-GFP:His3MX* *ura3-52 his3Δ200 leu2 lys2-801 trp1Δ63 Ade2+*	S288C	this study
14629	a	*Kip2-S63A-ΔT-3xsfGFP:KanMX4 Spc72-GFP:His3MX* *ura3-52 his3Δ200 leu2 lys2-801 trp1Δ63 Ade2+*	S288C	this study
10648	a	*Kip2-ΔN-3xsfGFP:KanMX4 Spc72-GFP:His3MX* *ura3-52 his3Δ200 leu2 lys2-801 trp1Δ63 Ade2+*	S288C	this study
10758	a	*Kip2-ΔN-ΔT-3xsfGFP:KanMX4 Spc72-GFP:His3MX* *ura3-52 his3Δ200 leu2 lys2-801 trp1Δ63 Ade2+*	S288C	this study
14698	a	*Kip2-allD-3xsfGFP:KanMX4 Spc72-GFP:His3MX* *ura3-52 his3Δ200 leu2 lys2-801 trp1Δ63 Ade2+*	S288C	this study
14699	a	*Kip2-allD-ΔT-3xsfGFP:KanMX4 Spc72-GFP:His3MX* *ura3-52 his3Δ200 leu2 lys2-801 trp1Δ63 Ade2+*	S288C	this study
14772	alpha	*Kip2-3xsfGFP:KanMX4 Spc72-GFP:His3MX Bim1-ΔETF* *ura3-52 his3Δ200 leu2 lys2-801 trp1Δ63 Ade2+*	S288C	this study
14963	a	*Kip2-K294A-R296A-3xsfGFP:KanMX4 Spc72-GFP:His3MX* *ura3-52 his3Δ200 leu2 lys2-801 trp1Δ63 Ade2+*	S288C	this study

14964	a	*Kip2-G374A-3xsfGFP:KanMX4 Spc72-GFP:His3MX ura3-52 his3Δ200 leu2 lys2-801 trp1Δ63 Ade2+*	S288C	this study
14965	a	*Kip2-R446A-3xsfGFP:KanMX4 Spc72-GFP:His3MX ura3-52 his3Δ200 leu2 lys2-801 trp1Δ63 Ade2+*	S288C	this study
14966	a	*Kip2-R384A-3xsfGFP:KanMX4 Spc72-GFP:His3MX ura3-52 his3Δ200 leu2 lys2-801 trp1Δ63 Ade2+*	S288C	this study
14939	a	*GFP-TUB1:LEU2 bik1Δ::NatMX ura3-52 his3-Δ200 trp1-Δ63*	S288C	this study
14936	a	*kip2Δ::Kip2-ΔN(93-536):(565-706)-3xsfGFP:KanMX4 Spc72-GFP:His3MX ura3-52 his3Δ200 leu2 lys2-801 trp1Δ63 Ade2+*	S288C	this study
14937	a	*kip2Δ::Kip2-allD(1-536):(565-706)-3xsfGFP:KanMX4 Spc72-GFP:His3MX ura3-52 his3Δ200 leu2 lys2-801 trp1Δ63 Ade2+*	S288C	this study
14935	a	*kip2Δ::Kip2-S63A(1-536):(565-706)-3xsfGFP:KanMX4 Spc72-GFP:His3MX ura3-52 his3Δ200 leu2 lys2-801 trp1Δ63 Ade2+*	S288C	this study
14931	a	*kip2Δ::Kip2-wt(1-536):(565-706)-3xsfGFP:KanMX4 Spc72-GFP:His3MX ura3-52 his3Δ200 leu2 lys2-801 trp1Δ63 Ade2+*	S288C	this study
14750	a	*Kip2-allD-Δmotor-3xsfGFP:KanMX4 Spc42-mCherry:NAT kip3Δ::URA ura3-52 his3Δ200 leu2 lys2-801 trp1Δ63 Ade2+*	S288C	this study
14773	a	*Kip2-allD-Δmotor-ΔT-3xsfGFP:KanMX4 Spc42-mCherry:NAT kip3Δ::URA ura3-52 his3Δ200 leu2 lys2-801 trp1Δ63 Ade2+*	S288C	this study
14662	a	*Kip2-S63A-Δmotor-3xsfGFP:KanMX4 Spc42-mCherry:NAT Δ ura3-52 his3Δ200 leu2 lys2-801 trp1Δ63 Ade2+*	S288C	this study
14858	a	*Kip2-S63A-Δmotor-ΔT-3xsfGFP:KanMX4 Spc42-mCherry:NAT ura3-52 his3Δ200 leu2 lys2-801 trp1Δ63 Ade2+*	S288C	this study
14663	a	*Kip2-ΔN-Δmotor-3xsfGFP:KanMX4 Spc42-mCherry:NAT kip3Δ::URA ura3-52 his3Δ200 leu2 lys2-801 trp1Δ63 Ade2+*	S288C	this study
14713	a	*Kip2-ΔN-Δmotor-ΔT-3xsfGFP:KanMX4 Spc42-mCherry:NAT kip3Δ::URA ura3-52 his3Δ200 leu2 lys2-801 trp1Δ63 Ade2+*	S288C	this study
14714	a	*Kip2-SNNN-S63A-Δmotor-3xsfGFP:KanMX4 Spc42-mCherry:NAT kip3Δ::URA ura3-52 his3Δ200 leu2 lys2-801 trp1Δ63 Ade2+*	S288C	this study
14715	a	*Kip2-SNNN-Δmotor-3xsfGFP:KanMX4 Spc42-mCherry:NAT kip3Δ::URA ura3-52 his3Δ200 leu2 lys2-801 trp1Δ63 Ade2+*	S288C	this study
14661	a	*Kip2-Δmotor-3xsfGFP:KanMX4 Spc42-mCherry:NAT kip3Δ::URA ura3-52 his3Δ200 leu2 lys2-801 trp1Δ63 Ade2+*	S288C	this study
14771	a	*Kip2-Δmotor-ΔT-3xsfGFP:KanMX4 Spc42-mCherry:NAT kip3Δ::URA ura3-52 his3Δ200 leu2 lys2-801 trp1Δ63 Ade2+*	S288C	this study
14913	a	*Kip2-ΔN-Δmotor-ΔHinge-3xsfGFP:KanMX4 Spc42-mCherry:NAT kip3Δ::URA ura3-52 his3Δ200 leu2 lys2-801 trp1Δ63 Ade2+*	S288C	this study
14912	a	*Kip2-allD-Δmotor-ΔHinge-3xsfGFP:KanMX4 Spc42-mCherry:NAT kip3Δ::URA ura3-52 his3Δ200 leu2 lys2-801 trp1Δ63 Ade2+*	S288C	this study
14911	a	*Kip2-S63A-Δmotor-ΔHinge-3xsfGFP:KanMX4 Spc42-mCherry:NAT kip3Δ::URA ura3-52 his3Δ200 leu2 lys2-801 trp1Δ63 Ade2+*	S288C	this study
14910	a	*Kip2-wt-Δmotor-ΔHinge-3xsfGFP:KanMX4 Spc42-mCherry:NAT kip3Δ::URA ura3-52 his3Δ200 leu2 lys2-801 trp1Δ63 Ade2+*	S288C	this study
14764	diploid	*KIP2/Kip2-Δmotor-3xsfGFP:KanMX4 Spc42-mCherry:NAT/ Spc42-mCherry:NAT KIP3/kip3Δ::URA ura3-52 his3Δ200 leu2 lys2-801 trp1Δ63 Ade2+*	S288C	this study

14765	diploid	*KIP2/Kip2-S63A-Δmotor-3xsfGFP:KanMX4 Spc42-mCherry:NAT/ Spc42-mCherry:NAT KIP3/kip3Δ::URA ura3-52 his3Δ200 leu2 lys2-801 trp1Δ63 Ade2+*	S288C	this study
14766	diploid	*KIP2/Kip2-ΔN-Δmotor-3xsfGFP:KanMX4 Spc42-mCherry:NAT/ Spc42-mCherry:NAT KIP3/kip3Δ::URA ura3-52 his3Δ200 leu2 lys2-801 trp1Δ63 Ade2+*	S288C	this study
14767	diploid	*KIP2/Kip2-allD-Δmotor-3xsfGFP:KanMX4 Spc42-mCherry:NAT/ Spc42-mCherry:NAT KIP3/kip3Δ::URA ura3-52 his3Δ200 leu2 lys2-801 trp1Δ63 Ade2+*	S288C	this study
14768	diploid	*KIP2/Kip2-ΔN-Δmotor-ΔT-3xsfGFP:KanMX4 Spc42-mCherry:NAT/ Spc42-mCherry:NAT KIP3/kip3Δ::URA ura3-52 his3Δ200 leu2 lys2-801 trp1Δ63 Ade2+*	S288C	this study
14769	diploid	*KIP2/Kip2-SNNN-S63A-Δmotor-3xsfGFP:KanMX4 Spc42-mCherry:NAT/ Spc42-mCherry:NAT KIP3/kip3Δ::URA ura3-52 his3Δ200 leu2 lys2-801 trp1Δ63 Ade2+*	S288C	this study
14770	diploid	*KIP2/Kip2-SNNN-Δmotor-3xsfGFP:KanMX4 Spc42-mCherry:NAT/ Spc42-mCherry:NAT KIP3/kip3Δ::URA ura3-52 his3Δ200 leu2 lys2-801 trp1Δ63 Ade2+*	S288C	this study
12394	a	*kip3Δ::Kip3(1-480):Kip2(510-706)::mNeonGreen::NAT Spc72-GFP:His3MX kip2Δ::hphNT1 ura3-52 his3Δ200 leu2 lys2-801 trp1Δ63 Ade2+*	S288C	this study
14580	?	*kip3Δ::Kip3(1-480)-Kip2(510-706)-mNeonGreen:NAT Spc72-GFP:His3MX kip2Δ::hphNT1 bik1Δ::NatMX ura3-52 his3Δ200 leu2 lys2-801 trp1Δ63 Ade2+*	S288C	this study
11875	a	*Kip3-3xsfGFP:KanMX4 Spc72-GFP:His3MX ura3-52 his3Δ200 leu2 lys2-801 trp1Δ63 Ade2+*	S288C	this study
14265	a	*kip3Δ::Kip3(694-806)-3xsfGFP:KanMX4 Spc72-mCherry:KanMX4 ura3-52 his3Δ200 leu2 lys2-801 trp1Δ63 Ade2+*	S288C	this study
14265	a	*kip3Δ::LZ-3HA-Kip3(694-806)-3xsfGFP:KanMX4 Spc42-mCherry:KanMX4 ura3-52 his3Δ200 leu2 lys2-801 trp1Δ63 Ade2+*	S288C	this study
13271	alpha	*kip3Δ::LZ-Kip3(440-806)-3xsfGFP:KanMX4 Spc72-GFP:His3MX ura3-52 his3Δ200 leu2 lys2-801 trp1Δ63 Ade2+*	S288C	this study
13117	a	*kip3Δ::Kip3-pp1-mNeonGreen:NAT Spc72-GFP:His3MX ura3-52 his3Δ200 leu2 lys2-801 trp1Δ63 Ade2+*	S288C	this study
11664	a	*kip3Δ::Kip3-wt-mNeonGreen:NAT Spc72-GFP:His3MX ura3-52 his3Δ200 leu2 lys2-801 trp1Δ63 Ade2+*	S288C	this study
11667	a	*kip3Δ::Kip3-pp1-3A-mNeonGreen:NAT Spc72-GFP:His3MX ura3-52 his3Δ200 leu2 lys2-801 trp1Δ63 Ade2+*	S288C	this study
13381	a	*kip3Δ::Kip3-3A-mNeonGreen:NAT Spc72-GFP:His3MX ura3-52 his3Δ200 leu2 lys2-801 trp1Δ63 Ade2+*	S288C	this study
12563	alpha	*Bik1-3xGFP:HYG Spc72-GFP:HIS kip2 Δ::Kip2-wt-TRP ura3-52 his3Δ200 leu2 lys2-801 Ade2+*	S288C	this study
11762	a	*Bik1-3xGFP:HYG Spc72-GFP:HIS kip2Δ::hphNT1 ura3-52 his3Δ200 leu2 lys2-801 Ade2+*	S288C	this study
11763	alpha	*Bik1-3xGFP:HYG Spc72-GFP:HIS kip2Δ::hphNT1 ura3-52 his3Δ200 leu2 lys2-801 trp1Δ63 Ade2+*	S288C	this study
12566	alpha	*Bik1-3xGFP:HYG Spc72-GFP:HIS kip2Δ::Kip2-ΔN:TRP ura3-52 his3Δ200 leu2 lys2-801 trp1Δ63 Ade2+*	S288C	this study
12577	a	*Bik1-3xGFP:HYG Spc72-GFP:HIS kip2Δ::Kip2-ΔN:TRP ura3-52 his3Δ200 leu2 lys2-801 trp1Δ63 Ade2+*	S288C	this study
12512	a	*Bik1-3xGFP:HYG Spc72-GFP:HIS kip2Δ::Kip2-SNNN:TRP ura3-52 his3Δ200 leu2 lys2-801 trp1Δ63 Ade2+*	S288C	this study
12781	alpha	*Bik1-3xGFP:HYG Spc72-GFP:HIS kip2Δ::Kip2-ΔT:TRP ura3-52 his3Δ200 leu2 lys2-801 trp1Δ63 Ade2+*	S288C	this study

12777	alpha	*Bik1-3xGFP:HYG Spc72-GFP:HIS kip2Δ::Kip2-ΔN-ΔT:TRP ura3-52 his3Δ200 leu2 lys2-801 trp1Δ63 Ade2+*	S288C	this study
11364	a	*Bik1-3xGFP:HYG Spc72-GFP:HIS kip2Δ::Kip2-S63A:TRP ura3-52 his3Δ200 leu2 lys2-801 trp1Δ63 Ade2+*	S288C	this study
13115	a	*Bik1-3xGFP:HYG Spc72-GFP:HIS kip2Δ::Kip2-SNNN-S63A:TRP ura3-52 his3Δ200 leu2 lys2-801 trp1Δ63 Ade2+*	S288C	this study
11077	a	*Bik1-3xGFP:HYG Spc72-GFP:HIS bim1Δ::hphNT1 ura3-52 his3Δ200 leu2 lys2-801 trp1Δ63 Ade2+*	S288C	this study
13120	a	*Bik1-3xGFP:HYG Spc72-GFP:HIS kip2Δ::Kip2-S63A-ΔT:TRP ura3-52 his3Δ200 leu2 lys2-801 trp1Δ63 Ade2+*	S288C	this study
13119	alpha	*Bik1-3xGFP:HYG Spc72-GFP:HIS kip2Δ::Kip2-S63A-ΔT:TRP ura3-52 his3Δ200 leu2 lys2-801 trp1Δ63 Ade2+*	S288C	this study
11338	alpha	*Bik1-3xGFP:HYG Spc72-GFP:HIS mck1Δ::KanMX4 ura3-52 his3Δ200 leu2 lys2-801 trp1Δ63 Ade2+*	S288C	this study
14454	a	*Bik1-3xGFP:HYG Spc72-GFP:HIS mck1Δ::KanMX4 kip2Δ::hphNT1 ura3-52 his3Δ200 leu2 lys2-801 trp1Δ63 Ade2+*	S288C	this study
13111	a	*Bik1-3xGFP:HYG Spc72-GFP:HIS dbf2-2 dbf20::hyg CFP-Tub1:URA ura3-52 his3Δ200 leu2 lys2-801 trp1Δ63 Ade2+*	S288C	this study
13113	alpha	*Bik1-3xGFP:HYG Spc72-GFP:HIS dbf2-2 dbf20::hyg CFP-Tub1:URA ura3-52 his3Δ200 leu2 lys2-801 trp1Δ63 Ade2+*	S288C	this study
14455	a	*Bik1-3xGFP:HYG Spc72-GFP:HIS dbf2-2 dbf20::hyg kip2Δ::hphNT1 ura3-52 his3Δ200 leu2 lys2-801 trp1Δ63 Ade2+*	S288C	this study
14855	alpha	*Bik1-3xGFP:HYG Spc72-GFP:HIS kip2Δ::Kip2-allD-6HA:NAT ura3-52 his3Δ200 leu2 lys2-801 trp1Δ63 Ade2+*	S288C	this study
14842	alpha	*Bik1-3xGFP:HYG Spc72-GFP:HIS kip2Δ::Kip2-S63A-Δmotor-6HA:NAT ura3-52 his3Δ200 leu2 lys2-801 trp1Δ63 Ade2+*	S288C	this study
14843	alpha	*Bik1-3xGFP:HYG Spc72-GFP:HIS kip2Δ::Kip2-SNNN-Δmotor-6HA:NAT ura3-52 his3Δ200 leu2 lys2-801 trp1Δ63 Ade2+*	S288C	this study
14853	alpha	*Bik1-3xGFP:HYG Spc72-GFP:HIS kip2Δ::Kip2-wt-Δmotor-6HA:NAT ura3-52 his3Δ200 leu2 lys2-801 trp1Δ63 Ade2+*	S288C	this study
14854	alpha	*Bik1-3xGFP:HYG Spc72-GFP:HIS kip2Δ::Kip2-ΔN-Δmotor-6HA:NAT ura3-52 his3Δ200 leu2 lys2-801 trp1Δ63 Ade2+*	S288C	this study
14859	alpha	*Bik1-3xGFP:HYG Spc72-GFP:HIS kip2Δ::Kip2-allD-Δmotor-6HA:NAT ura3-52 his3Δ200 leu2 lys2-801 trp1Δ63 Ade2+*	S288C	this study
14852	alpha	*Bik1-3xGFP:HYG Spc72-GFP:HIS kip2Δ::Kip2-SNNN-S63A-Δmotor-6HA:NAT ura3-52 his3Δ200 leu2 lys2-801 trp1Δ63 Ade2+*	S288C	this study
14991	alpha	*Bik1-3xGFP:HYG Spc72-GFP:HIS kip2Δ::Kip2-K294A-R296A:Trp ura3-52 his3Δ200 leu2 lys2-801 trp1Δ63 Ade2+*	S288C	this study
14994	alpha	*Bik1-3xGFP:HYG Spc72-GFP:HIS kip2Δ::Kip2-R446A:Trp ura3-52 his3Δ200 leu2 lys2-801 trp1Δ63 Ade2+*	S288C	this study
14996	alpha	*Bik1-3xGFP:HYG Spc72-GFP:HIS kip2Δ::Kip2-G374A:Trp ura3-52 his3Δ200 leu2 lys2-801 trp1Δ63 Ade2+*	S288C	this study
15010	alpha	*Bik1-3xGFP:HYG Spc72-GFP:HIS kip2Δ::Kip2-allD(1-536)-(565-706)-6HA:NAT ura3-52 his3Δ200 leu2 lys2-801 trp1Δ63 Ade2+*	S288C	this study
15011	alpha	*Bik1-3xGFP:HYG Spc72-GFP:HIS kip2Δ::Kip2-S63A(1-536)-(565-706)-6HA:NAT ura3-52 his3Δ200 leu2 lys2-801 trp1Δ63 Ade2+*	S288C	this study
15012	alpha	*Bik1-3xGFP:HYG Spc72-GFP:HIS kip2Δ::Kip2-wt(1-536)-(565-706)-6HA:NAT ura3-52 his3Δ200 leu2 lys2-801 trp1Δ63 Ade2+*	S288C	this study

15013	alpha	*Bik1-3xGFP:HYG Spc72-GFP:HIS kip2Δ::Kip2-ΔN(1-536)-(565-706)-6HA:NAT ura3-52 his3Δ200 leu2 lys2-801 trp1Δ63 Ade2+*	S288C	this study
14908	alpha	*Bik1-3xGFP:HYG Spc72-GFP:HIS kip2Δ::Kip3(1-480)-Kip2(510-706)-6HA:NAT ura3-52 his3Δ200 leu2 lys2-801 trp1Δ63 Ade2+*	S288C	this study
12119	alpha	*Bik1-3xGFP:HYG Spc72-GFP:HIS kip3Δ::URA3 ura3-52 his3Δ200 leu2 lys2-801 trp1Δ63 Ade2+*	S288C	this study
12118	alpha	*Bik1-3xGFP:HYG Spc72-GFP:HIS kip3Δ::URA3 kip2Δ::hyg ura3-52 his3Δ200 leu2 lys2-801 trp1Δ63 Ade2+*	S288C	this study
12119	alpha	*Bik1-3xGFP:HYG Spc72-GFP:HIS kip2Δ::hyg kip3Δ::Kip3-ΔCF-LZx2:KanMX ura3-52 his3Δ200 leu2 lys2-801 trp1Δ63 Ade2+*	S288C	this study
12390	alpha	*Bik1-3xGFP:HYG Spc72-GFP:HIS kip3Δ::Kip3-ΔCF-LZx2:KanMX ura3-52 his3Δ200 leu2 lys2-801 trp1Δ63 Ade2+*	S288C	this study
11367	a	*Bik1-3xGFP:HYG Spc72-GFP:HIS kip2Δ::Kip2-S63A:TRP kip3Δ::URA ura3-52 his3Δ200 leu2 lys2-801 trp1Δ63 Ade2+*	S288C	this study
11254	a	*Bik1-3xGFP:HYG Spc72-GFP:HIS kip2Δ::Kip2-ΔN-TRP kip3Δ::URA ura3-52 his3Δ200 leu2 lys2-801 trp1Δ63 Ade2+*	S288C	this study
11258	alpha	*Bik1-3xGFP:HYG Spc72-GFP:HIS kip2Δ::Kip2-SNNN:TRP kip3Δ::URA ura3-52 his3Δ200 leu2 lys2-801 trp1Δ63 Ade2+*	S288C	this study
11330	a	*Bik1-3xGFP:HYG Spc72-GFP:HIS kip2Δ::Kip2-ΔT:TRP kip3Δ::URA ura3-52 his3Δ200 leu2 lys2-801 trp1Δ63 Ade2+*	S288C	this study
11081	a	*Bik1-3xGFP:HYG Spc72-GFP:HIS kip2Δ::Kip2-SNNN:TRP bim1Δ::hphNT1 ura3-52 his3Δ200 leu2 lys2-801 trp1Δ63 Ade2+*	S288C	this study
13745	a	*Bik1-3xGFP:HYG Spc72-GFP:HIS Kip3-S299A ura3-52 his3Δ200 leu2 lys2-801 trp1Δ63 Ade2+*	S288C	this study
13748	a	*Bik1-3xGFP:HYG Spc72-GFP:HIS Kip3-S299E ura3-52 his3Δ200 leu2 lys2-801 trp1Δ63 Ade2+*	S288C	this study
14206	a	*Bik1-3xGFP:HYG Spc72-GFP:HIS Kip3-pp1 (V726AW728A) ura3-52 his3Δ200 leu2 lys2-801 trp1Δ63 Ade2+*	S288C	this study
14230	a	*Bik1-3xGFP:HYG Spc72-GFP:HIS Kip3-pp1-3A (V726AW728AS730AS734AS736A) ura3-52 his3Δ200 leu2 lys2-801 trp1Δ63 Ade2+*	S288C	this study
14231	a	*Bik1-3xGFP:HYG Spc72-GFP:HIS Kip3-3A (S730AS734AS736A) ura3-52 his3Δ200 leu2 lys2-801 trp1Δ63 Ade2+*	S288C	this study
14338	a	*Bik1-3xGFP:HYG Spc72-GFP:HIS kip3Δ::Kip3-ΔCF-LZ ura3-52 his3Δ200 leu2 lys2-801 trp1Δ63 Ade2+*	S288C	this study
14353	a	*Bik1-3xGFP:HYG Spc72-GFP:HIS kip3Δ::Kip3-ΔT ura3-52 his3Δ200 leu2 lys2-801 trp1Δ63 Ade2+*	S288C	this study
13219	a	*Bik1-3xGFP:HYG Spc72-GFP:HIS kip2Δ::hphNT1 kar3Δ::KAN ura3-52 his3Δ200 leu2 lys2-801 trp1Δ63 Ade2+*	S288C	this study
13223	a	*Bik1-3xGFP:HYG Spc72-GFP:HIS kar3Δ::KAN ura3-52 his3Δ200 leu2 lys2-801 trp1Δ63 Ade2+*	S288C	this study
12113	a	*Bik1-3xGFP:HYG Spc72-GFP:HIS dyn1Δ::TRP1 ura3-52 his3Δ200 leu2 lys2-801 trp1Δ63 Ade2+*	S288C	this study
13749	a	*Bik1-3xGFP:HYG Spc72-GFP:HIS Bim1-ΔETF ura3-52 his3Δ200 leu2 lys2-801 trp1Δ63 Ade2+*	S288C	this study
13965	a	*Bik1-3xGFP:HYG Spc72-GFP:HIS tub3Δ::hphNT1 CFP-Tub1:Trp1 ura3-52 his3Δ200 leu2 lys2-801 trp1Δ63 Ade2+*	S288C	this study
13725	a	*Bik1-3xGFP:HYG Spc72-GFP:HIS tub3Δ::hphNT1 ura3-52 his3Δ200 leu2 lys2-801 trp1Δ63 Ade2+*	S288C	this study

13479	a	*Bik1-3xGFP:HYG Spc72-GFP:HIS clb4Δ::NatMX ura3-52 his3Δ200 leu2 lys2-801 trp1Δ63 Ade2+*	S288C	this study
13603	alpha	*Bik1-3xGFP:HYG Spc72-GFP:HIS clb4Δ::NatMX dbf2-2 dbf20Δ::hyg ura3-52 his3Δ200 leu2 lys2-801 trp1Δ63 Ade2+*	S288C	this study
13726	a	*Bik1-3xGFP:HYG Spc72-GFP:HIS clb4Δ::NatMX kip2Δ::hphNT1 ura3-52 his3Δ200 leu2 lys2-801 trp1Δ63 Ade2+*	S288C	this study
14456	alpha	*Bik1-3xGFP:HYG Spc72-GFP:HIS clb4Δ::NatMX dbf2-2 dbf20Δ::hyg kip2Δ::hphNT1 ura3-52 his3Δ200 leu2 lys2-801 trp1Δ63 Ade2+*	S288C	this study
13437	alpha	*Bik1-3xGFP:HYG Spc72-GFP:HIS Kar9-S197A-TAP:LEU ura3-52 his3Δ200 leu2 lys2-801 trp1Δ63 Ade2+*	S288C	this study
13439	alpha	*Bik1-3xGFP:HYG Spc72-GFP:HIS kar9Δ::His ura3-52 his3Δ200 leu2 lys2-801 trp1Δ63 Ade2+*	S288C	this study
13452	alpha	*Bik1-3xGFP:HYG Spc72-GFP:HIS Kar9-S197A-TAP:LEU Kip2-S63A:TRP ura3-52 his3Δ200 leu2 lys2-801 trp1Δ63 Ade2+*	S288C	this study
13439	alpha	*Bik1-3xGFP:HYG Spc72-GFP:HIS kar9Δ::His kip2Δ::hphNT1 ura3-52 his3Δ200 leu2 lys2-801 trp1Δ63 Ade2+*	S288C	this study
14188	alpha	*Bik1-3xGFP:HYG Spc72-GFP:HIS cdc15-1 ura3-52 his3Δ200 leu2 lys2-801 trp1Δ63 Ade2+*	S288C	this study
13863	a	*Bik1-3xGFP:HYG Spc72-GFP:HIS swe1Δ::LEU2 ura3-52 his3Δ200 leu2 lys2-801 trp1Δ63 Ade2+*	S288C	this study
13866	alpha	*Bik1-3xGFP:HYG Spc72-GFP:HIS swe1Δ::LEU2 hsl1Δ::URA3 ura3-52 his3Δ200 leu2 lys2-801 trp1Δ63 Ade2+*	S288C	this study
13968	alpha	*Bik1-3xGFP:HYG Spc72-GFP:HIS kin3Δ::hyg ura3-52 his3Δ200 leu2 lys2-801 trp1Δ63 Ade2+*	S288C	this study
13728	a	*Bik1-3xGFP:HYG Spc72-GFP:HIS kin4Δ::KAN ura3-52 his3Δ200 leu2 lys2-801 trp1Δ63 Ade2+*	S288C	this study
14327	a	*Bik1-3xGFP:HYG Spc72-GFP:HIS Kin4-T209A Kip2-S63A:TRP ura3-52 his3Δ200 leu2 lys2-801 trp1Δ63 Ade2+*	S288C	this study
13857	alpha	*Bik1-3xGFP:HYG Spc72-GFP:HIS Kin4-T209A ura3-52 his3Δ200 leu2 lys2-801 trp1Δ63 Ade2+*	S288C	this study
13858	alpha	*Bik1-3xGFP:HYG Spc72-GFP:HIS Kin4-S508A ura3-52 his3Δ200 leu2 lys2-801 trp1Δ63 Ade2+*	S288C	this study
14458	a	*Bik1-3xGFP:HYG Spc72-GFP:HIS Kin4-T209A Kip2-S63A:TRP frk1Δ::KanMX ura3-52 his3Δ200 leu2 lys2-801 trp1Δ63 Ade2+*	S288C	this study
14479	alpha	*Bik1-3xGFP:HYG Spc72-GFP:HIS kin4Δ::KAN frk1Δ::KanMX ura3-52 his3Δ200 leu2 lys2-801 trp1Δ63 Ade2+*	S288C	this study
13723	a	*Bik1-3xGFP:HYG Spc72-GFP:HIS gin4Δ::HIS3 ura3-52 his3Δ200 leu2 lys2-801 trp1Δ63 Ade2+*	S288C	this study
13969	alpha	*Bik1-3xGFP:HYG Spc72-GFP:HIS hsl1Δ::hphNT1 ura3-52 his3Δ200 leu2 lys2-801 trp1Δ63 Ade2+*	S288C	this study
14127	alpha	*Bik1-3xGFP:HYG Spc72-GFP:HIS hsl1Δ::hphNT1 Kip2-S63A:TRP ura3-52 his3Δ200 leu2 lys2-801 trp1Δ63 Ade2+*	S288C	this study
14217	a	*Bik1-3xGFP:HYG Spc72-GFP:HIS bfa1Δ::TRP bub2Δ::KanMX ura3-52 his3Δ200 leu2 lys2-801 trp1Δ63 Ade2+*	S288C	this study
14218	a	*Bik1-3xGFP:HYG Spc72-GFP:HIS bfa1Δ::TRP ura3-52 his3Δ200 leu2 lys2-801 trp1Δ63 Ade2+*	S288C	this study
14544	a	*Bik1-3xGFP:HYG Spc72-GFP:HIS Bfa1-2A (S150A S180A) bub2::KanMX ura3-52 his3Δ200 leu2 lys2-801 trp1Δ63 Ade2+*	S288C	this study

14219	a	*Bik1-3xGFP:HYG Spc72-GFP:HIS bub2Δ::KanMX* *ura3-52 his3Δ200 leu2 lys2-801 trp1Δ63 Ade2+*	S288C	this study
13234	diploid	*Bik1-3xGFP:HYG/Bik1-3xGFP:HYG Spc72-GFP:HIS/ Spc72-GFP:HIS* *ura3-52 his3Δ200 leu2 lys2-801 trp1Δ63 Ade2+*	S288C	this study
13236	diploid	*Bik1-3xGFP:HYG/Bik1-3xGFP:HYG Spc72-GFP:HIS/ Spc72-GFP:HIS* *Kip2/kip2Δ::Kip2-ΔT:TRP* *ura3-52 his3Δ200 leu2 lys2-801 trp1Δ63 Ade2+*	S288C	this study
13237	diploid	*Bik1-3xGFP:HYG/Bik1-3xGFP:HYG Spc72-GFP:HIS/ Spc72-GFP:HIS* *Kip2/kip2Δ::Kip2-S63A:TRP* *ura3-52 his3Δ200 leu2 lys2-801 trp1Δ63 Ade2+*	S288C	this study
13251	diploid	*Bik1-3xGFP:HYG/Bik1-3xGFP:HYG Spc72-GFP:HIS/ Spc72-GFP:HIS* *Kip2/kip2Δ::hphNT1* *ura3-52 his3Δ200 leu2 lys2-801 trp1Δ63 Ade2+*	S288C	this study
14336	diploid	*Bik1-3xGFP:HYG/Bik1-3xGFP:HYG Spc72-GFP:HIS/ Spc72-GFP:HIS* *Kip2/kip2Δ::Kip2-ΔN:TRP* *ura3-52 his3Δ200 leu2 lys2-801 trp1Δ63 Ade2+*	S288C	this study
14839	diploid	*Bik1-3xGFP:HYG/Bik1-3xGFP:HYG Spc72-GFP:HIS/ Spc72-GFP:HIS* *Kip2/kip2Δ::Kip2-allD-6HA:NAT* *ura3-52 his3Δ200 leu2 lys2-801 trp1Δ63 Ade2+*	S288C	this study
13252	diploid	*Bik1-3xGFP:HYG/Bik1-3xGFP:HYG Spc72-GFP:HIS/ Spc72-GFP:HIS* *Kip3/kip3Δ::URA* *ura3-52 his3Δ200 leu2 lys2-801 trp1Δ63 Ade2+*	S288C	this study
13235	diploid	*Bik1-3xGFP:HYG/Bik1-3xGFP:HYG Spc72-GFP:HIS/ Spc72-GFP:HIS* *Kip3/kip3Δ::Kip3-ΔCF-LZx2:KanMX* *ura3-52 his3Δ200 leu2 lys2-801 trp1Δ63 Ade2+*	S288C	this study
15099	diploid	*Bik1-3xGFP:HYG/Bik1-3xGFP:HYG Spc72-GFP:HIS/ Spc72-GFP:HIS* *KIP2/kip2::Kip3(1-480)-Kip2(510-706)-6HA:NAT* *ura3-52 his3Δ200 leu2 lys2-801 trp1Δ63 Ade2+*	S288C	this study
14269	a	*kip2Δ::Kip2-6HA:NAT* *ura3-52 his3Δ200 leu2 lys2-801 trp1Δ63 Ade2+*	S288C	this study
14267	a	*kip2Δ::Kip2-ΔT-6HA:NAT* *ura3-52 his3Δ200 leu2 lys2-801 trp1Δ63 Ade2+*	S288C	this study
14407	alpha	*kip2Δ::Kip2-ΔT-6HA:NAT mad2::hyg* *ura3-52 his3Δ200 leu2 lys2-801 trp1Δ63 ade?*	S288C	this study
14271	?	*kip2Δ::Kip2-6HA:NAT Kip3-3xsfGFP:KanMX4 bik1Δ::hphNT1* *ura3-52 his3Δ200 leu2 lys2-801 trp1Δ63 Ade2+*	S288C	this study
14277	a	*kip2Δ::Kip2-6HA:NAT bim1Δ::hyg* *ura3-52 his3Δ200 leu2 lys2-801 trp1Δ63 Ade2+*	S288C	this study
14840	alpha	*kip2Δ::Kip2-6HA:NAT tem1::URA3 leu2::Tem1-Q79L:LEU2* *ade2-? Trp1-1 his3-11 can1-100?*	S288C/ W303	this study
14841	alpha	*kip2Δ::Kip2-ΔT-6HA:NAT tem1::URA3 leu2::Tem1-Q79L:LEU2* *ade2-? Trp1-1 his3-11 can1-100?*	S288C/ W303	this study
14744	a	*kip2Δ::Kip2-ΔT-6HA:NAT dbf2-2 dbf20Δ::HYG* *ura3-52 his3Δ200 leu2 lys2-801 trp1Δ63 ade?*	S288C	this study
14745	alpha	*kip2Δ::Kip2-6HA:NAT dbf2-2 dbf20Δ::HYG* *ura3-52 his3Δ200 leu2 lys2-801 trp1Δ63 ade?*	S288C	this study
14700	alpha	*kip2Δ::Kip2-ΔT-6HA:NAT dbf2Δ::Dbf2-SMNN:TRP Spc72-GFP:HIS* *ura3-52 his3Δ200 leu2 lys2-801 trp1Δ63 Ade2+*	S288C	this study
14701	a	*kip2Δ::Kip2-6HA:NAT dbf2::Dbf2-SMNN:TRP Bik1-3xGFP:hyg* *ura3-52 his3Δ200 leu2 lys2-801 trp1Δ63 Ade2+*	S288C	this study
14268	alpha	*kip2Δ::Kip2-ΔN-6HA:NAT* *ura3-52 his3Δ200 leu2 lys2-801 trp1Δ63 Ade2+*	S288C	this study
14405	a	*kip2Δ::Kip2-S63A-6HA:NAT* *ura3-52 his3Δ200 leu2 lys2-801 trp1Δ63 Ade2+*	S288C	this study

14284	a	*kip2Δ::Kip2-ΔN-ΔT-6HA:NAT ura3-52 his3Δ200 leu2 lys2-801 trp1Δ63 Ade2+*	S288C	this study
14406	a	*kip2Δ::Kip2-S63A-ΔT-6HA:NAT ura3-52 his3Δ200 leu2 lys2-801 trp1Δ63 Ade2+*	S288C	this study
13973	a	*kip3Δ::Kip3-wt-6HA:NAT ura3-52 his3Δ200 leu2 lys2-801 trp1Δ63 Ade2+*	S288C	this study
13975	a	*kip3Δ::Kip3-wt-6HA:NAT kip2Δ::hphNT1 ura3-52 his3Δ200 leu2 lys2-801 trp1Δ63 Ade2+*	S288C	this study
13990	a	*kip3Δ::Kip3-wt-6HA:NAT cdh1Δ::hphNT1 ura3-52 his3Δ200 leu2 lys2-801 trp1Δ63 Ade2+*	S288C	this study
13991	a	*kip3Δ::Kip3-wt-6HA:NAT pex2Δ::hphNT1 ura3-52 his3Δ200 leu2 lys2-801 trp1Δ63 Ade2+*	S288C	this study
13992	a	*kip3Δ::Kip3-wt-6HA:NAT pex4Δ::hphNT1 ura3-52 his3Δ200 leu2 lys2-801 trp1Δ63 Ade2+*	S288C	this study
13993	a	*kip3Δ::Kip3-wt-6HA:NAT bul1Δ::hphNT1 ura3-52 his3Δ200 leu2 lys2-801 trp1Δ63 Ade2+*	S288C	this study
14590	a	*kip3Δ::Kip3-wt-3xsfGFP:KanMX Spc42-mCherry:NatMX ura3-52 his3Δ200 leu2 lys2-801 trp1Δ63 Ade2+*	S288C	this study
15100	a	*kip2Δ::Kip2-wt-3xsfGFP:KanMX Spc42-mCherry:NatMX ura3-52 his3Δ200 leu2 lys2-801 trp1Δ63 Ade2+*	S288C	this study
15101	alpha	*kip2Δ::Kip2-ΔT-3xsfGFP:KanMX Spc42-mCherry:NatMX ura3-52 his3Δ200 leu2 lys2-801 trp1Δ63 Ade2+*	S288C	this study
15109	a	*kip2Δ::Kip2-wt-3xsfGFP:KanMX Spc42-mCherry:NatMX bik1::hphNT1 ura3-52 his3Δ200 leu2 lys2-801 trp1Δ63 Ade2+*	S288C	this study
15184	a	*kip2Δ::Kip2-ΔT-3xsfGFP:KanMX Spc42-mCherry:NatMX Spc72-3A ura3-52 his3Δ200 leu2 lys2-801 trp1Δ63 Ade2+*	S288C	this study
14747	a	*kip2Δ::Kip2-allD-3xsfGFP:KanMX Spc42-mCherry:NatMX ura3-52 his3Δ200 leu2 lys2-801 trp1Δ63 Ade2+*	S288C	this study
15102	a	*kip2Δ::Kip2-S63A-3xsfGFP:KanMX Spc42-mCherry:NatMX ura3-52 his3Δ200 leu2 lys2-801 trp1Δ63 Ade2+*	S288C	this study
14746	a	*kip2Δ::Kip2-ΔN-3xsfGFP:KanMX Spc42-mCherry:NatMX ura3-52 his3Δ200 leu2 lys2-801 trp1Δ63 Ade2+*	S288C	this study
15105	a	*kip2Δ::Kip2-G374A-3xsfGFP:KanMX Spc42-mCherry:NatMX ura3-52 his3Δ200 leu2 lys2-801 trp1Δ63 Ade2+*	S288C	this study
15104	a	*kip2Δ::Kip2-G374A-3xsfGFP:KanMX Spc42-mCherry:NatMX bik1Δ::NatMX ura3-52 his3Δ200 leu2 lys2-801 trp1Δ63 Ade2+*	S288C	this study
15106	a	*kip2Δ::Kip2-allD-G374A-3xsfGFP:KanMX Spc42-mCherry:NatMX ura3-52 his3Δ200 leu2 lys2-801 trp1Δ63 Ade2+*	S288C	this study
15107	a	*kip2Δ::Kip2-S63A-G374A-3xsfGFP:KanMX Spc42-mCherry:NatMX ura3-52 his3Δ200 leu2 lys2-801 trp1Δ63 Ade2+*	S288C	this study
15108	a	*kip2Δ::Kip2-ΔN-G374A-3xsfGFP:KanMX Spc42-mCherry:NatMX ura3-52 his3Δ200 leu2 lys2-801 trp1Δ63 Ade2+*	S288C	this study
15121	alpha	*kip2Δ::Kip2-G374A-3xsfGFP:KanMX Spc42-mCherry:NatMX kip3Δ::URA ura3-52 his3Δ200 leu2 lys2-801 trp1Δ63 Ade2+*	S288C	this study
15147	? sick	*kip2Δ::Kip2-G374A-3xsfGFP:KanMX Spc42-mCherry:NatMX kip3Δ::URA bik1Δ::NatMXura3-52 his3Δ200 leu2 lys2-801 trp1Δ63 Ade2+*	S288C	this study
15103	a	*kip2Δ::Kip2-G374A-3xsfGFP:KanMX Spc42-mCherry:NatMX stu2-13:URA ura3-52 his3Δ200 leu2 lys2-801 trp1Δ63 Ade2+*	S288C	this study

15149	a	*kip2Δ::Kip2-G374A-3xsfGFP:KanMX Spc42-mCherry:NatMX cdc5-2:URA ura3-52 his3Δ200 leu2 lys2-801 trp1Δ63 Ade2+*	S288C	this study
15148	a	*kip2Δ::Kip2-G374A-3xsfGFP:KanMX Spc42-mCherry:NatMX spc72-2:HIS3 ura3-52 his3Δ200 leu2 lys2-801 trp1Δ63 Ade2+*	S288C	this study
15144	a	*kip2Δ::Kip2-G374A-3xsfGFP:KanMX Spc42-mCherry:NatMX Spc72-ΔStu2(1-176::231-622) ura3-52 his3Δ200 leu2 lys2-801 trp1Δ63 Ade2+*	S288C	this study
15199	a	*kip2Δ::Kip2-G374A-3xsfGFP:KanMX Spc42-mCherry:NatMX nud1-44 ura3-52 his3Δ200 leu2 lys2-801 trp1Δ63 Ade2+*	S288C	this study
15150	a	*kip2Δ::Kip2-G374A-3xsfGFP:KanMX Spc42-mCherry:NatMX Spc72-3A ura3-52 his3Δ200 leu2 lys2-801 trp1Δ63 Ade2+*	S288C	this study
15155	a	*kip2Δ::Kip2-G374A-3xsfGFP:KanMX Spc42-mCherry:NatMX Spc72-wt ura3-52 his3Δ200 leu2 lys2-801 trp1Δ63 Ade2+*	S288C	this study
15166	a	*Bik1-3xGFP:HYG Spc72-GFP:HIS cdc5-2:URA ura3-52 his3Δ200 leu2 lys2-801 trp1Δ63 Ade2+*	S288C	this study
15164	a	*Bik1-3xGFP:HYG Spc72-ΔStu2(1-176::231-622)-GFP:HIS ura3-52 his3Δ200 leu2 lys2-801 trp1Δ63 Ade2+*	S288C	this study
15162	a	*Bik1-3xGFP:HYG Spc72-3A-GFP:HIS ura3-52 his3Δ200 leu2 lys2-801 trp1Δ63 Ade2+*	S288C	this study
15176	alpha	*kip2Δ::Kip2-G374A-3xsfGFP:KanMX Spc72-mCherry:hphNT1 ura3-52 his3Δ200 leu2 lys2-801 trp1Δ63 Ade2+*	S288C	this study
15177	alpha	*kip2Δ::Kip2-G374A-3xsfGFP:KanMX Nud1-mCherry:hphNT1 ura3-52 his3Δ200 leu2 lys2-801 trp1Δ63 Ade2+*	S288C	this study
15140	alpha	*Spc42-mCherry:NatMX Spc72-GFP:HIS3 ura3-52 his3Δ200 leu2 lys2-801 trp1Δ63 Ade2+*	S288C	this study
15191	a	*Spc42-mCherry:NatMX Spc72-3A-GFP:HIS3 ura3-52 his3Δ200 leu2 lys2-801 trp1Δ63 Ade2+*	S288C	this study
15192	a	*Spc42-mCherry:NatMX Spc72-ΔStu2(1-176::231-622)-GFP:HIS ura3-52 his3Δ200 leu2 lys2-801 trp1Δ63 Ade2+*	S288C	this study
15210	a	*Spc42-mCherry:NatMX Spc72-GFP:HIS3 cdc5-2::URA ura3-52 his3Δ200 leu2 lys2-801 trp1Δ63 Ade2+*	S288C	this study
15224	alpha	*kip2Δ::Kip2-mCherry:hphNT1 ura3-52 his3Δ200 leu2 lys2-801 trp1Δ63 Ade2+*	S288C	this study
15224b	a	*kip2Δ::Kip2-mCherry:hphNT1 ura3-52 his3Δ200 leu2 lys2-801 trp1Δ63 Ade2+*	S288C	this study
15323	a	*kip2Δ::Kip2-wt-3xsfGFP:KanMX Spc42-mCherry:NatMX clb4::HYG ura3-52 his3Δ200 leu2 lys2-801 trp1Δ63 Ade2+*	S288C	this study
15325	a	*kip2Δ::Kip2-wt-3xsfGFP:KanMX Spc42-mCherry:NatMX kar9::His3 ura3-52 his3Δ200 leu2 lys2-801 trp1Δ63 Ade2+*	S288C	this study
15330	diploid	*Kip2-3xsfGFP:KanMX/KIP2 Spc42-mCherry:NatMX/SPC42 Kar9-3xmKate:hphNT2/KAR9 ura3-52 his3Δ200 leu2 lys2-801 trp1Δ63 Ade2+ MET5+*	S288C	this study
15332	alpha	*kip2Δ::Kip2-R446A-3xsfGFP:KanMX Spc42-mCherry:NatMX ura3-52 his3Δ200 leu2 lys2-801 trp1Δ63 Ade2+*	S288C	this study
15333	alpha	*kip2Δ::Kip2-R384AR385A-3xsfGFP:KanMX Spc42-mCherry:NatMX ura3-52 his3Δ200 leu2 lys2-801 trp1Δ63 Ade2+*	S288C	this study
15334	alpha	*kip2Δ::Kip2-K294AR296A-3xsfGFP:KanMX Spc42-mCherry:NatMX ura3-52 his3Δ200 leu2 lys2-801 trp1Δ63 Ade2+*	S288C	this study
15335	diploid	*Kip2-ΔN-3xsfGFP:KanMX/Kip2-mCherry:hphNT1 ura3-52 his3Δ200 leu2 lys2-801 trp1Δ63 Ade2+*	S288C	this study

15336	diploid	*Kip2-S63A-3xsfGFP:KanMX/Kip2-mCherry:hphNT1 ura3-52 his3Δ200 leu2 lys2-801 trp1Δ63 Ade2+*	S288C	this study
15187	diploid	*Kip2-wt-3xsfGFP:KanMX/Kip2-mCherry:hphNT1 ura3-52 his3Δ200 leu2 lys2-801 trp1Δ63 Ade2+*	S288C	this study
15337	diploid	*Kip2-allD-3xsfGFP:KanMX/Kip2-mCherry:hphNT1 ura3-52 his3Δ200 leu2 lys2-801 trp1Δ63 Ade2+*	S288C	this study
15339	alpha	*kip2Δ::Kip2-7A-3xsfGFP:KanMX Spc42-mCherry:NatMX ura3-52 his3Δ200 leu2 lys2-801 trp1Δ63 Ade2+ (S13, T14, S18, S33, S47, S63, S69)*	S288C	this study
15340	alpha	*kip3::Kip3-E345A-3xsfGFP:KanMX Spc42-mCherry:NatMX ura3-52 his3Δ200 leu2 lys2-801 trp1Δ63 Ade2+*	S288C	this study
15341	diploid	*Kip2-mCherry:hphNT1/KIP2 Kip3-E345A-3xsfGFP:KanMX/KIP3 Spc42-mCherry:NatMX/Spc42 ura3-52 his3Δ200 leu2 lys2-801 trp1Δ63 Ade2+*	S288C	this study
15352	a	*kip2Δ::Kip2-wt-3xsfGFP:KanMX Spc42-mCherry:NatMX spc72-2:HIS3 ura3-52 his3Δ200 leu2 lys2-801 trp1Δ63 Ade2+*	S288C	this study
15353	a	*Kip2Δ::Kip2-K294AR296A(1-504)-polyGlycine-Kip2-K294AR296A(100-706)-3xsfGFP:KanMX ura3-52 his3Δ200 leu2 lys2-801 trp1Δ63 Ade2+*	S288C	this study
15354	a	*Kip2Δ::Kip2-R384R446A(1-504)-polyGlycine-Kip2-K294AR296A(100-706)-3xsfGFP:KanMX ura3-52 his3Δ200 leu2 lys2-801 trp1Δ63 Ade2+*	S288C	this study
15355	a	*Kip2Δ::Kip2-R384AR385A(1-504)-polyGlycine-Kip2-K294AR296A(100-706)-3xsfGFP:KanMX ura3-52 his3Δ200 leu2 lys2-801 trp1Δ63 Ade2+*	S288C	this study
15351	alpha	*Bik1-3xGFP:HYG Spc72-GFP:HIS Stu2-13:URA ura3-52 his3Δ200 leu2 lys2-801 trp1Δ63 Ade2+*	S288C	this study
15338	a	*kip2Δ::Kip2-wt-3xsfGFP:KanMX Spc42-mCherry:NatMX dbf2-2 dbf20Δ::HYG ura3-52 his3Δ200 leu2 lys2-801 trp1Δ63 Ade2+*	S288C	this study

Yeast (yYB) Strain number	Mating type	Plasmids	Genotype	source
14760	a	VN-allD-CH CF-VC	*Spc42-mCherry:NatMX kip2Δ::hyg* *ura3-52 his3Δ200 leu2 lys2-801 trp1Δ63 Ade2+*	this study
14783	a	VN-wt-CH-NES-LZ CF-VC	*Spc42-mCherry:NatMX kip2Δ::hyg* *ura3-52 his3Δ200 leu2 lys2-801 trp1Δ63 Ade2+*	this study
14761	a	VN-S63A-CH-NES-LZ CF-VC	*Spc42-mCherry:NatMX kip2Δ::hyg* *ura3-52 his3Δ200 leu2 lys2-801 trp1Δ63 Ade2+*	this study
14776	a	VN-ΔN-CH-NES-LZ CF-VC	*Spc42-mCherry:NatMX kip2Δ::hyg* *ura3-52 his3Δ200 leu2 lys2-801 trp1Δ63 Ade2+*	this study
14777	a	VN-allD-CH-NES-LZ CF-VC	*Spc42-mCherry:NatMX kip2Δ::hyg* *ura3-52 his3Δ200 leu2 lys2-801 trp1Δ63 Ade2+*	this study
14778	a	VN-allD-CH CF-ΔT-VC	*Spc42-mCherry:NatMX kip2Δ::hyg* *ura3-52 his3Δ200 leu2 lys2-801 trp1Δ63 Ade2+*	this study
14846	a	VN-wt-CH-NES-LZ CF-ΔT-VC	*Spc42-mCherry:NatMX kip2Δ::hyg* *ura3-52 his3Δ200 leu2 lys2-801 trp1Δ63 Ade2+*	this study
14847	a	VN-S63A-CH-NES-LZ CF-ΔT-VC	*Spc42-mCherry:NatMX kip2Δ::hyg* *ura3-52 his3Δ200 leu2 lys2-801 trp1Δ63 Ade2+*	this study
14878	a	VN-ΔN-CH-NES-LZ CF-ΔT-VC	*Spc42-mCherry:NatMX kip2Δ::hyg* *ura3-52 his3Δ200 leu2 lys2-801 trp1Δ63 Ade2+*	this study
14849	a	VN-allD-CH-NES-LZ CF-ΔT-VC	*Spc42-mCherry:NatMX kip2Δ::hyg* *ura3-52 his3Δ200 leu2 lys2-801 trp1Δ63 Ade2+*	this study
14864	a	NV-Kip2-wt-NF-NES-LZ CF-VC	*Spc42-mCherry:NatMX kip2Δ::hyg* *ura3-52 his3Δ200 leu2 lys2-801 trp1Δ63 Ade2+*	this study
14866	a	NV-Kip2-S63A-NF-NES-LZ CF-VC	*Spc42-mCherry:NatMX kip2Δ::hyg* *ura3-52 his3Δ200 leu2 lys2-801 trp1Δ63 Ade2+*	this study
14867	a	NV-Kip2-ΔN-NF-NES-LZ CF-VC	*Spc42-mCherry:NatMX kip2Δ::hyg* *ura3-52 his3Δ200 leu2 lys2-801 trp1Δ63 Ade2+*	this study
14865	a	NV-Kip2-allD-NF-NES-LZ CF-VC	*Spc42-mCherry:NatMX kip2Δ::hyg* *ura3-52 his3Δ200 leu2 lys2-801 trp1Δ63 Ade2+*	this study
14970	a	NV-Kip2-wt-NF-NES-LZ CF-ΔT-VC	*Spc42-mCherry:NatMX kip2Δ::hyg* *ura3-52 his3Δ200 leu2 lys2-801 trp1Δ63 Ade2+*	this study
14971	a	NV-Kip2-S63A-NF-NES-LZ CF-ΔT-VC	*Spc42-mCherry:NatMX kip2Δ::hyg* *ura3-52 his3Δ200 leu2 lys2-801 trp1Δ63 Ade2+*	this study
14972	a	NV-Kip2-ΔN-NF-NES-LZ CF-ΔT-VC	*Spc42-mCherry:NatMX kip2Δ::hyg* *ura3-52 his3Δ200 leu2 lys2-801 trp1Δ63 Ade2+*	this study
14973	a	NV-Kip2-allD-NF-NES-LZ CF-ΔT-VC	*Spc42-mCherry:NatMX kip2Δ::hyg* *ura3-52 his3Δ200 leu2 lys2-801 trp1Δ63 Ade2+*	this study